

University of Windsor

Scholarship at UWindor

Electronic Theses and Dissertations

Theses, Dissertations, and Major Papers

2012

Development and Testing of a Reconfigurable Gasoline Engine Control Module

Christopher John Kelly
University of Windsor

Follow this and additional works at: <https://scholar.uwindsor.ca/etd>

Recommended Citation

Kelly, Christopher John, "Development and Testing of a Reconfigurable Gasoline Engine Control Module" (2012). *Electronic Theses and Dissertations*. 5379.
<https://scholar.uwindsor.ca/etd/5379>

This online database contains the full-text of PhD dissertations and Masters' theses of University of Windsor students from 1954 forward. These documents are made available for personal study and research purposes only, in accordance with the Canadian Copyright Act and the Creative Commons license—CC BY-NC-ND (Attribution, Non-Commercial, No Derivative Works). Under this license, works must always be attributed to the copyright holder (original author), cannot be used for any commercial purposes, and may not be altered. Any other use would require the permission of the copyright holder. Students may inquire about withdrawing their dissertation and/or thesis from this database. For additional inquiries, please contact the repository administrator via email (scholarship@uwindsor.ca) or by telephone at 519-253-3000ext. 3208.

Development and Testing of a Reconfigurable Gasoline Engine Control Module

by

Christopher John Kelly

A Thesis

Submitted to the Faculty of Graduate Studies
through the Department of Mechanical, Automotive, and Materials Engineering
in Partial Fulfillment of the Requirements for
the Degree of Master of Applied Science at the
University of Windsor

Windsor, Ontario, Canada

2012

© 2012 Christopher John Kelly

Development and Testing of a Reconfigurable Gasoline Engine Control Module

by

Christopher John Kelly

APPROVED BY:

Dr. Xiaohong Xu, Outside Reader
Department of Civil and Environmental Engineering

Dr. Graham Reader, Program Reader
Department of Mechanical, Automotive and Materials Engineering

Dr. Jimi Tjong, Co-Advisor
Department of Mechanical, Automotive and Materials Engineering

Dr. Ming Zheng, Advisor
Department of Mechanical, Automotive and Materials Engineering

Dr. Bruce Minaker, Chair of Defense
Department of Mechanical, Automotive and Materials Engineering

December 16, 2011

DECLARATION OF ORIGINALITY

I hereby certify that I am the sole author of this thesis and that no part of this thesis has been published or submitted for publication.

I certify that, to the best of my knowledge, my thesis does not infringe upon anyone's copyright nor violate any proprietary rights and that any ideas, techniques, quotations, or any other material from the work of other people included in my thesis, published or otherwise, are fully acknowledged in accordance with the standard referencing practices. Furthermore, to the extent that I have included copyrighted material that surpasses the bounds of fair dealing within the meaning of the Canada Copyright Act, I certify that I have obtained a written permission from the copyright owner(s) to include such material(s) in my thesis and have included copies of such copyright clearances to my appendix.

I declare that this is a true copy of my thesis, including any final revisions, as approved by my thesis committee and the Graduate Studies office, and that this thesis has not been submitted for a higher degree to any other University or Institution.

ABSTRACT

A dynamometer laboratory may typically face the following issues on a daily basis: the lack/availability of a calibration, software limiters, hardware failure codes/modes, hardware/software level incompatibilities and the time/knowledge required to troubleshoot these issues. A Reconfigurable Engine Controller (REC), which provides freedom to operate the engine under any condition, eliminates many of these issues. The result is an accelerated engine development process which includes engine mapping and/or testing new algorithms before implementation on production hardware. A REC can provide a flexible tailored controller to suit the needs of the individual testing application.

This research used the dSPACE MicroAutoBox and RapidPro hardware and software with MATLAB/Simulink (the coding tool) to successfully develop and test a REC under a series of steady state engine operating conditions. Proportional Integral Derivative (PID) controllers were also successfully implemented for the throttle body position, lambda sensor heating and fuel pulse width modulation. The data collected from a combustion analysis system along with the production engine controller and the REC parameters was used to validate the new controller. The results indicated that the system performance was similar to that of the production controller.

DEDICATION

I would like to dedicate my thesis work to my fiancée Stephanie Masse and my parents, Ron and Suzanne Kelly. Without their understanding, support and guidance completing this thesis would have been a much more difficult and daunting task.

ACKNOWLEDGEMENTS

The work included in this thesis was conducted at the Ford Essex Engine Plant Dynamometer Lab also known as PERDC (Powertrain Engineering Research and Development Centre). I would like to thank the entire technician and engineering staff for their guidance and support. Countless times my co-workers pointed me in the proper direction to complete this thesis.

In particular I would like to acknowledge Dr. Jimi Tjong and Dr. Ming Zheng who provided me the opportunity to work on this exciting thesis topic. Without their drive and determination for engine testing this thesis would not have been possible.

I would like to also acknowledge Tony Fountaine who, over the years as I worked toward completing this thesis, has provided a wealth of knowledge on computer programming, electrical circuit design and operation. Without his guidance there would have been many more hours spent trying to find answers for the many problems encountered.

Darin Truman has been a wealth of knowledge, and he has helped me by accelerating my understanding of the production engine controller and its many complex algorithms. I would like to extend my thanks to Dr. Usman Asad, whom assisted me with the collection and analysis of my combustion data.

Editing this thesis has required numerous revisions and many of my co-workers, friends, fellow students and committee members have helped bring this thesis into its final form. I would like to thank everyone for their feedback in the process of completing this thesis.

TABLE OF CONTENTS

| | |
|---|--------|
| DECLARATION OF ORIGINALITY | iii |
| ABSTRACT | iv |
| DEDICATION | v |
| ACKNOWLEDGEMENTS | vi |
| LIST OF TABLES | xiv |
| LIST OF FIGURES | xviii |
| NOMENCLATURE | xxviii |
| CHAPTER 1 | |
| INTRODUCTION | |
| 1 | |
| 1.1 Four Stroke Gasoline Engine Process..... | 2 |
| 1.2 Electronic Engine Control..... | 3 |
| 1.3 Research Objectives..... | 5 |
| 1.4 Thesis Overview | 5 |
| CHAPTER 2 | |
| HARDWARE TECHNICAL BACKGROUND | |
| 8 | |
| 2.1 Sensors Used on Engines | 8 |
| 2.1.1 Engine Speed and Cam Position Sensors | 8 |
| 2.1.1.1 Crank Reluctor Wheel | 8 |

| | | |
|-----------|---|----|
| 2.1.1.2 | Cam Reluctor Wheel | 9 |
| 2.1.1.3 | Encoder | 10 |
| 2.1.1.4 | Variable Reluctance Sensor (VRS) | 10 |
| 2.1.1.4.1 | Missing Tooth Effect on the VRS Signal | 11 |
| 2.1.1.5 | Hall Sensor..... | 12 |
| 2.1.2 | Temperature Measurement/Thermistors | 14 |
| 2.1.2.1 | Intake Air Temperature (IAT)..... | 14 |
| 2.1.3 | Pressure Measurement | 15 |
| 2.1.3.1 | Strain Gauge/Piezo-Resistive Type..... | 15 |
| 2.1.3.2 | Manifold Absolute Pressure (MAP), Throttle Inlet Pressure (TIP) | 16 |
| 2.1.4 | Knock Detection | 16 |
| 2.1.4.1 | Using Knock Sensors for Feedback Control of Spark..... | 17 |
| 2.1.5 | Exhaust Gas Oxygen (EGO)/ Air to Fuel Ratio (AFR) | 18 |
| 2.1.6 | Mass Air Flow (MAF) | 21 |
| 2.1.6.1 | Hot-Film..... | 21 |
| 2.1.7 | Electronic Throttle Control (ETC) Position Feedback Sensors | 22 |
| 2.2 | Actuators Used on Engines | 23 |
| 2.2.1 | Throttle Body..... | 23 |

| | | |
|---------|--|----|
| 2.2.2 | Fuel Systems..... | 24 |
| 2.2.2.1 | Port Fuel Injection (PFI)..... | 24 |
| 2.2.3 | Ignition Systems | 26 |
| 2.2.3.1 | Ignition Coil Operation..... | 27 |
| 2.2.3.2 | Coil on Plug (COP) | 28 |
| 2.2.3.3 | Driver on Coil on Plug..... | 29 |
| 2.2.3.4 | Spark Plug..... | 29 |
| 2.3 | Types of Control Systems | 30 |
| 2.3.1 | Open Loop Control | 30 |
| 2.3.2 | Closed Loop Control (Feedback Control)..... | 30 |
| 2.3.3 | Closed Loop Control (Feedforward/Command Compensation) | 31 |
| 2.3.4 | Proportional Integral Derivative (PID) Control..... | 31 |
| 2.3.5 | Saturation, Integrator Windup and Anti-Windup | 34 |
| 2.3.6 | Bumpless Transfer and Integral Gain Parameter Changes..... | 35 |

CHAPTER 3

| | | |
|-----|--|-----------|
| | DESIGN AND METHODOLOGY | 36 |
| 3.1 | Engine Specifications | 36 |
| 3.2 | Engine Sensor/Instrumentation Setup..... | 37 |

| | | |
|-------|---|----|
| 3.2.1 | Production PCM via ETAS INCA vs. dSPACE Hardware | 38 |
| 3.2.2 | dSPACE MicroAutoBox Specifications | 40 |
| 3.2.3 | dSPACE RapidPro Stack Specifications..... | 41 |
| 3.2.4 | Combustion Analysis System..... | 43 |
| 3.3 | Dynamometer Setup | 44 |
| 3.3.1 | Load Points for Steady State Testing..... | 45 |
| 3.3.2 | Motoring..... | 45 |
| 3.3.3 | Engine Operation Production vs. dSPACE Hardware..... | 46 |
| 3.4 | Offline Testing | 46 |
| 3.5 | MATLAB/Simulink Model Overview..... | 47 |
| 3.6 | Throttle Body Controller..... | 49 |
| 3.6.1 | Throttle Body Motor Duty Cycle PID Controller Design..... | 49 |
| 3.6.2 | Controller Validation Tests | 50 |
| 3.7 | Air Fuel Ratio Controller | 51 |
| 3.7.1 | AFR Measurement Logic | 51 |
| 3.7.2 | Heater Duty Cycle PID Controller..... | 51 |
| 3.7.3 | Fuel Pulse Width/AFR PID Controller | 52 |
| 3.7.4 | Closed Loop AFR Controller Validation Tests | 54 |

CHAPTER 4

ANALYSIS OF RESULTS.....55

4.1 Throttle Body Test Results.....55

 4.1.1 Pyramid Test.....55

 4.1.2 Random Step Input Test (RSIT).....56

 4.1.3 Sine Wave Input Test (SWIT).....56

4.2 AFR Heater Controller Results57

4.3 AFR/Fuel Pulse Width Controller Results.....57

4.4 AFR Signal Noise due to Resistance Measurement59

4.5 Engine Operation Results.....60

 4.5.1 Data/Figure Overview60

 4.5.1.1 1000 RPM –17.7 inHg (Gauge).....62

 4.5.1.2 2000 RPM WOT67

 4.5.2 dSPACE Controller Open Loop Results71

 4.5.2.1 1000 RPM –17.7 inHg (Gauge) OL Control71

 4.5.2.2 2000 RPM WOT OL Control.....77

CHAPTER 5

CONCLUSIONS AND RECOMMENDATIONS81

5.1 Conclusions81

| | | |
|-----------------|--|-----|
| 5.2 | Recommendations for Future Work | 82 |
| APPENDICES..... | | 83 |
| APPENDIX I | : 5.0L Test Engine Figures | 83 |
| APPENDIX II | : Hardware Setup Diagrams | 84 |
| APPENDIX III | : Synchronization Routine/Example | 88 |
| APPENDIX IV | : Crank and Cam Sensors & Signals..... | 90 |
| | VRS & Hall Sensor Signals | 90 |
| | Magnetoresistive Sensor | 90 |
| APPENDIX V | : Cylinder Head Temperature (CHT)..... | 91 |
| APPENDIX VI | : Additional MAP Sensor Details | 92 |
| APPENDIX VII | : Knock Sensor Construction and Operation..... | 93 |
| APPENDIX VIII | : Additional HEGO/UHEGO Sensor Info..... | 94 |
| APPENDIX IX | : Additional MAF Sensor Designs..... | 96 |
| | Volume Air Flow (VAF)/Vane-Type | 96 |
| | Hot-Wire Type | 97 |
| APPENDIX X | : Spark Plug and Coil Construction | 98 |
| APPENDIX XI | : Actuator/Sensor Transfer Functions | 99 |
| APPENDIX XII | : MATLAB/Simulink Model Block Summary..... | 105 |

| | | |
|--------------------|---|-----|
| APPENDIX XIII | : Motoring Results | 153 |
| APPENDIX XIV | : Additional Engine Operation Results | 154 |
| APPENDIX XV | : Additional Throttle Body Results..... | 191 |
| APPENDIX XVI | : Coil Driver Circuit Design..... | 194 |
| APPENDIX XVII | : Offline Engine Simulator..... | 201 |
| APPENDIX XVIII | : MVEM Manifold Filling/Emptying | 205 |
| REFERENCES..... | | 209 |
| VITA AUCTORIS..... | | 219 |

LIST OF TABLES

| | |
|--|-----|
| Table 2.1: Missing Tooth Angle BTDC of Cylinder # 1 Intake Stroke | 9 |
| Table 2.2: EGO Sensor Interfaces, adapted from [36] | 18 |
| Table 3.1: Specifications for Engine and Fuel Used for Testing [55]..... | 36 |
| Table 3.2: Inputs and Outputs of the MicroAutoBox, adapted from [60] | 41 |
| Table 3.3: Load Points for Steady State Testing..... | 45 |
| Table 3.4: Closed and Open PID Controller Gains | 49 |
| Table 3.5: AFR Sensor Heater Duty Cycle PID Controller Gains..... | 52 |
| Table 3.6: AFR/Fuel Pulse Width PID Controller Gains | 54 |
| Table 4.1: AFR Sensor Delay Times..... | 59 |
| Table 4.2: Summary of Resistance and Averaging on AFR..... | 60 |
| Table 4.3: 1000 RPM –17.7 inHg Production PCM Data Summary | 66 |
| Table 4.4: 2000 WOT Production PCM Data Summary | 70 |
| Table 4.5: 1000 RPM –17.7 inHg dSPACE OL Controller Data Summary | 76 |
| Table 4.6: 2000 WOT dSPACE OL Control Data Summary | 80 |
| Table A-III-1: Left – Sync First Try, Right – Sync Second Try, adapted from [60] | 88 |
| Table A-XII-1: CrankAngleSimulatorSpark_TB_Inj Block Summary..... | 106 |
| Table A-XII-2: Constants Summary | 108 |

| | |
|---|-----|
| Table A-XII-3: Engine_Sensors Summary | 110 |
| Table A-XII-4: Inputs Summary | 112 |
| Table A-XII-5: AFR Summary | 114 |
| Table A-XII-6: Heater_Control1 Summary | 115 |
| Table A-XII-7: SampleHold_UA Summary | 116 |
| Table A-XII-8: SampleHold_UR Summary | 117 |
| Table A-XII-9: Heater_Control1 Summary | 118 |
| Table A-XII-10: Resistance_Switch Summary | 119 |
| Table A-XII-11: Heater_Switch Summary | 120 |
| Table A-XII-12: AFRHeater Summary | 121 |
| Table A-XII-13: Pedal Summary | 122 |
| Table A-XII-14: APPS1 & APPS2 Summary | 123 |
| Table A-XII-15: Throttle Summary | 124 |
| Table A-XII-16: TP_NS_ANG Summary | 125 |
| Table A-XII-17: TP_PS_ANG Summary | 125 |
| Table A-XII-18: MAP & TIP Summary | 126 |
| Table A-XII-19: MAF Summary | 128 |
| Table A-XII-20: CHT Summary | 129 |

| | |
|--|-----|
| Table A-XII-21: ETC Summary | 131 |
| Table A-XII-22: Source_Selector Summary..... | 133 |
| Table A-XII-23: Closed Summary | 134 |
| Table A-XII-24: Open Summary | 135 |
| Table A-XII-25: RPCU_Control_InjIgn Summary..... | 137 |
| Table A-XII-26: GBL_Fuel Summary | 138 |
| Table A-XII-27: GLOBAL_FUEL Summary..... | 139 |
| Table A-XII-28: GBL_Inj_Dur Summary | 141 |
| Table A-XII-29: GBL_Inj_Start_Ang Summary | 143 |
| Table A-XII-30: NumEventSelector Summary | 145 |
| Table A-XII-31: GBL_Fuel_Sch Summary..... | 147 |
| Table A-XII-1: AFR_Control Summary..... | 149 |
| Table A-XII-2: Integrator Summary..... | 150 |
| Table A-XII-3: iSwitch Summary | 151 |
| Table A-XII-4: Anti-Windup Summary | 152 |
| Table A-XIV-1: 1000 RPM 100 ft-lb Production Controller Data Summary | 157 |
| Table A-XIV-2: 1000 RPM WOT Production Controller Data Summary | 160 |
| Table A-XIV-3: 1500 RPM WOT Production Controller Data Summary | 163 |

| | |
|---|-----|
| Table A-XIV-4: 2000 RPM WOT Production Controller Data Summary | 166 |
| Table A-XIV-5: 1500 RPM –17.7 inHg Production Controller Data Summary | 169 |
| Table A-XIV-6: 1000 RPM 100 ft-lb dSPACE Controller Data Summary | 172 |
| Table A-XIV-7: 1000 RPM WOT dSPACE Controller Data Summary | 175 |
| Table A-XIV-8: 1500 RPM WOT dSPACE Controller Data Summary | 178 |
| Table A-XIV-9: 2000 RPM WOT dSPACE OL Controller Data Summary | 181 |
| Table A-XIV-10: 1500 RPM –17.7 inHg dSPACE OL Controller Data Summary | 184 |
| Table A-XIV-11: 1000 RPM –17.7inHg dSPACE CL Controller Data Summary | 187 |
| Table A-XIV-12: 2000 RPM WOT dSPACE CL Controller Data Summary | 190 |
| Table A-XVI-1: PCB Circuit Board Pad # to Connector Pin Numbers | 197 |

LIST OF FIGURES

| | |
|--|----|
| Figure 1.1: Four Stroke Gasoline Engine Process, adapted from [1]..... | 3 |
| Figure 1.2: Thesis Map | 7 |
| Figure 2.1: Crank Wheel Reluctors Left 36-1, Right 60-2 | 9 |
| Figure 2.2: All Cam Wheels Relative to each other and Overlaid at Base Timing | 9 |
| Figure 2.3: VRS Sensor Operation and Design, adapted from [5, 10]..... | 11 |
| Figure 2.4: Expected VRS Sensor Waveform due to the Missing Tooth Effect | 12 |
| Figure 2.5: Hall Sensor Operation Diagram, adapted from [5]..... | 13 |
| Figure 2.6: Hall IC Circuit, adapted from [28] | 13 |
| Figure 2.7: Left – Voltage Divider Circuit, Right – Basic Thermistor Curves | 14 |
| Figure 2.8: Two Strain Gage Pressure Sensor Designs, adapted from [3] | 15 |
| Figure 2.9: Knock Intensity and Spark Ignition Angle, adapted from [7, 8]..... | 17 |
| Figure 2.10: Narrow EGO Sensor Operating Range, adapted from [3] | 19 |
| Figure 2.11: HEGO Sensor BOSCH LSH25, adapted from [3] | 19 |
| Figure 2.12: Hot-Film Mass Air Flow Sensor Design, adapted from [3, 41]..... | 21 |
| Figure 2.13: 2 and 3 Track APPS Curves, adapted from [10] | 23 |
| Figure 2.14: Left – TPS Curve, Right – MLX90316 Hall Sensor, adapted from [42]..... | 23 |
| Figure 2.15: H-Bridge Driver Circuit for Throttle Body Motor, adapted from [43]..... | 24 |

| | |
|--|----|
| Figure 2.16: Port Fuel Injector Design and Wire Diagram, adapted from [3, 10] | 25 |
| Figure 2.17: Top – Prim. Coil Current, Bottom – Sec. Coil Voltage, adapted from [44] . | 27 |
| Figure 2.18: PCM with LSD and Current Sensing for COP Ignition..... | 28 |
| Figure 2.19: Circuits, Left – Driver On Coil, Right – IGBT, adapted from [46-49] | 29 |
| Figure 2.20: Open Loop Diagram | 30 |
| Figure 2.21: Closed Loop (Feedback Control) Diagram, adapted from [51] | 31 |
| Figure 2.22: Closed Loop Feedback/Feed Forward Diagram..... | 31 |
| Figure 2.23: PID Controller Diagram w/Feedforward, adapted from [51]..... | 33 |
| Figure 2.24: I-PD Controller Diagram w/Feed Forward, adapted from [52, 54]..... | 33 |
| Figure 2.25: Saturation, Anti-Windup Block Diagram, adapted from [51, 54]..... | 34 |
| Figure 3.1: Top View of Engine with Sensor/Instrumentation Locations..... | 37 |
| Figure 3.2: Left Side of the Engine Showing Sensor/Instrumentation Locations..... | 38 |
| Figure 3.3: ETAS Hardware Setup for Production PCM Communication..... | 39 |
| Figure 3.4: dSPACE MicroAutoBox and RapidPro Hardware Setup..... | 39 |
| Figure 3.5: Breakout Panel for dSPACE MicroAutoBox and RapidPro..... | 40 |
| Figure 3.6: RapidPro Stack Configuration used for Research of this Thesis | 42 |
| Figure 3.7: Cylinder Pressure Measurement AVL and NI Integration..... | 44 |
| Figure 3.8: Simulink Model Overview CrankAngleSimulatorSpark_TB_Inj.mdl..... | 48 |

| | |
|---|----|
| Figure 3.9: Closed PID Controller | 49 |
| Figure 3.10: AFRHeater, AFRHeater Duty Cycle PID Controller | 52 |
| Figure 3.11: Heater_DC_Switch, Duty Cycle Output Command to AFR Heater | 52 |
| Figure 3.12: Fuel Pulse Width (PW) PID Controller Option 1..... | 53 |
| Figure 3.13: Fuel Pulse Width (PW) PID Controller Option 2..... | 53 |
| Figure 4.1: Pyramid Test, Left – Engine Off, Right – Zoomed (7–13 s)..... | 55 |
| Figure 4.2: RSIT, Left – Engine Off, Right – Zoomed (37.6–38.6 s) | 56 |
| Figure 4.3: SWIT, Left – Engine Off, Right – Zoomed (0–4 s)..... | 56 |
| Figure 4.4: dSPACE UHEGO Resistance, 2000 RPM WOT Prod. PCM Control..... | 57 |
| Figure 4.5: RH AFR Control, Left – OL, Right – CL..... | 58 |
| Figure 4.6: RH AFR Control, Left – OL, Right – CL..... | 58 |
| Figure 4.7: Sequence for Checking AFR Noise due to Resistance/AFR Averaging | 59 |
| Figure 4.8: Production 1000 RPM –17.7 inHg Combustion Data..... | 64 |
| Figure 4.9: Production 1000 RPM –17.7 inHg PCM Measurements..... | 65 |
| Figure 4.10: Production 2000 RPM WOT Combustion Data..... | 68 |
| Figure 4.11: Production 2000 RPM WOT PCM Measurements | 69 |
| Figure 4.12: Bypassed Current Sensing Resistor by Voltage Measurement | 71 |
| Figure 4.13: dSPACE OL 1000 RPM –17.7 inHg Combustion Data..... | 74 |

| | |
|---|----|
| Figure 4.14: dSPACE OL 1000 RPM –17.7 inHg PCM Measurements | 75 |
| Figure 4.15: dSPACE OL 2000 RPM WOT Combustion Data..... | 78 |
| Figure 4.16: dSPACE OL 2000 RPM WOT PCM Measurements | 79 |
| Figure A-I-1: Ford F150 5.0L Engine Front View [55] | 83 |
| Figure A-I-2: Ford F150 5.0L Engine Rear View [55] | 83 |
| Figure A-II-1: ETAS Hardware Setup for Production PCM with Images | 85 |
| Figure A-II-2: dSPACE MicroAutoBox and RapidPro Hardware Setup with Images | 86 |
| Figure A-II-3: Cylinder Pressure Measurement, AVL and NI Integration with Images... | 87 |
| Figure A-III-1: CAD Calculation, Synchronization Flowchart, adapted from [60]..... | 89 |
| Figure A-IV-1: VRS and Hall Signals, Crank (36-1) and Cam (7 Teeth)..... | 90 |
| Figure A-V-1: Cylinder Head Temperature (CHT) Sensor, adapted from [3] | 91 |
| Figure A-VI-1: MAP Sensor with IAT Construction, adapted from [3] | 92 |
| Figure A-VI-2: Pressure Sensor Piezo-Resistor Arrangement, adapted from [5, 6]..... | 92 |
| Figure A-VII-1: Piezoceramic Knock Sensor Design, adapted from [3] | 93 |
| Figure A-VIII-1: HEGO & UHEGO Sensing Element Construction, adapted from [3] .. | 94 |
| Figure A-VIII-2: HEGO and UHEGO Operation, adapted from [3] | 94 |
| Figure A-IX-1: Volume Air Flow (VAF) Sensor, adapted from [6, 10]..... | 96 |
| Figure A-IX-1: Hot Wire Mass Air Flow (MAF) Sensor Design, adapted from [10] | 97 |

| | |
|--|-----|
| Figure A-X-1: Cross Section - Driver on Pencil Coil on Plug, adapted from [3]..... | 98 |
| Figure A-X-2: General Spark Plug Cross Section, adapted from [3, 10]..... | 98 |
| Figure A-XI-1: Fuel Injector Pulse Width Transfer Function | 99 |
| Figure A-XI-2: Pedal Rotation Transfer Function | 99 |
| Figure A-XI-3: Throttle Position Sensor Transfer Function..... | 100 |
| Figure A-XI-4: BOSCH LSU 4.9 Sensor Temperature Transfer Function | 100 |
| Figure A-XI-5: BOSCH LSU 4.9 O2 Concentration Transfer Function..... | 101 |
| Figure A-XI-6: BOSCH LSU 4.9 Lambda (λ) Transfer Function | 101 |
| Figure A-XI-7: CHT Sensor Resistance Transfer Function | 102 |
| Figure A-XI-8: CHT Sensor Voltage Transfer Function..... | 102 |
| Figure A-XI-9: MAF Sensor Voltage Temperature Transfer Function | 103 |
| Figure A-XI-10: MAP Sensor Voltage Temperature Transfer Function..... | 103 |
| Figure A-XI-11: MAF Sensor Frequency Transfer Function | 104 |
| Figure A-XI-12: MAP Sensor Voltage Transfer Function | 104 |
| Figure A-XII-1: CrankAngleSimulatorSpark_TB_Inj Model Root..... | 105 |
| Figure A-XII-2: Constants Subsystem | 107 |
| Figure A-XII-3: Engine_Sensors Subsystem..... | 109 |
| Figure A-XII-4: Inputs Subsystem | 111 |

| | |
|---|-----|
| Figure A-XII-5: AFR Subsystem, adapted from [80] | 113 |
| Figure A-XII-6: Control_Ri_mes Logic via Stateflow, adapted from [80] | 115 |
| Figure A-XII-7: Sample_Hold_UA, adapted from [80] | 116 |
| Figure A-XII-8: Sample_Hold_UR, adapted from [80] | 117 |
| Figure A-XII-9: Heater_Control1, adapted from [80] | 118 |
| Figure A-XII-10: Resistance_Switch, adapted from [80] | 119 |
| Figure A-XII-11: Heater_Switch, adapted from [80] | 120 |
| Figure A-XII-12: AFRHeater, adapted from [80] | 121 |
| Figure A-XII-13: Pedal Subsystem | 122 |
| Figure A-XII-14: APPS1 Subsystem | 123 |
| Figure A-XII-15: Throttle Subsystem | 124 |
| Figure A-XII-16: TP_NS_ANG Subsystem | 125 |
| Figure A-XII-17: TP_PS_ANG Subsystem | 125 |
| Figure A-XII-18: MAP Subsystem | 126 |
| Figure A-XII-19: MAF Subsystem | 127 |
| Figure A-XII-20: CHT Subsystem | 129 |
| Figure A-XII-21: ETC Subsystem | 130 |
| Figure A-XII-22: Source_Selector Subsystem | 133 |

| | |
|---|-----|
| Figure A-XII-23: Closed Subsystem | 134 |
| Figure A-XII-24: Open Subsystem | 135 |
| Figure A-XII-25: RPCU_Control_InjIgn Subsystem..... | 136 |
| Figure A-XII-26:GBL_Fuel Subsystem | 138 |
| Figure A-XII-27:GLOBAL_FUEL Subsystem..... | 139 |
| Figure A-XII-28: GBL_Inj_Dur Subsystem..... | 140 |
| Figure A-XII-29: GBL_Inj_Start_Ang Subsystem | 142 |
| Figure A-XII-30: dSPACE Crank Angle Commands vs Actual Crank Angle Domain.. | 143 |
| Figure A-XII-31: NumEventSelector Subsystem | 144 |
| Figure A-XII-32: GBL_Fuel_Sch, Global Fuel Pulse Width Control | 146 |
| Figure A-XII-33: AFR_Control Subsystem..... | 148 |
| Figure A-XII-1: Integrator Subsystem w/Bumpless Transfer..... | 149 |
| Figure A-XII-2: iSwitch Subsystem..... | 151 |
| Figure A-XII-3: Anti-Windup Subsystem | 152 |
| Figure A-XIII-1: 1000 RPM Motoring Curves..... | 153 |
| Figure A-XIII-2: 1500 RPM Motoring Curves..... | 153 |
| Figure A-XIII-3: 2000 RPM Motoring Curves..... | 153 |
| Figure A-XIV-1: Production 1000 RPM 100 ft-lb Combustion Data..... | 155 |

| | |
|--|-----|
| Figure A-XIV-2: Production 1000 RPM 100 ft-lb PCM Measurements | 156 |
| Figure A-XIV-3: Production 1000 RPM WOT Combustion Data | 158 |
| Figure A-XIV-4: Production 1000 RPM WOT PCM Measurements | 159 |
| Figure A-XIV-5: Production 1500 RPM WOT Combustion Data | 161 |
| Figure A-XIV-6: Production 1500 RPM WOT PCM Measurements | 162 |
| Figure A-XIV-7: Production 2000 RPM 35% Pedal Combustion Data..... | 164 |
| Figure A-XIV-8: Production 2000 RPM 35% Pedal PCM Measurements | 165 |
| Figure A-XIV-9: Production 1500 RPM –17.7 inHg Combustion Data..... | 167 |
| Figure A-XIV-10: Production 1500 RPM –17.7 inHg PCM Measurements | 168 |
| Figure A-XIV-11: dSPACE OL 1000 RPM 100 ft-lb Combustion Data..... | 170 |
| Figure A-XIV-12: dSPACE OL 1000 RPM 100 ft-lb PCM Measurements | 171 |
| Figure A-XIV-13: dSPACE OL 1000 RPM WOT Combustion Data | 173 |
| Figure A-XIV-14: dSPACE OL 1000 RPM WOT PCM Measurements | 174 |
| Figure A-XIV-15: dSPACE OL 1500 RPM WOT Combustion Data | 176 |
| Figure A-XIV-16: dSPACE OL 1500 RPM WOT PCM Measurements | 177 |
| Figure A-XIV-17: dSPACE OL 2000 RPM 35% Pedal Combustion Data..... | 179 |
| Figure A-XIV-18: dSPACE OL 2000 RPM 35% Pedal PCM Measurements | 180 |
| Figure A-XIV-19: dSPACE OL 1500 RPM –17.7 inHg Combustion Data..... | 182 |

| | |
|--|-----|
| Figure A-XIV-20: dSPACE OL 1500 RPM –17.7inHg PCM Measurements | 183 |
| Figure A-XIV-21: dSPACE CL 1000 RPM –17.7 inHg Combustion Data..... | 185 |
| Figure A-XIV-22: dSPACE CL 1000 RPM –17.7 inHg PCM Measurements | 186 |
| Figure A-XIV-23: dSPACE CL 2000 RPM WOT Combustion Data..... | 188 |
| Figure A-XIV-24: dSPACE CL 2000 RPM WOT PCM Measurements | 189 |
| Figure A-XV-1: Pyramid Diff. Plots, Left – Engine Off, Right – Zoomed (7-13 s) | 191 |
| Figure A-XV-2: Pyramid Diff. Plots, Left – Engine Off, Right – Motoring 2000..... | 191 |
| Figure A-XV-3: RSIT Diff. Plots, Left – Engine Off, Right – Zoomed (23-45 s)..... | 192 |
| Figure A-XV-4: RSIT Diff. Plots, Left – Engine Off, Right – Motoring 1500 RPM | 192 |
| Figure A-XV-5: SWIT Diff. Plots, Left – Engine Off, Right – Zoomed (0-4 s)..... | 193 |
| Figure A-XV-6: SWIT Diff. Plots, Left – Engine Off, Right – Motoring 2000 RPM ... | 193 |
| Figure A-XV-7: SWIT Engine Off, Zoomed (0.6-3 s)..... | 193 |
| Figure A-XVI-1: Final Assembled Coil on Driver (Box Bottom View)..... | 194 |
| Figure A-XVI-2: Coil Driver Board Layout/Pad Descriptions..... | 195 |
| Figure A-XVI-3: PCB Circuit Board Pad Numbers..... | 196 |
| Figure A-XVI-4: Driver Box Top View - Connector Locations Names | 198 |
| Figure A-XVI-5: Connection to dSPACE Bench & Components | 200 |
| Figure A-XVII-1: Engine Speed/Crank Simulator Setup for Offline Testing | 201 |

Figure A-XVII-2: Offline Injector and Spark Plug Test bench202

Figure A-XVII-3: Parallel Engine Hardware Testing203

Figure A-XVII-4: Proposed Offline Engine Simulator204

NOMENCLATURE

Abbreviations

| | | |
|-------|--|----------|
| .mdl | MATLAB Simulink Model (file extension) | |
| .tlc | Target Language Compiler (file extension) | |
| AC | Alternating Current | |
| ACT | Air Charge Temperature | [°C] |
| ADACS | Automatic Data Acquisition Control System | |
| AFR | Air Fuel Ratio | |
| AI | Analog Input | [V] |
| Ang | Angle | |
| APPS | Accelerator Pedal Position Sensor | |
| APPS1 | Accelerator Pedal Position Sensor Track 1 | [° or V] |
| APPS2 | Accelerator Pedal Position Sensor Track 2 | [° or V] |
| APPS3 | Accelerator Pedal Position Sensor Track 3 | [° or V] |
| ARS1 | BOSCH Hall Effect Sensor | |
| ARS2 | BOSCH Hall Effect Sensor | |
| ASAP3 | Arbeitskreis zur Standardisierung von Applikationssystemen (Working Group of Standardisation of Calibration and Diagnosis Systems) | |
| ATDC | After Top Dead Centre | [°CA] |
| avg | Average | |
| AVL | Anstalt für Verbrennungskraftmaschinen (Institute for Internal Combustion Engines) | |
| AWS | Chip Used by BOSCH to control EGO Sensors | |
| BDC | Bottom Dead Centre | |
| BIP | BOSCH Integrated Power | |
| BNC | Bayonet Neill–Concelman (Type of connector, RF/Coaxial) | |
| BTDC | Before Top Dead Centre | [°CA] |
| CA | Crank Angle | |
| CAC | Charge Air Cooler | |
| CAD | Crank Angle Domain | |
| CAN | Controller Area Network | |
| CC | Chassis Control | |
| CCDI | Camshaft/Crankshaft/Digital Input Card | |
| CHT | Cylinder Head Temperature | [°C] |
| CID | Cylinder Identification, Cam Position Sensor | |
| CJ125 | Chip Used by BOSCH to control EGO Sensors | |
| CKP | Crank Position Sensor | |

| | | |
|-------------|---|-------|
| CL | Closed Loop | |
| CMC | Cleveland Motion Controls | |
| CMOS | Complementary Metal Oxide Semiconductor | |
| CO | Carbon Monoxide | ppm |
| Coeff. Var. | Coefficient of Variance | |
| COP | Coil On Plug | |
| Cu | Copper | |
| Cyl | Cylinder | |
| D | Derivative | |
| DAC | Data Acquisition Card | |
| DC | Duty Cycle | |
| DC | Direct Current | [V] |
| DCCA | Drives Control Centre Aligned | |
| DCEA | Drives Control Edge Aligned | |
| DES | Desired | |
| DesETBAng | Desired Electronic Throttle Body Angle | [°] |
| DI | Direct Injection | |
| DOE | Design of Experiments | |
| DOHC | Double Over Head Cam | |
| Dur | Duration | [ms] |
| <i>e</i> | error (difference, setpoint-feedback) | |
| EA | Expected Angle | [°CA] |
| ECT | Engine Coolant Temperature | |
| EEC | Extended Engine Control | |
| EGO | Exhaust Gas Oxygen | |
| EGOS | Exhaust Gas Oxygen Sensor | |
| EOT | Engine Oil Temperature | [°C] |
| ETAS | Engineering Tools, Application and Services | |
| ETB | Electronic Throttle Body | |
| ETC | Electronic Throttle Control | |
| ETK | Emulator Test Probe | |
| EVC | Exhaust Valve Close | [°CA] |
| EVO | Exhaust Valve Open | [°CA] |
| ex. | Example | |
| EXH | Exhaust | |
| f_k_d | Derivative Gain | |
| f_k_i | Integral Gain | |
| f_k_p | Proportional Gain | |
| FET | Field Effect Transistor | |
| ff | feedforward | |
| fp | Fixed Period | |

| | | |
|----------|--|----------------------|
| FPM2.3 | BOSCH Hall Effect Sensor | |
| GBL | Global | |
| HC | Unburned Hydrocarbon | [ppmC ₁] |
| HEGO | Heated Exhaust Gas Oxygen | |
| HFM5 | Hot-Film Air-Mass Meter By BOSCH | |
| HFM6 | Hot-Film Air-Mass Meter By BOSCH | |
| I | Integral | |
| I/O | Input Output | |
| IAT | Intake Air Temperature | [°C] |
| IBM | International Business Machines Corporation | |
| IC | Integrated Circuit | |
| IGBT | Isolated Gate Bipolar Transistor | |
| Ign | Ignition | |
| IMC | Integrated Magneto-Concentrator | |
| IMEP | Indicated Mean Effective Pressure | [Bar] |
| INCA | INtegrated Calibration and Acquisition Systems | |
| Inj | Injection | |
| INT | Intake | |
| IntReset | Integrator Reset | |
| I-PD | Another Form of a PID Controller | |
| IVC | Intake Valve Close | [°CA] |
| IVO | Intake Valve Open | [°CA] |
| LH | Left Hand | |
| LHS | Left Hand Side | |
| LIN | Local Interconnect Network | |
| LSD | Low Side Driver | |
| LSF4 | Narrow-Band BOSCH Lambda Sensor | |
| LSU4.9 | Wide-Band BOSCH Lambda Sensor | |
| MA | Measured Angle | [°CA] |
| MABX | MicroAutoBox | |
| MAF | Mass Air Flow into Engine | [kg/hr] |
| MAFcyl | Mass Air Flow Per Cylinder | [kg/hr] |
| MAP | Manifold Absolute Pressure | [kPa] |
| MATLAB | MATrix LABoratory | |
| MBC | Model Based Control | |
| MFB | Mass Fraction Burned | [%] |
| MLX90316 | Throttle Body Hall Position Sensor | |
| MON | Motoring Octane Number | |
| MOSFET | Metal Oxide Semiconductor Field Effect Transistors | |
| MP | Manifold Pressure | [kPa] |

| | | |
|-----------|---|-------|
| MPC | Motorola PowerPC | |
| MPFI | Multiport Fuel Injection | |
| MVEM | Mean Value Engine Model | |
| N | Loop Counter for Synchronization of Crank Angle | |
| NA | Not Applicable | |
| Neg. | Negative Electrode | |
| NG | Next Generation | |
| NI | National Instruments | |
| Ni | Nickel | |
| NTC | Negative Temperature Coefficient | |
| numcyl | Number of Cylinders | |
| OBDII | On-Board Diagnostic II | |
| ode | Ordinary Differential Equation | |
| OL | Open Loop | |
| P | Proportional | |
| PC | Personal Computer | |
| PCB | Printed Circuit Board | |
| PCM | Powertrain Control Module | |
| PCMCIA | Personal Computer Memory Card International Association | |
| PCOP | Pencil on Coil On Plug | |
| PCT | Percent | [%] |
| PERDC | Powertrain Engine Research and Development Centre | |
| PFI | Port Fuel Injection | |
| PID | Proportional Integral Derivative | |
| P_{int} | Pressure Intake | [kPa] |
| Pos. | Positive Electrode | |
| PPC | PowerPC | |
| PSD | Pseudo-Derivative Feedback | |
| PTC | Positive Temperature Coefficient | |
| PV | Process Variable | |
| PW | Pulse Width | [ms] |
| PWM | Pulse Width Modulation | |
| RCP | Rapid Control Prototyping | |
| REC | Reconfigurable Engine Controller | |
| res. | Resolution | |
| RH | Right Hand | |
| RHS | Right Hand Side | |
| RON | Research Octane Number | |
| RPCU | RapidPro Control Unit | |
| RSIT | Random Step Input Test | |

| | | |
|-----------|---|----------|
| RTI | Real Time Interface | |
| SC | Signal Conditioning | |
| SEFI | Sequential Electronic Fuel Injection | |
| SFI | Sequential Port Fuel Injection | |
| <i>SP</i> | setpoint | |
| std. | Standard Deviation | |
| SWIT | Sine Wave Input Test | |
| T | Temperature | [°C] |
| TB | Throttle Body | |
| TDC | Top Dead Centre | |
| TIP | Throttle Inlet Pressure | [kPa] |
| TMAF | Temperature Mass Air Flow | [°C] |
| TMAP | Temperature Manifold Absolute Pressure | [°C] |
| TP_NS | Throttle Position Negative Slope | [° or V] |
| TP_PS | Throttle Position Positive Slope | [° or V] |
| TPS | Throttle Position Sensor | |
| TPS1 | Throttle Position Sensor Track 1 | [° or V] |
| TPS2 | Throttle Position Sensor Track 2 | [° or V] |
| TPU | Time Processor Unit | |
| TTIP | Temperature Throttle Inlet Pressure | [°C] |
| TTL | Transistor to Transistor Logic | |
| TWC | Three Way Catalyst | |
| <i>UA</i> | UHEGO Pumping Current Voltage from CJ125 | [Amp] |
| UHEGO | Universal Exhaust Gas Oxygen | |
| <i>UR</i> | UHEGO Resistance Voltage Measurement from CJ125 | [V] |
| <i>v</i> | vibration | |
| VAF | Volume Air Flow | [kg/hr] |
| VBAT | Battery Voltage | [V] |
| <i>vp</i> | Variable Period | |
| VRS | Variable Reluctance Sensor | |
| VVT | Variable Valve Timing | |
| WOT | Wide Open Throttle | |
| ZIF | Zero Insertion Force | |

Subscripts

| | | |
|----------------|-----------------------|-------|
| AFR_{Actual} | Actual Measured AFR | |
| Al_2O_3 | Aluminum Oxide | |
| I_{hall} | Hall Chip Current | [Amp] |
| I_p | UHEGO Pumping Current | [Amp] |
| K_d | Derivative Gain | |

| | | |
|--------------|--|--------------|
| K_{ff} | Feedforward Gain | |
| K_i | Integral Gain | |
| K_{new} | New Integral Gain | |
| K_{old} | Old Integral Gain | |
| K_p | Proportional Gain | |
| NO_x | Nitrogen Oxides | |
| O_2 | Oxygen | |
| Pa_{O_2} | Partial Pressure of Oxygen in Air | [kPa] |
| Pe_{O_2} | Partial Pressure of Oxygen in Exhaust | [kPa] |
| R_{pullup} | Pull Up Resistor Resistance | [Ω] |
| T_d | Derivative Time | [s] |
| T_i | Integral Time | [s] |
| V_{hall} | Hall Chip Voltage | [V] |
| V_{heater} | UHEGO/HEGO Heater Voltage | [V] |
| V_{in} | Sensor Supply Voltage | [V] |
| V_{out} | Sensor Output Voltage | [V] |
| V_{pump} | UHEGO Pumping Voltage | [V] |
| V_{ref} | Sensor Supply Voltage | [V] |
| ZrO_2 | Zirconia/Zirconium Dioxide (electrolyte) | |

Greek

| | | |
|-----------|--|--------------|
| ∞ | Infinity | |
| λ | Lambda (excess oxygen) = $AFR_{Actual}/AFR_{Stoich}$ | |
| Ω | Resistance | [Ω] |

Units

| | |
|--------------|---|
| % | Percent |
| $^{\circ}C$ | Degrees Celsius |
| $^{\circ}CA$ | Crank Angle Degree |
| $^{\circ}F$ | Degrees Fahrenheit = $(9/5)*(^{\circ}C) + 32$ |
| Amps | Amps |
| Bar | Bar |
| C | Coulomb |
| D | Delta |
| Deg | Degree |
| ft-lb | Foot Pound = 1.35582 Nm |
| HP | Horsepower = 745.6999 W |

| | |
|------------------------------|---|
| hr | Hour |
| Hz | Hertz |
| inHg | Inches of Mercury = 3.386388 kPa |
| J | Joule |
| K | Kelvin |
| kg | Kilogram |
| kHz | Kilohertz |
| kPa | Kilopascals |
| kV | Kilovolt |
| L | Litre |
| m | Meter |
| mA | Milli Amps |
| MB | Mega Byte |
| MHz | Mega Hertz |
| mm | Millimeter |
| mol | Mole |
| ms | Millisecond |
| mV | Millivolt |
| Nm | Newton Meter |
| ppm | Parts Per Million |
| ppm _{C₁} | Parts Per Million Carbon (C ₁ Basis) |
| rad | Radians |
| RPM | Revolutions Per Minute |
| s | Second |
| V | Voltage |
| W | Watt |

Constants

| | |
|-----------------------|--|
| F | Faradays Constant = 96485.3365 C/mol |
| R | Universal Gas Constant = 8.3145 J/molK |
| ν | UHEGO Constant used to Calculate Pumping Current |
| AFR _{Stoich} | AFR for Complete Combustion (Stoichiometry) = 14.6 |

CHAPTER 1

INTRODUCTION

The engine development process includes testing prototype engines. Development engines are typically ready for dynamometer (dyno) testing well ahead of the engine controller design process. Even when a production engine controller is available, there are often many issues and hurdles that must first be overcome for testing to begin. Typically when a production engine is tested in a dynamometer facility, a dyno-specific calibration is developed. In the dyno-specific calibration, the production vehicle (powertrain) calibration is modified, by shutting off switches that are present in the code. These switches may be present for safety reasons such as vehicle crash detection (disable fuel injection and spark), exhaust backpressure limits (detect a plugged exhaust pipe, due to a failed catalyst for example), vehicle/engine speed and torque limiters (limit the engine operating range) or even anti-theft algorithms. After such features have been disabled and testing has commenced, it is not uncommon for other unforeseen software features or limits to present themselves, halting engine testing. One example might be due to a failed sensor, which causes the engine to enter a limp/failure mode. Depending on the failure mode, it may be detected through the On-Board Diagnostic II (OBDII) codes using a code reader.

Production engine calibrations are designed by many different calibration groups, and are often the result of a global effort. For this reason the engine calibration features are documented in a manual that may contain upwards of 15,000 pages. Troubleshooting faults then becomes a very time consuming issue, as engineers sift through pages of documentation and contact hardware specific calibrators for support. Simple engine tests which adjust specific parameters such as Air Fuel Ratio (AFR), throttle plate position and cam position for instance may require this same process of troubleshooting, in order to find the correct parameter to achieve the desired control of the specific hardware available.

The calibration and its complex algorithms may also delay engine testing, as a result of software/hardware incompatibilities or even software/hardware revision level issues. It is not uncommon for a calibration to go through many software level revisions on an hourly or daily basis. Changing hardware such as the injectors, sensors or engine wiring harness for instance may require a new calibration.

In summary the main issues that a dynamometer lab faces on a daily basis include: lack/availability of a calibration, software limiters, hardware failure codes/modes, hardware/software level incompatibilities and the time/knowledge required to troubleshoot these issues. It would be beneficial to have a generic controller that can be updated to match the specific hardware of any engine, while facilitating steady state engine operation. A tool with this capability would then accelerate the development of engine maps, which may be used for production calibrations. New control algorithms can also be tested before implementation on a production controller. With a REC, only the required features for engine testing can be implemented reducing complexity.

1.1 Four Stroke Gasoline Engine Process

The four stroke gasoline engine process begins with the piston at Top Dead Centre (TDC). As the piston travels away from TDC, the open intake valve allows for a fresh charge of fuel and air to enter the combustion chamber. Figure 1.1 shows a naturally aspirated engine with Port Fuel Injection (PFI). After the piston has reached Bottom Dead Centre (BDC), the intake valve is closed and the piston changes direction and begins to compress the fresh charge. With the piston approaching TDC again, the spark plug fires and combustion is initiated causing a rapid rise in the cylinder pressure, hence commencing the power stroke. The power stroke is complete when the piston again reaches BDC and reverses direction, at which point the exhaust valve is open allowing the piston to force out the combustion products (exhaust stroke) until the piston approaches TDC again. The four stroke engine must rotate the crankshaft twice for an entire combustion cycle to occur [1, 2].

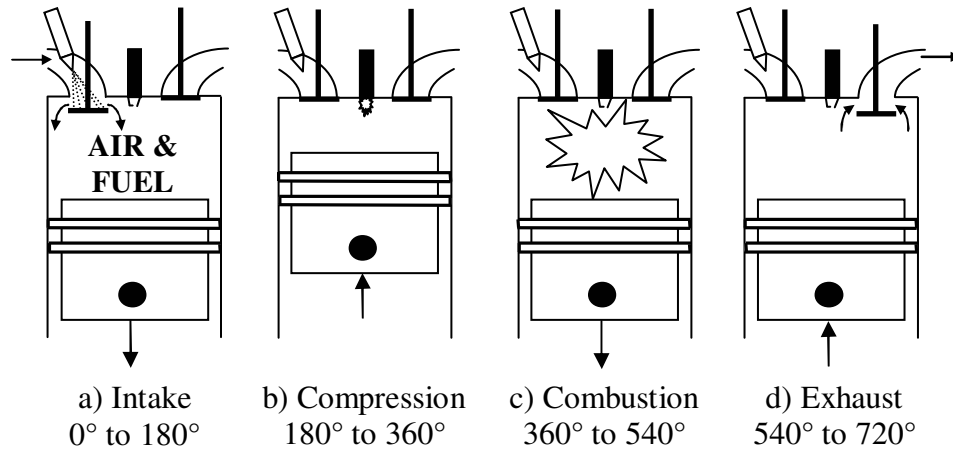


Figure 1.1: Four Stroke Gasoline Engine Process, adapted from [1]

1.2 Electronic Engine Control

The four stroke internal combustion engine process previously defined in section 1.1 has not changed with the implementation of electronics [3]. However, various electronic components have been added to the engine such as actuators (throttle body, exhaust gas recirculation valve, injectors, cam phasers, solenoids, etc.), while a number of sensors have been implemented to provide feedback (closed loop control) on the many processes occurring (throttle position, air fuel ratio, speed, mass flow rates, temperatures, pressures, knock, etc.) [4-11]. By using these sensors, it has been possible to:

- 1) Improve idle noise and combustion noise
- 2) Improve engine efficiency and fuel economy
- 3) Increase power and torque
- 4) Reduce engine out emissions

As manufacturers implement the various electronics and the associated control algorithms to improve the operation of the engine, it is also a goal to reduce engine cost and improve engine quality in order to remain competitive in the market. The result of the reduced cost criteria requires minimizing the time to generate and calibrate the complex engine control algorithms used on production engine controllers, while utilizing the available sensors to estimate or predict other signals that may not be available through the use of Mean Value Engine Models MVEM. Some examples of desired signals are Mass Air Flow (MAF), Manifold Absolute Pressure (MAP) [12], torque [7, 13, 14], turbo

speed, exhaust pressure and temperature [15, 16]. Improving quality requires engine control algorithms that have been tested and proven to work. Reduced cost and improved quality can be achieved by testing and development in a facility such as a dynamometer lab, as the engine is mapped under steady state conditions (various speeds and loads) using advanced modeling techniques such as DOE (Design of Experiments) [17]. The engine does not operate under steady state conditions in vehicle, but steady state conditions are used to approximate the transient operation of the engine. Another way of reducing cost and improving the quality of engine controllers was to replace hand coded algorithms (c-code), with automatically generated c-code through the use of software packages such as MATLAB/Simulink with Real-Time Workshop and TargetLink [18-25].

Previously, it was demonstrated that it is possible to develop an Internal Combustion engine model based controller using LabVIEW and operate an engine using a modern PC (Personal Computer) with a Data Acquisition Card (DAC) [26]. Research has also been conducted to develop MVEM's within MATLAB/Simulink to validate engine controller designs [27]. dSPACE developed the MicroAutoBox (MABX) and RapidPro Control Unit (RPCU) with some associated Simulink blocks to allow the controller design to be completed using MATLAB/Simulink. Standard c-code can then be quickly generated and flashed (programmed) onto the MABX. The micro controller and associated hardware used by dSPACE is the same as that found onboard a production engine controller. An additional benefit of using MATLAB/Simulink would be the possibility of potentially applying some of the MVEM's which were previously developed and utilize them in real time on an engine controller.

1.3 Research Objectives

The main objectives of this thesis are listed below:

- 1) Design, develop and implement a custom engine controller using MATLAB/Simulink software with dSPACE MicroAutoBox and RapidPro hardware
- 2) Test the production engine under the same steady state conditions using the production engine controller and the REC
- 3) Compare the results from both engine controllers and determine if the REC is capable of operating an engine, similar to a production engine controller

It was considered necessary to review the sensors, actuators and control algorithms used for engine control in order to complete the main goals of this thesis. The function, operation and purpose of each will be reviewed prior to completing the main goals of the thesis.

1.4 Thesis Overview

Chapter 2 focuses on reviewing the various sensors, actuators and associated control theory that is typically applied for engine control purposes. The reviewed hardware was included in the design of the REC. Chapter 3 focuses on the engine setup that was used for all the experiments which were conducted; the various test cell hardware that was used to collect data is also introduced. An overview of the designed MATLAB/Simulink model is then presented, followed by a detailed review on the implemented throttle body position controller, Air Fuel Ratio (AFR) heater controller and fuel Pulse Width (PW) controller. The test methods used to validate these various controllers are presented, as well as the various load points for testing both the production engine controller and the REC. Chapter 4 focuses on presenting the empirical data that was collected, from both the production and REC. Results from the various tests that were conducted to validate the designed closed loop controllers are also presented.

Chapter 5 includes conclusions and recommendations for the future work and opportunities for improvement to continue the advancement of the REC.

APPENDIX I contains images of the test engine. APPENDIX II includes some diagrams with photos of the hardware used for testing. APPENDIX III reviews the synchronization routine used to determine the crank angle domain. APPENDIX IV presents some example crank and cam signals as well as an alternate sensor which is available. APPENDIX V reviews the Cylinder Head Temperature (CHT) sensor which could be used in future calibrations. APPENDIX VI shows the construction of the MAP sensor. APPENDIX VII illustrates the knock sensor construction and explains its operation. APPENDIX VIII focuses on the construction and operation of the exhaust gas oxygen sensors. APPENDIX IX provides background for some additional MAF sensor designs. APPENDIX X includes illustrations of the pencil coil on plug and spark plug construction. APPENDIX XI provides the sensor and actuator transfer functions. APPENDIX XII summarizes the MATLAB/Simulink model subsystems used. APPENDIX XIII groups the motoring curves for the speeds and throttle angles tested. APPENDIX XIV has additional results showing the test points that were not discussed in the main body. APPENDIX XV contains additional throttle body results. APPENDIX XVI describes and provides the required information to build a coil driver box. APPENDIX XVII presents an offline engine simulator that may be developed for conducting offline engine control model development. APPENDIX XVIII includes an overview of the mean value engine model equations that may be applied or investigated in future work.

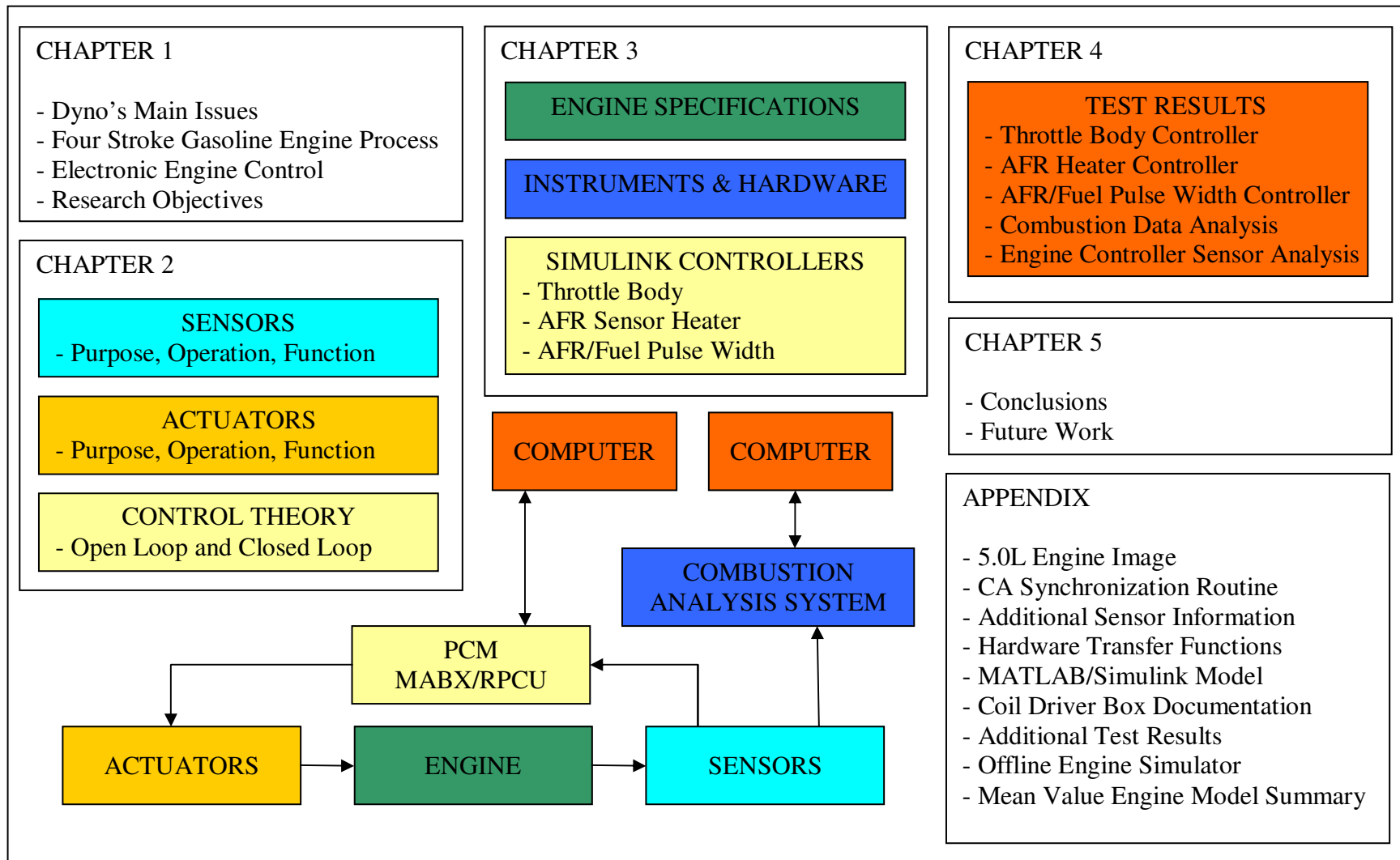


Figure 1.2: Thesis Map

CHAPTER 2

HARDWARE TECHNICAL BACKGROUND

The research conducted as part of this thesis uses the production Ford 5.0 L naturally aspirated gasoline truck engine. In order to properly design the controller it was necessary to understand the purpose, function and operation of the sensors and actuators used on the engine. Additional sensor or actuator information (ex. construction, alternate designs and transfer functions) can be found in APPENDIX IV to XI.

2.1 Sensors Used on Engines

2.1.1 Engine Speed and Cam Position Sensors

For engine control purposes, both the engine speed (Crank Position, CKP) and the cam position (Cylinder Identification, CID) are required. Using these two signals the engine controller may calculate the Crank Angle Domain (CAD), which enables the scheduling, of fuel and spark in the CAD. For a detailed description of the engine synchronization process in order to determine the CAD see APPENDIX III.

2.1.1.1 Crank Reluctor Wheel

The majority of production engines use either 36-1 (36 teeth evenly spaced, one tooth missing) or 60-2 (60 teeth evenly spaced, two teeth missing) reluctor wheels for the calculation of the engine speed and position. Using 60-2 provides a higher resolution than the 36-1 wheel (10°CA between teeth vs. 6°CA , Note: CA = Crank Angle). Figure 2.1 shows the two common crank wheel patterns. In either case for a four stroke internal combustion engine the crankshaft must rotate twice for an entire combustion cycle (720°CA). Using the crankshaft wheel alone does not provide sufficient information to identify the engine position in the combustion cycle, as the missing tooth will appear twice in the combustion cycle (once for each rotation of the engine). The missing tooth is used to identify the location of the engine rotation relative to TDC of cylinder # 1 (intake stroke). Table 2.1 provides some typical angles for the location of the missing tooth

(where I = Inline, V = V engine configuration). These locations are angles Before Top Dead Centre (BTDC) of cylinder # 1 for various engine configurations.

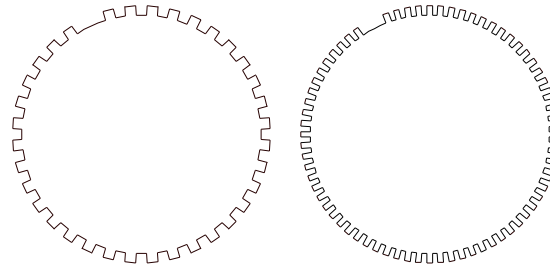


Figure 2.1: Crank Wheel Reluctors Left 36-1, Right 60-2

Table 2.1: Missing Tooth Angle BTDC of Cylinder # 1 Intake Stroke

| Engine Type | I4 | V6 | V8 | V10 |
|-----------------------|----|----|----|-----|
| Missing Tooth (°BTDC) | 90 | 60 | 50 | 36 |

2.1.1.2 Cam Reluctor Wheel

A unique signal is required to identify where the engine is in the combustion cycle. The reluctor wheel on the cam provides a unique pattern relative to the missing tooth gap (crank reluctor wheel) as the cam makes only one rotation in the combustion cycle (crank reluctor wheel makes two rotations in one combustion cycle). Figure 2.2 shows the base timing position of all the cam wheels relative to one another. With the image on the far right showing all the cam wheels overlaid.

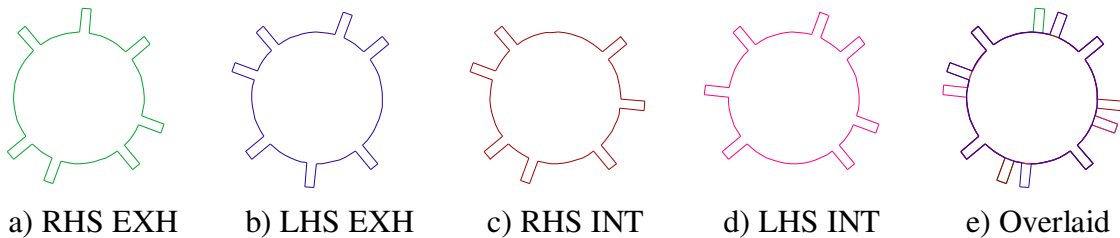


Figure 2.2: All Cam Wheels Relative to each other and Overlaid at Base Timing

2.1.1.3 Encoder

For research purposes typically the CAD can be calculated fairly easily with high precision (0.1°CA), through the use of an encoder. There are many different encoders available for this purpose, but would be too expensive for production use. After an encoder is installed on an engine, it is necessary to know the position of the encoder disc relative cylinder # 1.

2.1.1.4 Variable Reluctance Sensor (VRS)

The VRS is one of the most common sensors used in production to detect the crank and cam wheel profiles. The VRS can be identified by the number of pins on the sensor (two pins). Hall sensors which are reviewed later have three pins. The sensor consists of a permanent magnet on one end and a ferrite pin in the middle. A coil is wrapped around the ferrite pin and it is this coil that generates the varying voltage detected by the engine controller. The voltage generated by the sensor will resemble that of an Alternating Current (AC) sine wave. The signal is a function of the rate of change in the magnetic flux/field intensity around the sensor. Typically the wires for these sensors are shielded and twisted together until the signal reaches the engine controller, where the shield is then connected to ground. This helps reduce cross-talk and inductive interference which may lead to noise in the signal [6]. An example of a noise source may be the ignition coils.

The VRS operation can be explained as follows with the help of Figure 2.3. As the leading edge of a tooth or tab enters the sensors magnetic field, the voltage will first go to zero, and as the center of the tab reaches the edge of the sensor, the voltage will reach its maximum value (magnetic field contracting, intensity/flux increasing). Once the centres of the sensor and the tab are aligned the voltage will return to zero again with a negative slope (magnetic field rate of change = 0, intensity/flux at a maximum). It is this negative slope, zero crossing that is generally used for engine control purposes. As the centre of the tab rotates away from the sensors centre, the voltage continues to decrease and reaches a minimum when the edge of the sensor aligns with the tabs centre (magnetic

field expanding, intensity/flux reducing). As this initial tab exits the sensors magnetic field the next tab is beginning to enter the sensors magnetic field and the voltage approaches zero with a positive slope (magnetic field rate of change = 0, intensity/flux at a minimum) [5, 10]. See APPENDIX IV for an example signal.

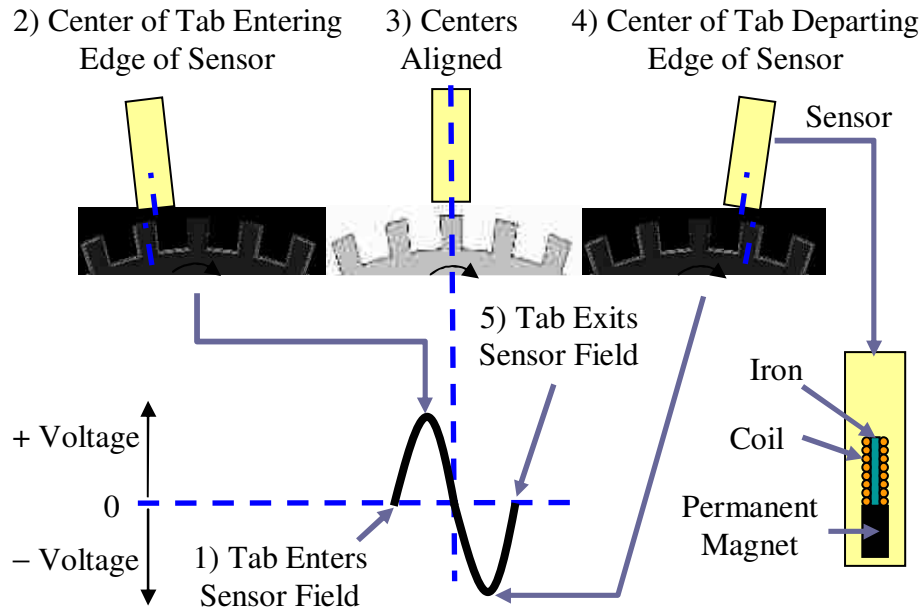


Figure 2.3: VRS Sensor Operation and Design, adapted from [5, 10]

2.1.1.4.1 Missing Tooth Effect on the VRS Signal

A missing tooth on a wheel will cause a significant change in the signal of the VRS sine wave and it can be expected to follow the following pattern seen in Figure 2.4, which is using the 36-1 tooth pattern as an example. It is important to note that the voltage will experience a slight spike in amplitude due to the missing tooth and will approach its positive slope zero voltage over a larger increased crank angle. Assuming constant speed, the frequency would be temporarily cut in half due to the missing tooth. The voltage that is generated by the VRS is relative to the rate of change of the magnetic flux/field intensity around the sensor. When the missing tooth passes the sensor the magnetic field reaches its lowest state and this affects the rate of change of the magnetic flux causing the increased voltage [11]. See APPENDIX IV for an example signal.

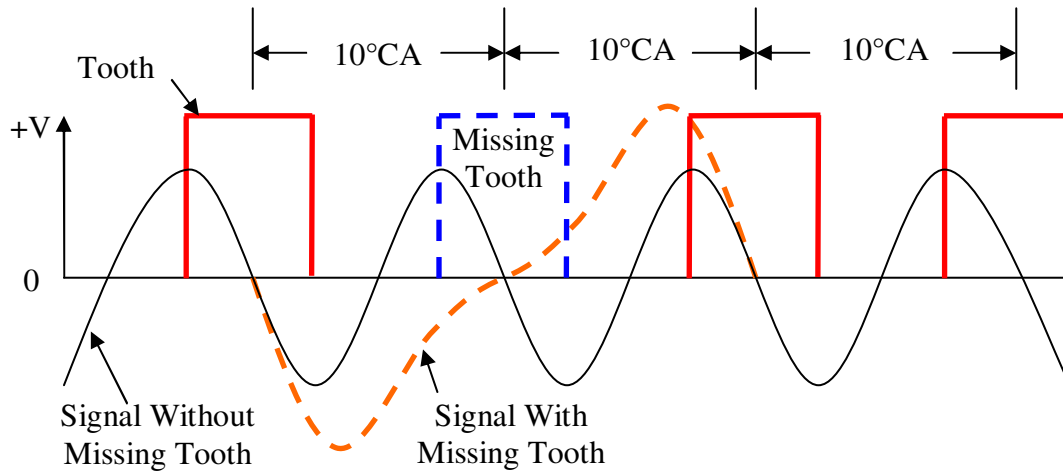


Figure 2.4: Expected VRS Sensor Waveform due to the Missing Tooth Effect

2.1.1.5 Hall Sensor

Hall sensors can be identified by the number of pins (three). These sensors also do not generate a voltage, while the VRS does. The three pins are used for a voltage supply, which is typically between five and 12 volts DC, a ground and the output signal. These sensors typically require the use of a pull-up resistor located between the sensor voltage supply and the sensor output voltage. A typical pull up resistor value is around 1.5 k Ω .

The hall sensor utilizes both the Hall Effect and the Lorentz Force. The Hall Effect is known as a generated voltage that is dependant on a magnetic field [5] and was first discovered by Dr. Edwin Hall in 1879 [28]. The Lorentz Force is what causes the Hall voltage to be generated. It is defined as a force that is exerted on an electron that is traveling through a magnetic field and is proportional to the velocity of the electron and the strength of the magnetic flux exerted on the electron [5]. The hall sensor has an Integrated Circuit (IC) and Hall chip on the end of it with a permanent magnet on top as shown on the left of Figure 2.5. The magnet creates the magnetic field which travels perpendicular to the hall chip. The PCM supplies ' V_{ref} ' to the sensor and the current ' I_{hall} ' flows through the hall chip. The Lorentz Force acts perpendicular to the electron flow, deflecting electrons and generates the Hall voltage (see Figure 2.5). If the current ' I_{hall} ' is fixed then the Hall voltage varies based on the magnetic flux strength [5], which changes as a tooth enters the sensors magnetic field.

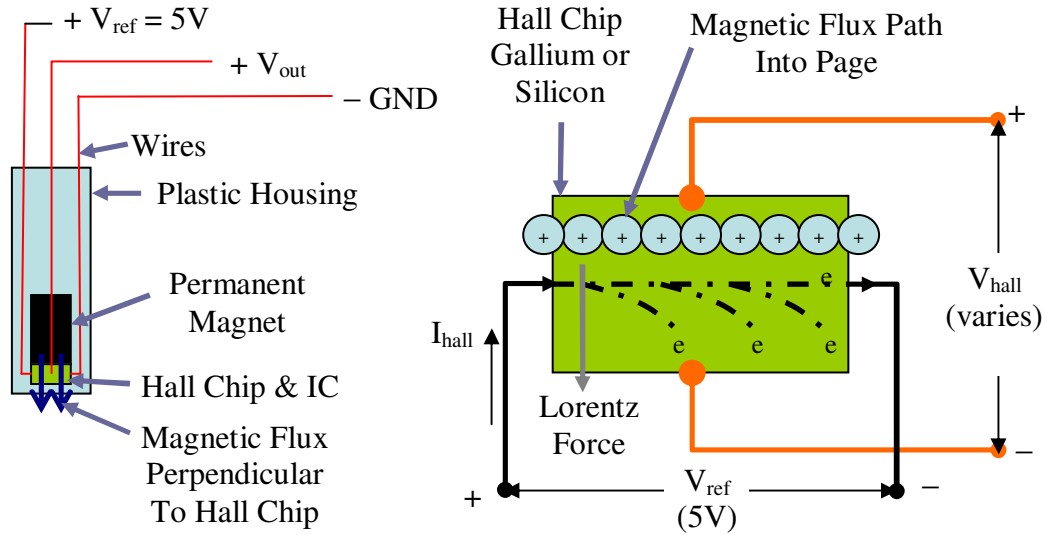


Figure 2.5: Hall Sensor Operation Diagram, adapted from [5]

The Hall voltage is typically small; it is amplified using an op-amp circuit as shown in Figure 2.6 on the right. In order for this sensor to generate a clean square waveform a Schmitt Trigger is used. The Schmitt Trigger is designed to switch a transistor when the Hall voltage and flux density reach a designed limit (see Figure 2.6 on the left). Switching the transistor in the circuit below will draw ‘ V_{out} ’ to ground causing a square wave as shown in Figure 2.6. See APPENDIX IV for an example signal.

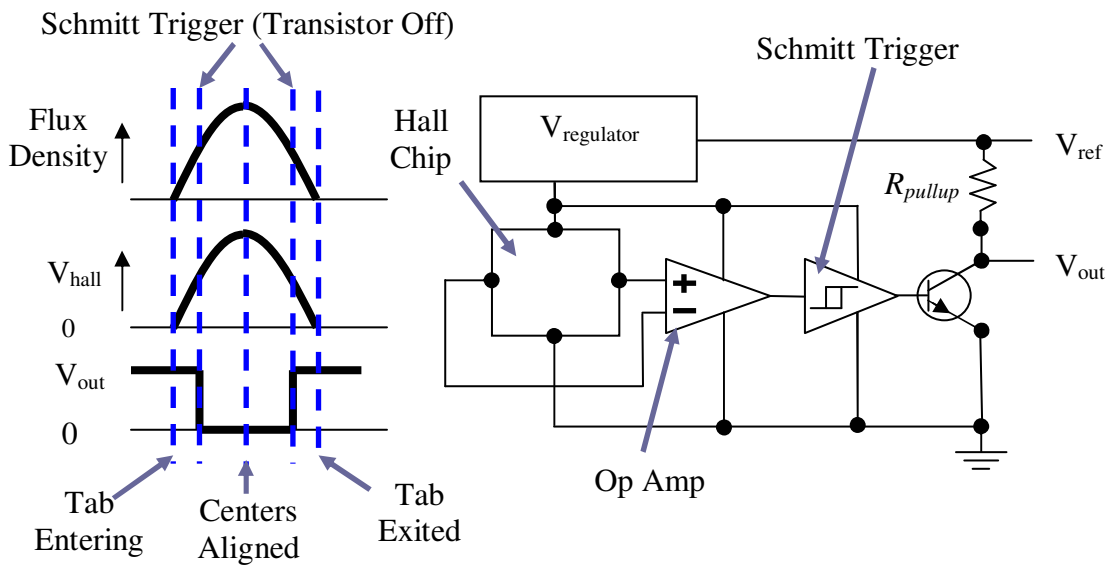


Figure 2.6: Hall IC Circuit, adapted from [28]

2.1.2 Temperature Measurement/Thermistors

Thermistors come in two forms; Positive Temperature Coefficient (PTC - as temperature increases, electronic resistance increases) and Negative Temperature Coefficient (NTC - as temperature increases, electronic resistance decreases). Figure 2.7 (right) shows how the electronic resistance may change with temperature, for these two sensor designs. Both of these sensors use a voltage divider circuit similar to the one found on the left side of Figure 2.7, where the pull up resistor (R_{pullup}) is connected to a five volt power supply. The value of R_{pullup} can vary anywhere in the range of 0.95 to 20 k Ω . The analog voltage across the thermistor (V_{out}) is then supplied to an analog input on the Powertrain Control Module (PCM) for measurement and changes relative to the thermistor resistance as shown in Eq. 2-1. Temperature measurement of the intake air will be reviewed and implemented. For background on the Cylinder Head Temperature (CHT) sensor which may be used see APPENDIX V.

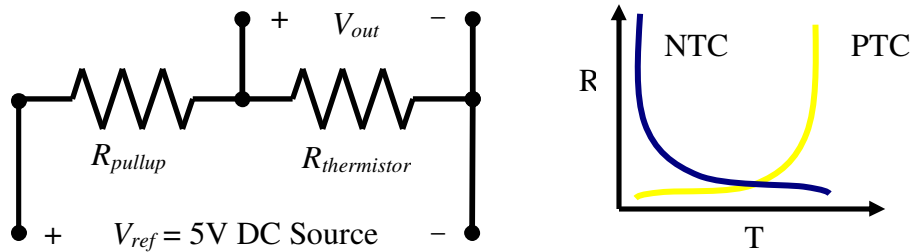


Figure 2.7: Left – Voltage Divider Circuit, Right – Basic Thermistor Curves

$$V_{out} = V_{ref} \frac{R_{thermistor}}{R_{pullup} + R_{thermistor}} \quad \text{Eq. 2-1}$$

2.1.2.1 Intake Air Temperature (IAT)

The IAT sensor can be located in various positions on the engine, but is most commonly found either before or after the throttle body. It may be a standalone sensor or incorporated into the design of other sensors such as the following (T = Temperature):

- 1) Mass Air Flow (MAF) - TMAF
- 2) Manifold Absolute Pressure (MAP) - TMAP
- 3) Throttle Inlet Pressure (TIP) - TTIP

The IAT sensor can be used to calculate the Charge Air Cooler (CAC) efficiency if present on an engine, it may be used to infer the density of the air for correcting the MAF or MAP sensor measurements. The IAT sensor is also used for adjusting the spark advance angle. Another name used for this sensor may be Air Charge Temperature (ACT). See APPENDIX XI for sensor transfer functions.

2.1.3 Pressure Measurement

2.1.3.1 Strain Gauge/Piezo-Resistive Type

Strain gauge type pressure transducers are commonly used to measure the pressure of the intake manifold, fuel rail, ambient and oil. These sensors use a silicon-diaphragm diffused strain gauge, which measures the deflection/displacement of a diaphragm. The circuit for these sensors utilizes the Wheatstone bridge. As the diaphragm deforms, two of the resistors increase in electronic resistance and two reduce [3]. Pressure is measured with respect to a reference vacuum port as can be seen in Figure 2.8.

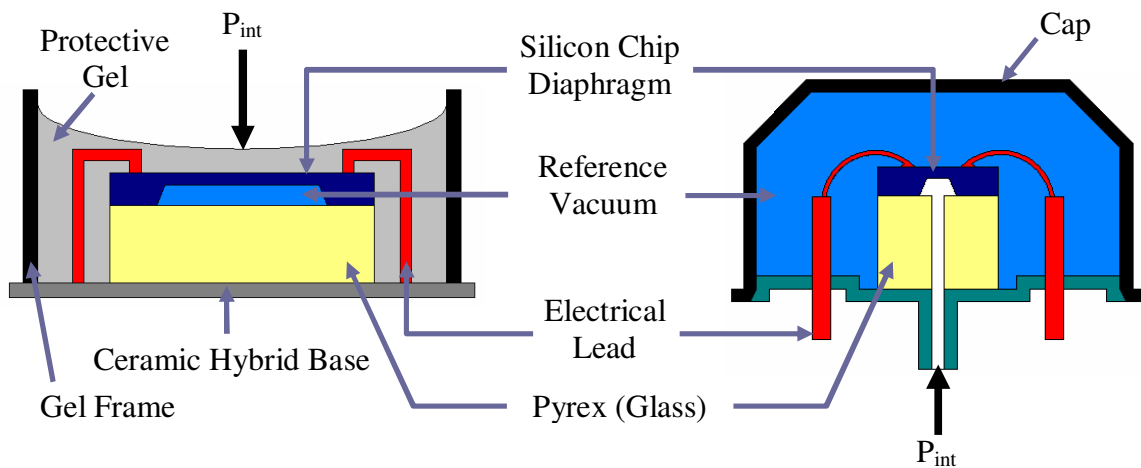


Figure 2.8: Two Strain Gage Pressure Sensor Designs, adapted from [3]

Additional figures contained in APPENDIX VI show how these piezo-resistive elements are arranged and installed in an actual sensor. See APPENDIX XI for sensor transfer functions.

2.1.3.2 Manifold Absolute Pressure (MAP), Throttle Inlet Pressure (TIP)

The MAP sensor is used to monitor the pressure in the intake manifold. By knowing this pressure it is possible to calculate the amount of air entering the cylinder using the speed-density equations found in APPENDIX XVIII. The TIP sensor is commonly used on turbo charged engines as a feedback sensor to adjust the turbo waste gate or vane angles to obtain the desired throttle inlet pressure.

2.1.4 Knock Detection

The term 'knock' is the term given to describe the noise that transmits through the engine structure due to spontaneous ignition of the end gas (fuel, air, residual gas mixture), which occurs before the propagating flame (flame initiated by spark ignition) arrives. The noise heard is the result of the propagation of the end gas high pressure waves throughout the cylinder. The spontaneous ignition may occur due to surface ignition (hot spots such as valves, spark plugs and carbon deposits) and over advanced spark timing. Advancing spark timing can increase knock intensity, while retarding the spark timing can reduce knock intensity. Assuming the base spark of an engine is at 20°BTDC (compression), 30°BTDC would be considered advanced and 10°BTDC would be considered retarded. In other words, advanced spark timing would be further from compression TDC, while retarding moves the spark closer to compression TDC. If adjusting the timing does not reduce knock, this would be known as surface ignition. When it is possible to adjust the spark timing and eliminate knock, it is referred to as spark knock [1].

Knock is monitored on production gasoline engines in part to protect the engine from damage, and to attain high fuel efficiency even when the operating environment or fuel properties change. Knock is detected on the cylinder block, the intake manifold and the cylinder heads if instrumented with an accelerometer or in-cylinder through pressure measurement [29, 30] or ion-current measurement (uses the spark plug as a sensor) [31–33]. The most common method used on gasoline engines utilizes the measurement of vibrations with a form of accelerometer. Research has been conducted on the use of the

magnetostrictive transducer [5, 34, 35]; however, the most widely used sensor is the piezoceramic knock sensor, which has been tuned to a frequency where knock is typically detected (5 to 18 kHz). For more details on the construction and operation of this sensor see APPENDIX VII. Some of the key benefits of this sensor include:

- 1) Cost/Quantity of sensors required
 - Cylinder pressure/ion current is required in each cylinder while one or two knock sensors may be used per bank depending on the engine design
 - Cylinder pressure sensors are also corrected for sensor drift by pegging the pressure relative to a MAP sensor while the intake valve is open, requiring additional instrumentation
- 2) Reliability/Maintenance
 - The knock sensor is not exposed to hot exhaust gases and soot, while the in-cylinder pressure sensor on the other hand is, which requires regular cleaning/maintenance

2.1.4.1 Using Knock Sensors for Feedback Control of Spark

The knock sensor is part of a closed loop control system for spark timing, where the spark timing is usually advanced until knock occurs. Once the PCM detects the knock event on a conditioned sensor signal, the engine controller retards timing by a predefined amount, typically between 1 to 2°CA. Figure 2.9 below shows how spark advance may change when using a knock sensor for closed loop spark timing control [7, 8]. See APPENDIX XI for sensor transfer functions.

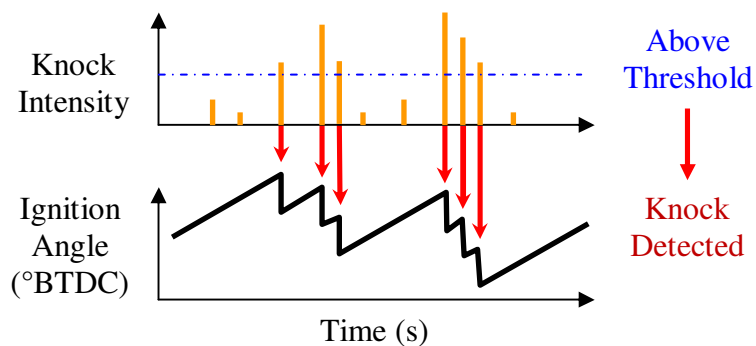


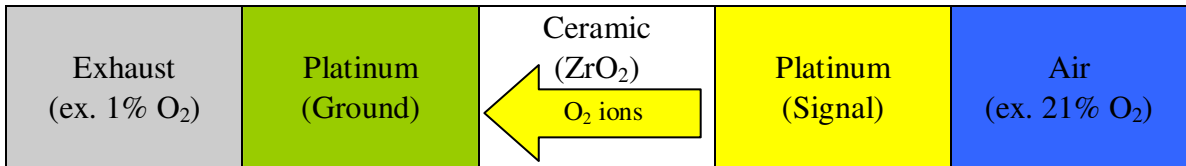
Figure 2.9: Knock Intensity and Spark Ignition Angle, adapted from [7, 8]

2.1.5 Exhaust Gas Oxygen (EGO)/ Air to Fuel Ratio (AFR)

Controlling emissions has been an ever increasing concern, which resulted in the government increasing the requirements on engine manufactures to reduce the emissions produced. For gasoline engines, the three way catalytic converter or three way catalyst (TWC) was introduced to reduce carbon monoxide (CO), unburned hydrocarbons (HC), and nitrogen oxides (NO_x). Using the TWC requires strict control of the AFR to within approximately one percent of stoichiometry (14.6 AFR). As a result, the Exhaust Gas Oxygen (EGO) sensor was introduced to provide feedback on the oxygen content in the exhaust to help protect the TWC [2].

The EGO sensor provides a voltage signal that is dependant on the oxygen concentration in the exhaust gas and operates similar to a battery/galvanic cell [36]. The EGO sensor interface can be represented using Table 2.2.

Table 2.2: EGO Sensor Interfaces, adapted from [36]



On the platinum electrodes, an electrochemical process takes place and oxygen ions transport a current across the ceramic/Zirconia (ZrO₂). The Nernst equation can be used to relate the cell output voltage (V_{out}) to the oxygen partial pressures for the exhaust and air (see Eq. 2-2) [1].

$$V_{out} = \frac{RT}{4F} \ln \left(\frac{Pa_{O_2}}{Pe_{O_2}} \right) \quad \text{Eq. 2-2}$$

where F is the Faraday Constant (96485.3365 C/mol), R is the gas constant (8.3145J/molK), T is the temperature in Kelvin, Pa_{O_2} and Pe_{O_2} are the air and exhaust gas partial pressures respectively. EGO sensors, which directly output a voltage operate over a very narrow range and in order to maintain an AFR of 14.6 ($\lambda = 1$) required the fuelling strategy to alternate between rich and lean conditions (see Figure 2.10).

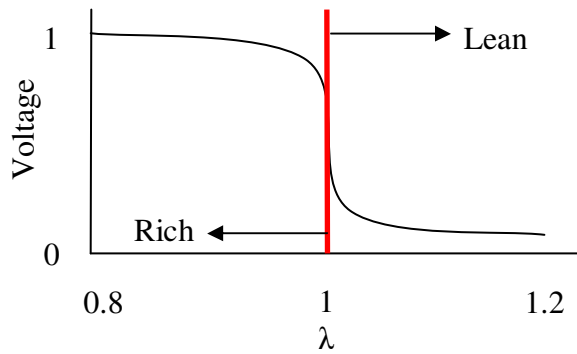


Figure 2.10: Narrow EGO Sensor Operating Range, adapted from [3]

However, the EGO sensor does not provide desired measurements until it exceeds 350°C, as the ceramic element is not conductive and cannot support the transport of oxygen ions below 350°C. Furthermore, the sensor is optimum at around 600°C as the response time for the sensor drops from a few seconds to approximately 50 ms [3]. When the engine is first started up, the EGO sensor is cold and must heat up. This requires open loop fuel control until the temperature exceeds ~ 350°C. This limitation resulted in the development of the HEGO (Heated Exhaust Gas Oxygen) sensor. The heater helps burn off deposits, keeps the sensor warm when idling, and provides more flexibility for locating the sensor in the exhaust (it may be located further from the engine), while still reaching operating temperature quicker [10]. The EGO sensor interface shown in Table 2.2 can be utilized inside a sensor as either a thimble design (see Figure 2.11) or a planar design (see APPENDIX VIII) [3]. Figure 2.11 shows the cross section of an entire HEGO sensor.

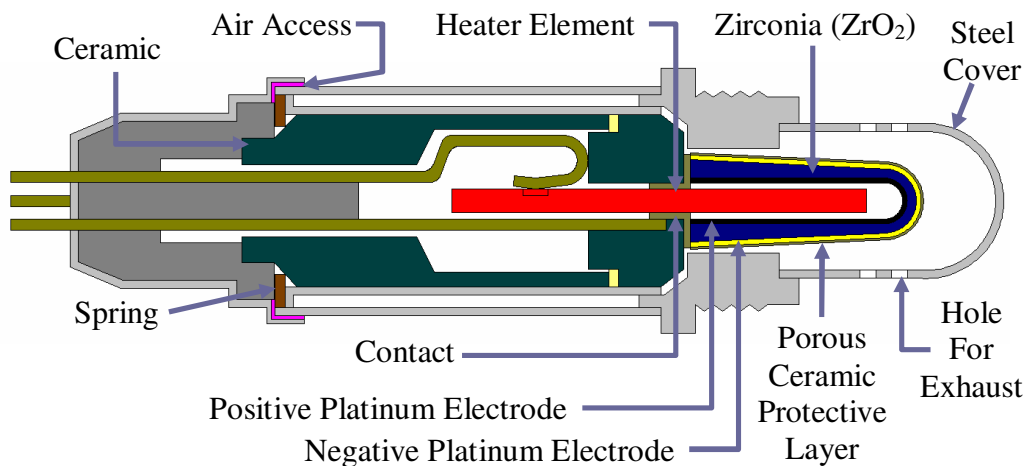


Figure 2.11: HEGO Sensor BOSCH LSH25, adapted from [3]

The UHEGO (Universal Heated Exhaust Gas Oxygen) sensor which is also known as a Wide-Band Lambda sensor can report back lambda values between 0.65 and ∞ (Air). The sensor transfer function for the BOSCH LSU4.9 sensor only reports up to a lambda (λ) value of 2.42, which would give a gasoline AFR range of (9.5-35.3 AFR). The UHEGO eliminates the need to switch around 14.6 AFR, as was required with the basic EGO and HEGO; as it provides a continuous AFR measurement allowing for more precise control of the AFR. The UHEGO sensor maintains a temperature of around 780°C (1436°F) and uses a resistor, built into the UHEGO for feedback control of the on-board heater element. The acceptable temperature range for the UHEGO is between 650 and 900°C (1202-1652°F). In order to maintain the sensor in the acceptable temperature range, the resistor must be held between 143 and 955 Ω with the ideal resistance being 300 Ω [3, 37-39]. For additional details on the construction of the HEGO and UHEGO sensors, as well as details on the control of the UHEGO sensor, see APPENDIX VIII. See APPENDIX XI for sensor transfer functions.

2.1.6 Mass Air Flow (MAF)

The purpose of the MAF sensor is to measure the quantity of air the engine is consuming, in order to properly schedule the fuel that needs to be injected into each cylinder. Assuming the measured air is equally distributed between each cylinder, the mass air flow rate into each cylinder would be calculated using Eq. 2-3.

$$MAF_{cyl} = \frac{MAF}{numcyl} \quad \text{Eq. 2-3}$$

For additional background on the VAF (Volume Air Flow) and hot-wire MAF sensors see APPENDIX IX. See APPENDIX XI for sensor transfer functions. The next section will focus on the hot-film sensor which is now commonly used in industry.

2.1.6.1 Hot-Film

Hot-wire MAF sensors were not very effective at detecting backflow and fast changes during engine transients, which would cause problems under high load conditions. With the emergence of micro silicon technology the hot-film MAF sensor was designed and enabled compensation for backflow [41]. Figure 2.12 shows a few BOSCH sensor designs (HFM5 and HFM6) and the temperature profile across the sensor element with the effect of the flow. The main improvements of the HFM6 over the HFM5 was the switch from analog to digital, improving accuracy and a trap in the flow path to catch heavy particles and water droplets [3]. MAF Sensors can either output an analog voltage or a digital frequency, which varies with the air flow rate (see APPENDIX XI).

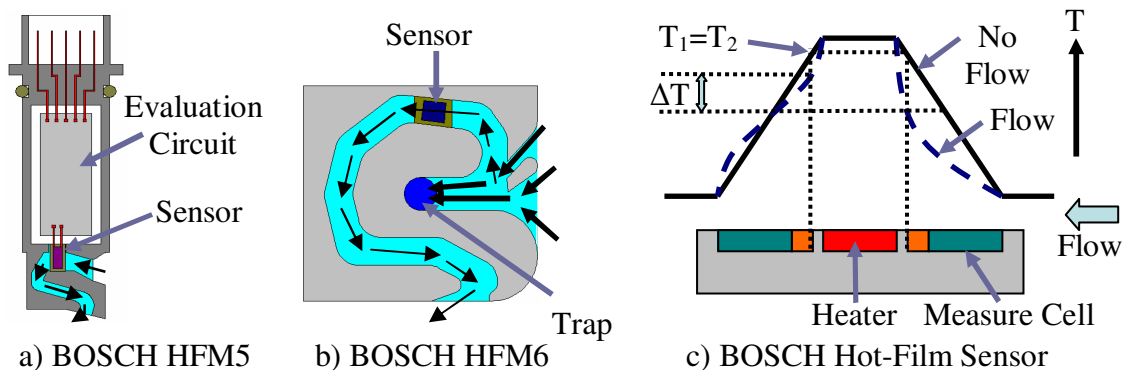


Figure 2.12: Hot-Film Mass Air Flow Sensor Design, adapted from [3, 41]

2.1.7 Electronic Throttle Control (ETC) Position Feedback Sensors

With the emergence of electronics, the pedal which was once connected to the throttle body through a direct cable linkage was converted to a "throttle by wire" design. In order to ensure safety, these electronic pedals would have multiple tracks and would be used together to determine if the circuit tracks were properly functioning. These pedals may use either a potentiometer with a voltage divider design or more recently a hall sensor design, with the main difference being that the hall design is a contact-less design [3, 10]. Figure 2.13 shows two different pedal configurations, two track and three track pedals (Accelerator Pedal Position Sensor is referred to as APPS, while the number following APPS is the track). For the two track pedal, APPS2 is typically half of APPS1 [3]. For the three track pedal APPS1 would have a negative slope. The throttle body would also have multiple tracks and typically opposite slopes, see Figure 2.14. TPS is Throttle Position Sensor and the number is the track.

Both the throttle body and the pedal, as mentioned earlier may incorporate new hall technology which differs from that previously discussed for detecting cam and crank position. BOSCH has designed the following contact-less hall sensor systems ARS1, ARS2 and FPM2.3, with the last design being the newest [3]. Melexis has released a product similar to the BOSCH FPM2.3 and is known as the MLX90316 which uses Triaxis hall technology. This technology differs from the standard hall sensor technology previously described, which is sensitive to flux changes perpendicular to the IC surface. Triaxis allows a hall sensor to be sensitive to flux changes in the planar direction, by using an Integrated Magneto-Concentrator (IMC®) deposited on the CMOS (Complementary Metal Oxide Semiconductor) die. The MLX90316 is only sensitive to the planar magnetic flux changes. Absolute rotary position (0-360°) can be detected by placing a small magnet (diametrically magnetized) on the rotating element parallel to and above the IC chip (see Figure 2.14) [42]. See APPENDIX XI for sensor transfer functions.

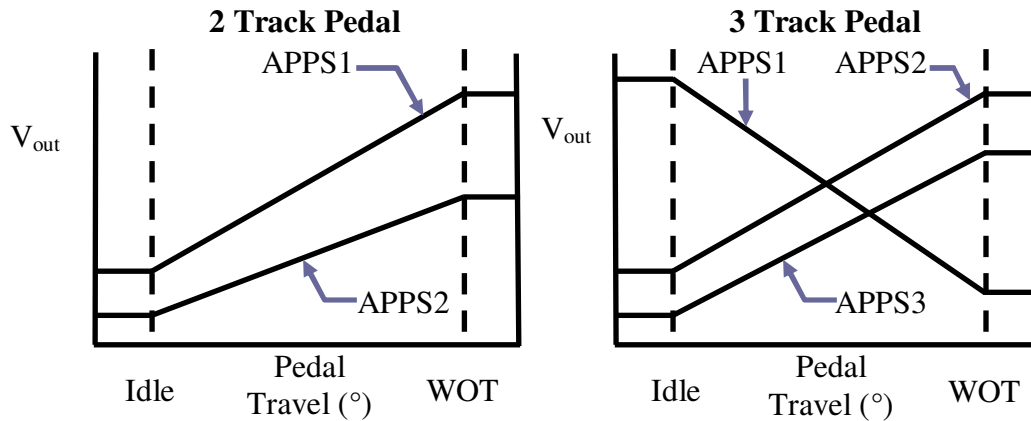


Figure 2.13: 2 and 3 Track APPS Curves, adapted from [10]

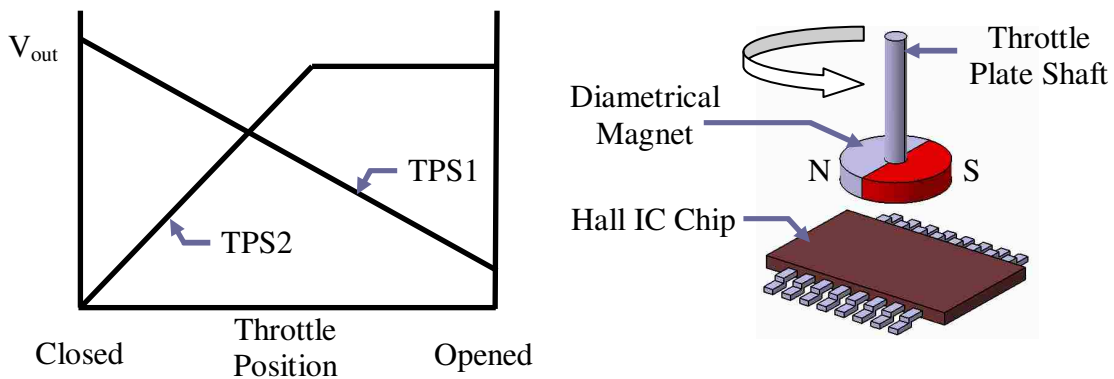


Figure 2.14: Left – TPS Curve, Right – MLX90316 Hall Sensor, adapted from [42]

2.2 Actuators Used on Engines

2.2.1 Throttle Body

The throttle body is installed on the engine in order to throttle or limit the amount of air that the engine has access to, allowing control of the engine load produced. As was previously mentioned, ETC or throttle by wire systems have been implemented. These systems use the pedal to send a signal to the PCM, which then interprets the signal along with other sensors (MAP, MAF and TPS) and decides the most optimal throttle angle for the current conditions. The throttle body is actuated using a DC motor and Pulse Width Modulation (PWM). This motor is capable of both forward and reverse rotation, however a spring is still present on the throttle body to help the throttle return to the idle/closed position (should the motor fail). The motor is driven using a full bridge (also known as

H-Bridge) driver circuit (see Figure 2.15). The H-Bridge driver uses Metal Oxide Semiconductor Field Effect Transistors (MOSFET) connected to the motor in the shape of an “H”. As shown in Figure 2.15 by activating MOSFETs 2 and 3 the motor will rotate one way and then activating 1 and 4 will rotate the motor in the opposite direction. ETC control has allowed the implementation of cruise control [10].

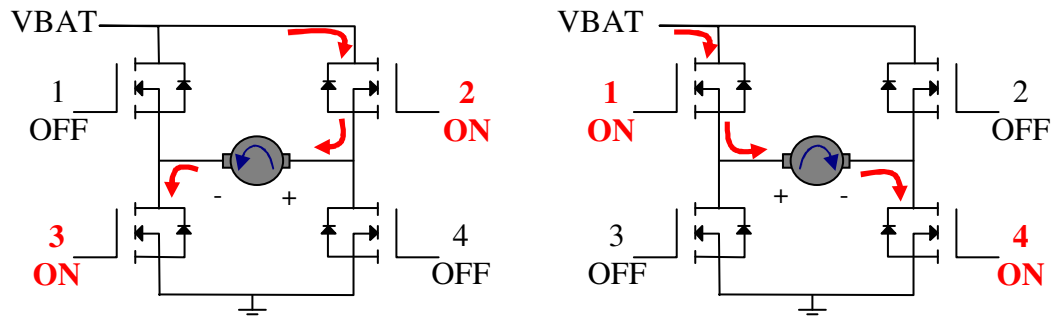


Figure 2.15: H-Bridge Driver Circuit for Throttle Body Motor, adapted from [43]

2.2.2 Fuel Systems

Before the advent of electronics, fuel was mixed with the air through the use of the carburetor. This would allow for the fuel and air mixture to vaporize in the intake manifold and mix before reaching the cylinder, but could not guarantee even fuel distribution. Fuel would also puddle in the intake manifold. Many different carburetor designs are explained by Heisler [9] and BOSCH [3, 4] as it is beyond the scope of this work. As electronics became more common, various injector designs were developed to allow for fuel to be injected through the throttle body, intake manifold, and intake port or directly into combustion chamber (direct injection DI). Port injection will be reviewed in further detail as this method is used on the 5.0 L test engine.

2.2.2.1 Port Fuel Injection (PFI)

Two types of port injection are Multiport Fuel Injection (MPFI), which would fire multiple injectors at once using one Low Side Driver (LSD), or Sequential Port Fuel Injection (SFI), which may also be called SEFI (Sequential Electronic Fuel Injection). SEFI is the most common method of PFI as it injects fuel before the intake valve opens

for each cylinder (all cylinders are controlled individually using their own LSD). SEFI has been found to improve fuel economy and idle quality [10]. SEFI may operate as a MPFI system if desired by commanding multiple injectors to fire at the same time.

The injector used for port fuel injection is essentially a solenoid. One of the injector pins is connected to the battery, which always supplies energy to the solenoid. The LSD inside the PCM is triggered by the PCM and connects the other pin of the injector to ground. Care must be taken not to connect the low side of the coil accidentally to ground, since the injector will inject fuel and could be dangerous or damage the engine. Once grounded the coil charges and then actuates an armature, which is connected to a pintle with a tapered tip. Moving the pintle off the discharge orifice/nozzle allows fuel to then flow/inject into the intake manifold. Removing the connection to ground allows a spring to force the injector pintle to seat on the discharge orifice/nozzle, in turn stopping fuel injection. The PW is defined as the time the injector remains open to inject the required amount of fuel. The PCM varies the PW according to the MAF into the cylinder and the feedback from the UHEGO sensor. See APPENDIX XI for the injector transfer function. Figure 2.16 illustrates the injector open as well as the circuit diagram showing how the injector is wired.

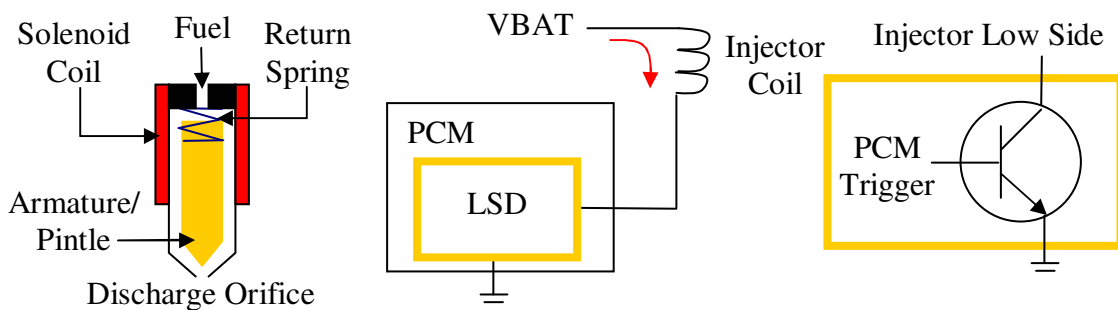


Figure 2.16: Port Fuel Injector Design and Wire Diagram, adapted from [3, 10]

2.2.3 Ignition Systems

The purpose of the ignition system [10] is to:

- 1) Distribute spark to the proper cylinder corresponding to the desired firing order
- 2) Produce enough high voltage to ignite the air-fuel mixture while maintaining complete combustion
 - a. Minimum secondary voltage is between 8 to 12 kV for engine idle
 - b. Secondary coils can have voltages up to 60 kV
- 3) Adjust spark timing with the following factors in mind
 - a. Desired peak cylinder pressure around 10 to 20°ATDC compression
 - b. Higher speed requires advancing (spark earlier) to allow more time to burn
 - c. Light loads have high manifold vacuum and lower combustion pressure which results in slower combustion (advance spark)
 - d. High loads have low manifold vacuum and higher combustion pressure which results in faster combustion (retard/spark later)
 - e. Higher octane fuel requires more time to burn since it is harder to ignite (advance spark)
 - f. More fuel vaporization and turbulence speeds combustion (retard spark)
 - g. Intake air temperature, barometric pressure and humidity also affect the timing and scheduling of the spark
 - h. Adjust the dwell time to achieve the desired spark energy

Ignition systems have gone through a vast amount of changes through the years and many of the great developments are reviewed by BOSCH [3] or Pickerill [10]. The main components of modern ignition systems include a battery, ignition switch, ignition coil, high tension cables, PCM and spark plugs. The work conducted in this thesis uses the coil on plug design and incorporates the same triggering technique used in the driver on coil on plug design. Both of these systems will be reviewed in further detail.

2.2.3.1 Ignition Coil Operation

Through the use of magnetic induction, the ignition coil (also known as a pulse transformer) converts power supplied by the battery into a high voltage low current signal used by the spark plug. The ignition coil consists of a primary winding and a secondary winding, wrapped around an iron or steel core that has low inductive reluctance. The primary coil consists of 20 gauge wire with 100 to 200 turns, while the secondary coil is made from very fine copper and can be up to 25,000 or more turns. Dwell is the time the current flows through the primary wire and must be controlled to limit the coil current. Longer dwell time allows the coil to approach saturation, where the coil reaches its maximum current and magnetic field strength. The time it takes for a coil to saturate, is due to reactance, as the magnetic field of one loop of the primary winding will oppose the direction of the current flow of the next loop of wire [10].

The primary circuit current flow when stopped causes the magnetic field around both primary and secondary coils to collapse. The result is the generation of the ionization voltage in the secondary coil. Increasing the spark plug gap or cylinder pressure requires a higher secondary voltage in order to force the spark to jump the gap (see Figure 2.17).

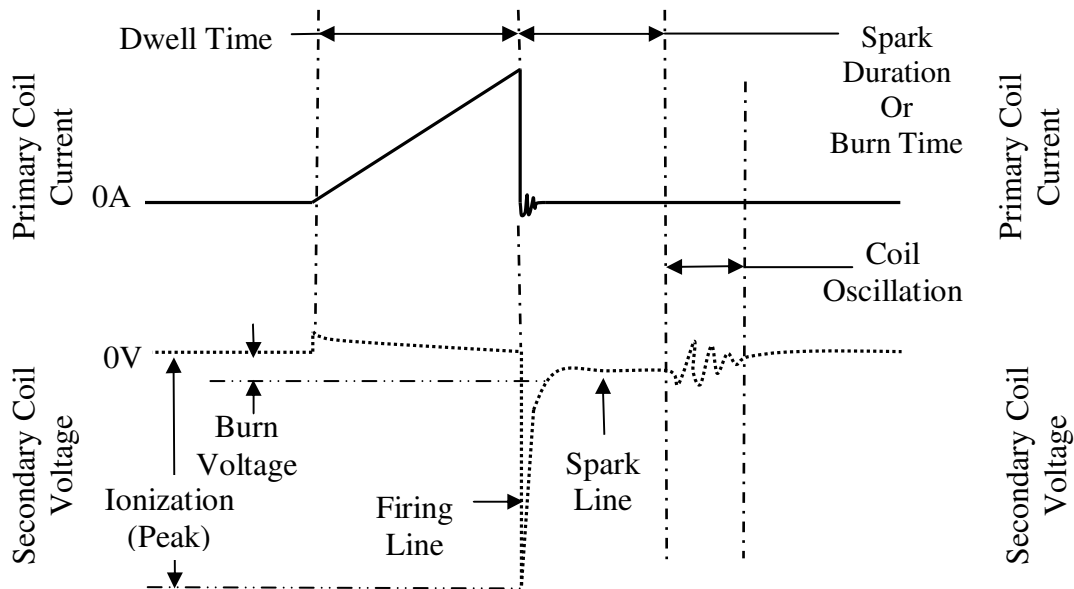


Figure 2.17: Top – Prim. Coil Current, Bottom – Sec. Coil Voltage, adapted from [44]

2.2.3.2 Coil on Plug (COP)

The ignition coil for a COP system would be located locally at the spark plug. Coils of this type would have two pins both for the primary coil: one for the constant battery power and the second is the low side of the primary coil. The latter returns back to the PCM, where it is grounded using a LSD. Unlike the injectors the coil draws significant current (up to 10 Amps) and requires the use of one of the following driver chips: BOSCH Integrated Power (BIP) using a Darlington transistor setup [9], Field Effect Transistors (FET) or Isolated Gate Bipolar Transistors (IGBT) to switch the coil to ground [3]. The IGBT provides the following advantages [3]:

- 1) Uses voltage actuation instead of current (reduces power consumption)
- 2) Low saturation voltage
- 3) Increased current capability
- 4) Reduced switching times
- 5) Increased clamp voltage
- 6) Increased holding temperature
- 7) Voltage reversal protection

The main advantage of having the coil LSD on the PCM is that the dwell time can be controlled by measuring the primary current through a resistor (ex. 0.2 Ω , Vishay WSR5R2000FEA) [45] in series with the LSD. If the resistance is a known value, the voltage across the resistor can be measured and used to calculate the current by ohms law ($V=IR$). Figure 2.18 shows the circuit diagram for a COP system.

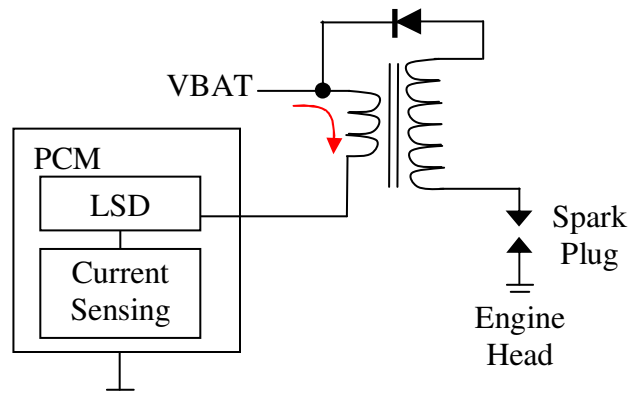


Figure 2.18: PCM with LSD and Current Sensing for COP Ignition

2.2.3.3 Driver on Coil on Plug

The LSD driver that is used to control the dwell time was removed from the PCM and relocated onboard the coil, in order to reduce the complexity of the PCM. Coils of this type can be identified as they have three pins on the connector: battery voltage, ground and the third is a low voltage control/trigger signal that is switched between zero and five volts. When the control signal is switched to five volts the IGBT or driver will switch on, which will close the primary circuit to ground, allowing current to flow. Figure 2.19 shows the modified circuit diagram for the driver on coil on plug setup as well as the internal circuit diagram of a basic IGBT chip [46-49]. Special smart IGBT's have been designed to allow for this current measurement [50]. See APPENDIX X for a cross section of a driver on PCOP (Pencil on Coil On Plug) cross section.

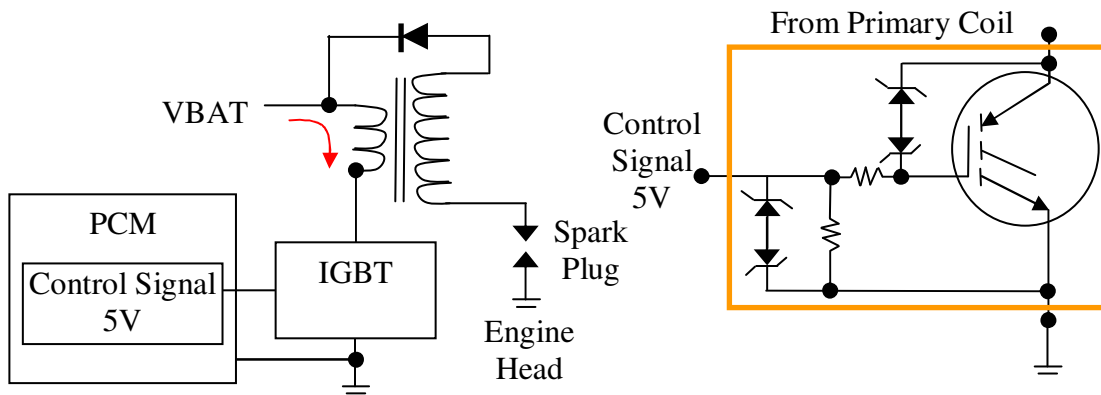


Figure 2.19: Circuits, Left – Driver On Coil, Right – IGBT, adapted from [46-49]

2.2.3.4 Spark Plug

There are various designs of spark plugs with different heating characteristics and different tip shapes. A typical spark plug cross section may look similar to that shown in APPENDIX X. Most of the time, a cylinder will have only one spark plug, however some larger production engines may use multiple spark plugs in one cylinder to initiate the combustion in more locations at once, resulting in a slight power increase, reduced emissions or even possible ignition offset of the spark plugs. It is important to note that the spark plug threads into the head on the engine, which allows for the spark plug to dissipate heat as well as provides the ground for the spark plug to complete its circuit [3].

2.3 Types of Control Systems

The following section will discuss the various controllers that may be incorporated on a production engine controller in order to fully utilize the data coming from the sensors, instrumented on the engine.

2.3.1 Open Loop Control

Open loop controllers do not use sensors to provide engine performance feedback for control purposes; instead these controllers make adjustments according to a predefined schedule. These controllers are typically cheaper but require a system that is repeatable and predictable [51]. Open loop control may be used for spark and fuel injection control purposes in order to get the engine warm, or when failure modes are present due to a failed sensor for instance. Open loop control is typically done by using tables of data that were previously mapped in a dynamometer test cell and stored in the PCM (see Figure 2.20).

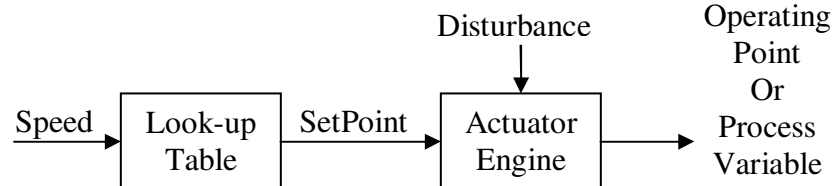


Figure 2.20: Open Loop Diagram

2.3.2 Closed Loop Control (Feedback Control)

Control systems using closed loop control measure the output (system performance) or Process Variable (*PV*) and feed it back to the controller to help the system achieve the desired setpoint (*SP*). The error term is simply the difference between the desired setpoint and the feedback from the measured parameter (*PV*) that is being controlled (see Figure 2.21). The engine controller uses feedback control for many purposes; some examples include throttle body angle, AFR, spark dwell and ignition timing etc.

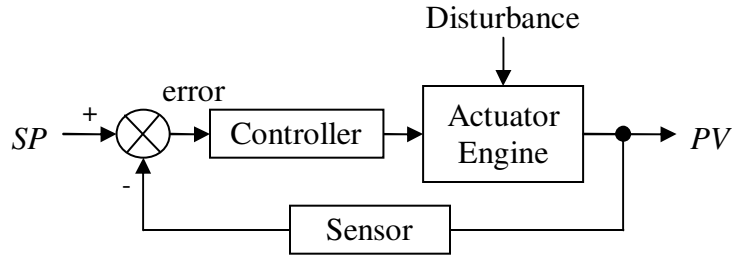


Figure 2.21: Closed Loop (Feedback Control) Diagram, adapted from [51]

2.3.3 Closed Loop Control (Feedforward/Command Compensation)

The technique of feedforward control may supply a percentage of the setpoint, and use a look-up table or an equation to supply a value, which is added to the feedback controller output (see Figure 2.22). By doing this, it is possible to help the controller arrive at a required setpoint when step or ramp inputs are requested. The feedback controller works to hold and maintain the required setpoint as disturbances occur. Feedforward is also known as command compensation [51].

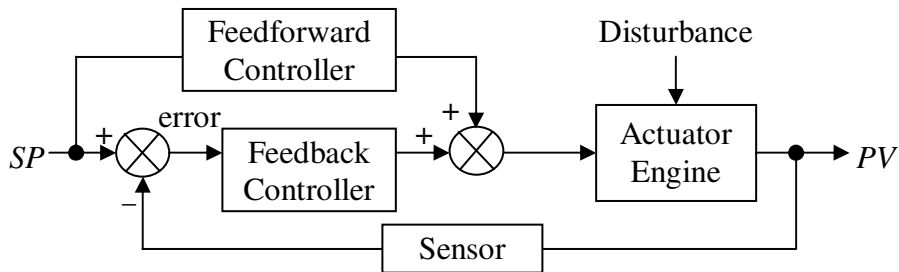


Figure 2.22: Closed Loop Feedback/Feed Forward Diagram

2.3.4 Proportional Integral Derivative (PID) Control

Together the proportional controller, the integral controller and the derivative controller make up what is known as a PID controller and can be expressed using Eq. 2-4 or Figure 2.23. Where $e(t)$ is the error/difference over time (setpoint – sensor feedback), K_p is the proportional gain, K_i is the integral gain, K_d is the derivative gain, T_i is the integral time constant and T_d is the derivative time constant.

$$u(t) = K_p e(t) + K_i \int_0^t e(t) dt + K_d \frac{de(t)}{dt} \quad \text{Eq. 2-4}$$

$$\text{Where: } K_i = \frac{K_p}{T_i}, \quad K_d = K_p T_d$$

The proportional controller adjusts the control signal proportional to the error, but the output often comes with an offset from the desired setpoint that can not be accounted for. Increasing the proportional gain will help reduce the error, but cannot eliminate it and will result in increased oscillations and overshoot [52]. As a result integral controllers are proportional to the integral of the error and can eliminate this steady state error. Increasing the integral gain too much will also lead to overshoot and oscillations [52]. Derivative control was introduced to help ease the controller to an error of zero (predicts what the error will be) by reacting to the rate of change of the error [52]. Derivative control helps to minimize/dampen oscillations in the process variable [53]. Derivative control is not always necessary and may be left out if the control signal contains excessive noise, or does not have a properly filtered signal available.

Both derivative and proportional controllers will experience a kick when the setpoint is subjected to a step change. To eliminate the proportional and derivative kick, it has been recommended to move the supply signal for these calculations from the error to the sensor feedback signal of the process variable as shown in Figure 2.24. This system would be called an I-PD system [54]. Connecting the derivative term to the sensor feedback is also referred to as pseudo-derivative feedback (PSD) [51]. It is not uncommon for controllers to have different combinations of the P, I and D components for controlling hardware (actuators), another option is to use cascade control which may include a second PID controller in series with the sensor feedback of the process variable [51].

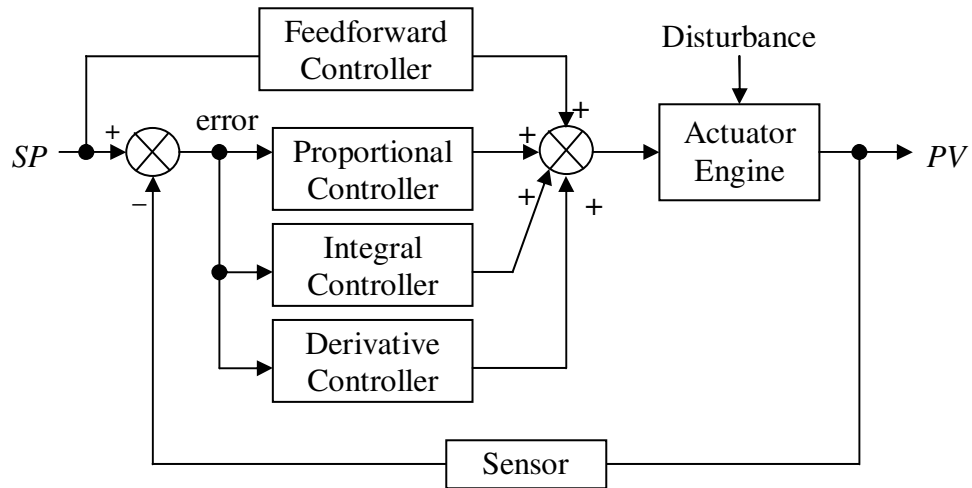


Figure 2.23: PID Controller Diagram w/Feedforward, adapted from [51]

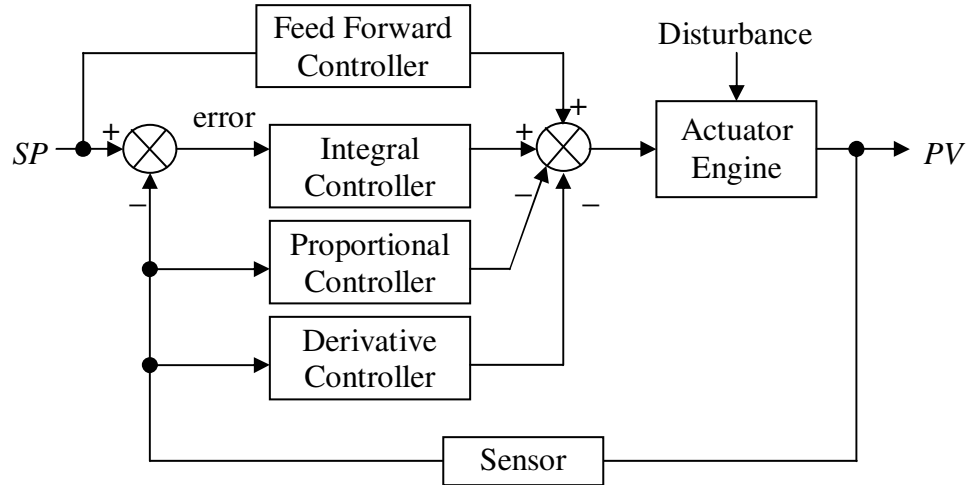


Figure 2.24: I-PD Controller Diagram w/Feed Forward, adapted from [52, 54]

Figure 2.24 above can be expressed with Eq. 2-5 where K_{ff} is the feedforward gain and PV is the process variable measured by the sensor and SP is the commanded setpoint.

$$u(t) = K_{ff} SP(t) - K_p PV(t) + K_i \int_0^t e(t) dt - K_d \frac{dPV(t)}{dt} \quad \text{Eq. 2-5}$$

2.3.5 Saturation, Integrator Windup and Anti-Windup

Saturation occurs when the controller cannot achieve a desired setpoint and requests for an actuator to continue to open beyond its limits. An example of where this may be applied for engine control would be throttle body control. The throttle body can only rotate 90° , requesting a rotation of 100° would be beyond the limits of the actuator and would result in saturation as the integrator from the PID controller will continually increase by accumulating error (wind-up) in an attempt to achieve the unachievable setpoint. When the actuator is commanded to return to a lower angle the integrator must unwind, which may require some time depending on how long it was allowed to windup. In order to resolve this issue, anti-windup was introduced. An example block diagram is shown below in Figure 2.25. U_{max} is the cut-off or maximum limit (where the controller becomes saturated). When the controller saturates E will be greater than zero and a switch disables integration to prevent wind-up.

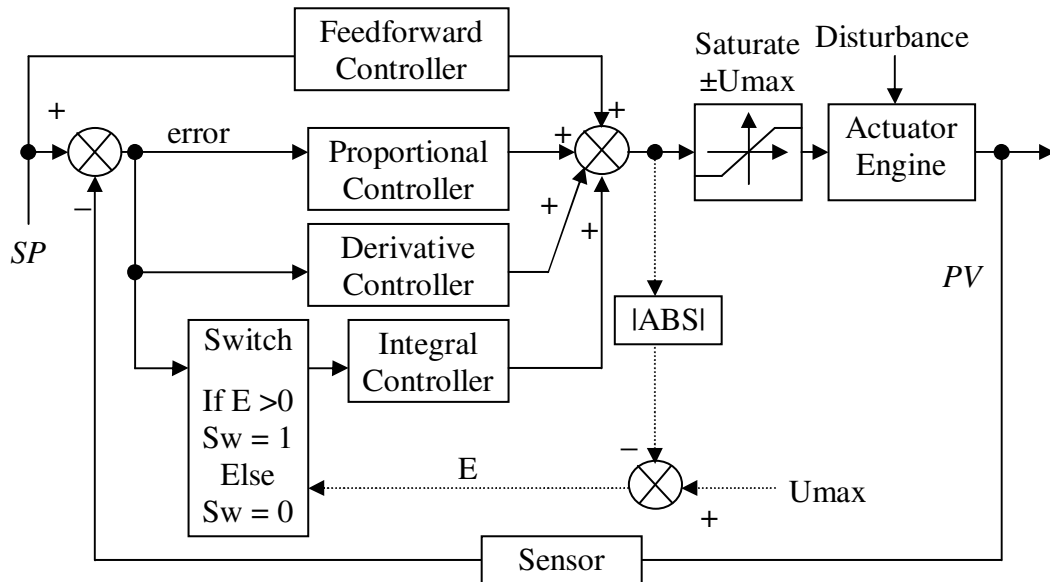


Figure 2.25: Saturation, Anti-Windup Block Diagram, adapted from [51, 54]

2.3.6 Bumpless Transfer and Integral Gain Parameter Changes

The purpose of bumpless transfer is to allow the user to switch between open loop and closed loop control. In other words the user can bypass a PID controller and manually input a commanded setpoint to the engine hardware. In order for bumpless transfer to work, at the time of a transition between open loop control and closed loop control, the outputs must be the same. This would require the error to be zero, and the integral initial condition would be the last manual setpoint value [52]. Similarly when attempting to change the integral gain K_i (let K_{old} be the last known integral gain), it is necessary to reset the integral to a new initial condition, which is a known value relative to the new K_i (or K_{new}) and the last known output from the integral x_{old} . x_{new} is the new integral initial condition (see Eq. 2-6 and Eq. 2-7).

$$x_{old} = K_{old} \int_0^t e(t) dt \quad \text{Eq. 2-6}$$

$$x_{new} = K_{new} \int_0^t e(t) dt + x_{old} \left(\frac{K_{old}}{K_{new}} \right) \quad \text{Eq. 2-7}$$

CHAPTER 3

DESIGN AND METHODOLOGY

3.1 Engine Specifications

For the purpose of this thesis, all research was conducted using a Ford F150 5.0 L truck engine. The specifications for this engine can be found in Table 3.1. See APPENDIX I for images of the engine used for testing.

Table 3.1: Specifications for Engine and Fuel Used for Testing [55]

| | |
|-----------------------|---|
| Manufacture | Ford of Canada (Essex Engine Plant) |
| Model Year | 2010 |
| Vehicle | Naturally Aspirated F150 Truck |
| # of Cylinders | 8 |
| Displacement | 5.0 L |
| Compression Ratio | 10.5:1 |
| Peak Power | 360 HP @ 6000 RPM |
| Peak Torque | 380 ft-lb @ 4250 RPM |
| Bore | 92.2 mm |
| Stroke | 92.73 mm |
| Connecting Rod Length | 150.7 mm |
| Piston Pin Offset | 0.80 mm |
| Firing Order | 1-5-4-8-6-3-7-2 |
| # of Valves | 2 Intake, 2 Exhaust Per Cylinder, 32 Valves Total |
| Variable Valve Timing | DOHC Twin Independent Cams with Phasing 50°CA Max |
| Base IVO | 30°CA (or 330°BTDC) |
| Base IVC | 270°CA (or 90°BTDC) |
| Base EVO | 521°CA (or 161°ATDC) |
| Base EVC | 9°CA (or 351°BTDC) |
| Fuel Injection | SEFI Port Injectors |
| # of Injectors | 8 |
| Fuel Type | Gasoline |
| Fuel MON # | 86.73 |
| Fuel RON # | 96.53 |
| Fuel Antiknock Index | 91.63 |
| Fuel Density | 710.9 kg/m ³ |

3.2 Engine Sensor/Instrumentation Setup

Figure 3.1 shows the top view of the engine as it has been instrumented for testing purposes. Figure 3.2 shows the left side of the engine and its respective sensor and instrumentation locations as well.

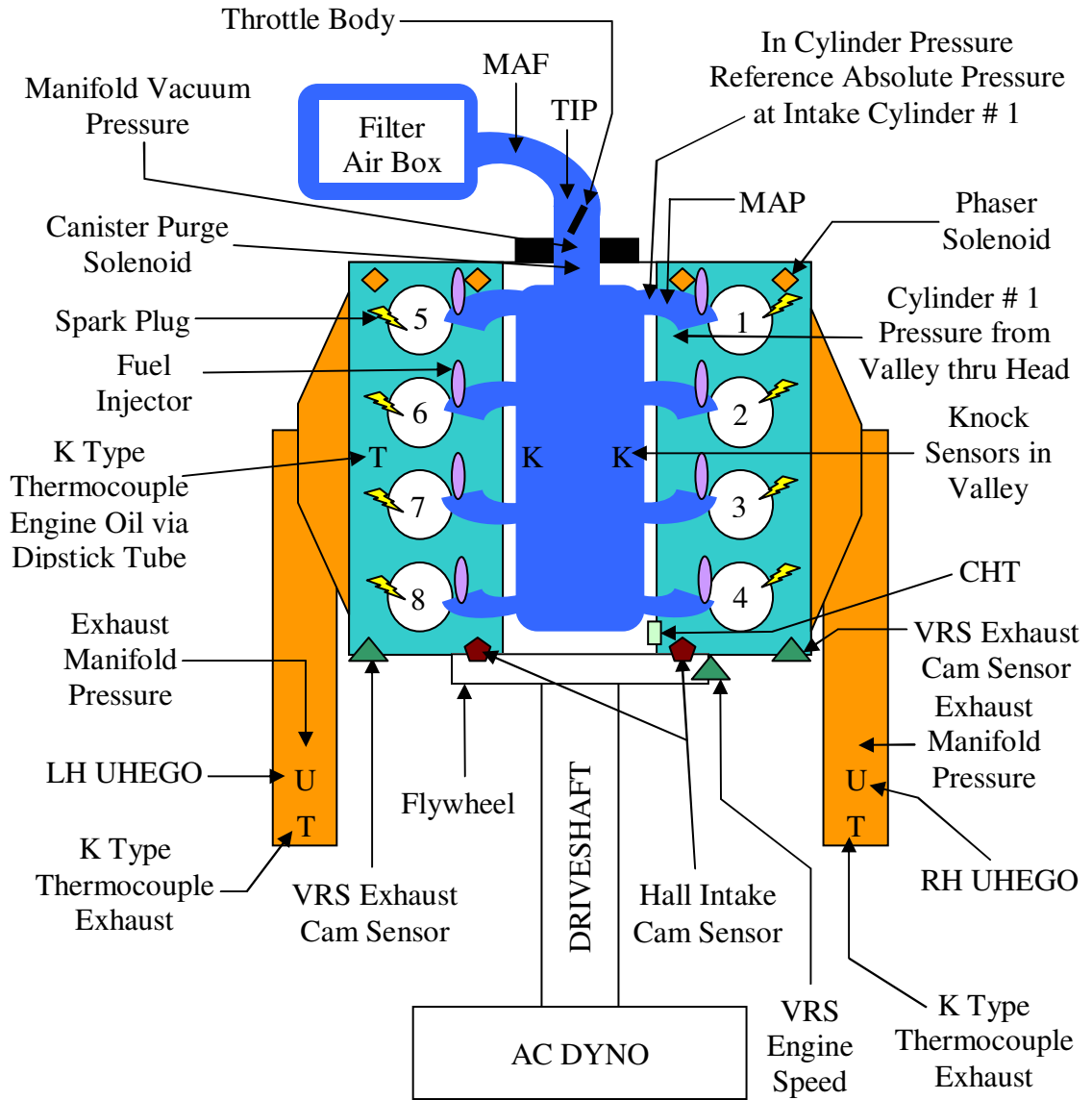


Figure 3.1: Top View of Engine with Sensor/Instrumentation Locations

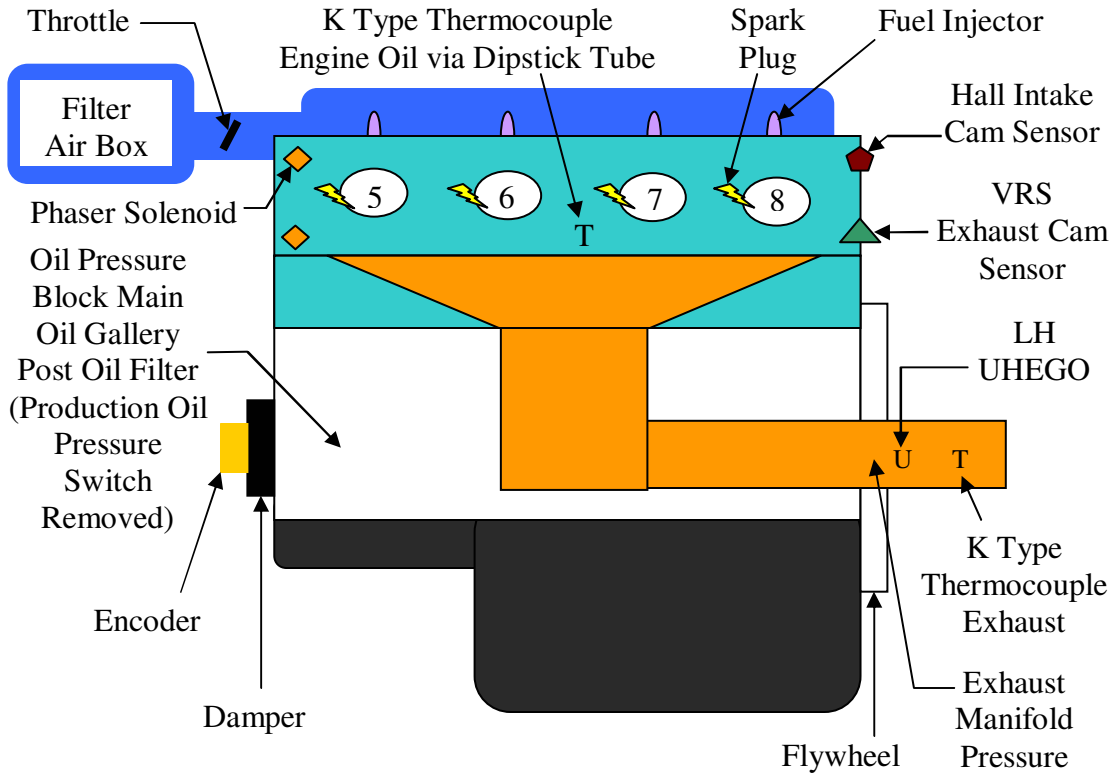


Figure 3.2: Left Side of the Engine Showing Sensor/Instrumentation Locations

3.2.1 Production PCM via ETAS INCA vs. dSPACE Hardware

The research for this thesis was conducted by operating the engine and collecting data using the production engine controller (using its respective ETAS INCA 5.4.1 calibration setup). The production cam phasers were disabled through the INCA calibration in order to fix cam timing at its base values. This was necessary, since the calibration that was developed and presented later in this thesis does not utilize the capabilities of the phasers (variable valve timing, VVT) as it was beyond the scope of this thesis. The data that was collected from these initial tests was used to help aid in the design of the new engine Model Based Controller (MBC). Communication with the production engine controller was achieved by using the ETAS ES600 network module [56] and ES690 interface module (CAN, ETK connections) [57]. The ES650 (analog and thermocouple input) module [58] was used to acquire dyno data.

The MBC was developed using the MATLAB/Simulink software, with the Real-Time Workshop and TargetLink to compile the c-code that was flashed (loaded) onto the

dSPACE MicroAutoBox and RapidPro hardware, which controls the engine. Figures 3.3 and 3.4 illustrate the different hardware setups that were required for the production and REC. A larger version of these same diagrams with hardware photos can be found in APPENDIX II. Input/Output (I/O) modules from the ADACS (Automatic Data Acquisition Control System) test cell included frequency, analog and thermocouple inputs and a trigger output to synchronize data collection between systems.

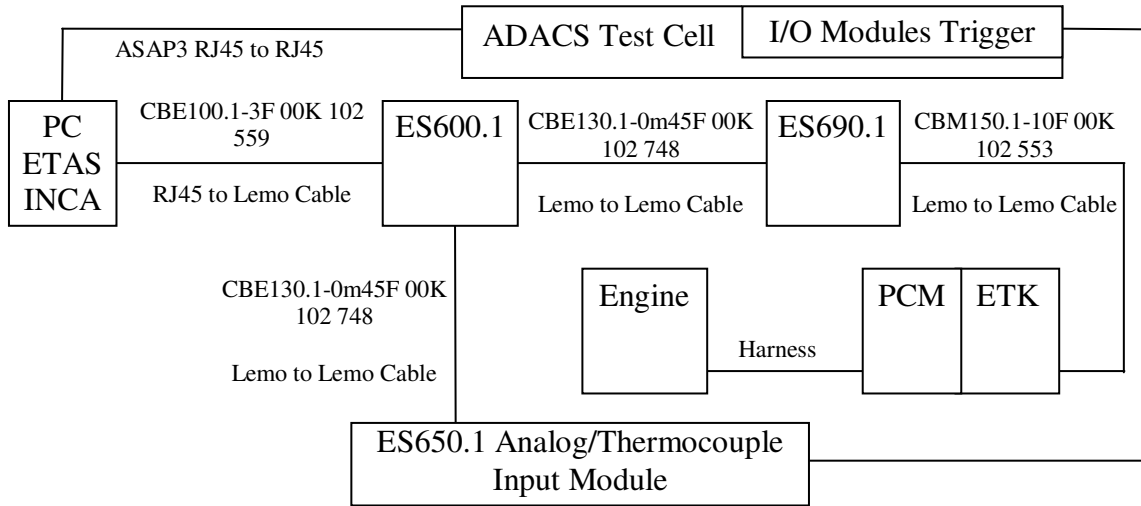


Figure 3.3: ETAS Hardware Setup for Production PCM Communication

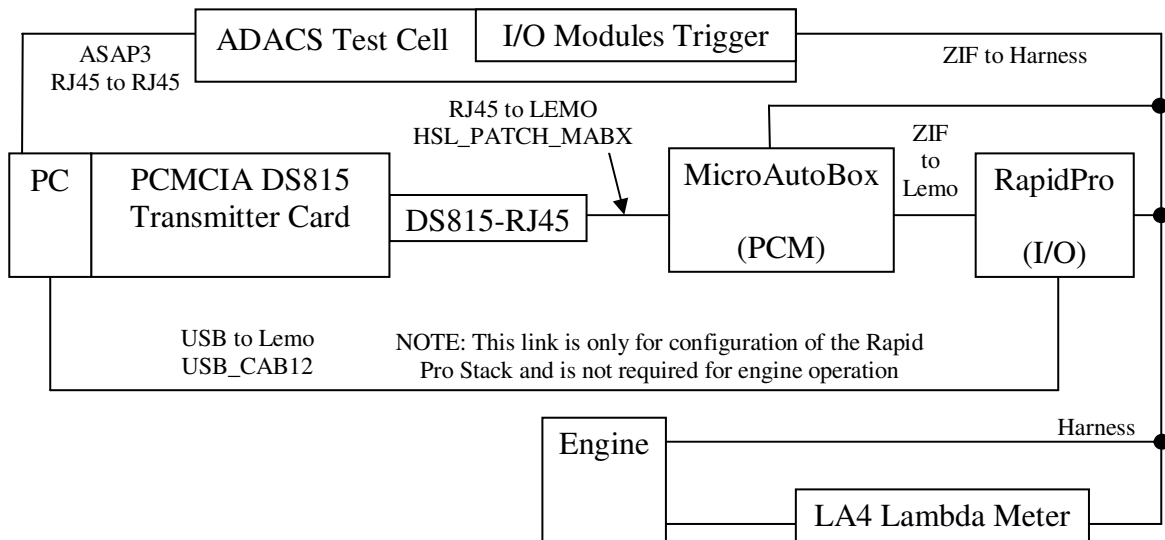


Figure 3.4: dSPACE MicroAutoBox and RapidPro Hardware Setup

Figure 3.5 shows the breakout panel that was used to connect the MicroAutoBox and RapidPro hardware to the engine harness.

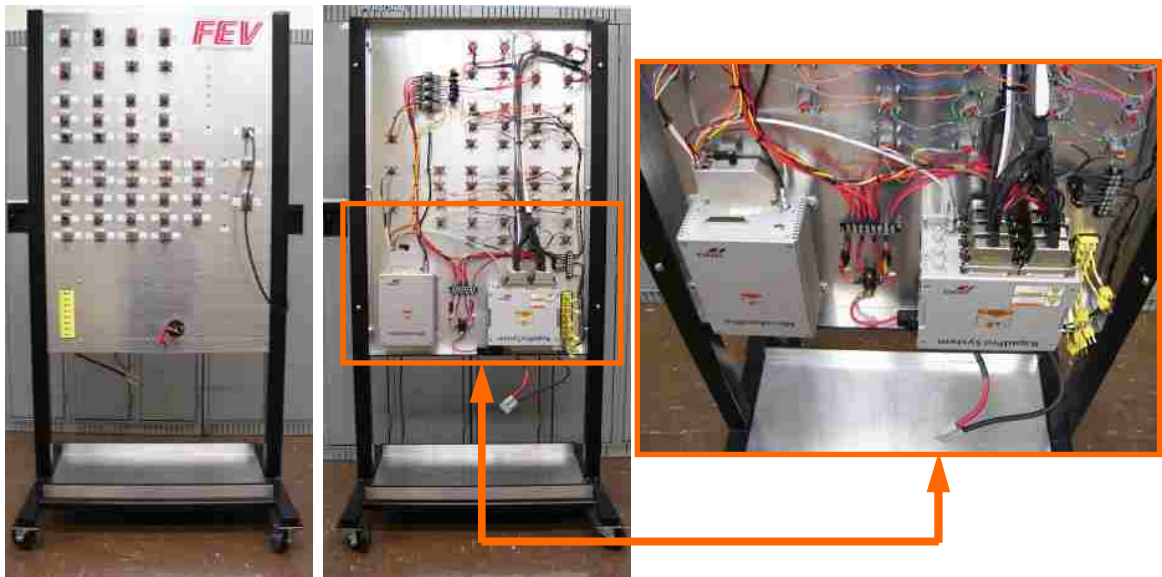


Figure 3.5: Breakout Panel for dSPACE MicroAutoBox and RapidPro

3.2.2 dSPACE MicroAutoBox Specifications

The dSPACE MicroAutoBox was used to replace the production PCM. The updating of dSPACE has since replaced this version of the MicroAutoBox with the MicroAutoBox II [59]. The details for the specific MicroAutoBox system used for this thesis are as follows [60]:

- Processor: IBM PPC 750FX, 800 MHz
- Memory: 8 MB Main, 4 MB Communication, 16 MB for code and data
- 4 CAN, 2 RS232 & 2 LIN interfaces
- Analog Channels
 - Input: 16 channels, 12 bit (0-5 V)
 - Output: 8 channels, 12 bit (0-4.5 V), 5 mA max
- Digital Channels:
 - 16 discreet inputs, 16 bit
 - 10 discreet outputs, 16 bit, 5 mA max
 - 16 shared discreet inputs/outputs

- 16 TPU (Time Processor Unit) Channels
- The digital input channels are configured while designing the engine controller in MATLAB/Simulink. It is not possible to mix the four available configuration setups to choose the optimal channel setup. The user must select one of the four methods listed in Table 3.2.

Table 3.2: Inputs and Outputs of the MicroAutoBox, adapted from [60]

| | | EEC | CC | DCEA | DCCA |
|---------|---|-------|-------|------|------|
| INPUTS | Frequency/Pulse Width Measurement, 1.25 Hz-100 kHz | 2 | 4 | 4 | 4 |
| | Edge Aligned, 5 Hz-50 kHz, 15 Bit res. | 0 | 0 | 3 | 0 |
| | Center Aligned with Dead Time, 5 Hz-20 kHz, | 0 | 0 | 0 | 6 |
| | Incremental Encoder Digital Inputs using an Index | 0 | 0 | 3 | 0 |
| | Incremental Encoder Digital Inputs without an Index | 0 | 0 | 0 | 1 |
| | Wheel Speed Inputs | 0 | 4 | 0 | 0 |
| OUTPUTS | 2.5 Hz-100 kHz, 15 Bit res, DC 0-100% | 14 fp | 12 vp | 0 | 0 |
| | 0.625 Hz-100 kHz, 16 Bit res, DC 0-100%, vp | 4 | 4 | 4 | 4 |
| | Stepper Motor Control | 1 | 0 | 0 | 0 |

Note: DC = Duty Cycle EEC = Extended Engine Control
 vp = Variable Period CC = Chassis Control
 fp = Fixed Period DCEA = Drives Control Edge Aligned
 res. = Resolution DCCA = Drives Control Centre Aligned

3.2.3 dSPACE RapidPro Stack Specifications

The RapidPro unit is used to enhance the capabilities of the MicroAutoBox system. It allows for additional inputs and outputs, for the specific engine control application. Figure 3.6 shows the configuration of the RapidPro stack used for the research conducted in this thesis. The number of layers in the RapidPro stack depends on the number of additional I/O cards desired for the application or engine sensor configuration.

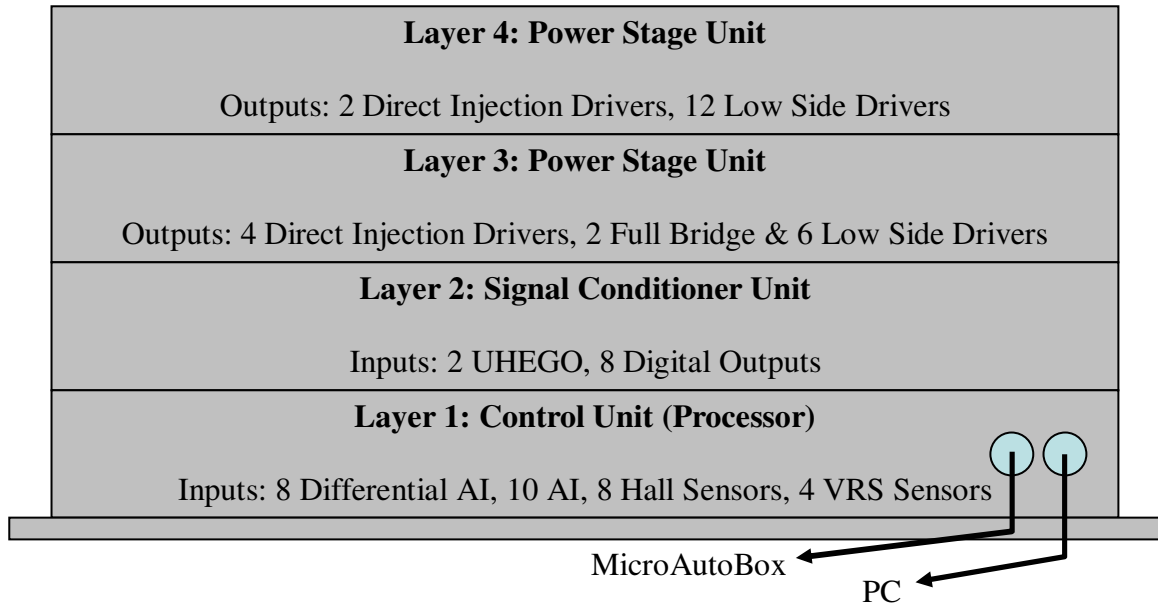


Figure 3.6: RapidPro Stack Configuration used for Research of this Thesis

The specifications for the RPCU used in this thesis work are summarized below [43, 61]:

- Processor: MPC565, 56 MHz
- Signal Conditioning and Power Units are user configured
- SC-AI 4/1 : (2 cards)
 - 4 channel differential analog input ± 100 mV to ± 50 V
 - With 1st order low pass filter (10 Hz, 50 Hz, 100 Hz, 1 kHz)
- SC-AI 10/1 :
 - 10 channel analog input
 - 5 V, 1 W sensor power supply
 - 1st or 2nd order low pass filtering
- SC-DO 8/1 :
 - 8 channel digital output, 40 V, 1 Amp total
- SC-CCDI 6/1 : Crankshaft/Camshaft Module (2 cards)
 - 2 VRS channels ± 200 VAC, 4 Hall channels (± 60 VDC)
- SC-EGOS 2/1 :
 - 2 channels, BOSCH LSU4.2 or LSU4.9 capable
 - Lambda measurement range of 0.65 to Air
 - Pump Current 0 to 150 μ A

3.2.4 Combustion Analysis System

A combustion analysis system was utilized to monitor the combustion stability and the ignition/fuel timing. In particular, the AVL IndiCom software [62] was used with AVL IndiSmart 612 hardware [63]. The crank angle domain was obtained by using the AVL Angle Encoder 364CC with a light tube and pulse converter 365Z01C to generate TTL (Transistor to Transistor Logic) signals [64]. The manifold pressure was measured using a Kistler 4005BA5F transducer [65, 66] and amplified by a Kistler 4618A0 amplifier [67, 68], while cylinder pressure was measured using an AVL GU22CK transducer [69] with amplification occurring internal to the AVL IndiSmart 612.

The coil current and fuel injector current signals were monitored using the Fluke 80i-110s AC/DC current probes [70, 71]. One current probe monitored the main current supply for all ignition coils, a second probe monitored the main injector current drawn by all injectors and a third probe was used to monitor the injector for cylinder # 1. The third current probe was necessary since the fuel injection pulses may overlap at higher speeds and loads, making it hard to distinguish when cylinder # 1 starts/ends injecting fuel. A National Instruments (NI) LabVIEW system (PXI-1031) [72, 73] was operated in parallel with the AVL IndiSmart system in order to ensure that valid data was being recorded with the AVL IndiCom/IndiSmart system. The TTL encoder signal was split off the AVL system and input into the BNC-2110 [74, 75]. The MAP signal was also split off, while the cylinder pressure signal was amplified internal to the IndiSmart 612 and output as an analog voltage, which was sent to the BNC-2110. Both AVL & LabVIEW systems were triggered to begin recording at the same time as the ETAS INCA 5.4.1 and dSPACE ControlDesk Next Generation 4.0 data sets. See Figure 3.7 for a diagram showing how the combustion analysis system was connected. For a more detailed figure see APPENDIX II.

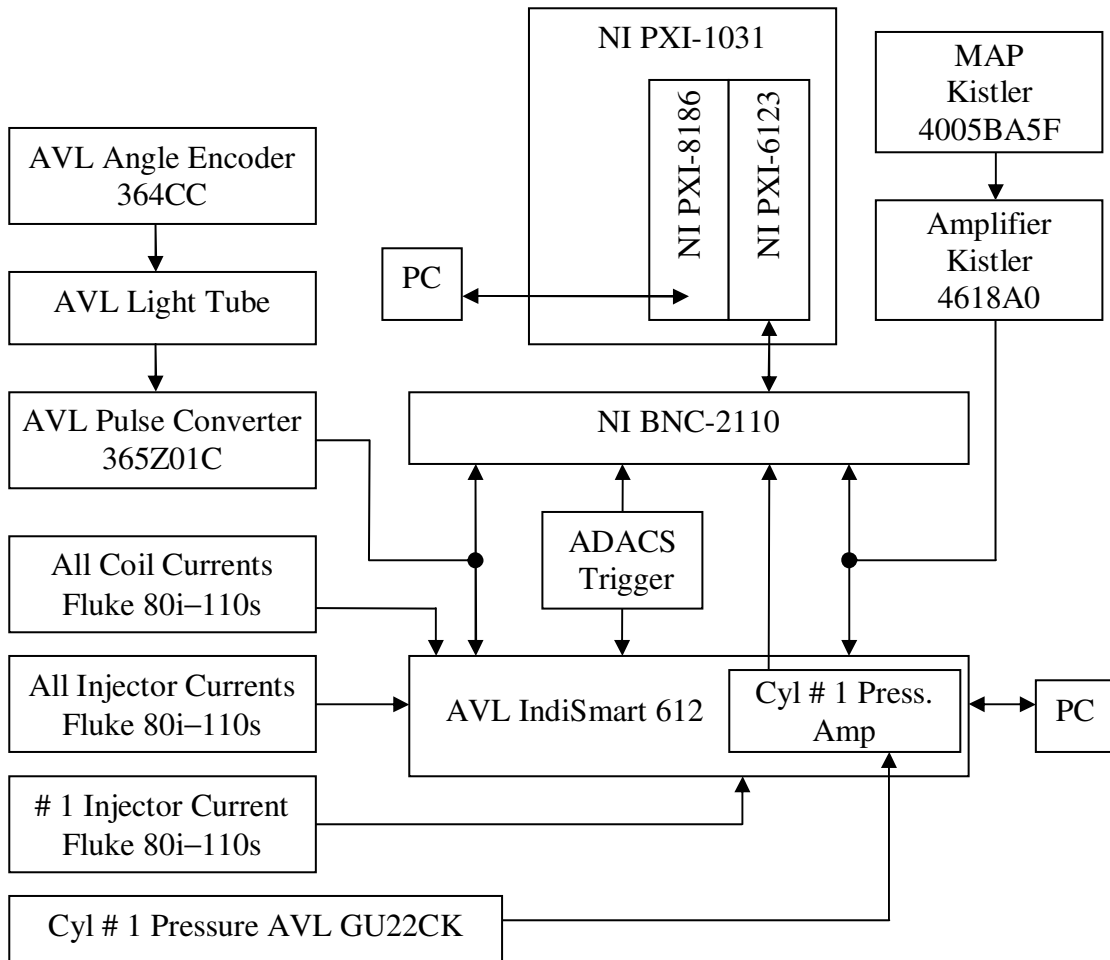


Figure 3.7: Cylinder Pressure Measurement AVL and NI Integration

3.3 Dynamometer Setup

All testing was conducted using an AC dynamometer system. By using an AC dyno, the engine can be motored (rotated without combustion), since the AC dyno acts as an electric motor and turns the engine over at the commanded speed setpoint. This eliminates the need for using a production starter motor to get the engine spinning, and also eliminates the need to code a start up sequence in the MATLAB/Simulink model that was developed. Instead the model can focus on steady state conditions/operation.

3.3.1 Load Points for Steady State Testing

For the purpose of validating the operation of the engine controller designed in this thesis, the following load points were run until the oil and coolant temperatures stabilized. The coolant was held to approximately 88°C (190°F), while the oil temperatures are listed below in Table 3.3. Once stable temperatures were achieved, the engine data was recoded for one minute using the production PCM and REC, while 200 cycles of combustion data from cylinder # 1 was collected, using both AVL IndiCom and LabVIEW systems. The engine operating points were chosen to vary the speed and load conditions, while applying different control methods typically used by a dyno facility. The different control methods included torque, Manifold Pressure (MP), Wide Open Throttle (WOT, maximum load), and pedal position.

Table 3.3: Load Points for Steady State Testing

| # | Speed RPM | Load (Nm / ft-lb) | Oil (°C/°F) | Control Method MP = Manifold Pressure |
|---|--------------|----------------------|----------------|--|
| 1 | 1000 | 135.6 / 100 | 101 / 214 | Torque |
| 2 | 1000 | 31.6 / 23.3 | 96 / 205 | MP @ -59.94 kPa (-17.7 inHg), PT |
| 3 | 1000 | 292.9 / 216 | 107 / 225 | WOT |
| 4 | 1500 | 316.3 / 233.3 | 113 / 236 | WOT |
| 5 | 2000 | 333.1 / 245.7 | 119 / 246 | WOT |
| 6 | 2000 | 275.9 / 203.5 | 117 / 243 | 35% Pedal, PT |
| 7 | 1500 | 43.5 / 32.1 | 100 / 212 | MP @ -59.94 kPa (-17.7 inHg), PT |

3.3.2 Motoring

After the engine was operated at all the various conditions above, the engine was motored with the throttle body held at the same angle as when operating the engine. These motoring curves were recorded with the engine oil temperature around 77°C (170°F) and were used to overlay with the combustion curves. See APPENDIX XIII for a summary of the motoring results.

3.3.3 Engine Operation Production vs. dSPACE Hardware

When operating the engine using the REC OL controller, the injection start angle, duration, and spark start and end angles were manually specified. These were all measured using the AVL IndiSmart 612 system, when running the engine using the production controller. Similarly, the throttle body position used for the REC tests conducted was not directly controlled through the pedal as was the case with the production PCM. While running the engine on the production PCM the throttle position was measured by the REC along with the MAF and AFR. These measured values were used as the basis to start control of the engine in OL or CL mode.

First, the throttle body was set to the same angle as previously measured and then the injection duration was set to the measured value. After the engine temperatures had stabilized, adjustments were made to match the conditions used to control the production engine. The throttle position was adjusted manually to ensure the same manifold vacuum was achieved, as that of the operation by the production PCM. Then the fuel injection duration was adjusted to match the RH (Right Hand) AFR that was previously measured. When the engine was operated under WOT conditions, the throttle angle was set to its maximum value (as measured under production operation) and the injection duration was adjusted until the RH AFR matched the previous operating conditions. When operating torque and pedal load points on the REC, the throttle was adjusted to match the MAF conditions previously measured on the production PCM and the injection duration was adjusted to obtain the same RH AFR that was previously measured. LA4 Lambda meters provided a second AFR measurement when operating the REC to validate AFR measurements [76, 77] (see Figure 3.4).

3.4 Offline Testing

Before attempting to operate the engine using the dSPACE MicroAutoBox and RapidPro hardware, three intermediate steps were required to ensure safe operation and enable full understanding of all the hardware being utilized. The additional details regarding the setup used to test the model and hardware offline are presented in APPENDIX XVII.

The three steps used for offline testing included:

- 1) Test dSPACE hardware functionality
- 2) Test injection and spark functions offline using an engine simulator
- 3) Operate a second set of hardware in parallel with production engine

3.5 MATLAB/Simulink Model Overview

The model presented in the following pages was developed from a dSPACE demo model for the RPCU [78]. The model was extensively reworked in this thesis and the following page includes a summary of the overall model before the main topics of interest (the controllers for the throttle body and the AFR/fuel PW) are presented. In the following pages, block names and/or variables used in the MATLAB/Simulink model are typed in **bold** font so that they are distinguishable as model parameters that can be found in the referenced figures. Throughout the model, signals/variables that were designed for viewing in Control Desk NG, but were not required elsewhere in the model were terminated using MATLAB terminators. Gains with a value of one have also been implemented in order to control how variables are available in Control Desk NG, but otherwise have no purpose or do not change the signals in the model.

The model was compiled using:

- 1) A fixed time step of “0.001 s (1000 Hz)”
- 2) The solver used was “ode1 (Euler)”
- 3) The only optimization applied when building was “Implement logic signals as boolean data (vs. double)”
- 4) The system target file used for compiling was “rti1401.tlc”
- 5) The RTI (Real Time Interface) variable description was set to include both “signal labels” and “virtual blocks”

See Figure 3.8 for the overview of the MATLAB/Simulink model root or APPENDIX XII for the summary of the entire MATLAB/Simulink model.

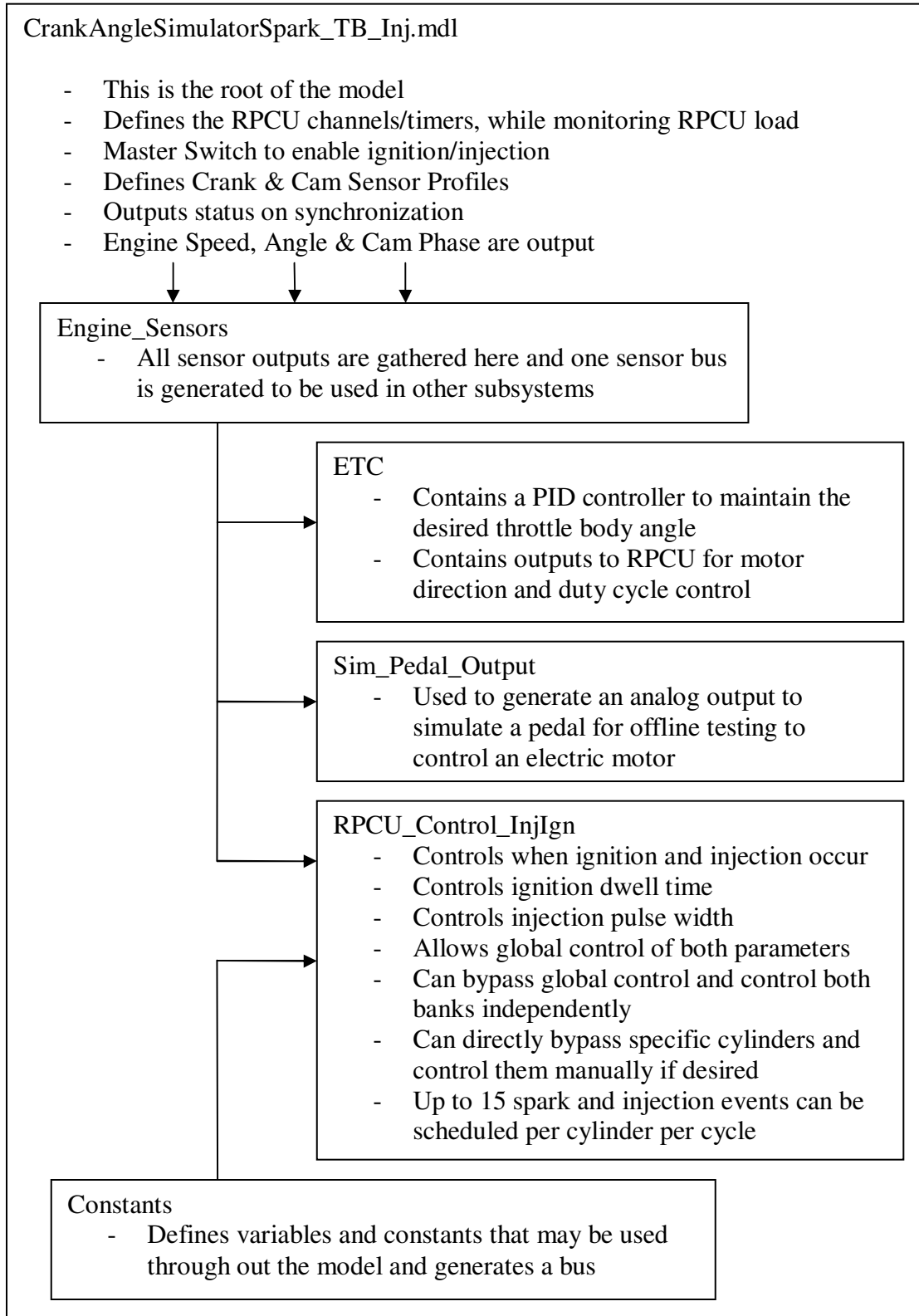


Figure 3.8: Simulink Model Overview CrankAngleSimulatorSpark_TB_Inj.mdl

3.6 Throttle Body Controller

The throttle body PID controller that was implemented was based on a demo model supplied by dSPACE [79]. For more details on the model see APPENDIX XII. When the throttle body opens, a spring on the throttle body opposes the direction of rotation (in addition to the moment of inertia of the throttle plate); however the spring helps close the throttle body when commanded. In order to allow more freedom and flexibility when tuning the PID controller gains and account for the effect of the spring, the controller was designed to have two independent PID controllers. One PID controller would act in order to open the throttle, while the other PID controller would act to close the throttle.

3.6.1 Throttle Body Motor Duty Cycle PID Controller Design

The two controllers implemented for the PID duty cycle controller had the form of Figure 3.9. The PID gains were calibrated manually until the desired controller response was achieved. The final gains that were chosen are summarized in Table 3.4.

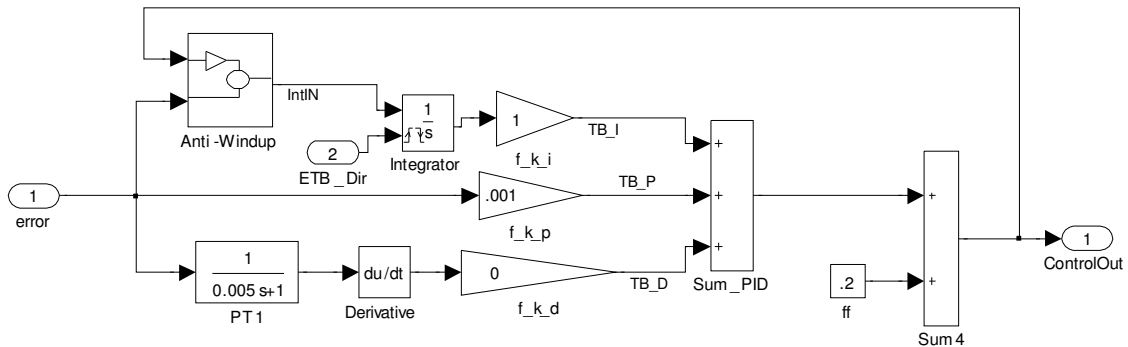


Figure 3.9: Closed PID Controller

Table 3.4: Closed and Open PID Controller Gains

| Gain | Open | Closed |
|-------|--------|--------|
| f_k_p | 0.15 | 0.001 |
| f_k_i | 2.5 | 1 |
| f_k_d | 0.0001 | 0 |

Excessive throttle chatter was observed when derivative control was added to the **Closed** PID controller. For this reason, no derivative action was used on the **Closed** PID controller. While operating the PID controller, it was found that the motor required a duty cycle of approximately 0.2 to hold any throttle angle. For this reason the feedforward term (**ff**) was fixed at 0.2. **Anti-Windup** was used to prevent the integrator from winding up when the duty cycle output went outside ± 1 . Every time the motor direction was flipped, the integrator constant was also reset to zero. **PT1** is a filter that was applied to the error signal before the derivative was taken. This filter was the default filter from the demonstration model and could be modified to provide better results [79].

3.6.2 Controller Validation Tests

After the throttle body controller was designed, several tests were conducted to analyze the robustness of the controller throughout its operating range. Three different tests were used either with engine off or motoring, at 1000, 1500 and 2000 RPM. These tests included:

1.) Pyramid Test

- a. Throttle angle was incremented every 2.5 s from the idle position up to WOT and then stepped back to the base idle position over 60 seconds. All angles are ramped over a period of 250 ms.
- b. 15° , 22° , 29° , 36° , 43° , 50° , 57° , 64° , 71° , 78° , 85° , 92° , 97°

2.) Random Step Input Test (RSIT)

- a. The throttle angle was commanded through a series of large openings and was also closed past its base idle position using the following sequence
- b. Each ramp to a different angle occurs over 250 ms
- c. 15° (0-3.75 s), 60° (4-10.75 s), 10° (11-18.75 s), 80° (19-25.75 s), 30° (26-32.75 s), 90° (33-39.75 s), 40° (40-49.75 s), 70° (50-54.75 s), 15° (55-60 s)

3.) Sine Wave Input Test (SWIT)

- a. A sine wave with a bias of 53.5° , amplitude of 43.5° and frequency of 2 rad/s was commanded to observe the throttle body response.

3.7 Air Fuel Ratio Controller

The AFR controller requires three controllers: one controller executes logic to switch between measuring resistance and AFR, the second controller focuses on maintaining the sensor temperature at the sensors operating point, the third controller uses AFR feedback to adjust the fuel injection duration to obtain the desired AFR.

3.7.1 AFR Measurement Logic

The RPCU used was equipped with the dSPACE SC-EGO 2/1 card which contains the BOSCH CJ125 chip to control and take measurements with the BOSCH LSU4.9 UHEGO sensors. dSPACE provided a demo model [80, 81] which was developed for BOSCH LSU4.2 UHEGO's; this model was used as a basis to start the development of a user customizable model to control and take measurements with the LSU4.9 UHEGO sensors. The demo model had implemented some logic to alternate between measuring AFR and sensor resistance. This was necessary as measuring the resistance introduced noise on the AFR signal, see Section 4.4. For additional details on the sequencing logic used see APPENDIX XII.

3.7.2 Heater Duty Cycle PID Controller

The heater duty cycle PID controller was developed using the throttle body PID controller as a starting point. The main difference in this controller was new gain values (see Table 3.5) and an added **Constant** to allow manually resetting the integration block (see Figure 3.10). The integrator reset was required in order to address the issue of calibrating the integrator gain as discussed in section 2.3.6. Changing the integrator gain **f_k_i**, without reinitializing the integrator would cause the integrator to eventually windup, (see Figure 3.10). The output from **AFRHeater (ControlOut)** was then sent to **Heater_DC_Switch (UHEGO1_DC)** see Figure 3.11), where the controller could be bypassed (flipped to manual control) using **Switch**. The heating rate was limited by **Rate Limiter 1** (rising slew rate = 1 and falling slew rate = -1). Using this slew rate, it would take a total of 1 second to go from a duty cycle of 0 to 1 (or 1 to 0), this was the default settings used in the dSPACE demo model and was not modified. BOSCH does have a

specific heating profile that should be investigated and implemented [39]. For safety, a second saturation block was added before the duty cycle was commanded to the heater on the sensor by **RPCU_PWM_MIOS_BL2**.

Table 3.5: AFR Sensor Heater Duty Cycle PID Controller Gains

| Gain | Value |
|-------|---------|
| f_k_p | -0.0015 |
| f_k_i | -0.001 |
| f_k_d | -0.0001 |

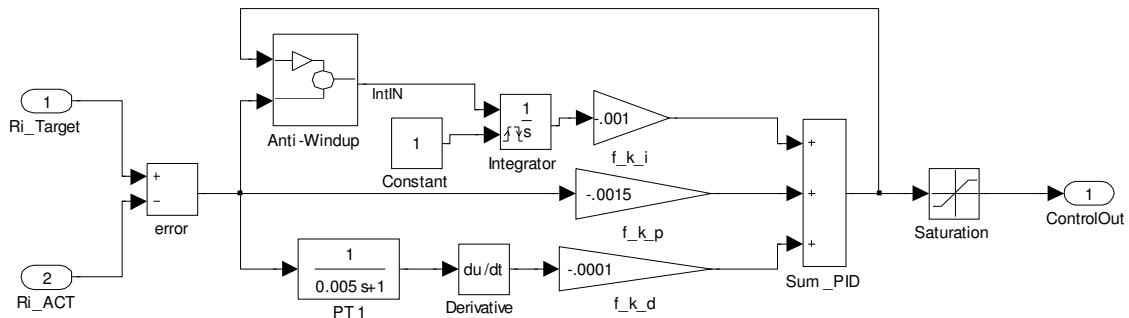


Figure 3.10: AFRHeater, AFRHeater Duty Cycle PID Controller

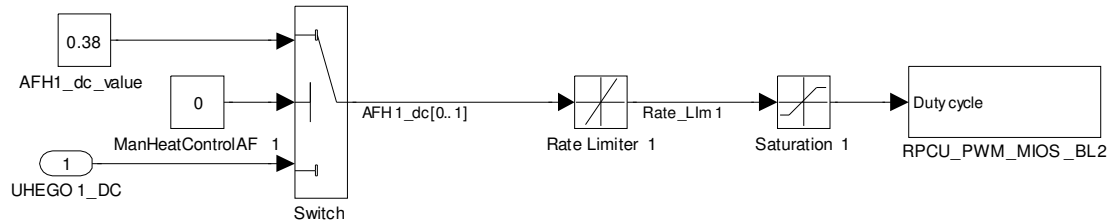


Figure 3.11: Heater_DC_Switch, Duty Cycle Output Command to AFR Heater

3.7.3 Fuel Pulse Width/AFR PID Controller

The fuel PW controller consisted of several different options. The model was designed to maximize the capabilities of the system, while still maintaining flexibility for various aspects of testing. The model was setup with the following intentions:

- 1) Allow a single AFR sensor the ability to control the fuel PW for the entire engine (both right hand and left hand banks, global). Presently the right bank AFR sensor was setup to control both banks but may easily be changed
- 2) Allow bank specific AFR control and bypass the global controller setup. Each AFR sensor should be able to control its own bank
- 3) Allow the ability to bypass the fuel PW controller for any number of cylinders and directly input a desired manual fuel PW
- 4) Allow the user the ability to command the maximum number of injection events possible. dSPACE software/hardware allows the user to command up to 15 injection events per cylinder per cycle (720°CA)

Two possible options for inserting the PID controller were reviewed (see Figure 3.12 and Figure 3.13). The second option was ultimately used, since it allowed the ability to bypass the PID controller and instead use the desired AFR (**DES_AFR**) as the commanded setpoint (instead of **Final AFR** see Figure 3.13). The second option indirectly controls the fuel PW by correcting **DES_AFR** to achieve the desired setpoint, while the first option uses the PID controller to directly output a PW or injection duration. When doing this, it is not possible to directly use **DES_AFR**, since it is not a PW.

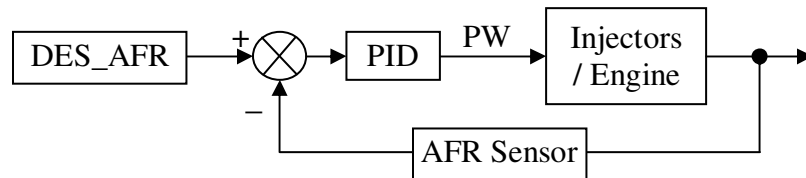


Figure 3.12: Fuel Pulse Width (PW) PID Controller Option 1

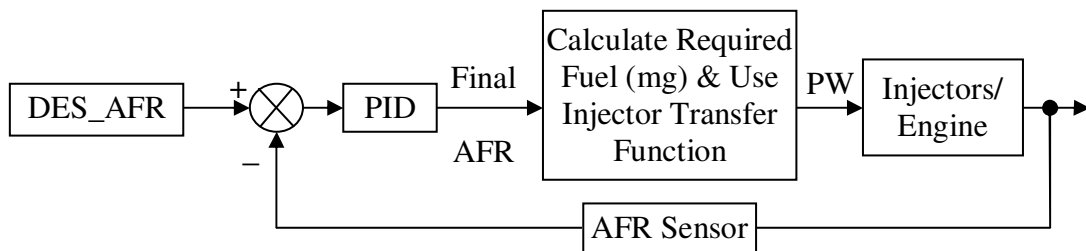


Figure 3.13: Fuel Pulse Width (PW) PID Controller Option 2

The PID controller that was implemented to control the fuel PW was an advanced technique. The entire integrator and anti-windup subsystems were re-worked. The anti-windup subsystem was now setup to saturate when AFR is above 20 or below 0. The integrator was setup to include bumpless transfer and parameters changes for the integral gain. Derivative kick was eliminated by moving the derivative from the error calculation to the sensor feedback. The feedforward term was also applied directly on the setpoint. For more details on the injection duration/PW controller see APPENDIX XII. The final parameters used for the implemented controller are summarized below in Table 3.6

Table 3.6: AFR/Fuel Pulse Width PID Controller Gains

| Gain | Value |
|-------|-------|
| f_k_p | 0.25 |
| f_k_i | 0.2 |
| f_k_d | 0.01 |
| ff | 0.5 |

3.7.4 Closed Loop AFR Controller Validation Tests

The response of the Air Fuel Ratio controller was checked by subjecting the AFR setpoint for the PID controller to a step response, which alternated between 14.7 and 16 AFR every 10 seconds. This same response was also applied to the open loop/manual setpoint in order to show the steady state offset between the commanded and actual applied setpoints.

CHAPTER 4

ANALYSIS OF RESULTS

4.1 Throttle Body Test Results

The throttle body tests that are presented in the following sections will only focus on the engine off conditions. It was found that the motoring tests did not present any significant differences, when testing the throttle body response. See APPENDIX XV for additional results including motoring data.

4.1.1 Pyramid Test

Figure 4.1 shows the results from the pyramid test with the engine off. The results showed the controller to be more stable near wide open throttle. The controller tracked the commanded profile within a few degrees. The zoomed region on the right of Figure 4.1 shows that the controller response is able to respond transiently with minimal overshoot, while some slight disturbances are observed periodically after the throttle body has stabilized. These disturbances may be resolved by adding a filter to the measured throttle body position before using it for control purposes. The plotted signals in the figures below are not filtered. See APPENDIX XV for more details.

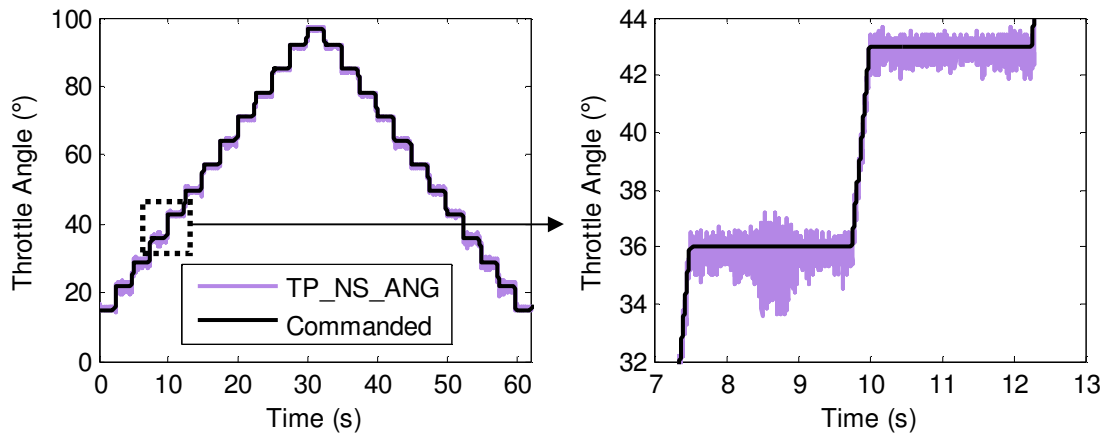


Figure 4.1: Pyramid Test, Left – Engine Off, Right – Zoomed (7–13 s)

4.1.2 Random Step Input Test (RSIT)

Figure 4.2 shows a set of data from the random step input test that was conducted. A zoomed region on the right side of this figure shows overshoot, which stabilizes after 260 ms. The other random ramps that were tested do not show these same overshoot conditions. See APPENDIX XV for more details.

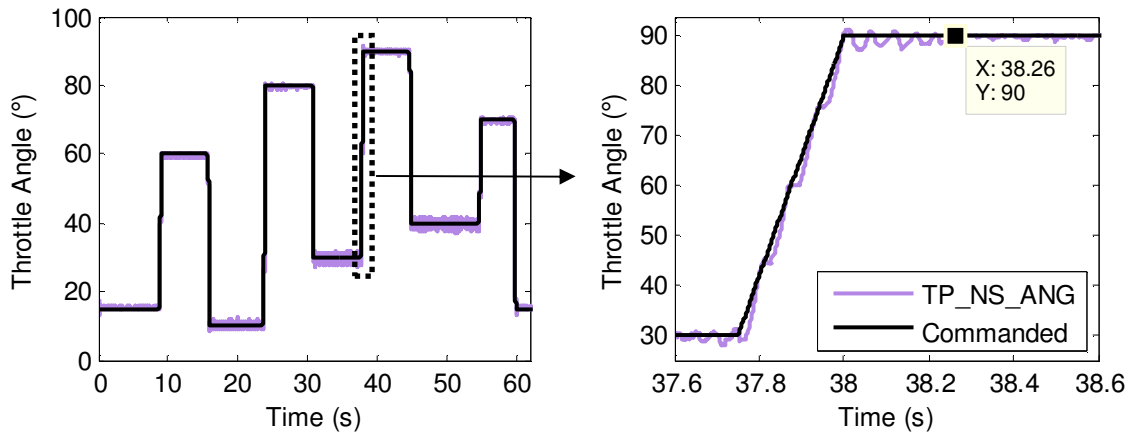


Figure 4.2: RSIT, Left – Engine Off, Right – Zoomed (37.6–38.6 s)

4.1.3 Sine Wave Input Test (SWIT)

Figure 4.3 shows that the throttle position follows the setpoint with satisfactory accuracy, while the zoomed region also shows encouraging results. As the throttle approaches wide open the throttle response is closer to the setpoint. For additional details see APPENDIX XV for more details.

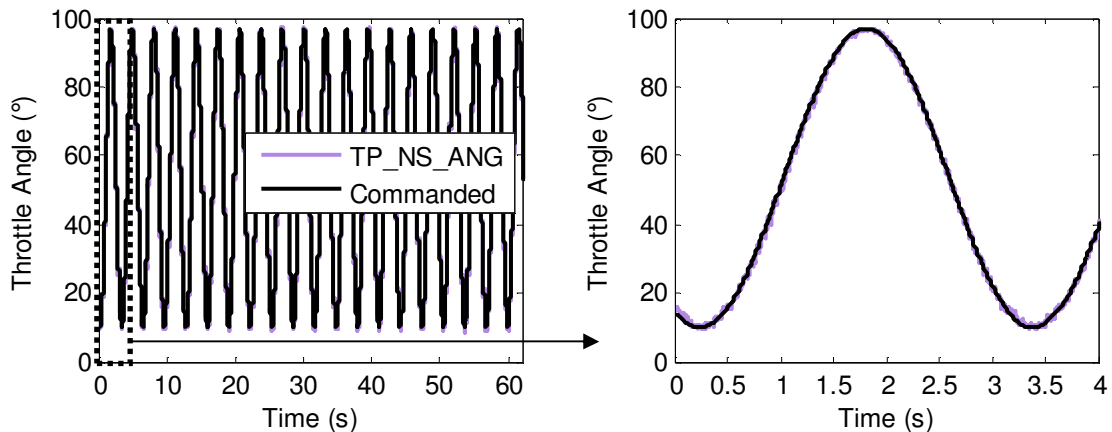


Figure 4.3: SWIT, Left – Engine Off, Right – Zoomed (0–4 s)

4.2 AFR Heater Controller Results

The following data was collected from the REC, while the engine was controlled by the production PCM. Of the seven load points that were tested, data from 2000 RPM WOT was chosen to summarize the ability of the controller to control and maintain the desired resistance of 300 Ω . The RH AFR sensor was capable of holding its internal resistance to within approximately ± 2 Ω , while the LH (Left Hand) AFR sensor was capable of holding its internal resistance to within approximately ± 5 Ω (see Figure 4.4). The control of the LH bank AFR sensor resistance was not nearly as tight as the RH bank AFR sensor. The PID gains were originally tuned using the RH bank AFR sensor. The difference in the control of the AFR sensor resistance may be a direct result of differences within the sensor manufacturing process.

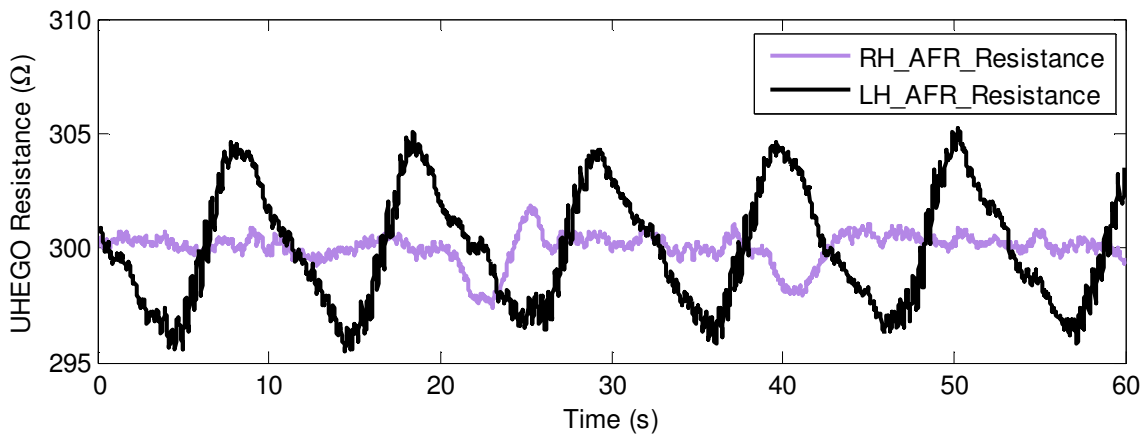


Figure 4.4: dSPACE UHEGO Resistance, 2000 RPM WOT Prod. PCM Control

4.3 AFR/Fuel Pulse Width Controller Results

The AFR/fuel PW controller was tested using both OL and CL control. When attempting to manually control the AFR to specific values in OL mode, it was determined that there was approximately a steady state offset of about five percent. In order to get the system to go to an AFR of 16, the system required a commanded value of approximately 15.2 or 95 percent of **DES_AFR**. Figure 4.5 shows the results from the OL controller (left), applying this percentage to **DES_AFR** still results in a slight steady state offset from **DES_AFR** (see Figure 4.6, left). The results of the CL controller response to the

same step function are shown on the right side of Figure 4.5. There was an obvious difference between the OL and CL controllers. In particular the CL controller commands the system to overshoot and also undershoot the setpoint. This was due to the fact that the AFR measurement has a delay from when fuel is injected. The delay was due to the time required for the fuel combustion to occur and then reach the AFR sensor downstream in the exhaust pipe. This delay causes the PID integral to steadily wind up, as it waits for the sensor to respond to the fuelling changes. Once the sensor responds the PID controller quickly corrects itself to obtain the desired AFR. The OL controller on the other hand was held at a setpoint which shows an offset from the desired, the delay times and sensor response was found to vary from cycle to cycle. Figure 4.6 shows the ability of the CL controller to eliminate the steady state offset, unlike the OL controller.

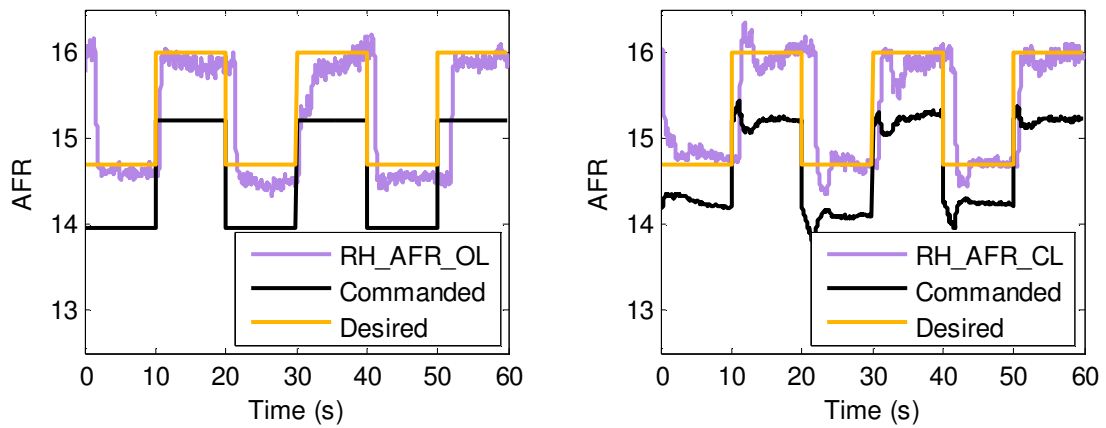


Figure 4.5: RH AFR Control, Left – OL, Right – CL

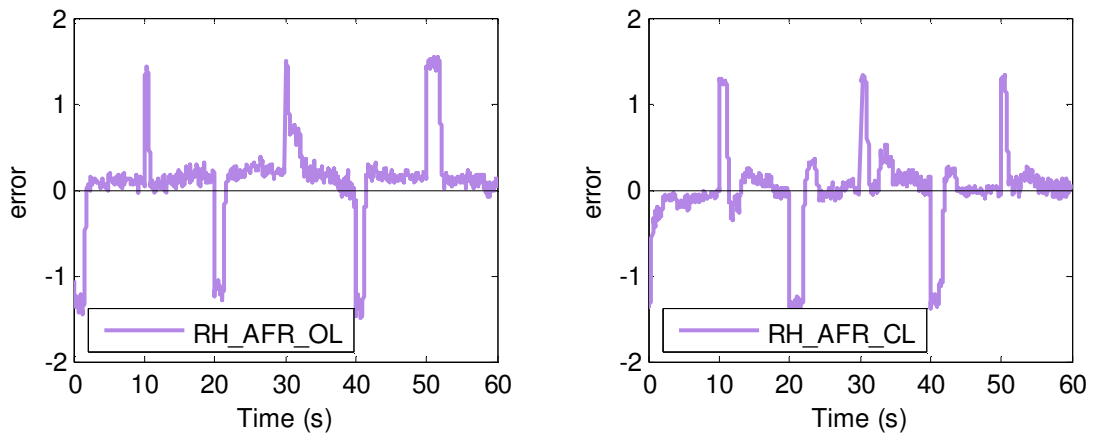


Figure 4.6: RH AFR Control, Left – OL, Right – CL

The delay times for the sensor response shown in Figure 4.5 have been summarized in Table 4.1.

Table 4.1: AFR Sensor Delay Times

| Time (s) | AFR Change | OL Delay Time (s) | CL Delay Time (s) |
|----------|------------|-------------------|-------------------|
| 10 | 14.7 to 16 | 0.5 | 1.08 |
| 20 | 16 to 14.7 | 1.2 | 1.82 |

4.4 AFR Signal Noise due to Resistance Measurement

Figure 4.7 illustrates the sequence that was used to check the effect of resistance measurement and averaging on the AFR measurement. The data between 30 and 50 s is representative of data that would have been recorded using the REC for testing and has a slight offset of 0.09 AFR. The LA4 Peak to Peak (PK to PK) is 0.18 AFR which is about the same as the REC (see Table 4.2).

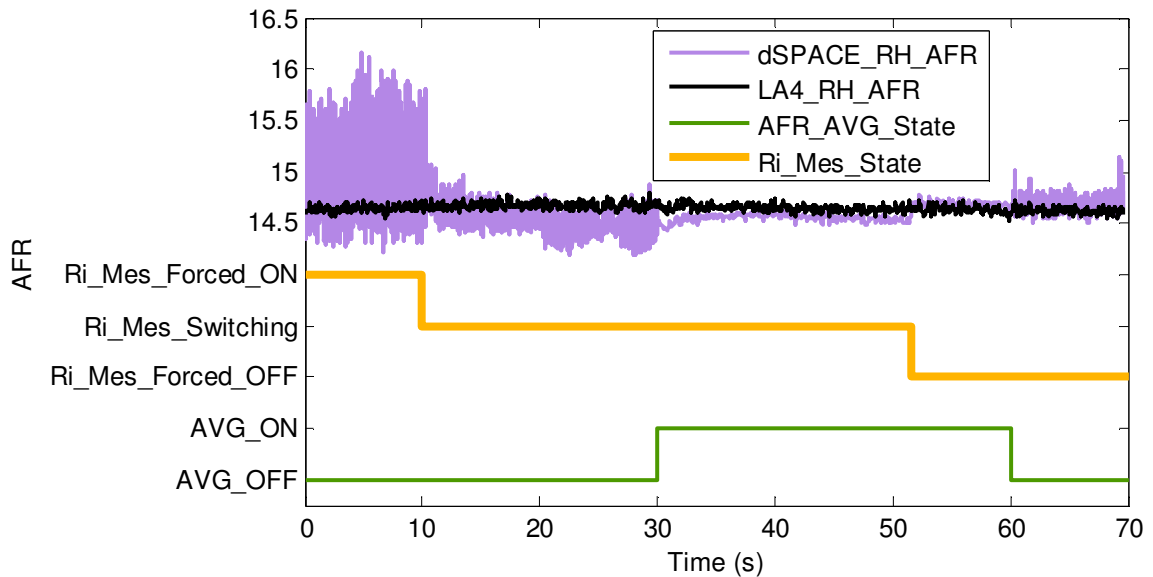


Figure 4.7: Sequence for Checking AFR Noise due to Resistance/AFR Averaging

Table 4.2: Summary of Resistance and Averaging on AFR

| Settings | Ri_Mes - on AVG - off | Ri_Mes - sw AVG - off | Ri_Mes - sw AVG - on | Ri_Mes - off AVG - on | Ri_Mes - off AVG - off |
|----------------------|--------------------------|--------------------------|-------------------------|--------------------------|---------------------------|
| Time Range | 0-10 s | 10-30 s | 30-50 s | 50-60 s | 60-70 s |
| AFR Band PK to PK | 1.85 | 0.5 | 0.14 | 0.11 | 0.4 |

4.5 Engine Operation Results

4.5.1 Data/Figure Overview

From the series of load points that were chosen to test the engine, the main results presented in this section, focus on a low speed/load (1000 RPM / – 17.7 inHg) and a high speed/load (2000 RPM WOT), to show the range of operation of the engine controller. The CL controller did not exhibit any significant differences from those that were observed for the OL controller, since only steady state testing was conducted. Extra test results not included in this section can be found in the APPENDIX XIV. Each load point has a summary table, including mean, standard deviation (std.) and Coefficient of Variation (Coeff. Var.) for the various figures that were plotted. Also included in the summary table is the CA50 (crank angle 50 percent Mass Fraction Burned - MFB), which was not plotted. Each load point has two figures containing a series of eight sub figures. The layout and purpose of these sub figures is described below.

The first figure includes the combustion analysis data; one common set of axes has been chosen for each sub figure to allow easy comparison between all load points. This combustion analysis figure was organized as follows:

- A) Shows the coil and injector currents to identify when each injector or coil is in use. The coil and injector current profiles were measured using separate current probes, located on the main current supply for all injectors and/or coils. An additional current probe was located on injector # 1, to allow easy identification of the # 1 cylinder injection event. At higher speeds and loads it was not possible to easily identify when injector # 1 was operating. The generic current probe measuring the main current feed for the injectors has overlapping current profiles,

which merge together. The coil current profile has been labelled with the respective cylinder firing order. The same sequence can be applied starting at injector # 1. This sub figure shows one entire combustion cycle of data.

- B) Illustrates the spark angle and the Cumulative Mass Fraction Burned (MFB) of fuel that was injected. The cumulative MFB was calculated using the mean MFB data for 200 cycles, which is shown in sub figure F. The star in the figure identifies the point of ignition. The crank angle has been limited to the region $\pm 100^\circ\text{CA}$ of TDC. This figure may be compared to sub figure C.
- C) Plots the average of 200 motoring cycles along with 200 sequential combustion cycles. The star in the figure identifies the point of ignition. This plot shows the wide range of cyclic cylinder pressure variation within the spark ignition engine. The crank angle has been limited to the region $\pm 100^\circ\text{CA}$ of TDC.
- D) Provides a top view of sub figure C, where the CA for both spark and peak cylinder pressure are plotted for 200 sequential combustion cycles, within the region $\pm 100^\circ\text{CA}$ of TDC.
- E) 200 sequential combustion cycles are overlaid showing cylinder # 1 coil current and the cyclic variability present. The CA is limited between 70°BTDC and TDC
- F) The MFB curve can be compared with sub figures B to D. The plotted MFB curve is the mean MFB of 200 combustion cycles and is limited within the region $\pm 100^\circ\text{CA}$ of TDC.
- G) 200 cycles of peak cylinder pressure (P_{\max}) and peak motoring cylinder pressure. This figure provides a side view of sub figure C.
- H) Indicated Mean Effective Pressure (IMEP) for 200 sequential combustion cycles.

The second figure provides a zoomed view of the important PCM measurements.

The list of the sub figures contained in these plots includes:

- A) Temperatures measured by MAF, TIP and MAP sensors (TMAF, TTIP, TMAP)
- B) Pressures measured by MAP and TIP sensors
- C) Commanded injection duration (PCM) and measured fuel flow rates

- D) Left bank AFR as measured by the production PCM (ETAS), the dSPACE hardware and the LA4 Lambda meters. The LA4 Lambda meters were used only when the production PCM was not controlling the engine.
- E) Torque as measured by the test cell for the various operating conditions. This torque was the observed torque.
- F) Throttle position sensor angle (negative slope only) as measured by the production PCM and the dSPACE hardware
- G) MAF values as measured by the production PCM and the dSPACE hardware
- H) Same as D but using the Right bank AFR sensor.

4.5.1.1 1000 RPM –17.7 inHg (Gauge)

Figures 4.8D and E illustrate the variation of the spark angle which is a direct result of the PCM implementing a spark control algorithm similar to the one, described in section 2.1.4.1 (advance spark until knock is detected, then retard spark). Figure 4.8A shows that the injector duration was very small in order to obtain the low load. Injection began around 295.4°CA and ended at approximately 307.4°CA. Assuming a constant speed of 1000 RPM, results in approximately 2 ms for the injection duration. The commanded injection duration by the production PCM (1.1 ms), did not match the measured injection duration by the current probe (see Figure 4.9C). The variable, which was chosen to represent the commanded injection duration, does not appear to be the final commanded duration by the PCM. This variable however, does provide insight on the decisions made by the PCM (fuel is cycling with the MAF signal, see Figure 4.9C).

Figures 4.8C and G show that peak cylinder pressure was similar to that of the motoring curve for a number of the combustion cycles. Figures 4.8B and F show that the spark must be initiated early (38.4°BTDC) compared to the actual start of combustion. Figures 4.9D and H show the AFR as measured by both the dSPACE and production PCMs. Both sets of hardware follow the same cyclic trends, with similar amounts of variation in the signal. Figure 4.9F shows that the PCM was cycling the throttle body position, resulting in similar fluctuations in the commanded injection duration, measured MAP, MAF and torque signals.

It is important to note that this load point was actually controlled by the ADACS test cell, which was measuring the intake manifold pressure directly after the throttle body. The test cell would control the pressure at this location to approximately -17.7 inHg (gauge), which is approximately 40 kPa (absolute) (see Figure 3.1). The test cell controlled the pedal position, which would then command the PCM to adjust the throttle position. This setup replicates how the PCM operates on a vehicle. ADACS continually adjusted the pedal position until the desired manifold vacuum was achieved. Reviewing Figure 4.9B however, does not reflect that the MAP was controlled to 40 kPa as expected. Instead MAP was reading around 30 kPa. The difference in the MAP readings is due to the differences in the sensor locations.

The MAP sensor for the dSPACE hardware and the AVL combustion system were installed as close to cylinder # 1 intake as possible. Comparing the combustion and dSPACE MAP sensors confirmed that the dSPACE MAP sensor was accurately reading 30 kPa, when the pressure after the throttle body was controlled to 40 kPa. This indicates that there was an additional pressure drop from the throttle body to the cylinder intake port. The fuel flow rate shown in Figure 4.9C does not show any signs of fluctuation, while they are present in the commanded injection duration. The variation in the fuel flow rate may be attributed to the rail pressure and battery voltage fluctuations instead.

The dSPACE MAF temperature shown in Figure 4.9A was slightly lower than the production PCM and is suspected to be a result of corrections made by the production PCM. Further work can be conducted to improve the temperature measurements from the MAF sensor. The air temperature increased as it entered the engine, with the coldest point being the MAF sensor, which measures the fresh air charge after the air filter (farthest point from the engine). A slight increase in the temperature is seen at the throttle inlet (TIP sensor). As the air passes through the intake, additional heat is transferred from the engine and the MAP sensor measures the highest temperature. Therefore heat dissipated by the engine was being absorbed as the intake air traveled through the intake system and into the cylinder. See Table 4.3 for a summary of the results for this load point

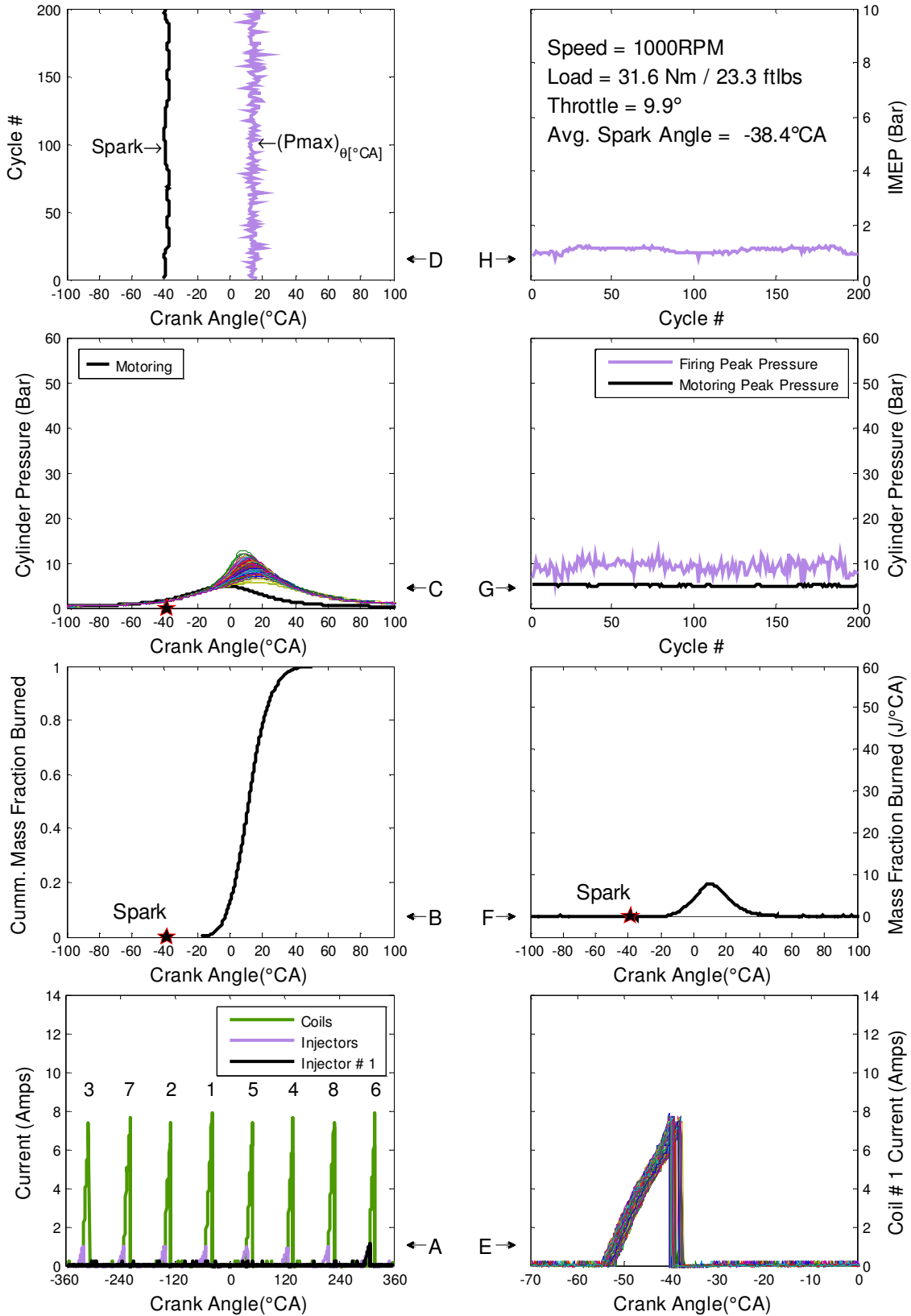


Figure 4.8: Production 1000 RPM -17.7 inHg Combustion Data

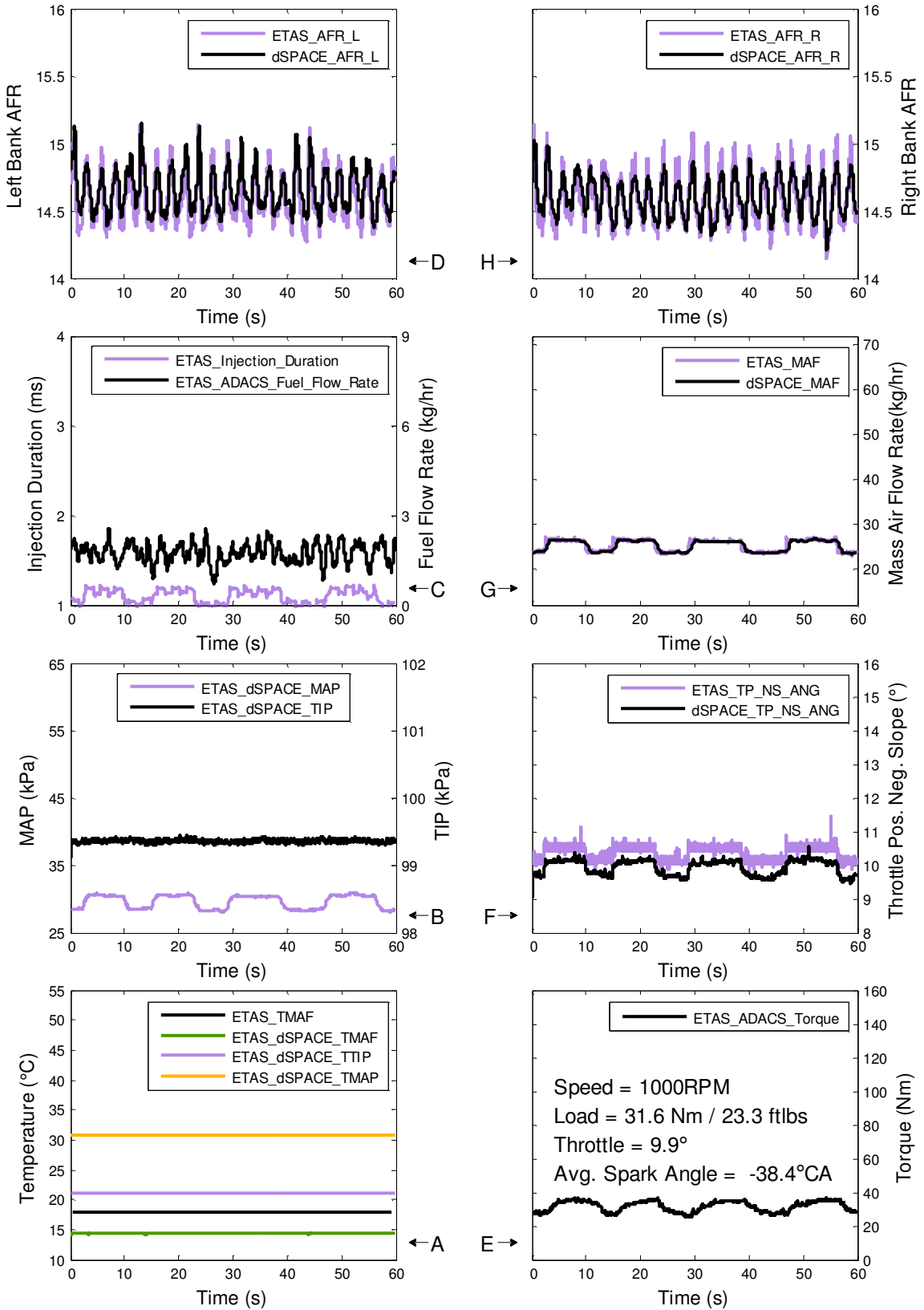


Figure 4.9: Production 1000 RPM -17.7 inHg PCM Measurements

Table 4.3:1000 RPM –17.7 inHg Production PCM Data Summary

| | Left Bank AFR | | | Right Bank AFR | | |
|-----------------|---------------|-----|--------|----------------|-----|--------|
| | ETAS | LA4 | dSPACE | ETAS | LA4 | dSPACE |
| Mean | 14.59 | NA | 14.65 | 14.58 | NA | 14.60 |
| Std. | 0.18 | NA | 0.16 | 0.18 | NA | 0.15 |
| Coeff. Var. (%) | 1.25 | NA | 1.10 | 1.26 | NA | 1.03 |

| | Inj. Dur. (ms) | | Fuel Flow (kg/hr) | | MAF (kg/hr) | |
|-----------------|----------------|--------|-------------------|--------|-------------|--------|
| | ETAS | dSPACE | ETAS | dSPACE | ETAS | dSPACE |
| Mean | 1.10 | NA | 1.74 | NA | 25.30 | 25.23 |
| Std. | 0.07 | NA | 0.33 | NA | 1.30 | 1.23 |
| Coeff. Var. (%) | 6.74 | NA | 19.21 | NA | 5.13 | 4.87 |

| | MAP (kPa) | | TIP (kPa) | | TP_NS (°) | |
|-----------------|-----------|--------|-----------|--------|-----------|--------|
| | ETAS | dSPACE | ETAS | dSPACE | ETAS | dSPACE |
| Mean | 29.58 | NA | 99.36 | NA | 10.35 | 9.93 |
| Std. | 1.01 | NA | 0.02 | NA | 0.21 | 0.22 |
| Coeff. Var. (%) | 3.40 | NA | 0.02 | NA | 1.99 | 2.24 |

| | TMAP (°C) | | TTIP (°C) | | TMAF (°C) | |
|-----------------|-----------|--------|-----------|--------|-----------|--------|
| | ETAS | dSPACE | ETAS | dSPACE | ETAS | dSPACE |
| Mean | 30.72 | NA | 21.09 | NA | 17.97 | 14.38 |
| Std. | 0.03 | NA | 0.02 | NA | 0.02 | 0.04 |
| Coeff. Var. (%) | 0.11 | NA | 0.08 | NA | 0.09 | 0.26 |

| | Torque (Nm) | | CA50 (°CA) | | Spark (°CA) | |
|-----------------|-------------|--------|------------|--------|-------------|--------|
| | ETAS | dSPACE | ETAS | dSPACE | ETAS | dSPACE |
| Mean | 31.57 | NA | 12.25 | NA | -38.42 | NA |
| Std. | 3.08 | NA | 3.90 | NA | 0.93 | NA |
| Coeff. Var. (%) | 9.75 | NA | 31.83 | NA | 2.42 | NA |

| | Pmax (bar) | | CA Pmax (°CA) | | IMEP (bar) | |
|-----------------|------------|--------|---------------|--------|------------|--------|
| | ETAS | dSPACE | ETAS | dSPACE | ETAS | dSPACE |
| Mean | 9.22 | NA | 14.28 | NA | 1.09 | NA |
| Std. | 1.30 | NA | 2.34 | NA | 0.10 | NA |
| Coeff. Var. (%) | 14.15 | NA | 16.38 | NA | 8.92 | NA |

4.5.1.2 2000 RPM WOT

Figure 4.10A illustrates the need for the third current probe to distinguish and identify when injector # 1 was operating. With the higher load, the injectors operated for longer durations, which overlapped from one cylinder to the next. The slight peaks and dips in the main injector current probe are indications of multiple injectors overlapping and injecting at the same time. This can be noticed when comparing the current from cylinder # 1 with the main current from all injectors.

Figures 4.10B to F show that the spark angle has moved closer to TDC, when compared to the low load condition shown in section 4.5.1.1 (20.5° BTDC vs. 38.4° BTDC). The spark has to be advanced for the light load conditions since it is much harder to ignite/initiate combustion. Figures 4.10D and E indicate a constant spark angle. During the WOT conditions the PCM no longer applies a knock control algorithm, but instead switched to an open loop control method, where a fixed spark angle stored on the PCM is executed. The higher load point required an increase in the amount of energy released as shown in Figure 4.10F. Figures 4.10C and G both show that the spark ignition engine still has substantial peak cylinder pressure variation at high loads, but does now consistently exceed the motoring peak pressure.

Figure 4.11 does not show any fluctuations in the measurements that were observed in the previous data set, since ADACS commands and holds the pedal at its maximum angle, which forces the PCM to hold the throttle wide open. The fuel flow rate (Figure 4.11C) shows similar variation as present in the light load point. The measured air temperatures entering the engine also increased from the MAF to MAP sensor as previously observed (see Figure 4.11A). Figure 4.11H shows a slight steady offset in the measured AFR (0.24 AFR), while Figure 4.11D does not show such a significant offset (0.06 AFR). This could be due to sensor to sensor variation. The AFR under WOT conditions runs rich in order to produce the required torque and maintain durability. Figure 4.11B shows MAP and TIP sensors measured ambient pressure, as expected since the throttle is unable to create a restriction. See Table 4.4 for a summary of the results for this load point.

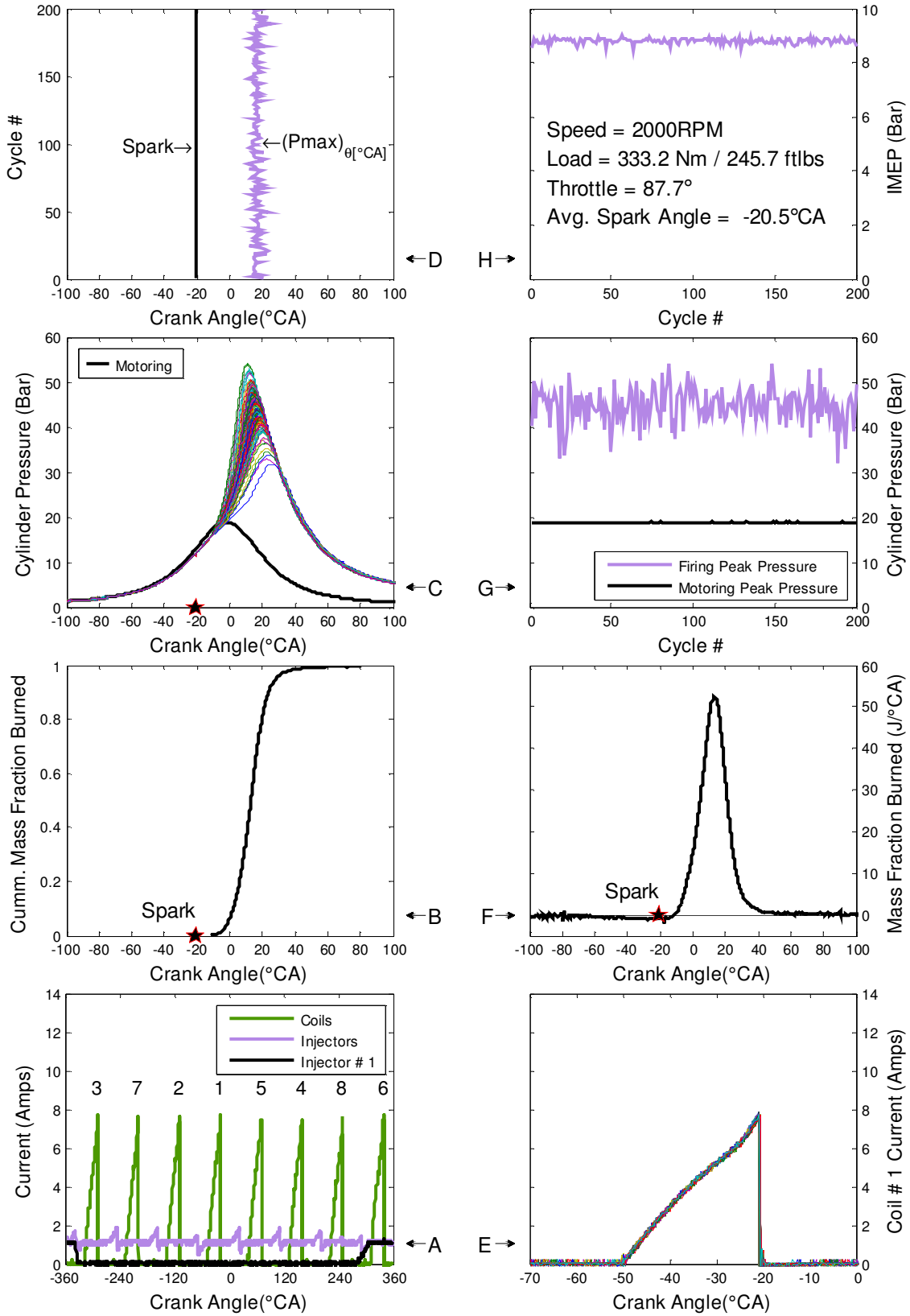


Figure 4.10: Production 2000 RPM WOT Combustion Data

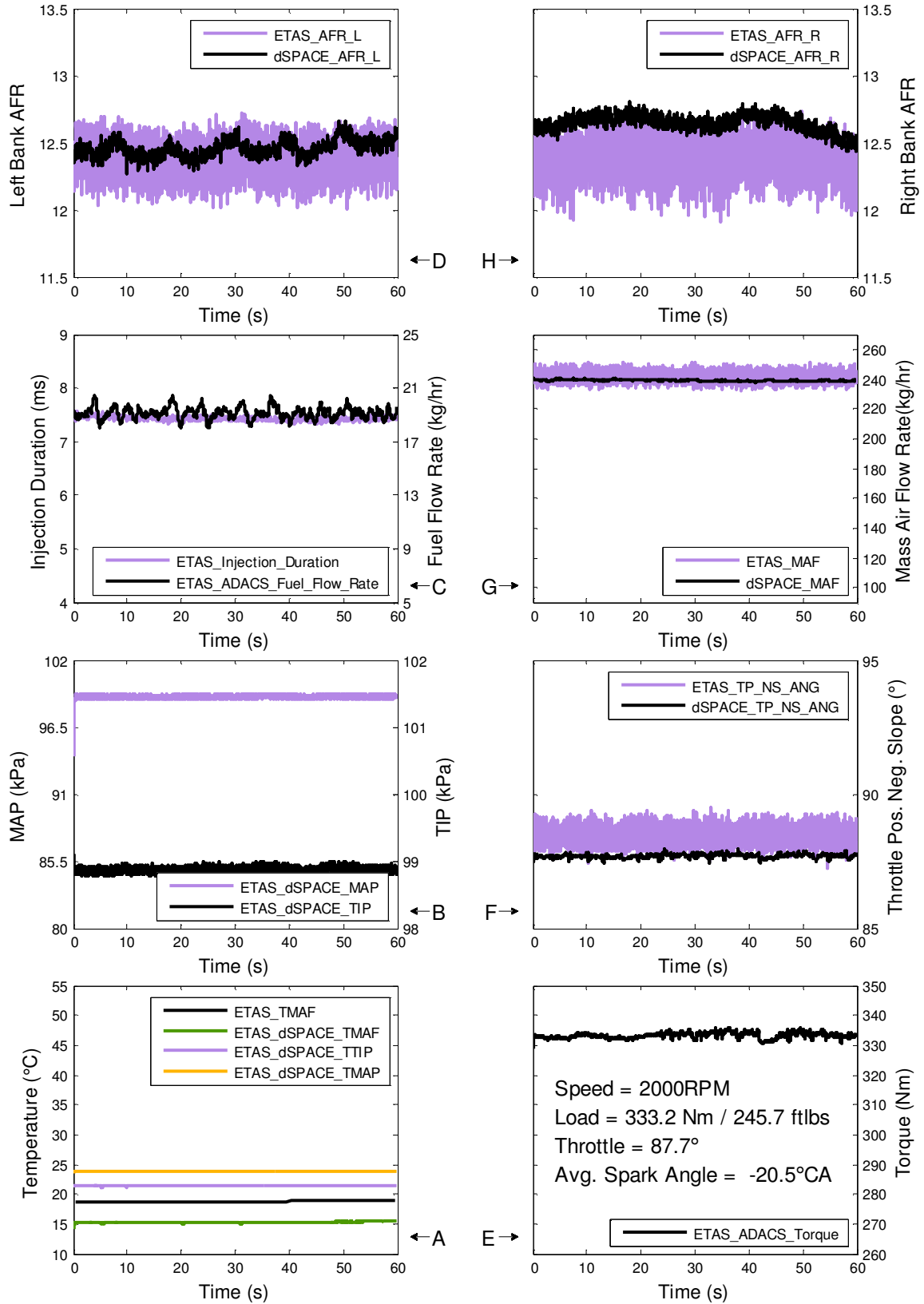


Figure 4.11: Production 2000 RPM WOT PCM Measurements

Table 4.4: 2000 WOT Production PCM Data Summary

| | Left Bank AFR | | | Right Bank AFR | | |
|-----------------|---------------|-----|--------|----------------|-----|--------|
| | ETAS | LA4 | dSPACE | ETAS | LA4 | dSPACE |
| Mean | 12.40 | NA | 12.46 | 12.40 | NA | 12.64 |
| Std. | 0.13 | NA | 0.06 | 0.14 | NA | 0.06 |
| Coeff. Var. (%) | 1.04 | NA | 0.49 | 1.16 | NA | 0.48 |

| | Inj. Dur. (ms) | | Fuel Flow (kg/hr) | | MAF (kg/hr) | |
|-----------------|----------------|--------|-------------------|--------|-------------|--------|
| | ETAS | dSPACE | ETAS | dSPACE | ETAS | dSPACE |
| Mean | 7.43 | NA | 19.12 | NA | 240.84 | 238.99 |
| Std. | 0.04 | NA | 0.43 | NA | 3.28 | 0.49 |
| Coeff. Var. (%) | 0.49 | NA | 2.23 | NA | 1.36 | 0.21 |

| | MAP (kPa) | | TIP (kPa) | | TP_NS (°) | |
|-----------------|-----------|--------|-----------|--------|-----------|--------|
| | ETAS | dSPACE | ETAS | dSPACE | ETAS | dSPACE |
| Mean | 99.00 | NA | 98.87 | NA | 88.36 | 87.69 |
| Std. | 0.15 | NA | 0.03 | NA | 0.34 | 0.08 |
| Coeff. Var. (%) | 0.15 | NA | 0.04 | NA | 0.39 | 0.09 |

| | TMAP (°C) | | TTIP (°C) | | TMAF (°C) | |
|-----------------|-----------|--------|-----------|--------|-----------|--------|
| | ETAS | dSPACE | ETAS | dSPACE | ETAS | dSPACE |
| Mean | 23.80 | NA | 21.34 | NA | 18.85 | 15.22 |
| Std. | 0.04 | NA | 0.06 | NA | 0.06 | 0.10 |
| Coeff. Var. (%) | 0.18 | NA | 0.29 | NA | 0.34 | 0.64 |

| | Torque (Nm) | | CA50 (°CA) | | Spark (°CA) | |
|-----------------|-------------|--------|------------|--------|-------------|--------|
| | ETAS | dSPACE | ETAS | dSPACE | ETAS | dSPACE |
| Mean | 333.17 | NA | 12.70 | NA | -20.49 | NA |
| Std. | 0.96 | NA | 2.19 | NA | 0.16 | NA |
| Coeff. Var. (%) | 0.29 | NA | 17.22 | NA | 0.77 | NA |

| | Pmax (bar) | | CA Pmax (°CA) | | IMEP (bar) | |
|-----------------|------------|--------|---------------|--------|------------|--------|
| | ETAS | dSPACE | ETAS | dSPACE | ETAS | dSPACE |
| Mean | 44.71 | NA | 16.67 | NA | 8.81 | NA |
| Std. | 3.84 | NA | 2.46 | NA | 0.10 | NA |
| Coeff. Var. (%) | 8.59 | NA | 14.73 | NA | 1.08 | NA |

4.5.2 dSPACE Controller Open Loop Results

4.5.2.1 1000 RPM –17.7 inHg (Gauge) OL Control

The coil current profile shown in Figures 4.13A and E was slightly lower for the entire right bank of the engine (cylinders 1 to 4). The coil currents did not exhibit these low currents, when controlled by the production PCM. After reviewing the coil driver box that was designed and assembled, the following observation was made. The coil current sensing resistor was bypassed and grounded (reversed wires). The leads used to measure the voltage across the current sensing resistor for all the coils on the LH bank of the driver box were reversed, which essentially removed the $0.2\ \Omega$ current sensing resistor for the entire LH bank of coils, increasing current flow. Assuming a constant coil/battery supply voltage of 13.8 volts, and using the maximum measured current for each bank (RH = 7 Amps, LH = 8 Amps) it is possible to apply ohms law ($V = IR$). This resulted in the following resistance values (RH = $1.971\ \Omega$, LH = $1.725\ \Omega$). Taking the difference between the two banks gave a delta of $0.246\ \Omega$, approximately the value of the current sensing resistor. See Figure 4.12 for a diagram of how the circuit was wired bypassing the coil current sensing resistor for the LH bank.

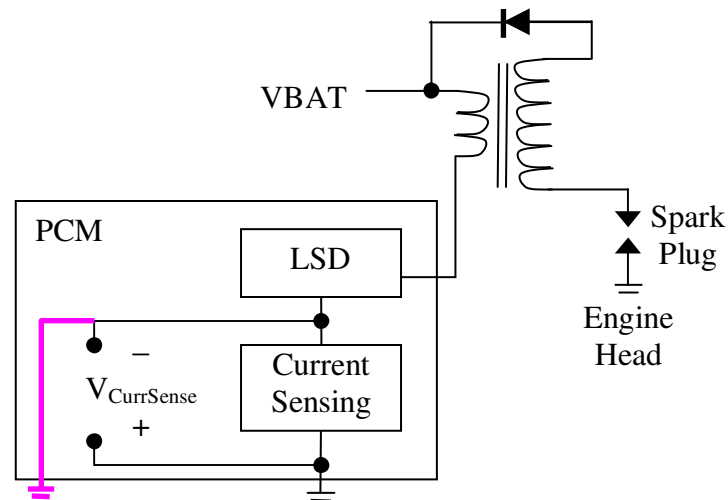


Figure 4.12: Bypassed Current Sensing Resistor by Voltage Measurement

A larger current sensing resistor effectively increases the time it takes for the coil to charge. In order to match the coil current charge time previously observed from the production engine controller, the current sensing resistor would need to be further reduced or a different IGBT driver with a lower resistance would be required. An alternate option would be to use the current sensing resistor to adjust the dwell time until the desired coil current is achieved. This was the original intention of the current sensing resistor, which was previously wired but not fully utilized. Figures 4.13D and E show the spark angle was held constant across all 200 cycles. The production engine controller was applying a CL controller with knock sensors as the feedback signal, to adjust the point of ignition. The REC controller was not setup for CL control of ignition.

The intake air temperature shows an increase of nearly 10°C (see Figure 4.14A) above the production PCM results (see Figure 4.9A). While testing the engine using the production PCM heat was radiated from the engine into the test cell, increasing the room temperature. The intake air temperature was not controlled, and was supplied by the ambient air in the test cell. With the intake ambient air already warm from testing the production engine, no further increases were observed between the MAF and TIP sensor. However, it was noticed that the MAP temperature did see an increase of 10°C when compared to the TIP sensor. This may be attributed to heat transfer from the engine, between the throttle and the intake port.

MAF, MAP, throttle position and fuel injection duration do not cycle in Figure 4.14 as was previously shown in Figure 4.9 (production PCM with ADACS controlling the pedal to achieve the desired MAP setpoint of -17.7 inHg (gauge)). When testing with the REC, the throttle body position was directly fixed at the desired angle to achieve the desired manifold vacuum as shown in Figure 4.14F. The fixed angle used for testing with the REC was slightly higher on average (0.24° above production), which resulted in the MAP, MAF, cylinder pressure, IMEP and torque showing similar results (slight increases see Table 4.5). To get the RH AFR to match the fuel injection duration was also increased.

The fuel flow rate data in Figure 4.14C shows that it was approximately the same for both systems (production/REC), which contradicts the commanded injection duration data which shows different durations. This is best explained by measuring the injection duration from Figure 4.14A as was discussed in section 4.5.1.1. Previously it was found that the commanded injection duration was approximately 2 ms for the production PCM, while the applied injection duration for dSPACE OL control was 2.08 ms. These injection duration values are more realistic and closer together, which supports the fuel flow rate measurements.

The RH AFR was controlled to the original setpoint (see Figure 4.14H), while both Figure 4.14D and H show that measuring the AFR with a third device such as the LA4 Lambda meter produces similar results (both readings and trends were nearly identical). The offset LH AFR shown in Figure 4.14D is a result of using the same injection duration for all cylinders and adjusting the injection duration to achieve only a desired RH AFR. It appears that the engine was receiving more air on the LH bank of the engine and would require increased fuel on this bank. Alternatively closing the throttle slightly and reducing injection duration on the RH bank, while increasing the LH bank injection duration could have provided closer results for both banks. Increasing the injection duration on the LH bank, will change the output torque and increase the fuel flow rate.

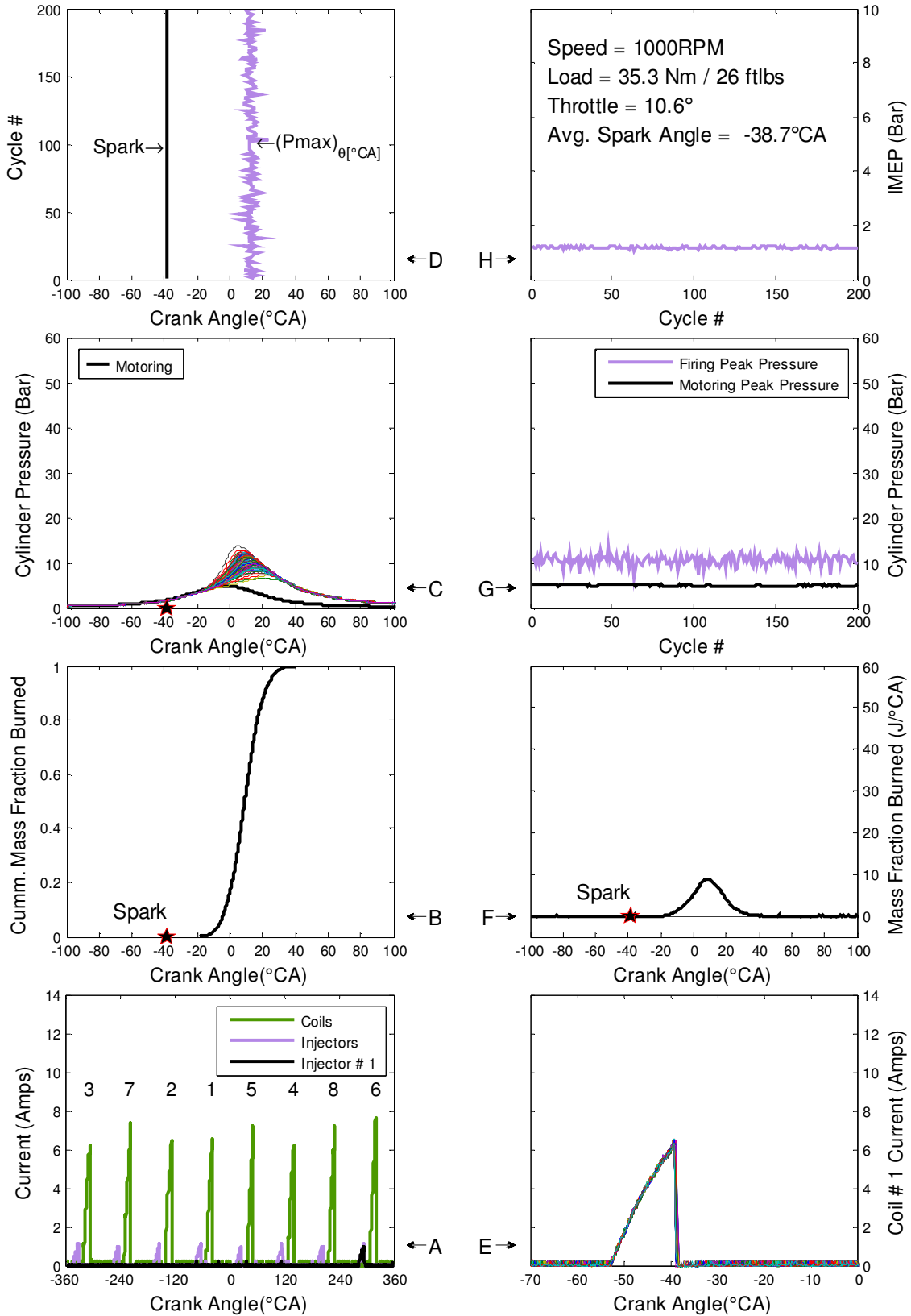


Figure 4.13: dSPACE OL 1000 RPM -17.7 inHg Combustion Data

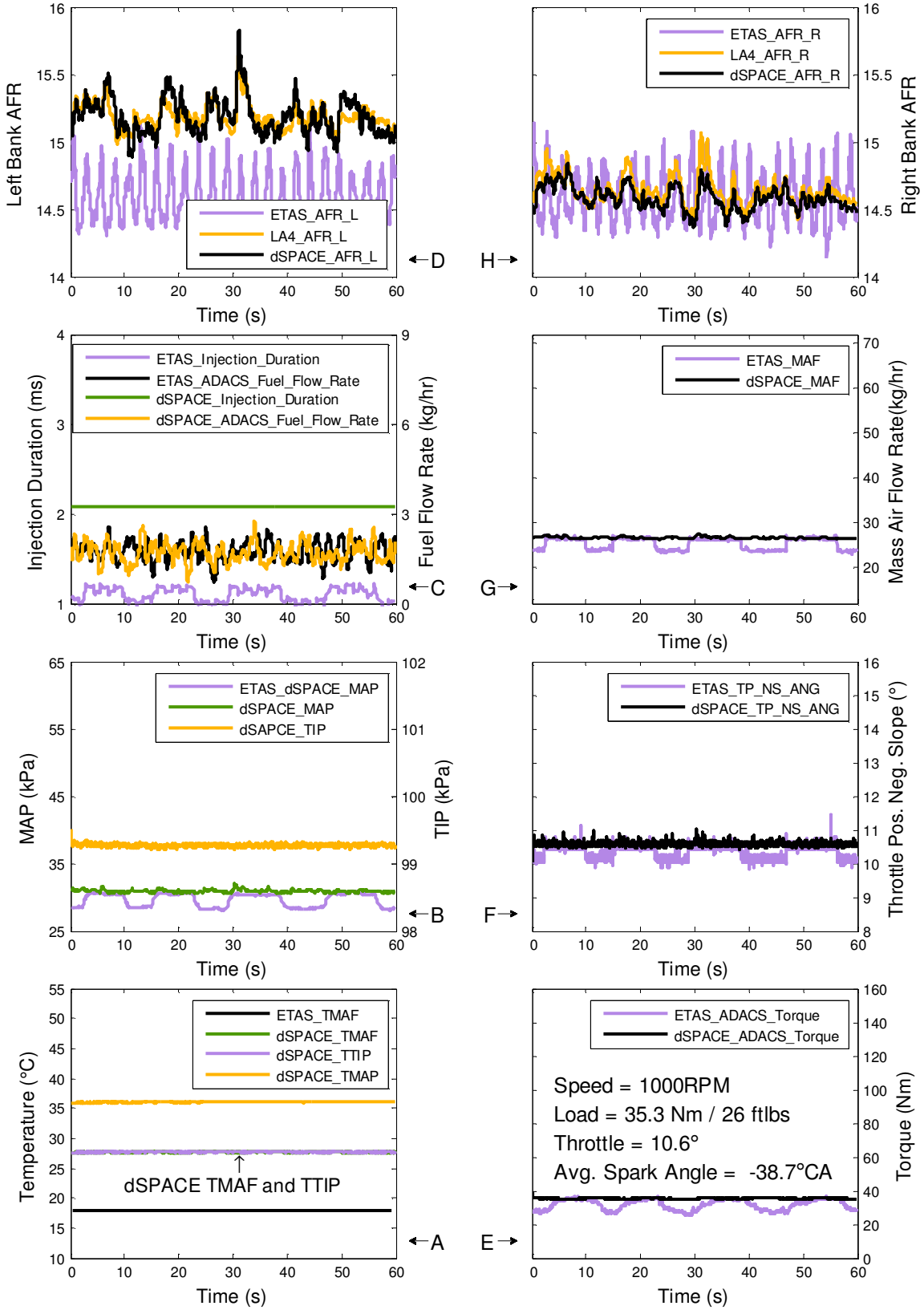


Figure 4.14: dSPACE OL 1000 RPM -17.7 inHg PCM Measurements

Table 4.5: 1000 RPM –17.7 inHg dSPACE OL Controller Data Summary

| | Left Bank AFR | | | Right Bank AFR | | |
|-----------------|---------------|-------|--------|----------------|-------|--------|
| | ETAS | LA4 | dSPACE | ETAS | LA4 | dSPACE |
| Mean | 14.59 | 15.19 | 15.19 | 14.58 | 14.64 | 14.58 |
| Std. | 0.18 | 0.10 | 0.14 | 0.18 | 0.11 | 0.09 |
| Coeff. Var. (%) | 1.25 | 0.63 | 0.92 | 1.26 | 0.76 | 0.61 |

| | Inj. Dur. (ms) | | Fuel Flow (kg/hr) | | MAF (kg/hr) | |
|-----------------|----------------|--------|-------------------|--------|-------------|--------|
| | ETAS | dSPACE | ETAS | dSPACE | ETAS | dSPACE |
| Mean | 1.10 | 2.08 | 1.74 | 1.70 | 25.30 | 26.66 |
| Std. | 0.07 | 0.00 | 0.33 | 0.34 | 1.30 | 0.21 |
| Coeff. Var. (%) | 6.74 | 0.00 | 19.21 | 20.00 | 5.13 | 0.79 |

| | MAP (kPa) | | TIP (kPa) | | TP_NS (°) | |
|-----------------|-----------|--------|-----------|--------|-----------|--------|
| | ETAS | dSPACE | ETAS | dSPACE | ETAS | dSPACE |
| Mean | 29.58 | 30.86 | 99.36 | 99.27 | 10.35 | 10.59 |
| Std. | 1.01 | 0.19 | 0.02 | 0.02 | 0.21 | 0.06 |
| Coeff. Var. (%) | 3.40 | 0.62 | 0.02 | 0.02 | 1.99 | 0.61 |

| | TMAP (°C) | | TTIP (°C) | | TMAF (°C) | |
|-----------------|-----------|--------|-----------|--------|-----------|--------|
| | ETAS | dSPACE | ETAS | dSPACE | ETAS | dSPACE |
| Mean | 30.72 | 36.02 | 21.09 | 27.69 | 17.97 | 27.68 |
| Std. | 0.03 | 0.03 | 0.02 | 0.01 | 0.02 | 0.02 |
| Coeff. Var. (%) | 0.11 | 0.09 | 0.08 | 0.05 | 0.09 | 0.07 |

| | Torque (Nm) | | CA50 (°CA) | | Spark (°CA) | |
|-----------------|-------------|--------|------------|--------|-------------|--------|
| | ETAS | dSPACE | ETAS | dSPACE | ETAS | dSPACE |
| Mean | 31.57 | 35.28 | 12.25 | 9.49 | -38.42 | -38.73 |
| Std. | 3.08 | 0.32 | 3.90 | 3.36 | 0.93 | 0.10 |
| Coeff. Var. (%) | 0.00 | 0.90 | 31.83 | 35.36 | 2.42 | 0.25 |

| | Pmax (bar) | | CA Pmax (°CA) | | IMEP (bar) | |
|-----------------|------------|--------|---------------|--------|------------|--------|
| | ETAS | dSPACE | ETAS | dSPACE | ETAS | dSPACE |
| Mean | 9.22 | 10.55 | 14.28 | 12.89 | 1.09 | 1.18 |
| Std. | 1.30 | 1.12 | 2.34 | 2.61 | 0.10 | 0.03 |
| Coeff. Var. (%) | 14.15 | 10.66 | 16.38 | 20.22 | 8.92 | 2.35 |

4.5.2.2 2000 RPM WOT OL Control

The same trends with the lower coil currents on the RH bank of the engine (cylinders 1 to 4) can be observed in Figures 4.15A and E. Figure 4.15F has a slight spike in the MFB near the location of the spark. The offset between the spike and the star (ignition point) is believed to be the time required for the combustion pressure wave to propagate from the spark plug to the in-cylinder pressure transducer. The remaining data in this figure does not pose any significant differences from the production engine results, which is supported by Table 4.6.

Figure 4.16A shows that the intake air temperature is slightly higher (by nearly 10°C). It is believed that the increased intake air temperature also resulted in a reduced torque output as shown in Figure 4.16E. The RH AFR between the LA4 Lambda meter and the dSPACE system shows a steady offset of approximately 0.36 AFR. The offset on the LH bank was not nearly as large. The LH AFR appears to have a cyclic trend which seems to match that from the AFR resistance measurements taken previously (see Figure 4.4). Further research may be conducted to understand the relationship of the AFR resistance under rich AFR conditions. The response near stoichiometric AFR did not show this behaviour.

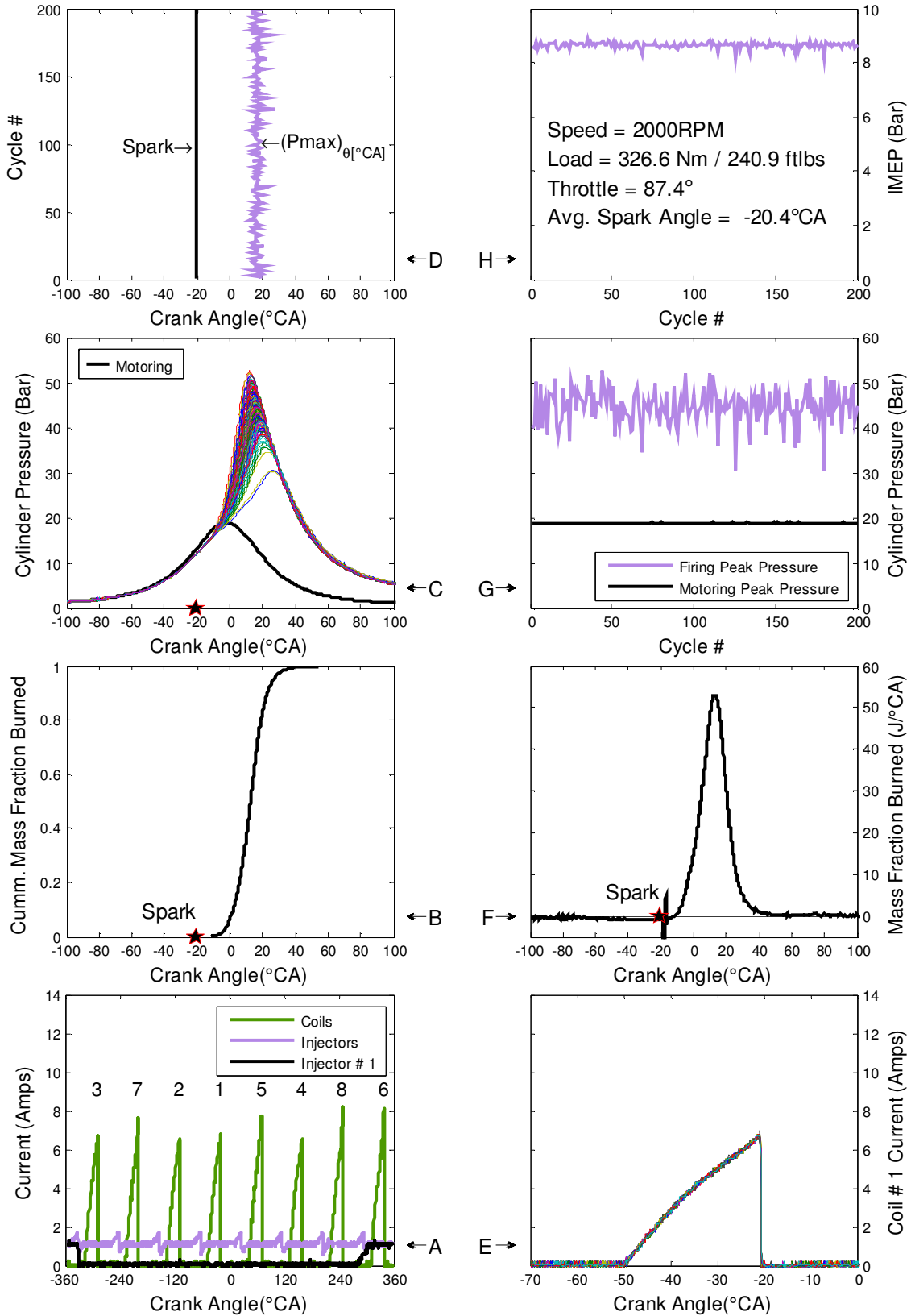


Figure 4.15: dSPACE OL 2000 RPM WOT Combustion Data

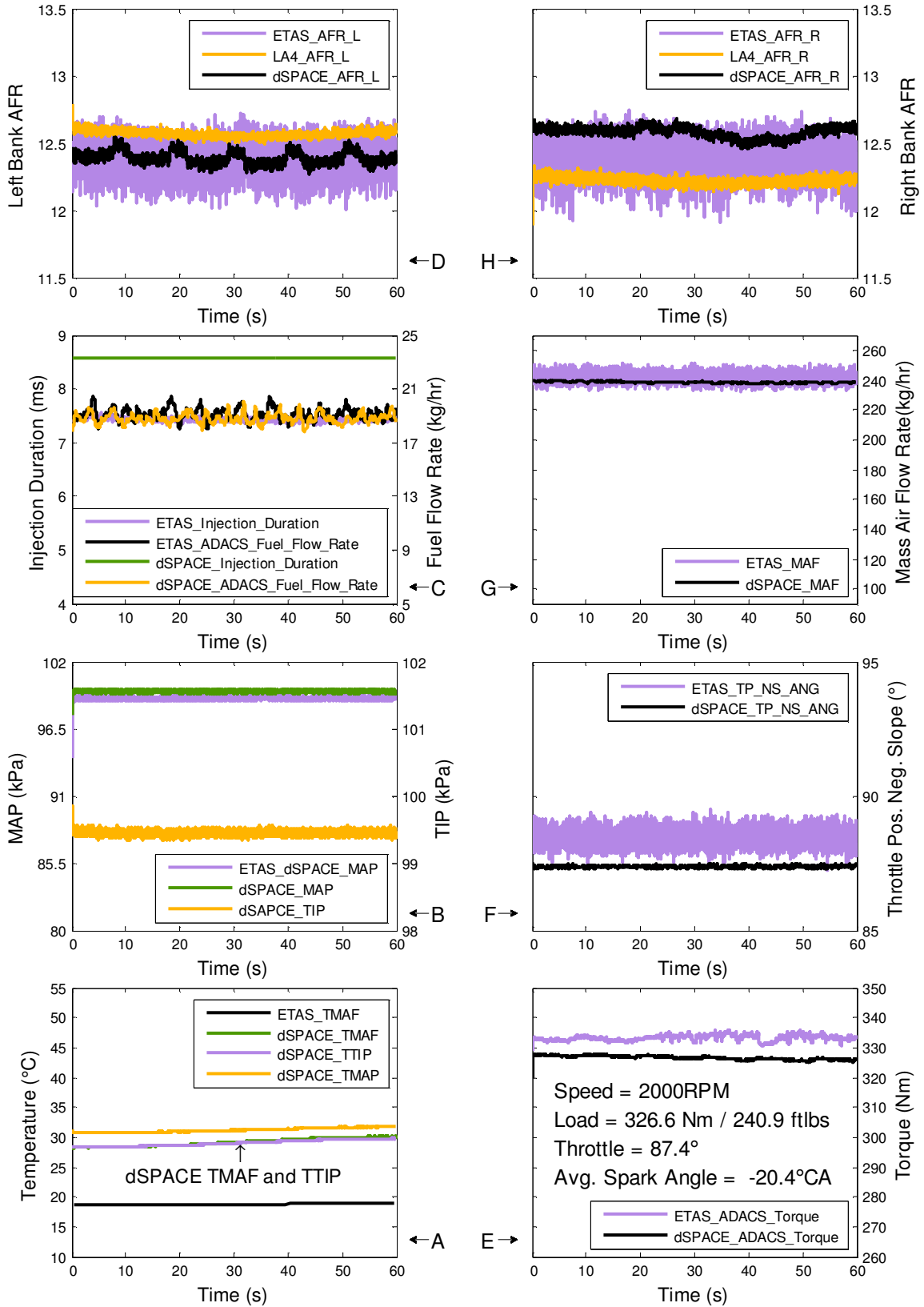


Figure 4.16: dSPACE OL 2000 RPM WOT PCM Measurements

Table 4.6: 2000 WOT dSPACE OL Control Data Summary

| | Left Bank AFR | | | Right Bank AFR | | |
|-----------------|---------------|-------|--------|----------------|-------|--------|
| | ETAS | LA4 | dSPACE | ETAS | LA4 | dSPACE |
| Mean | 12.40 | 12.57 | 12.39 | 12.40 | 12.22 | 12.58 |
| Std. | 0.13 | 0.02 | 0.05 | 0.14 | 0.03 | 0.04 |
| Coeff. Var. (%) | 1.04 | 0.19 | 0.38 | 1.16 | 0.23 | 0.33 |

| | Inj. Dur. (ms) | | Fuel Flow (kg/hr) | | MAF (kg/hr) | |
|-----------------|----------------|--------|-------------------|--------|-------------|--------|
| | ETAS | dSPACE | ETAS | dSPACE | ETAS | dSPACE |
| Mean | 7.43 | 8.56 | 19.12 | 18.80 | 240.84 | 238.30 |
| Std. | 0.04 | 0.00 | 0.43 | 0.39 | 3.28 | 0.55 |
| Coeff. Var. (%) | 0.49 | 0.00 | 2.23 | 2.06 | 1.36 | 0.23 |

| | MAP (kPa) | | TIP (kPa) | | TP_NS (°) | |
|-----------------|-----------|--------|-----------|--------|-----------|--------|
| | ETAS | dSPACE | ETAS | dSPACE | ETAS | dSPACE |
| Mean | 99.00 | 99.56 | 98.87 | 99.45 | 88.36 | 87.36 |
| Std. | 0.15 | 0.08 | 0.03 | 0.03 | 0.34 | 0.03 |
| Coeff. Var. (%) | 0.15 | 0.08 | 0.04 | 0.03 | 0.39 | 0.03 |

| | TMAP (°C) | | TTIP (°C) | | TMAF (°C) | |
|-----------------|-----------|--------|-----------|--------|-----------|--------|
| | ETAS | dSPACE | ETAS | dSPACE | ETAS | dSPACE |
| Mean | 23.80 | 31.20 | 21.34 | 29.03 | 18.85 | 29.15 |
| Std. | 0.04 | 0.34 | 0.06 | 0.50 | 0.06 | 0.66 |
| Coeff. Var. (%) | 0.18 | 1.09 | 0.29 | 1.72 | 0.34 | 2.27 |

| | Torque (Nm) | | CA50 (°CA) | | Spark (°CA) | |
|-----------------|-------------|--------|------------|--------|-------------|--------|
| | ETAS | dSPACE | ETAS | dSPACE | ETAS | dSPACE |
| Mean | 333.17 | 326.56 | 12.70 | 12.43 | -20.49 | -20.40 |
| Std. | 0.96 | 0.62 | 2.19 | 2.45 | 0.16 | 0.00 |
| Coeff. Var. (%) | 0.00 | 0.19 | 17.22 | 19.68 | 0.77 | 0.00 |

| | Pmax (bar) | | CA Pmax (°CA) | | IMEP (bar) | |
|-----------------|------------|--------|---------------|--------|------------|--------|
| | ETAS | dSPACE | ETAS | dSPACE | ETAS | dSPACE |
| Mean | 44.71 | 44.61 | 16.67 | 16.60 | 8.81 | 8.66 |
| Std. | 3.84 | 3.87 | 2.46 | 2.48 | 0.10 | 0.11 |
| Coeff. Var. (%) | 8.59 | 8.68 | 14.73 | 14.95 | 1.08 | 1.24 |

CHAPTER 5

CONCLUSIONS AND RECOMMENDATIONS

The implementation of dSPACE hardware and software for engine control is a viable alternative to using a production engine controller or NI hardware with a standard PC [26]. dSPACE provides the end-user with the tools (various MATLAB blocks) to allow integration of the desired control algorithms with the MicroAutoBox and RapidPro hardware. The user must still have knowledge of the fundamental principles that are being applied underneath the supplied dSPACE blocks and hardware purchased. An understanding of the algorithms used for engine crank angle synchronization, position and speed are critical. The same applies when attempting to control the throttle body (H-Bridge driver) or take AFR measurements with an AFR sensor such as the UHEGO sensor. Prior to using any hardware or software to control an engine, one should have reasonable understanding of the engine cycle and the combustion process, in addition to a working knowledge of the hardware and associated controls.

5.1 Conclusions

The main objectives of this thesis were achieved as follows:

- 1) A REC was successfully designed using MATLAB/Simulink and compiled into c-code using Real-Time Workshop and TargetLink. The compiled code was flashed (programmed) onto the dSPACE MicroAutoBox and RapidPro Hardware, which successfully replaced the production engine controller
- 2) The production engine controller and REC were both operated under a series of test conditions successfully
- 3) The results from the operating points were compared using cylinder pressure combustion data along with data measured by the engine control modules and were found to show similar results

5.2 Recommendations for Future Work

Engine control has endless opportunities for improvement and advancement, as the search will always continue in an effort to reduce emissions, while improving the fuel economy, response, output and cost effectiveness of the engine. From the work that has been conducted thus far the following recommendations are suggested in order of importance:

- 1) Improve AFR measurement noise concerns due to heater resistance measurement
- 2) Continue to implemented bank specific AFR control
- 3) Implement CL dwell time control with primary coil current sensing resistors
- 4) Continue to develop intake air temperature measurement corrections
- 5) Implement CL spark advance/ignition timing using knock sensor feedback
- 6) Add the ability to estimate MAF using the MAP sensor/speed density equations
- 7) Configure the RPCU to allow both port and direct injection methods
- 8) Implement cam phasing control
- 9) Replace PID controllers with different controllers including sliding mode control, H-infinity control, neural networks to name a few
- 10) Update the controller to account for the effect of EGR on MAF
- 11) Implement an estimate of combustion torque and detect misfire by analyzing the speed from the engine crank position sensor [7, 8]
- 12) Implement turbocharger vane position/wastegate position control in order to achieve the desired boost setpoint or prevent the turbocharger from going beyond its speed limits
- 13) Develop an engine simulator bench to allow for new algorithms to be developed outside of a test cell that could simplify the testing of controller algorithms.

APPENDICES

APPENDIX I : 5.0L TEST ENGINE FIGURES

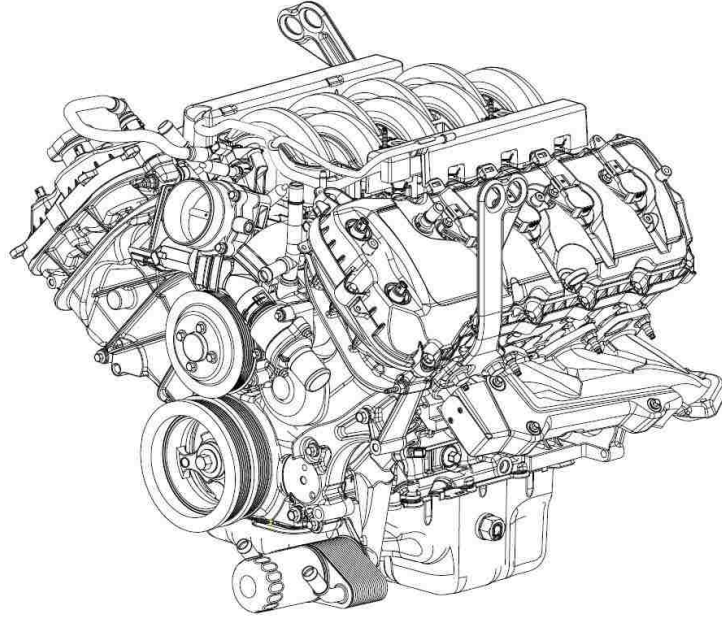


Figure A-I-1: Ford F150 5.0L Engine Front View [55]

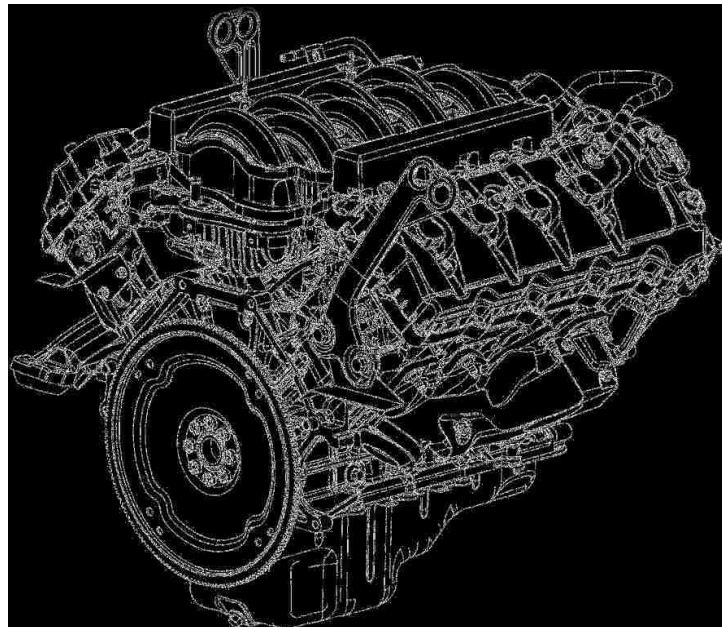


Figure A-I-2: Ford F150 5.0L Engine Rear View [55]

APPENDIX II : HARDWARE SETUP DIAGRAMS

The following diagrams describe the setup used for the production engine controller, the dSPACE hardware controller and the combustion system that was used.

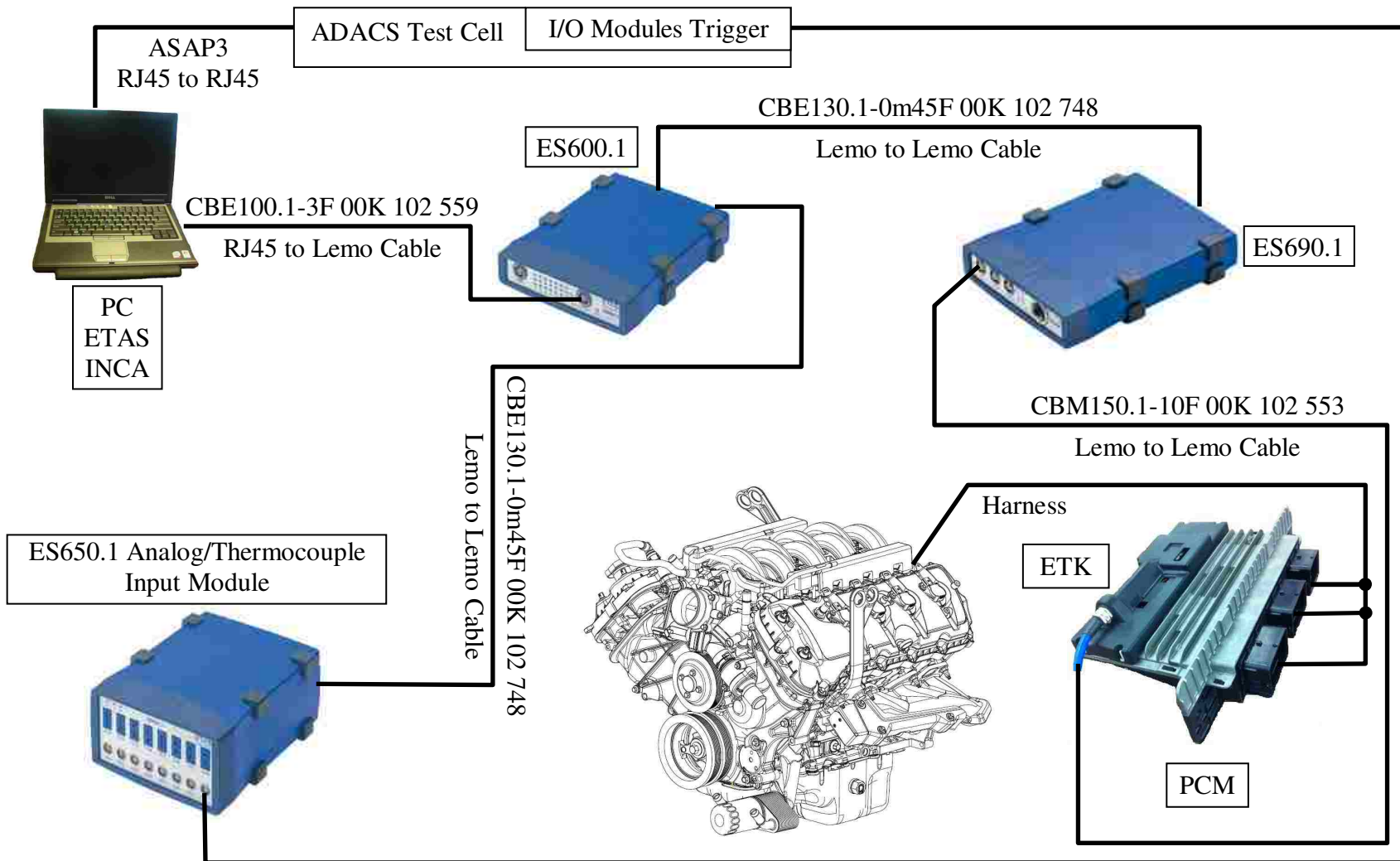


Figure A-II-1: ETAS Hardware Setup for Production PCM with Images

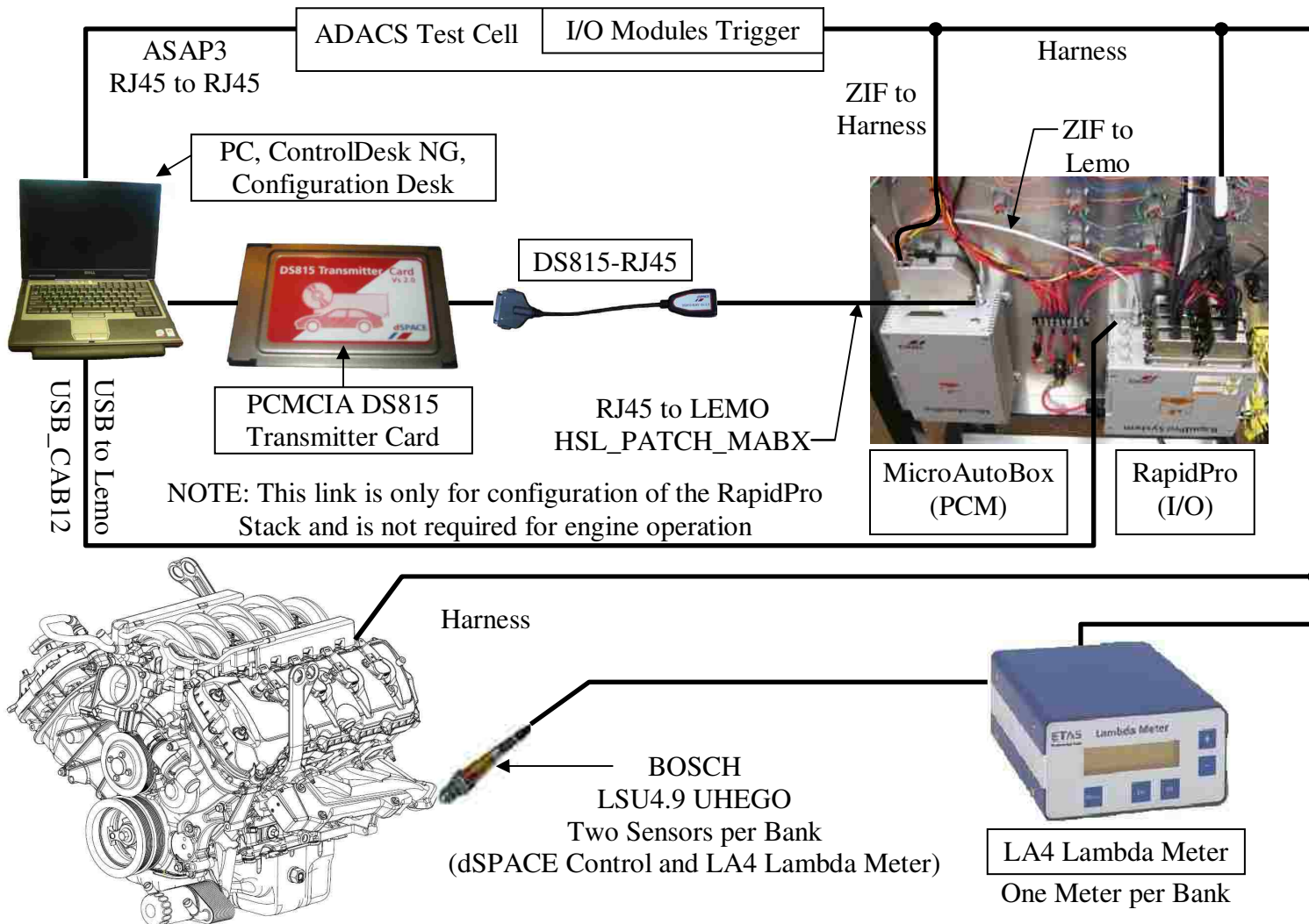


Figure A-II-2: dSPACE MicroAutoBox and RapidPro Hardware Setup with Images

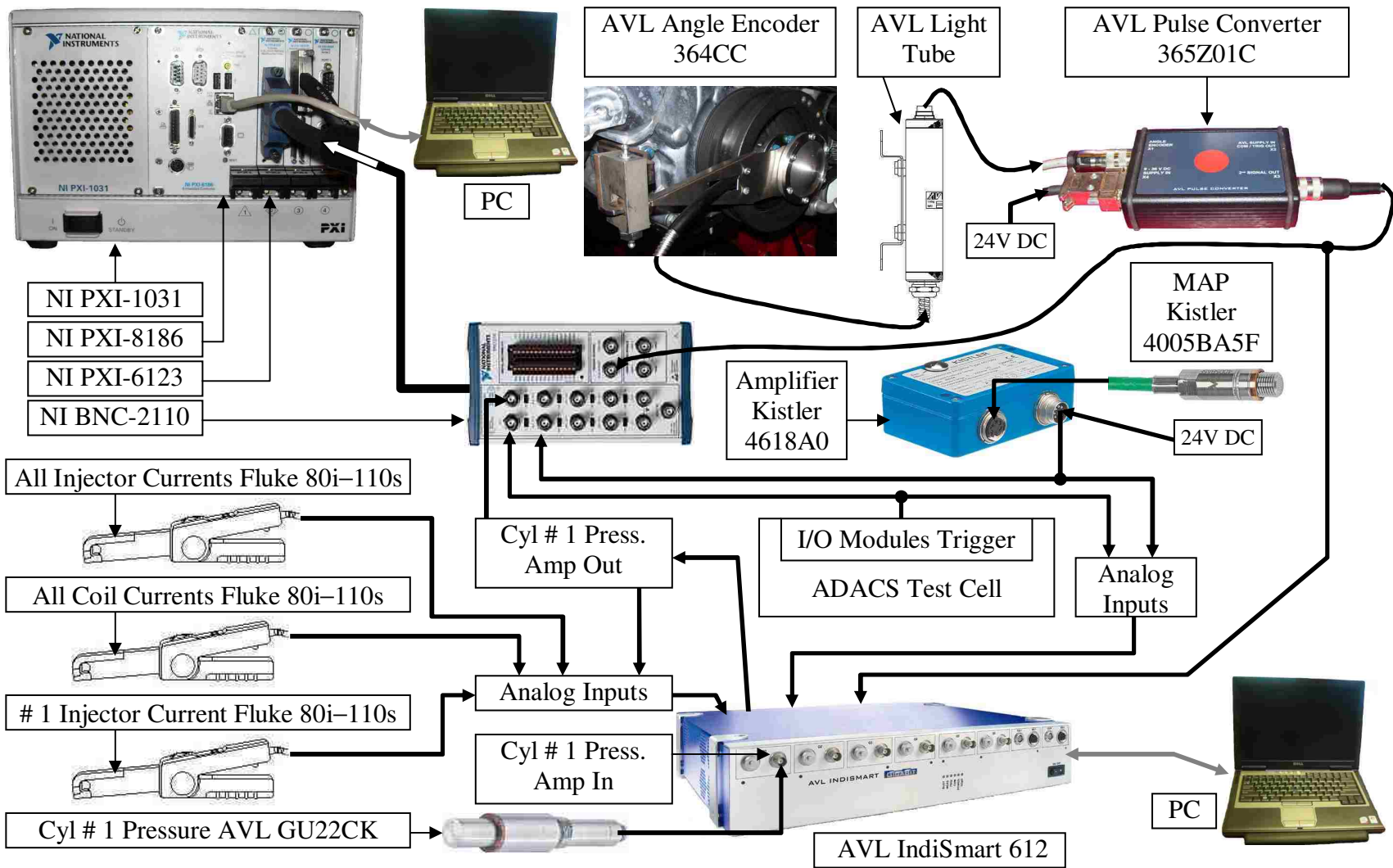


Figure A-II-3: Cylinder Pressure Measurement, AVL and NI Integration with Images

APPENDIX III : SYNCHRONIZATION ROUTINE/EXAMPLE

Synchronization occurs by first detecting the location of the missing tooth and assuming a predefined crank angle start position (310 or 670°CA) [60]. Then the engine controller detects the first cam tab that follows the missing tooth, the angle is logged relative to the assumed missing tooth position (310°CA). This detected cam angle is compared back to a table of expected angles and if the angle matches within a tolerance ($\pm 15^\circ\text{CA}$) the engine will be synchronized and calculation of the crank angle domain can continue. It is important to note that synchronization is only possible when the cam is not phased (base timing is required). If synchronization failed, the next attempt would occur when the next missing tooth is detected. Only this time an offset of 360°CA will be added to the assumed start angle ($310 + 360 = 670^\circ\text{CA}$). Table A-III-1 shows two examples using a single cam for synchronization (EA = Expected Angle, MA = Measured Angle). The table on the left shows sync achieved on the first attempt and the table on the right shows sync failing on the first attempt and achieved on the second attempt. Figure A-III-1 shows a flow diagram of this synchronization process.

Table A-III-1: Left – Sync First Try, Right – Sync Second Try, adapted from [60]

| Sync First Attempt Assuming 310 | | | Failed Sync, First Attempt Assuming 310 | | | Sync Second Attempt Assuming 310 + 360 | | |
|------------------------------------|-----|-------|---|-----|-------|---|-----|-------|
| EA | MA | Match | EA | MA | Match | EA | MA | Match |
| 400 | 401 | Yes | 400 | 371 | No | 10 | 11 | Yes |
| 460 | 459 | Yes | 460 | 459 | Yes | 100 | 99 | Yes |
| 640 | 640 | Yes | 640 | 582 | No | 220 | 222 | Yes |
| 10 | 11 | Yes | 10 | 641 | No | 280 | 281 | Yes |
| 100 | 99 | Yes | 100 | 41 | No | 400 | 401 | Yes |
| 220 | 222 | Yes | 220 | 99 | No | 460 | 459 | Yes |
| 280 | 281 | Yes | 280 | 280 | No | 640 | 640 | Yes |

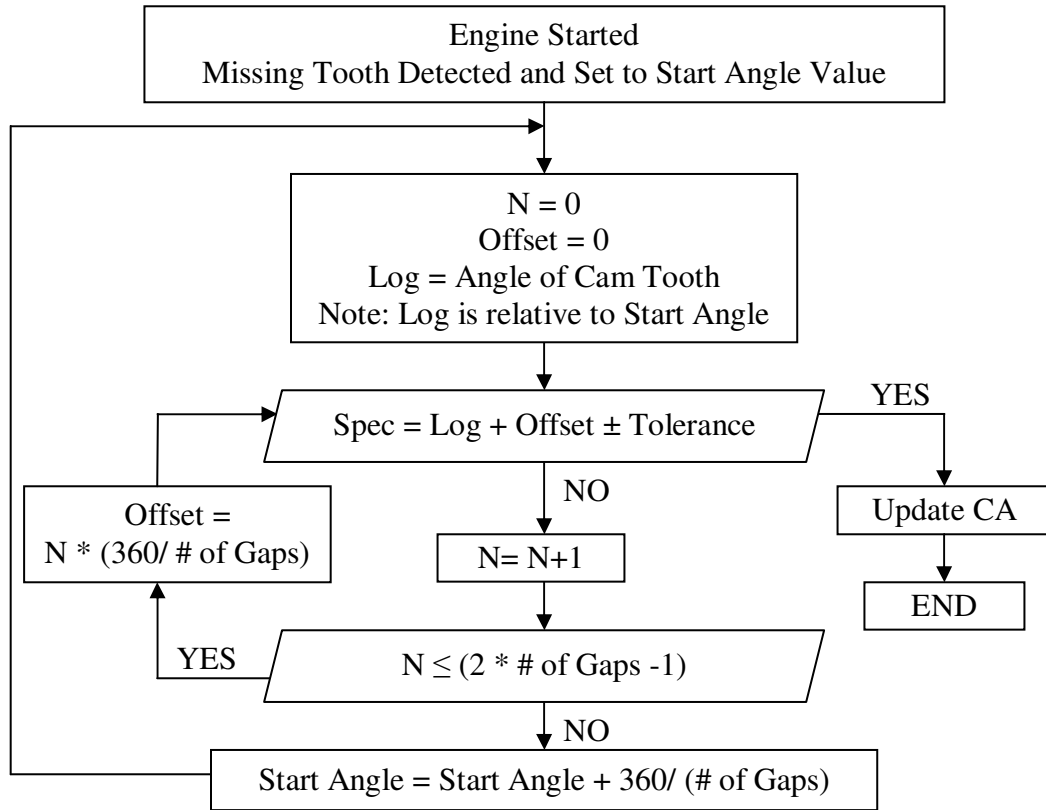


Figure A-III-1: CAD Calculation, Synchronization Flowchart, adapted from [60]

APPENDIX IV : CRANK AND CAM SENSORS & SIGNALS

VRS & Hall Sensor Signals

Figure A-IV-1 shows one entire combustion cycle and the cam and crank position sensor signals. This is a typical pattern that can be expected from an engine that uses a VRS for the crank position, and cams. Hall sensors are used on this engine for the intake cam sensors. The crank reluctor wheel in this example has the 36-1 tooth profile while the cam sensors have a total of 7 teeth. The crank position sensor (CKP), LH and RH Exhaust (Exh) use the VRS, while the RH and LH Intake (Int) use Hall sensors. The following data was collected by motoring the engine at 1000 RPM.

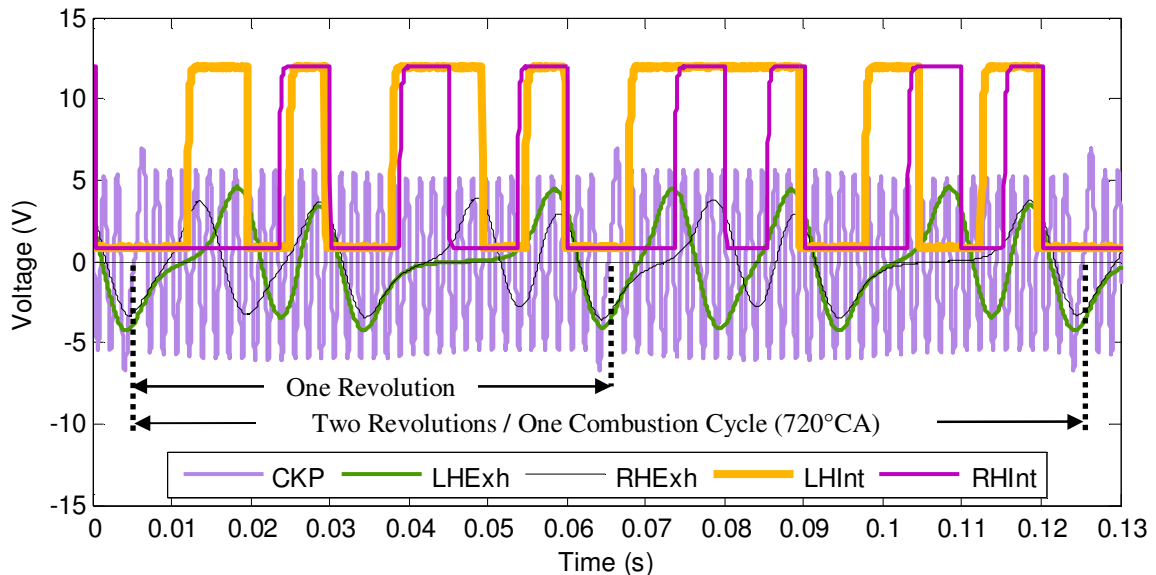


Figure A-IV-1: VRS and Hall Signals, Crank (36-1) and Cam (7 Teeth)

Magneto-resistive Sensor

Magneto-resistive sensors may also be referred to as AMR (Anisotropic Magneto Resistive) sensors. These sensors are not common in industry, but have been designed and used on some vehicles. This sensor will not be reviewed in detail as it is not being used for the research in this thesis. However, it could be used for detecting both crank and cam position [3, 82-84].

APPENDIX V : CYLINDER HEAD TEMPERATURE (CHT)

During the design of an internal combustion engine, the cylinder heads are typically instrumented with thermocouples in every possible location in order to determine the most optimal position to locate the CHT sensor. The CHT replaces the Engine Coolant Temperature (ECT) sensor, which was installed in a coolant passage on the engine and the Engine Oil Temperature (EOT) sensor, which was installed in an oil gallery. By sensing the CHT it is possible to infer the ECT and EOT by mapping out the engine at various conditions and forming a relationship between the measured temperatures. Switching to the CHT sensor eliminates the interaction between fluids and sensors, which can lead to cost savings and increased reliability. Figure A-V-1 shows a cross section of a CHT thermistor that is commonly used. When the engine is started up the CHT sensor provides feedback to the PCM on the engines temperature. When the engine is cold the PCM will inject extra fuel (fuel enrichment) in order to help the engine start and warm up quicker. This is required as cold cylinder walls promote fuel precipitation. The precipitated fuel on the walls then does not participate in the combustion process [3, 5]. See APPENDIX XI for a sensor transfer function.

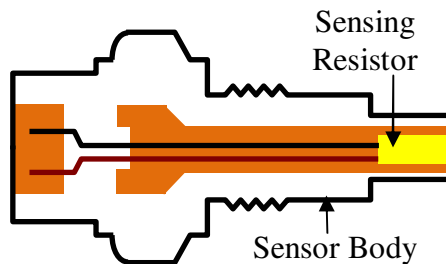


Figure A-V-1: Cylinder Head Temperature (CHT) Sensor, adapted from [3]

APPENDIX VI : ADDITIONAL MAP SENSOR DETAILS

Figure A-VI-1 shows how the various pressure sensor designs can be installed in a sensor, while Figure A-VI-2 shows how the piezo-resistive elements may be arranged on the sensor to get the proper orientation. Note the bottom right image is the cross section A-A. It is important to note that the thermistor for IAT measurement has been incorporated into this one component.

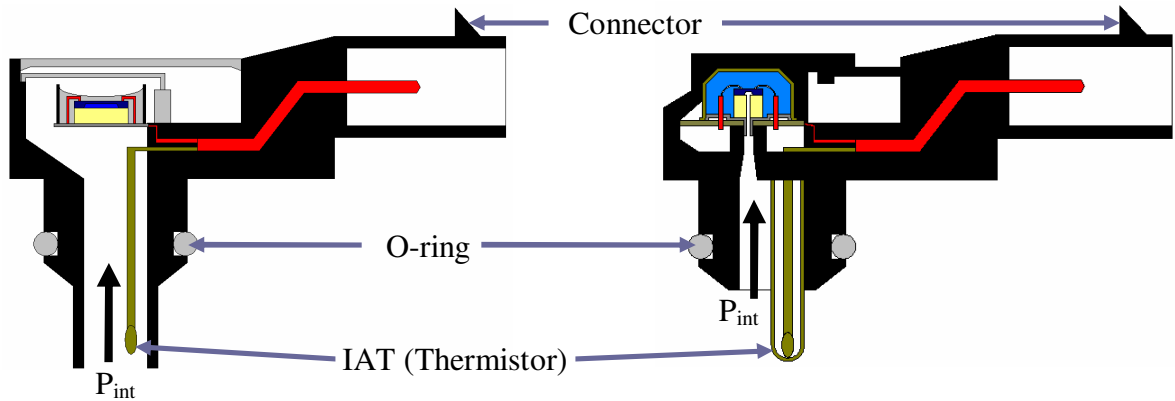


Figure A-VI-1: MAP Sensor with IAT Construction, adapted from [3]

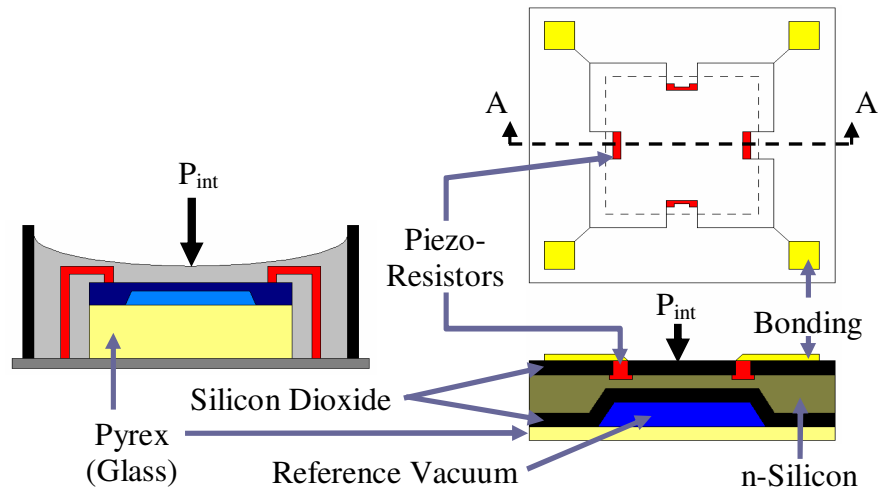


Figure A-VI-2: Pressure Sensor Piezo-Resistor Arrangement, adapted from [5, 6]

APPENDIX VII : KNOCK SENSOR CONSTRUCTION AND OPERATION

The most popular way to detect engine knock in production engines is by using a piezoceramic knock sensor as can be seen in the Figure A-VII-1 where 'v' is the vibration caused by combustion knock. Typically knock sensor wires are twisted pairs and shielded up to the PCM similar to the VRS sensor to help reduce noise.

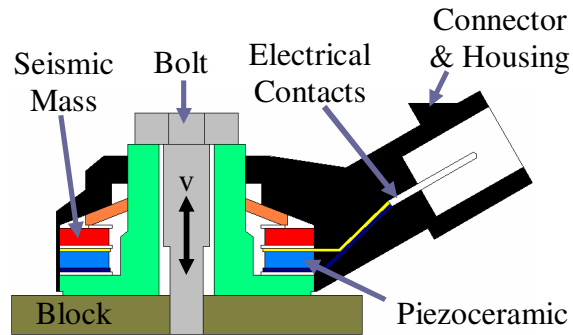


Figure A-VII-1: Piezoceramic Knock Sensor Design, adapted from [3]

To understand the operation of a knock sensor requires an understanding of the piezoelectric effect. The piezoelectric effect states that a suitably sized quartz crystal with an applied alternating voltage will vibrate at the same frequency as the applied alternating voltage. This vibration is due to the motor effect which states that the quartz crystal will undergo a mechanical strain from the constantly reversing polarity. The knock sensor utilizes the opposite process, which is to apply a strain through an applied force such as engine knock. This changes the crystal's polarity and generates a voltage and is known as the generator effect [6].

APPENDIX VIII : ADDITIONAL HEGO/UHEGO SENSOR INFO

Figure A-VIII-1 and Figure A-VIII-2 compare the construction of the BOSCH LSF4 planar HEGO to the BOSCH LSU4 UHEGO. The LSU4 sensor has an additional zirconia layer with added oxygen pumping electrodes. Lean measurements on the UHEGO are shown by positive pumping currents while rich measurements have negative pumping currents. For each type of EGO sensor, it is important that the sensor has access to ambient air through the body of the sensor for the reference cell. When the reference air supply is plugged or lost the sensor will stop working properly.

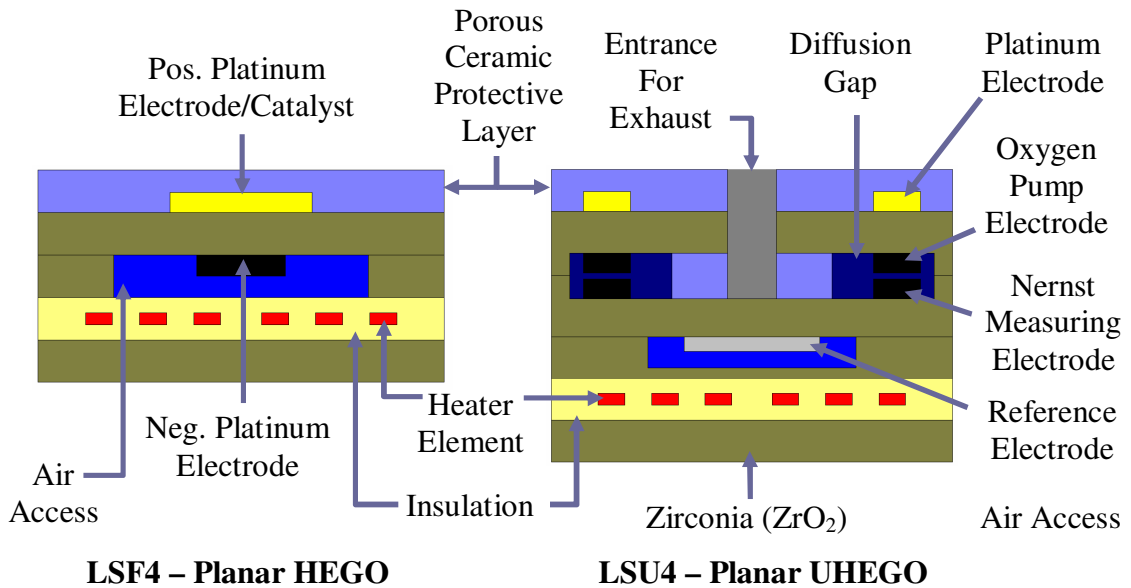


Figure A-VIII-1: HEGO & UHEGO Sensing Element Construction, adapted from [3]

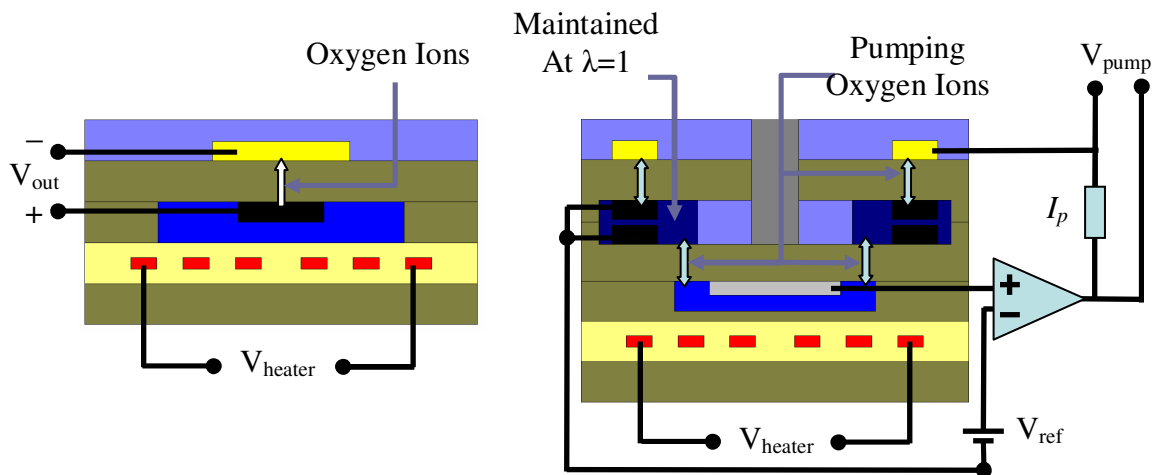


Figure A-VIII-2: HEGO and UHEGO Operation, adapted from [3]

There are two control units available in order to properly measure the pumping current and the sensor resistance. These units include the BOSCH AWS and the BOSCH CJ125. The information below pertains to the BOSCH CJ125 when used with the LSU4.9 sensor as the following formulas change with different sensors. The work contained in this thesis will be using the CJ125 and LSU4.9 hardware with a λ range of 0.75 to air.

$$R = \frac{UR - 0.294}{0.00245} \quad \text{Eq. A-VIII-1}$$

$$I_p = \frac{UA - 1.5}{61.9 * \nu} \quad \text{Eq. A-VIII-2}$$

Where: UR is the output voltage of the CJ125 control unit representing the resistance and UA is the output voltage of the CJ125 control unit representing the pumping current, $\nu = 8$ if the λ range will be between 0.65 and air or $\nu = 17$ if using a λ range between 0.8 and air. Setting ν as 17 gives 1052.3, however dSPACE recommended using 1053 [40] instead with its hardware as the range is 0.75 to air, leading to:

$$I_p = \frac{UA - 1.5}{1053} \quad \text{Eq. A-VIII-3}$$

APPENDIX IX : ADDITIONAL MAF SENSOR DESIGNS

Volume Air Flow (VAF)/Vane-Type

The VAF sensor was one of the first devices designed to measure the flow of air into the engine (see Figure A-IX-1). As the air passed through the intake, it would force the VAF sensor flap to rotate about a shaft, which was connected to a potentiometer. Rotating the flap would change the resistance of the potentiometer and by using a voltage divider similar to Figure 2.7, it was possible to measure the air flow rate. The flap would return to the closed position by using the force of a helical spring. The second flap was put there to help reduce flutter of the flap assembly. This sensor also has an idle bypass valve which could be adjusted using a screw [6, 10].

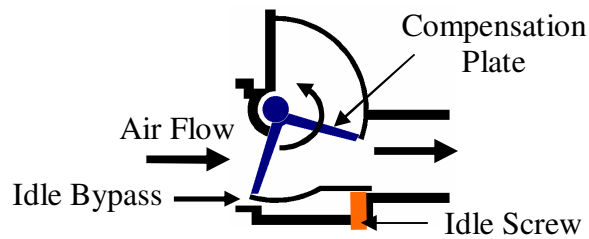


Figure A-IX-1: Volume Air Flow (VAF) Sensor, adapted from [6, 10]

Hot-Wire Type

Hot-Wire type MAF sensors were designed to reduce the number of moving components. These sensors required a wire screen to smooth the flow out. The thermistor measured the air temperature and was also referred to as a cold wire (see Figure A-IX-1). When powered up, the Hot-Wire was held constantly between 100 and 200°C (212–392°F) above the thermistor/cold wire. As the airflow increased, the circuit increased the current to maintain a constant delta between the thermistor and the hot wire. The equations required to convert the current flow into a mass air flow were derived in [85]. When ignition is turned off, the hot wire can be heated up to high temperatures to burn off any contaminants [10].

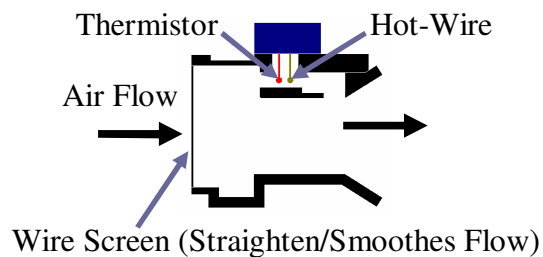


Figure A-IX-1: Hot Wire Mass Air Flow (MAF) Sensor Design, adapted from [10]

APPENDIX X : SPARK PLUG AND COIL CONSTRUCTION

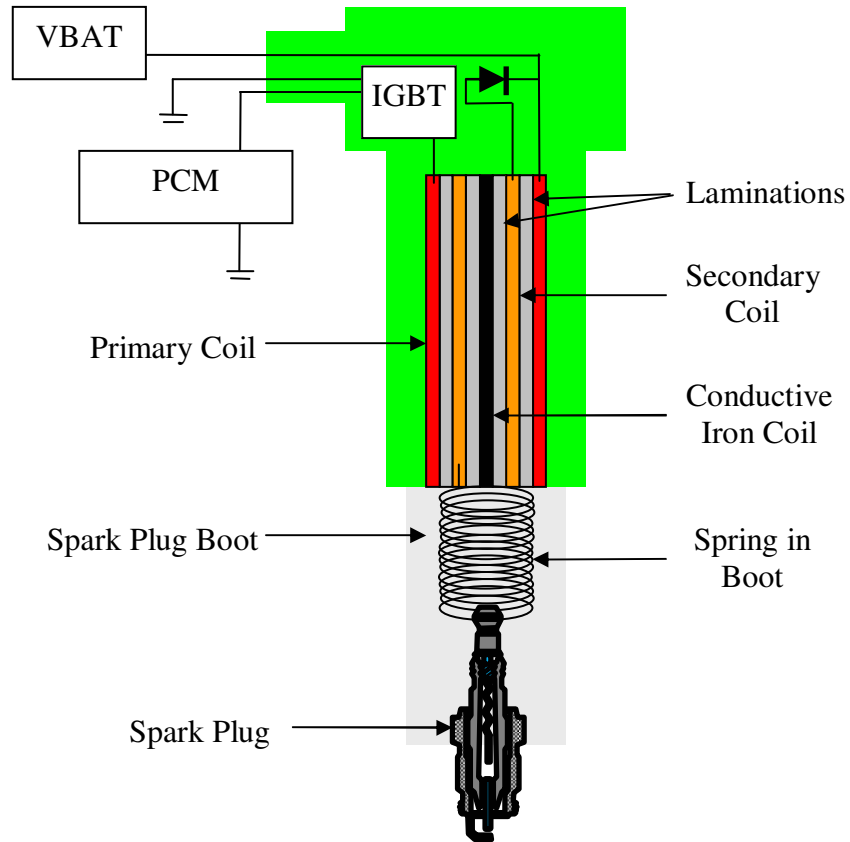


Figure A-X-1: Cross Section - Driver on Pencil Coil on Plug, adapted from [3]

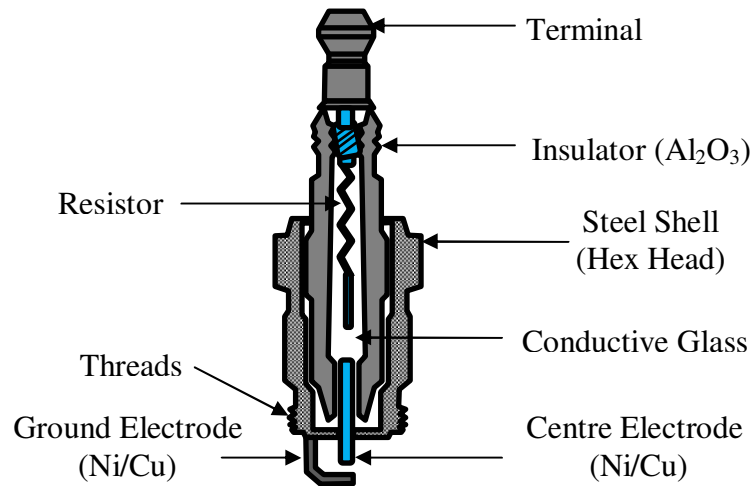


Figure A-X-2: General Spark Plug Cross Section, adapted from [3, 10]

APPENDIX XI : ACTUATOR/SENSOR TRANSFER FUNCTIONS

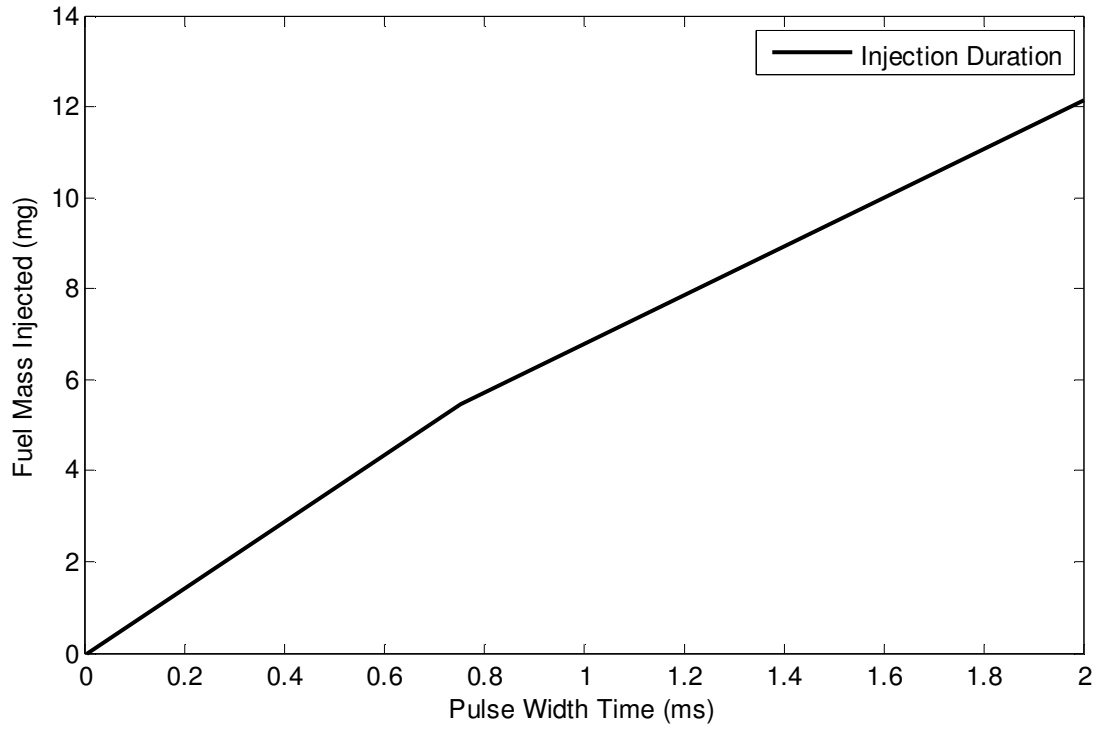


Figure A-XI-1: Fuel Injector Pulse Width Transfer Function

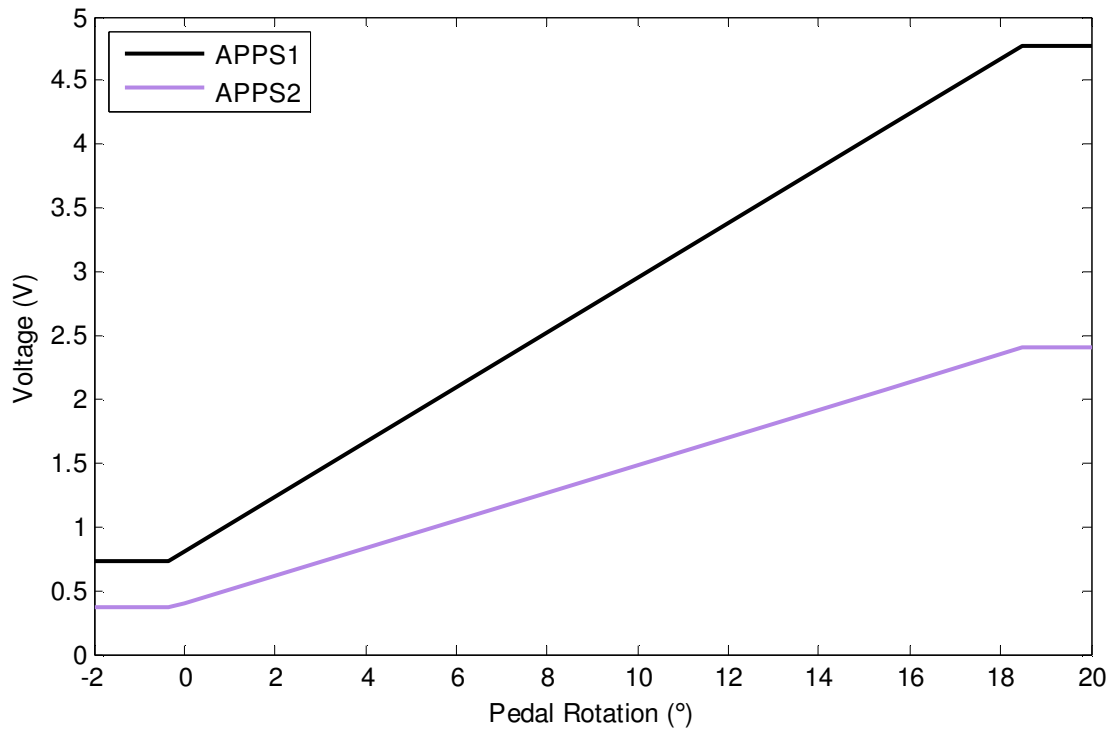


Figure A-XI-2: Pedal Rotation Transfer Function

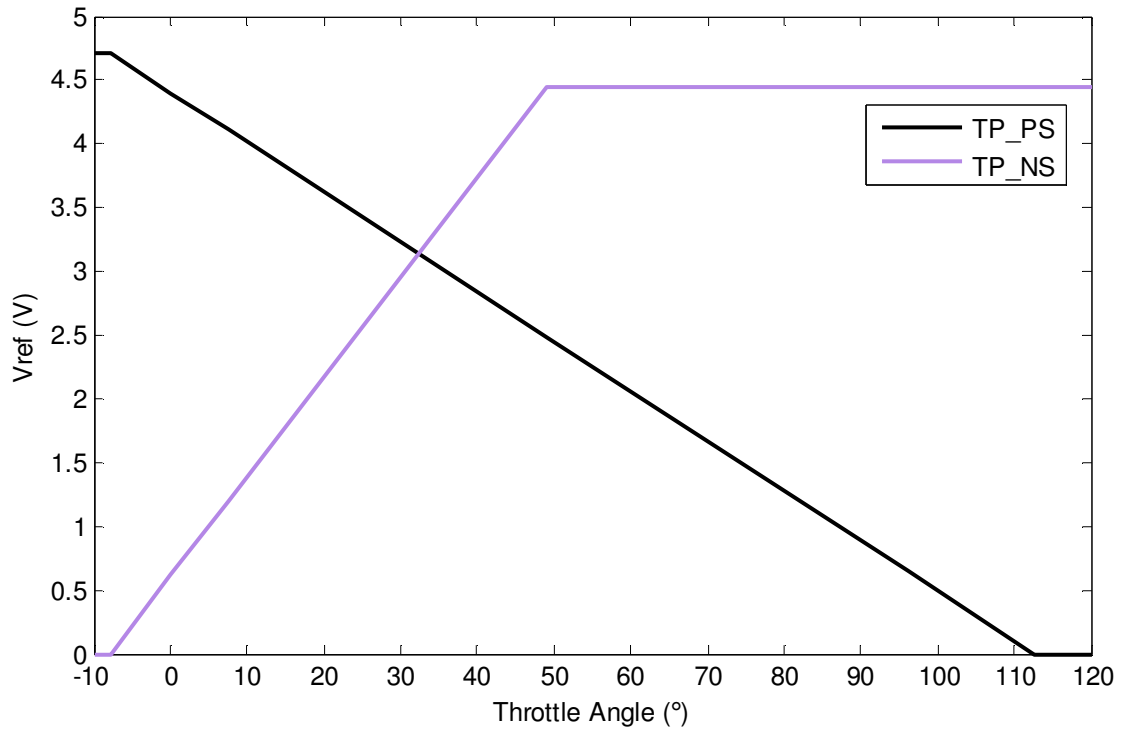


Figure A-XI-3: Throttle Position Sensor Transfer Function

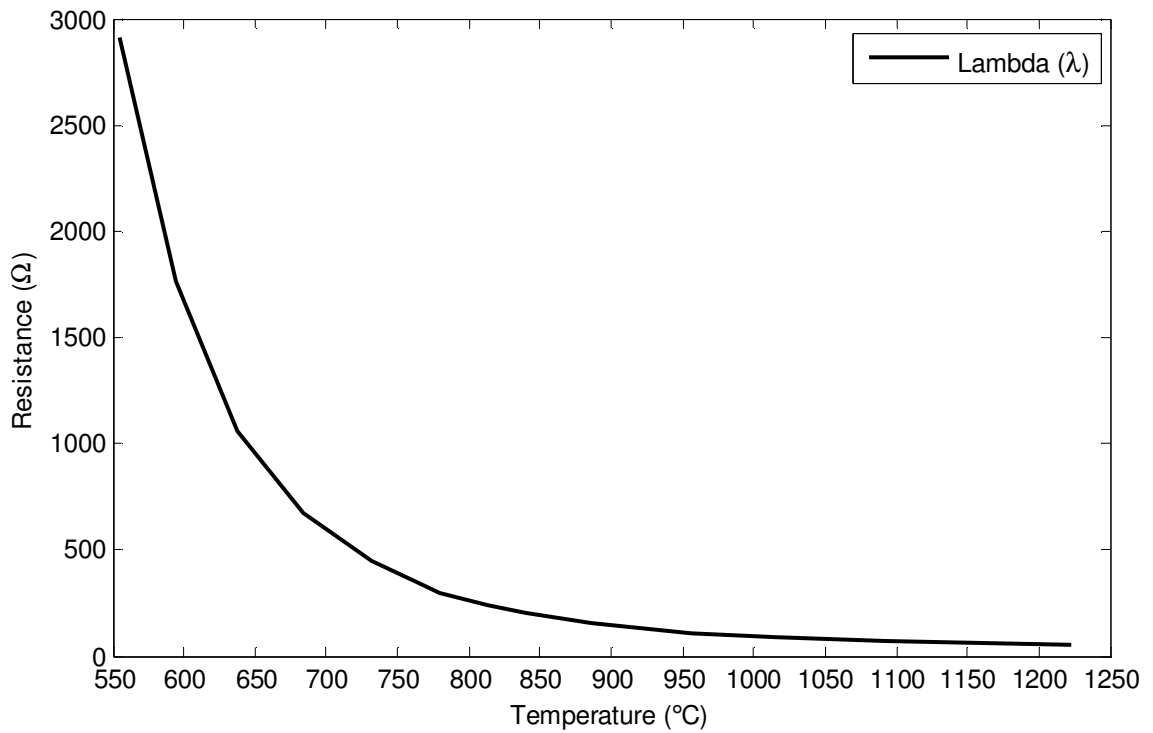


Figure A-XI-4: BOSCH LSU 4.9 Sensor Temperature Transfer Function

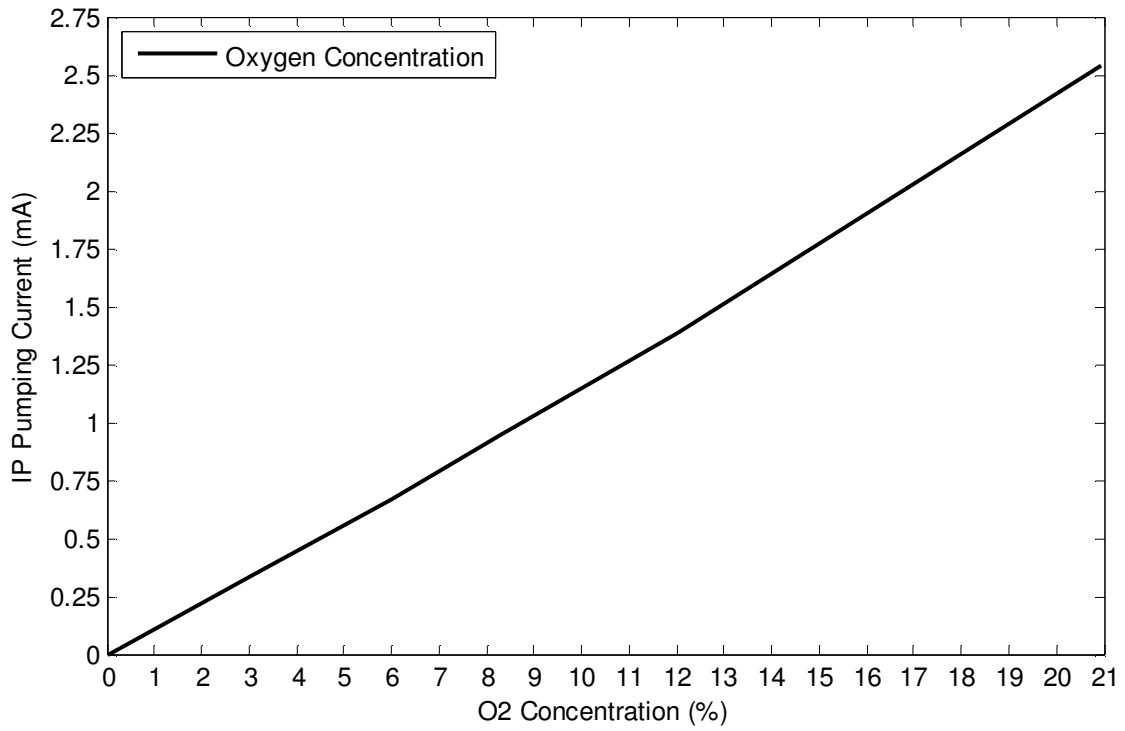


Figure A-XI-5: BOSCH LSU 4.9 O₂ Concentration Transfer Function

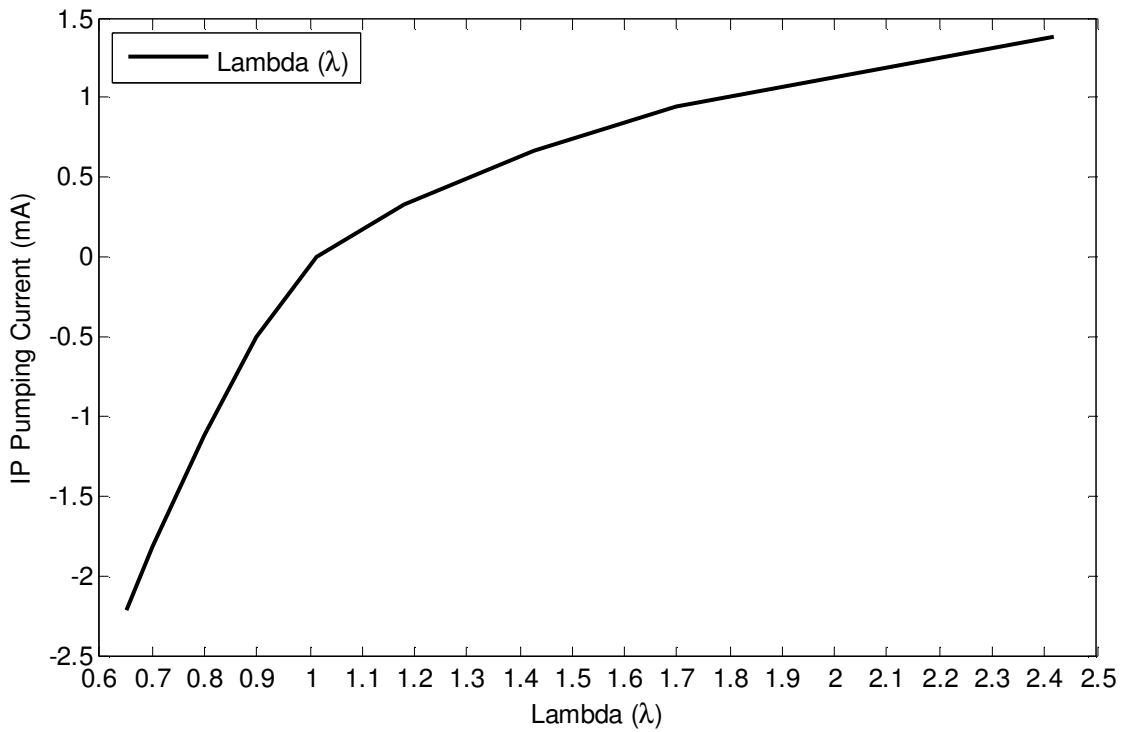


Figure A-XI-6: BOSCH LSU 4.9 Lambda (λ) Transfer Function

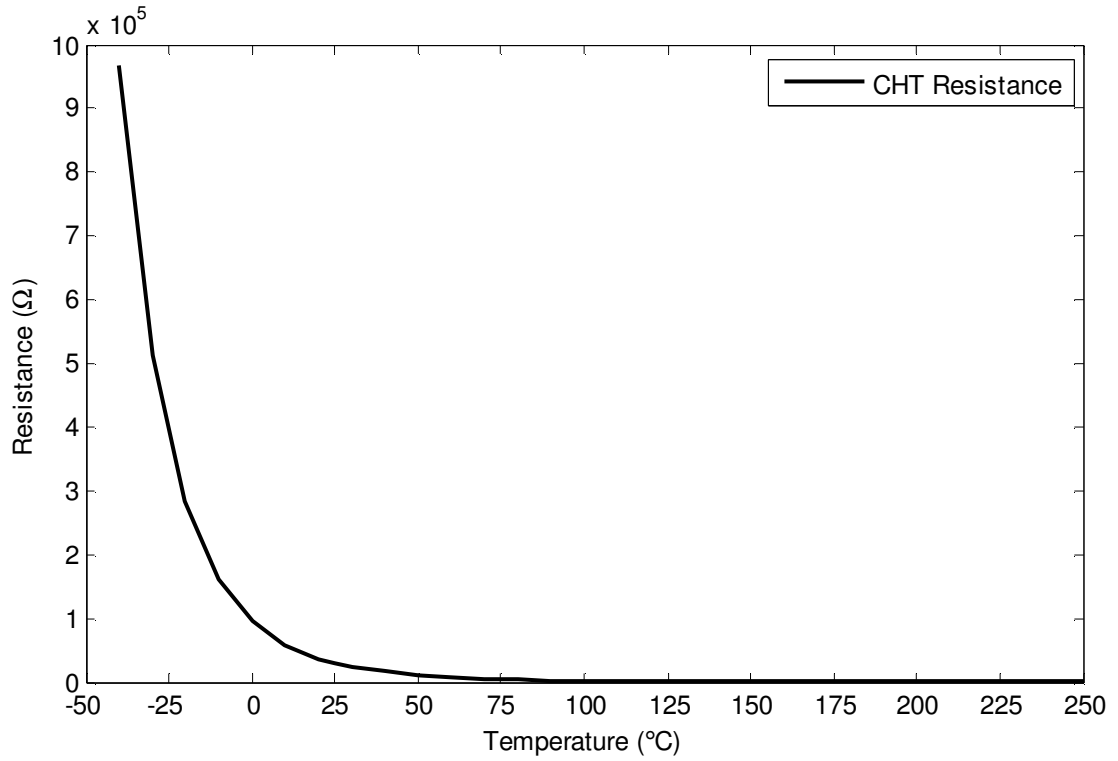


Figure A-XI-7: CHT Sensor Resistance Transfer Function

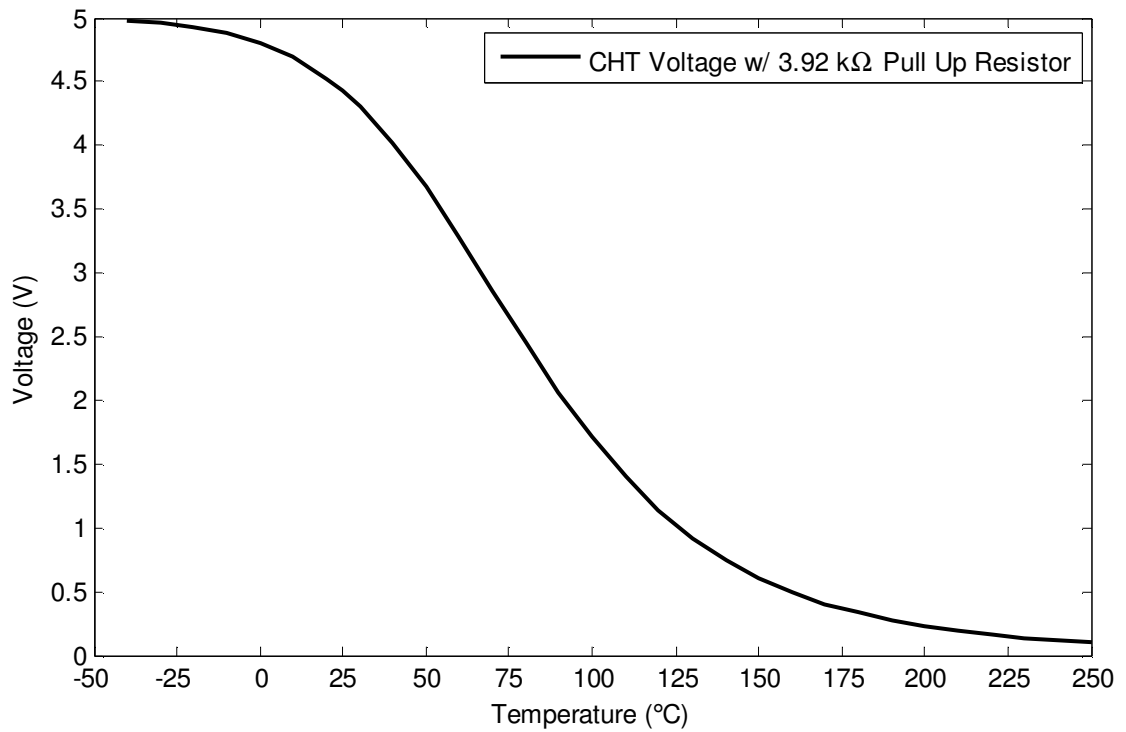


Figure A-XI-8: CHT Sensor Voltage Transfer Function

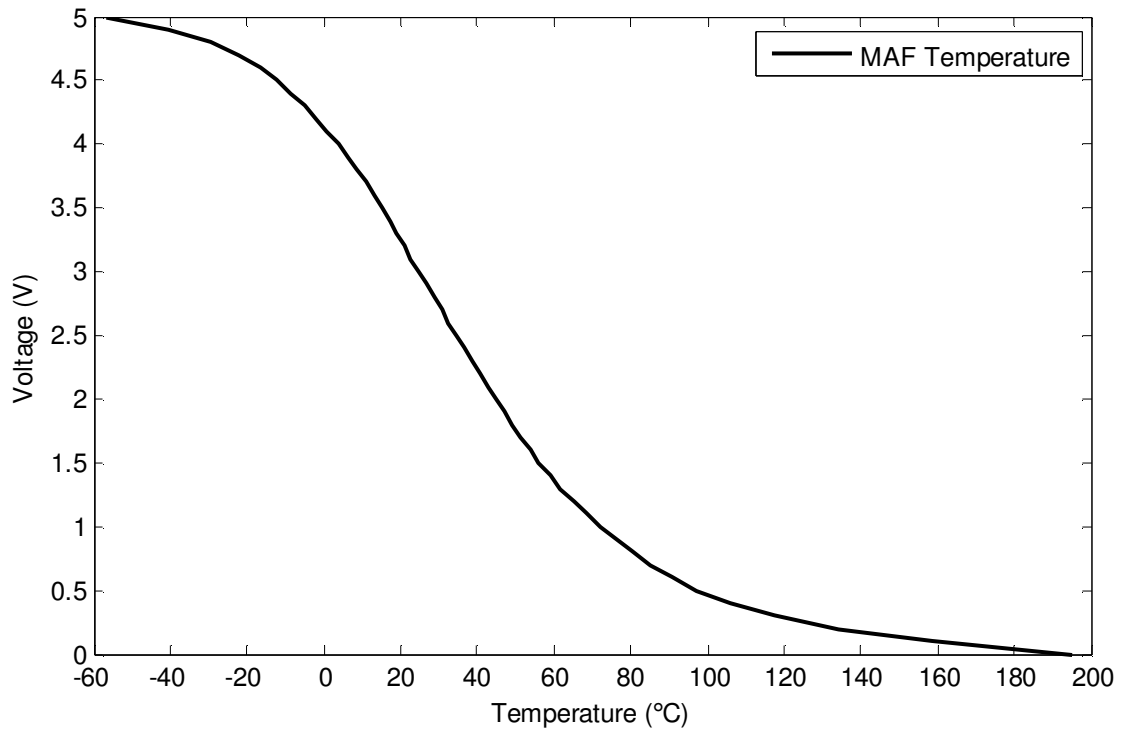


Figure A-XI-9: MAF Sensor Voltage Temperature Transfer Function

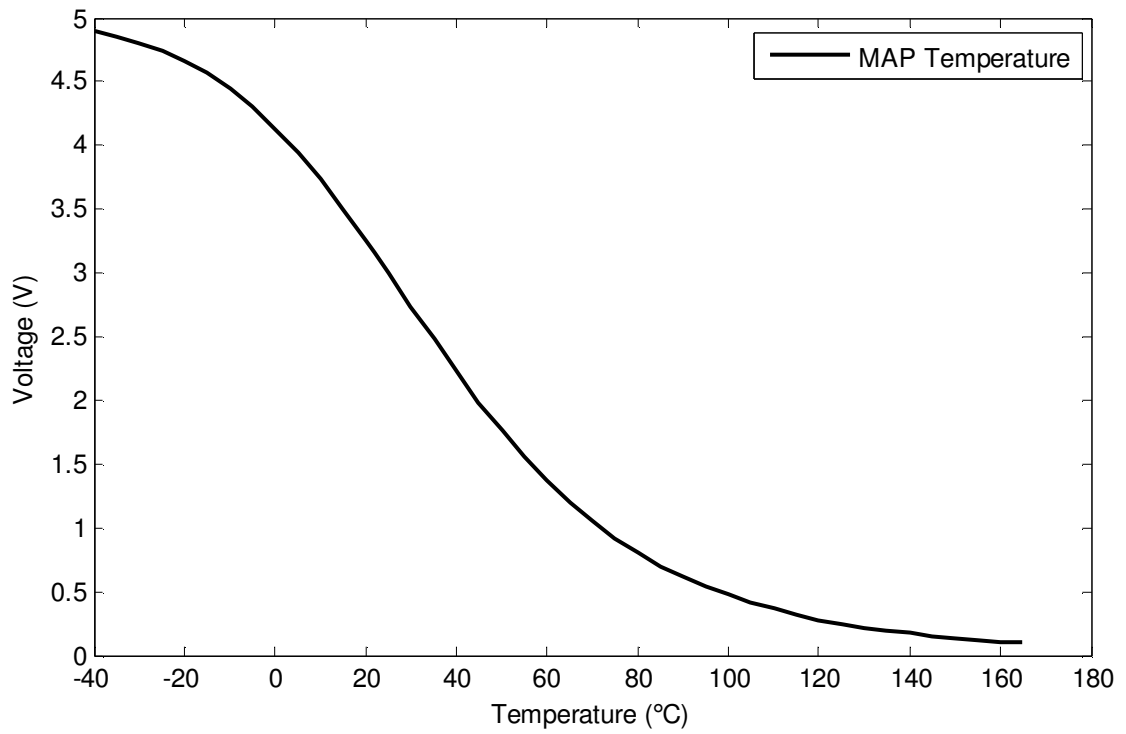


Figure A-XI-10: MAP Sensor Voltage Temperature Transfer Function

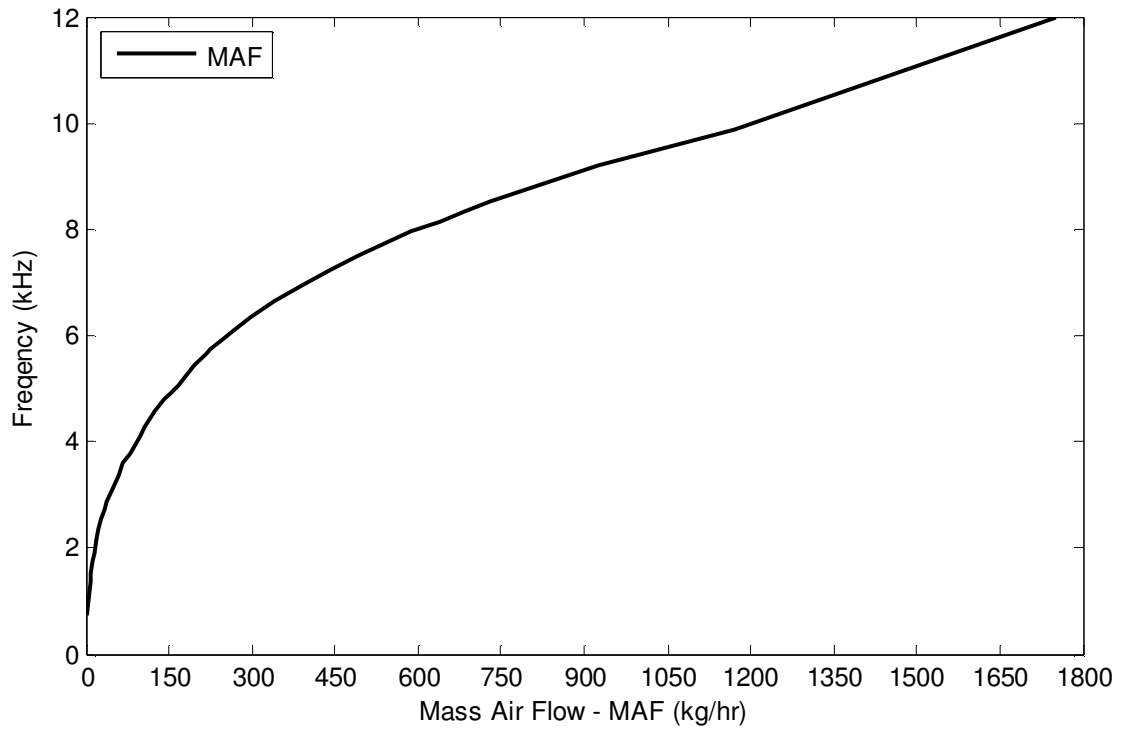


Figure A-XI-11: MAF Sensor Frequency Transfer Function

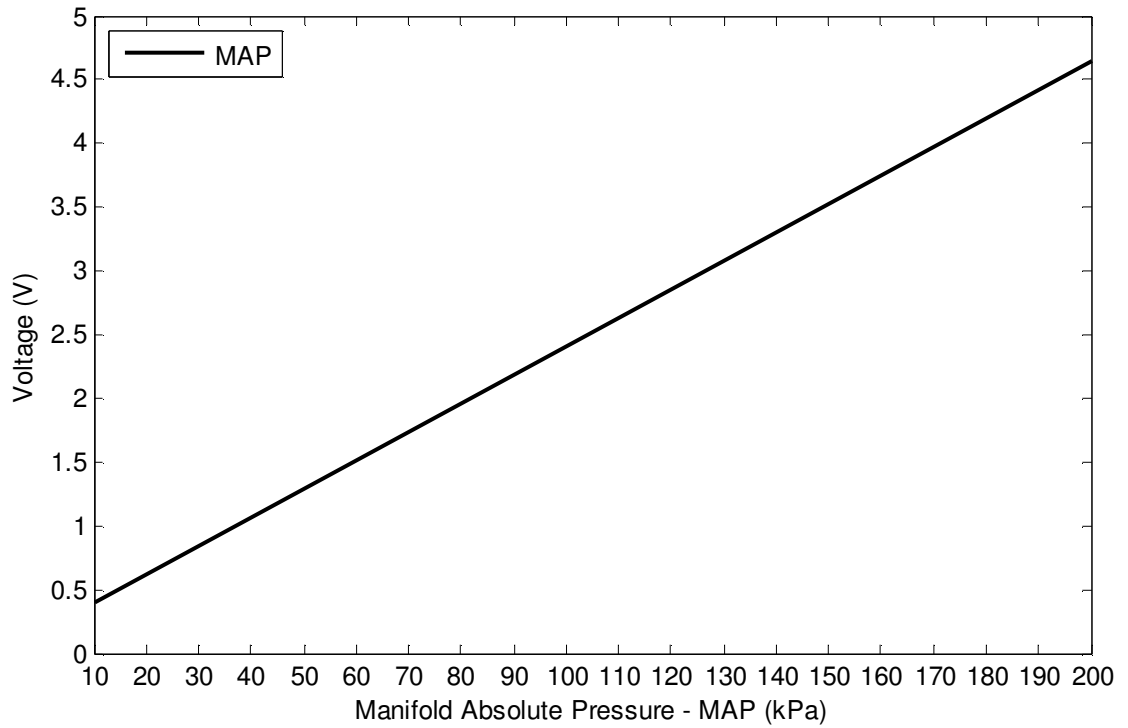


Figure A-XI-12: MAP Sensor Voltage Transfer Function

APPENDIX XII : MATLAB/SIMULINK MODEL BLOCK SUMMARY

The following subsystem is the root of the entire model. For each model shown it will be followed by a table describing the blocks contained in the model.

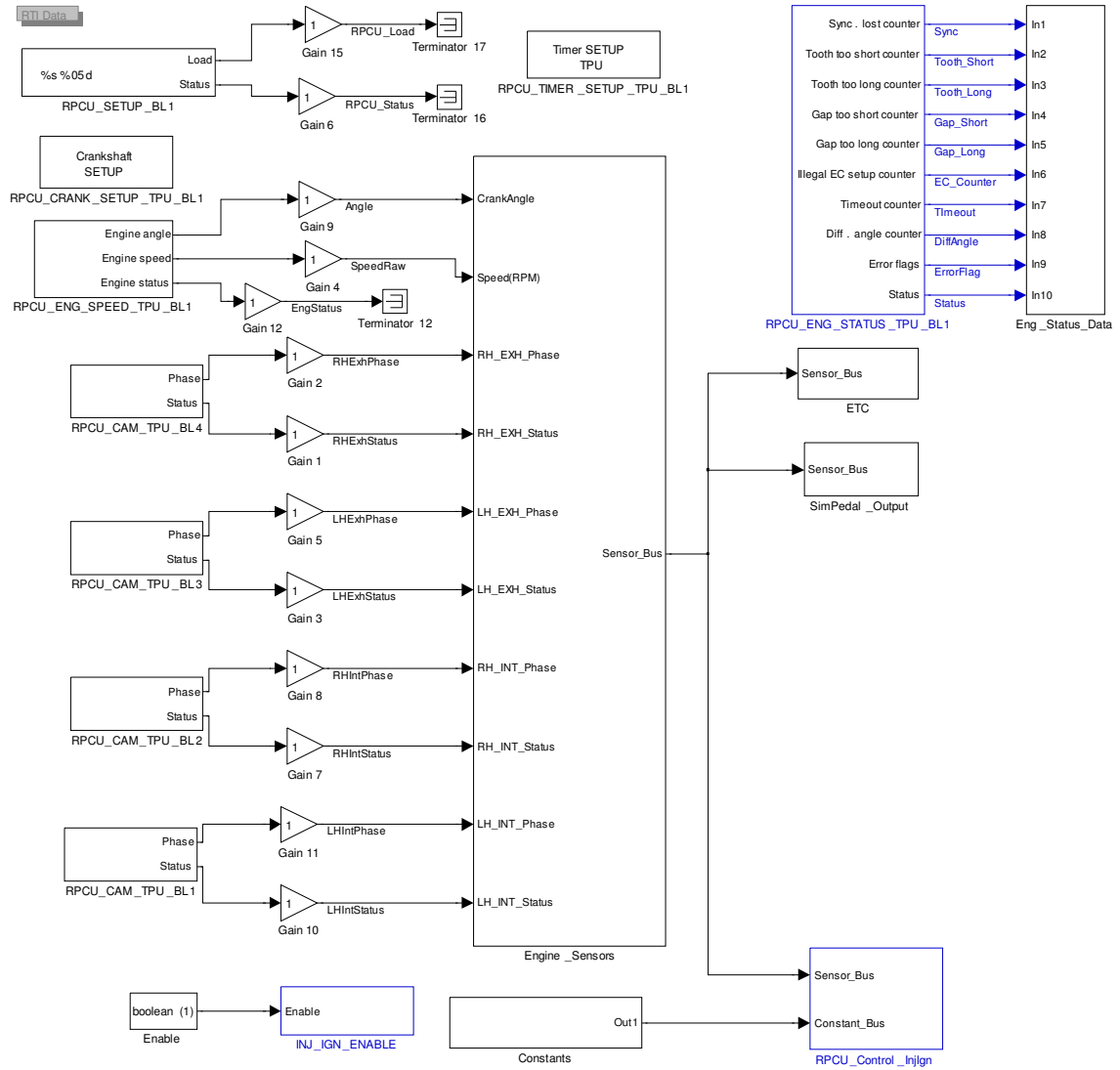


Figure A-XII-1: CrankAngleSimulatorSpark_TB_Inj Model Root

Table A-XII-1: CrankAngleSimulatorSpark_TB_Inj Block Summary

| # | Block Name | Description |
|----|--------------------------|--|
| 1 | RPCU_Setup_BL1 | Supplies RapidPro hardware setup and configuration to the model for selecting channels when designing the subsystems |
| 2 | RPCU_TIMER_SETUP_TPU_BL1 | Configures the resolution of the TPU timers on the RPCU for engine control |
| 3 | RPCU_CRANK_SETUP_TPU_BL1 | Configures the crankshaft wheel for calculating engine speed and synchronization/calculation of the CAD |
| 4 | RPCU_ENG_SPEED_TPU_BL1 | Provides the calculated results for engine speed and crank angle for control purposes |
| 5 | RPCU_CAM_TPU_BL1 to 4 | Configures the cam wheel configurations for cam phase measurement and synchronization of the crank angle domain |
| 6 | RPCU_ENG_STATUS_TPU_BL1 | Outputs information on the present status of the engine crank signal |
| 7 | Eng_Status_Data | Stores outputs from RPCU_ENG_STATUS |
| 8 | Engine_Sensors | Collects all sensor signals and forms a bus to supply sensor signals to other blocks |
| 9 | ETC | Contains the Electronic Throttle Controller, which includes two PID controllers to open and close the throttle |
| 10 | SimPedal_Output | Used to simulate a pedal output using an analog output from the MicroAutoBox |
| 11 | Constants | Contains all engine constants to form a bus which is supplied to various subsystems |
| 12 | INJ_IGN_ENABLE | Used to enable and disable injection/ignition for all cylinders (1 = enabled, 0 = disabled) |
| 13 | RPCU_Control_InjIgn | Contains several submodels to specify the injection and ignition events such as timing, duration and number of events per combustion cycle |

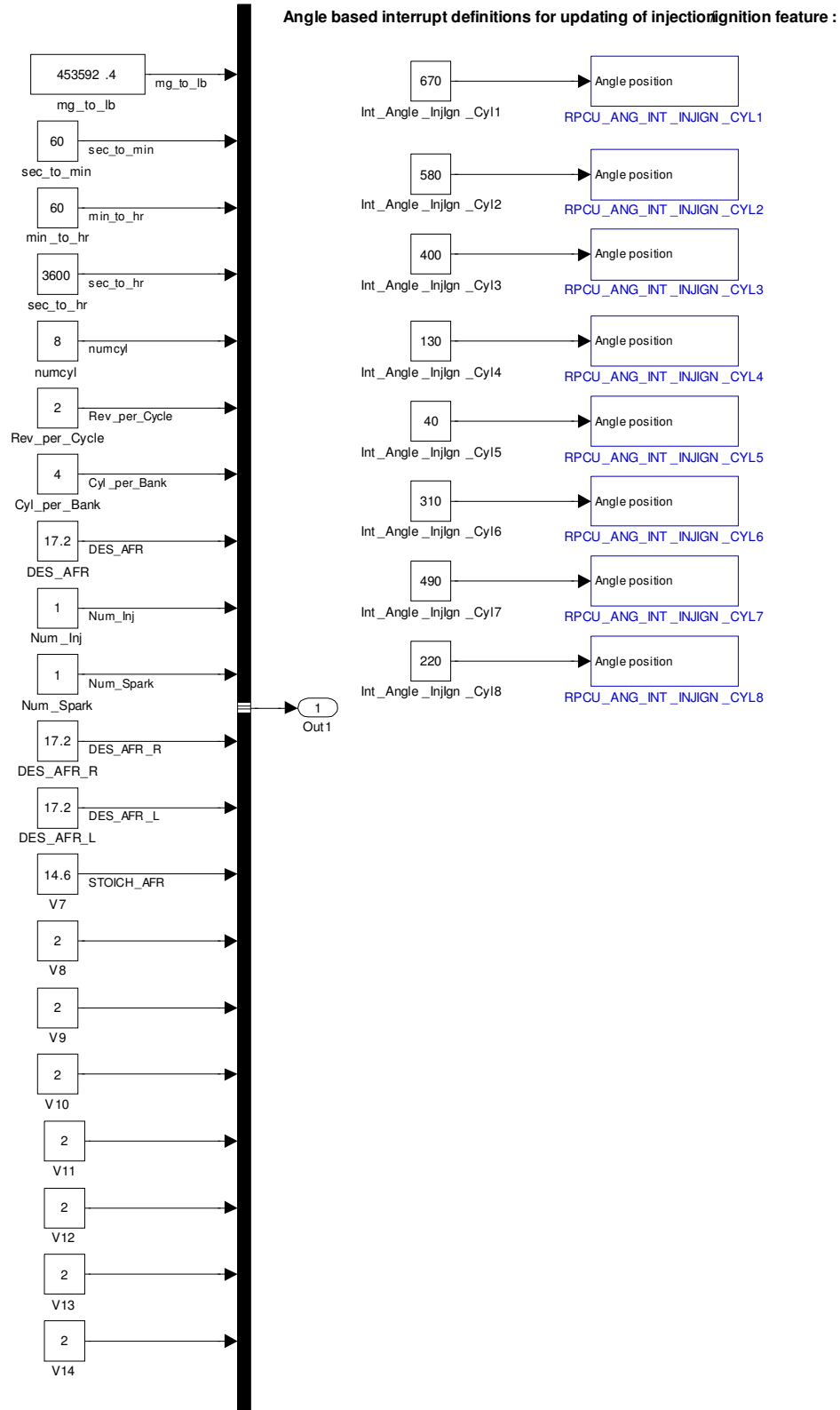


Figure A-XII-2: Constants Subsystem

The **Constants** subsystem was used to create a bus that stores all constant parameters. This bus can then carry all the required constants to various subsystems.

Table A-XII-2: Constants Summary

| # | Block Name | Description |
|----|--------------------------------|--|
| 1 | mg_to_lb | Used to convert mass (mg to lb) |
| 2 | sec_to_min | Converts time (seconds to minutes) |
| 3 | min_to_hr | Converts time (minutes to hours) |
| 4 | sec_to_hr | Converts time (seconds to hours) |
| 5 | numcyl | Number of cylinders on the engine |
| 6 | Rev_per_Cycle | Number of engine revolutions in one engine combustion cycle. 4 Stroke = 2 2 Stroke = 1 |
| 7 | Cyl_per_Bank | Number of cylinders per bank V8 = 4 V6 = 3 V4 = 2 |
| 8 | DES_AFR | Desired Air Fuel Ratio for use with Global AFR control |
| 9 | Num_Inj | Number of injection events per combustion cycle, Max = 15 |
| 10 | Num_Spark | Number of spark events per combustion cycle, Max = 15 |
| 11 | DES_AFR_R | Desired Air Fuel Ratio setpoint for use with Right Bank AFR control |
| 12 | DES_AFR_L | Desired Air Fuel Ratio setpoint for use with Left Bank AFR control |
| 13 | V7 | Stores the stoichiometric AFR |
| 14 | V8 to V14 | Extra variables not presently used |
| 15 | Int_Angle_InjIgn_Cyl1 to 8 | This is the angle that is used to trigger the injection and ignition subsystem |
| 16 | RPCU_ANG_INT_INJIGN_CYL_1 to 8 | These blocks are used trigger the hardware interrupts for spark and injection |

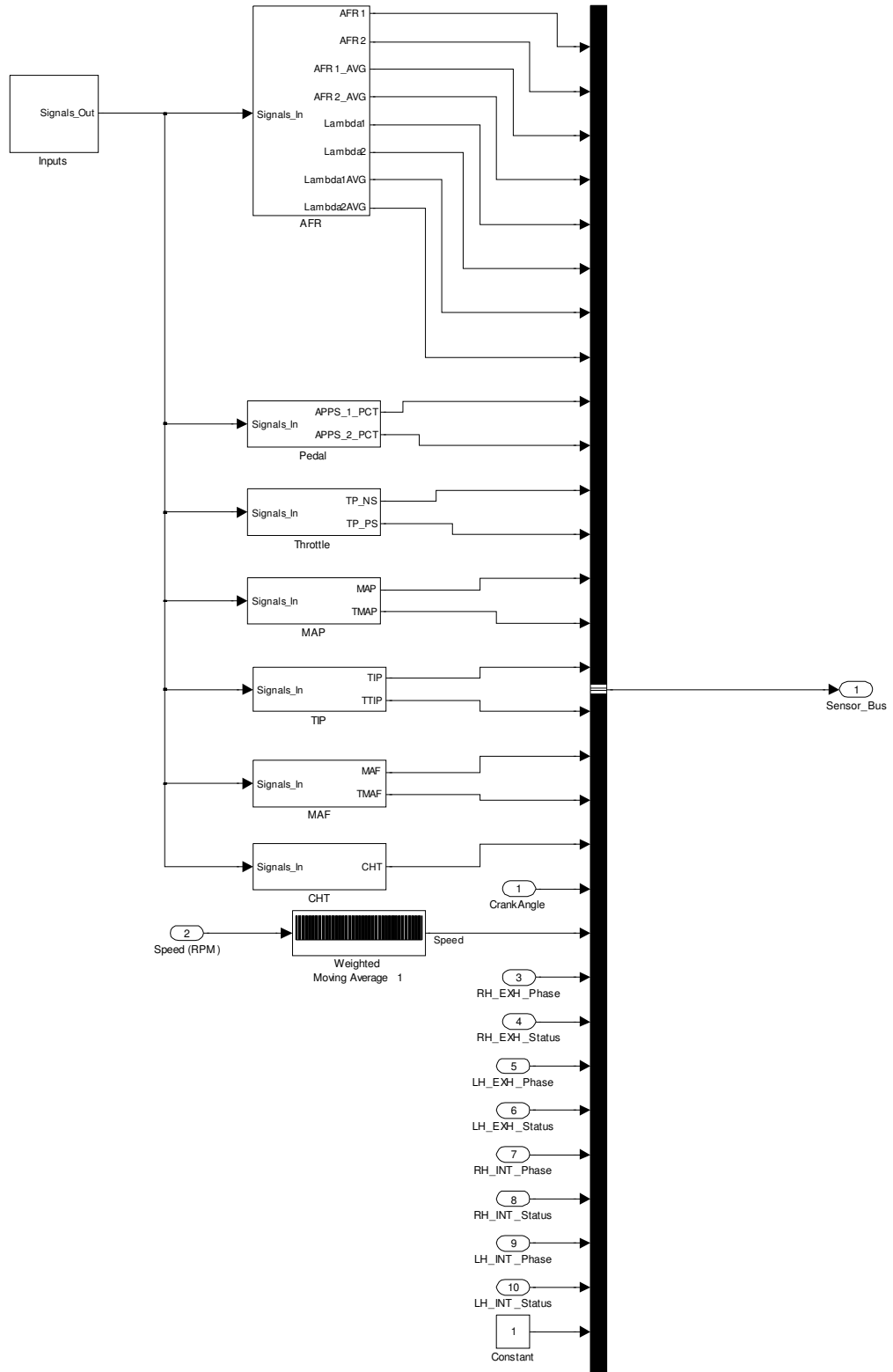


Figure A-XII-3: Engine_Sensors Subsystem

The **Engine_Sensors** subsystem is used to create a bus of sensor signals that can be carried to other model subsystems.

Table A-XII-3: Engine_Sensors Summary

| # | Block Name | Description |
|---|--------------------------|---|
| 1 | Inputs | This submodel is used to collect all the various sensor signals (Analog/Digital) monitored by the MicroAutoBox or the RPCU used in the model. |
| 2 | AFR | This submodel controls the AFR signal conditioning, transfer function, measurement sequencing and controllers to maintain the AFR sensor temperature |
| 3 | Pedal | This block has the transfer function to convert the raw voltages into pedal angles |
| 4 | Throttle | This block acts as the transfer function to convert the raw voltages into throttle angles |
| 5 | MAP | This block acts as the transfer function to convert the raw voltages into Manifold Absolute Pressure. Temperature is also converted in this block. |
| 6 | TIP | This block acts as the transfer function to convert the raw voltages into Throttle Inlet Pressure. Throttle inlet temperature is also converted. |
| 7 | MAF | This block acts as the transfer function to convert the raw frequencies into Mass Air Flow into the engine. Also the MAF sensor temperature is converted. |
| 8 | CHT | This block acts as the transfer function to convert the raw voltage into Cylinder Head Temperature |
| 9 | Weighted Moving Average1 | Applies an equal weight rectangular moving average over the last 500 data points (0.5s) |

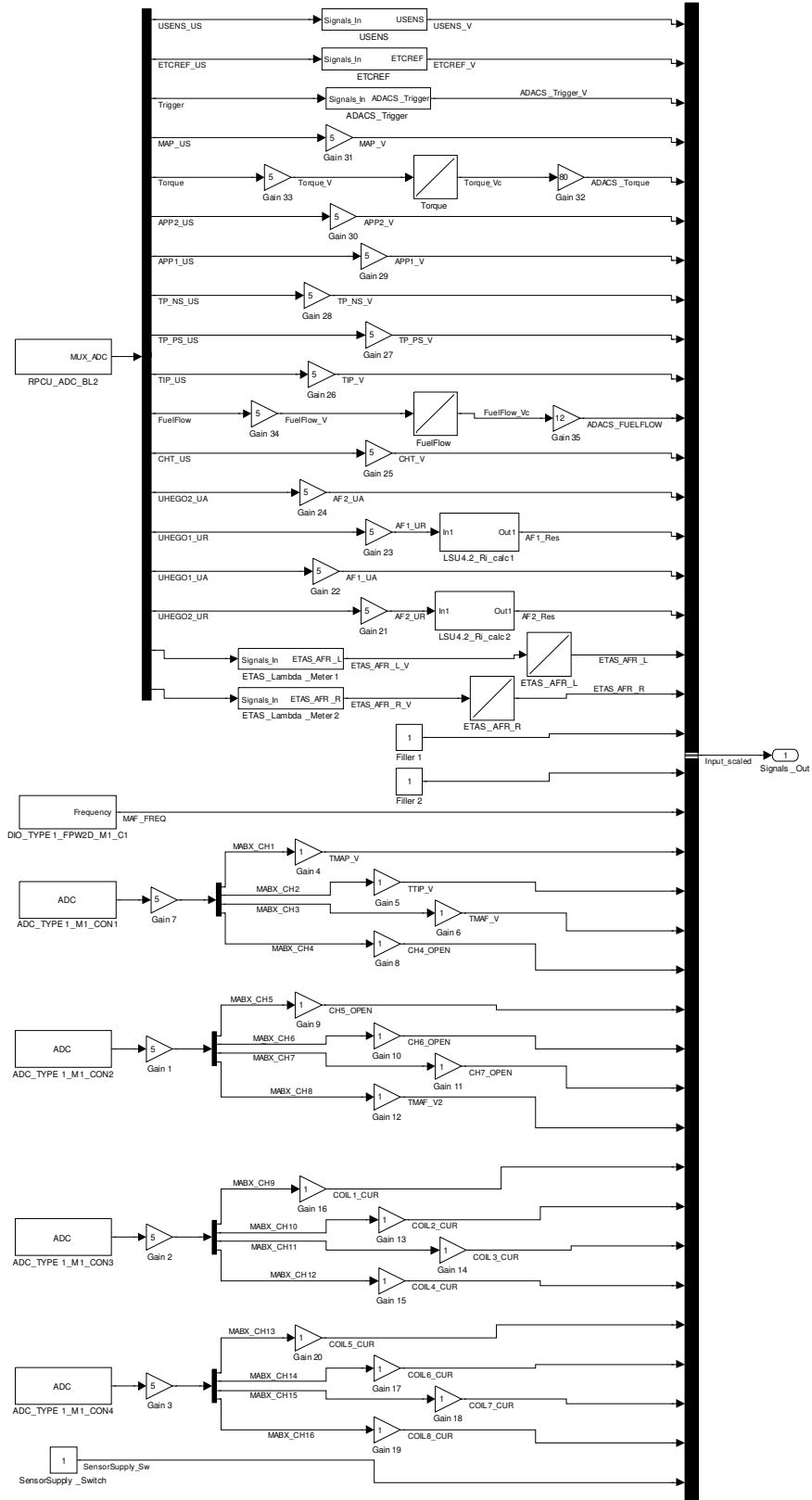


Figure A-XII-4: Inputs Subsystem

Sensor signals that require transfer functions are collected by the **Inputs** subsystem.

Table A-XII-4: Inputs Summary

| # | Block Name | Description |
|---|------------------------|--|
| 1 | RPCU_ADC_BL2 | Provides read access to the 40 A/D converters of the RPCU |
| 2 | DIO_TYPE1_FPW2D_M1_C1 | Provides read access to either frequency or pulse width for square wave signals input to the MicroAutoBox. This particular input is used for measuring the frequency of the MAF sensor. Extended engine control with active sensor was chosen, with falling edge detection between 10Hz and 100KHz |
| 3 | ADC_TYPE1_M1_CON1 to 4 | Provides read access to the 16 analog inputs of the MicroAutoBox, 8 Channels are used to measure the individual coil currents, MAP, TIP and MAF Temperature sensor voltages are also collected |
| 4 | USENS | Converts the differential input which is measuring the sensor supply voltage from a value of 0-1 to a voltage between -10 and +10 V |
| 5 | ETCREF | Converts the differential input which is measuring the Electronic Throttle Controller voltage from a value of 0-1 to a voltage between -10 and +10 V |
| 6 | ADACS_Trigger | Converts the differential input which is measuring the ADACS_Trigger voltage from a value of 0-1 to a voltage between -5 and +5 V |
| 7 | Torque | Transfer function to account for analog output errors from the ADACS system, the output is converted to torque (ft-lb) using Gain32 |
| 8 | FuelFlow | Transfer function to account for analog output errors from the ADACS system, the output is converted to Fuel Flow (lb/hr) using Gain35 |

| | | |
|----|------------------------|--|
| 9 | LSU4.2_Ri_calc1 & 2 | Used to convert the analog voltage measured from the AFR sensors into a resistance value. This signal provides feedback on the sensor temperature, 300Ω would be the desired operating point |
| 10 | ETAS_Lambda_Meter1 & 2 | Converts the differential input which is measuring the voltage from ETAS LA4 Lambda meters from a value of 0-1 to a voltage between -10 and +10 V |
| 11 | ETAS_AFR_L & R | Transfer function to convert from voltage to AFR for the ETAS LA4 Lambda meters |

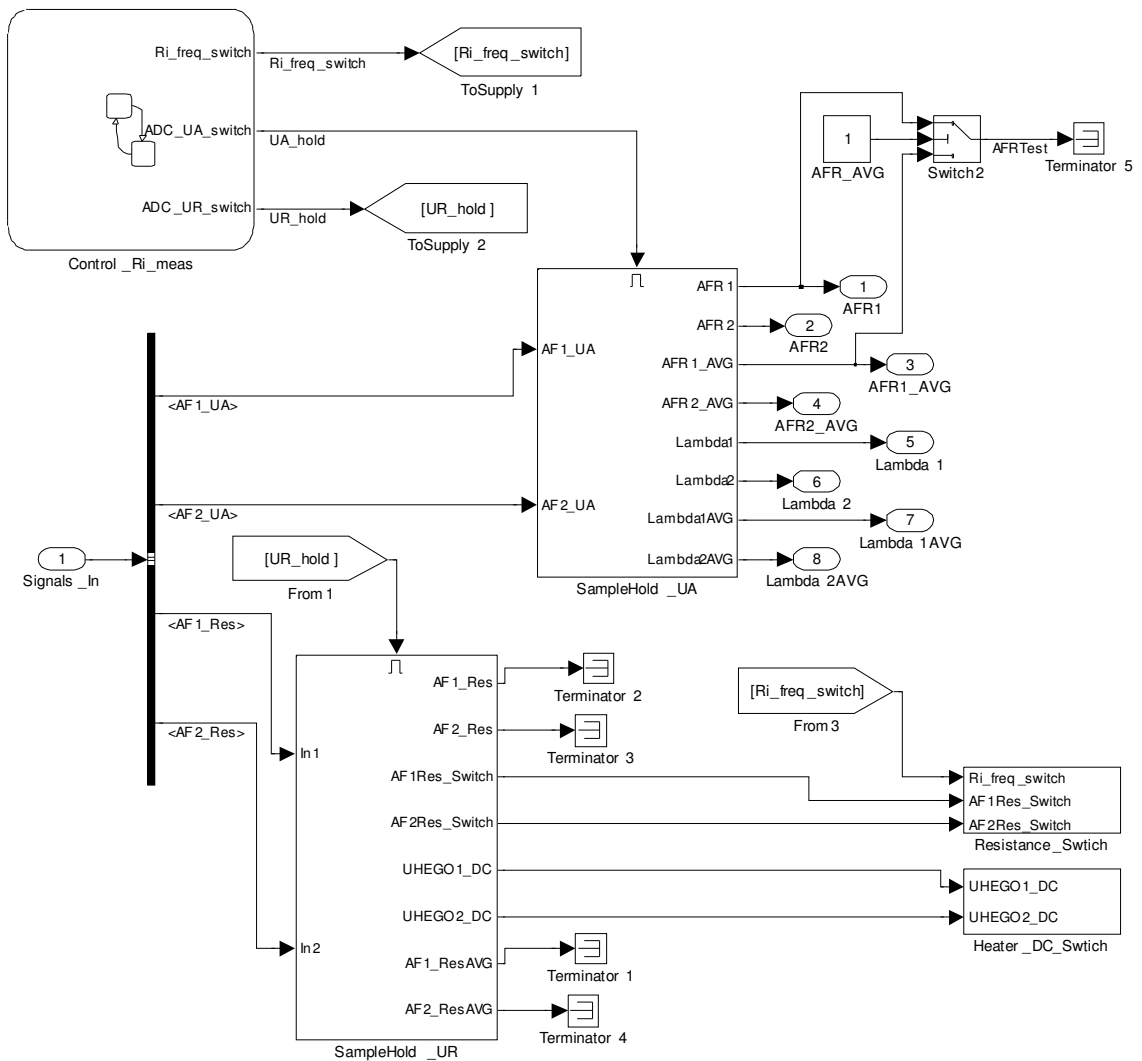


Figure A-XII-5: AFR Subsystem, adapted from [80]

The **AFR** Subsystem was designed to control the AFR sensor heating, while sequencing sensor resistance and AFR measurements to limit noise.

Table A-XII-5: AFR Summary

| # | Block Name | Description |
|---|-------------------|---|
| 1 | Control_Ri_meas | Stateflow chart which provides the logic to switch between AFR measurement and AFR sensor resistance measurement to maintain the sensor at its operating temperature (300Ω). Total cycle time = 20ms. |
| 2 | SampleHold_UA | This block is used to sample and hold the AFR measurement and convert the measured voltage to a pumping current then into a Lambda value which is then converted into AFR |
| 3 | SampleHold_UR | This block is used to sample and hold the AFR resistance measurement which is used to control the sensor heater to maintain 300 Ω, The resistance value is also converted into a temperature value |
| 4 | Resistance_Switch | Used to enable and disable the switching of the resistance measurement signal for the UHEGO sensors |
| 5 | Heater_DC_Switch | Outputs the AFR sensor heater DC, and limits the rate at which the sensor heats |
| 6 | Switch2 | Switches the variable AFRTest between Average and Raw AFR measurement for the right bank AFR sensor |

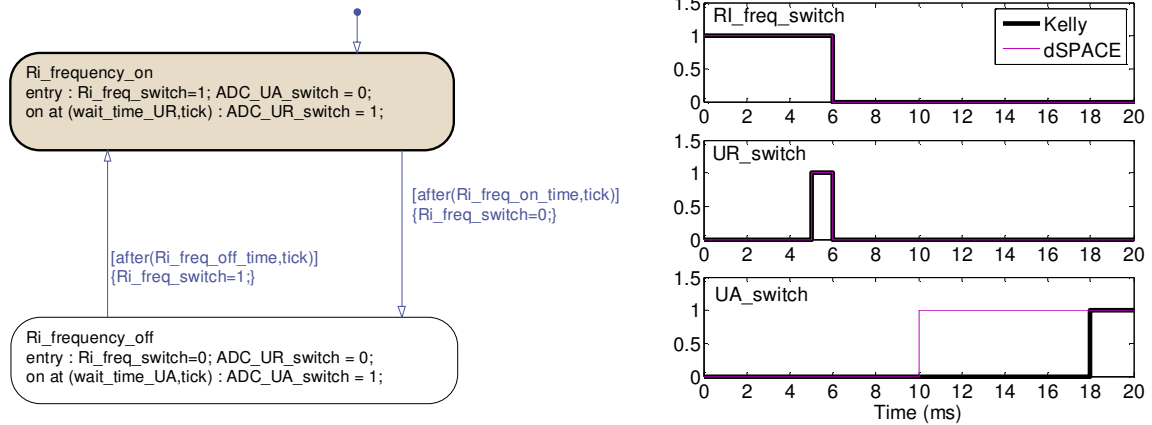


Figure A-XII-6: Control_Ri_mes Logic via Stateflow, adapted from [80]

Control_Ri_mes is the stateflow diagram that was used to sequence resistance and AFR measurements. The entire cycle time of the stateflow diagram is set to 20ms.

Table A-XII-6: Heater_Control1 Summary

| # | Block Name | Description |
|---|------------------|--|
| 1 | Ri_frequency_on | When this block is active Ri_freq_switch = 1 |
| 2 | Ri_frequency_off | When this block is active Ri_freq_switch = 0 |
| 3 | Ri_freq_switch | This variable is used to enable resistance measurement |
| | Ri_freq_off_time | This is the period of time the model waits to measure resistance = 14ms |
| | Ri_freq_on_time | This is the period of time the model is able to measure resistance = 6ms |
| 4 | ADC_UA_switch | Switches on AFR measurement between 18 and 20ms of the cycle |
| 5 | wait_time_UA | This timer is set to 12ms |
| 6 | ADC_UR_switch | Switches on resistance measurement between 5 and 6ms of the cycle |
| 7 | wait_time_UR | This timer is set to 5ms |

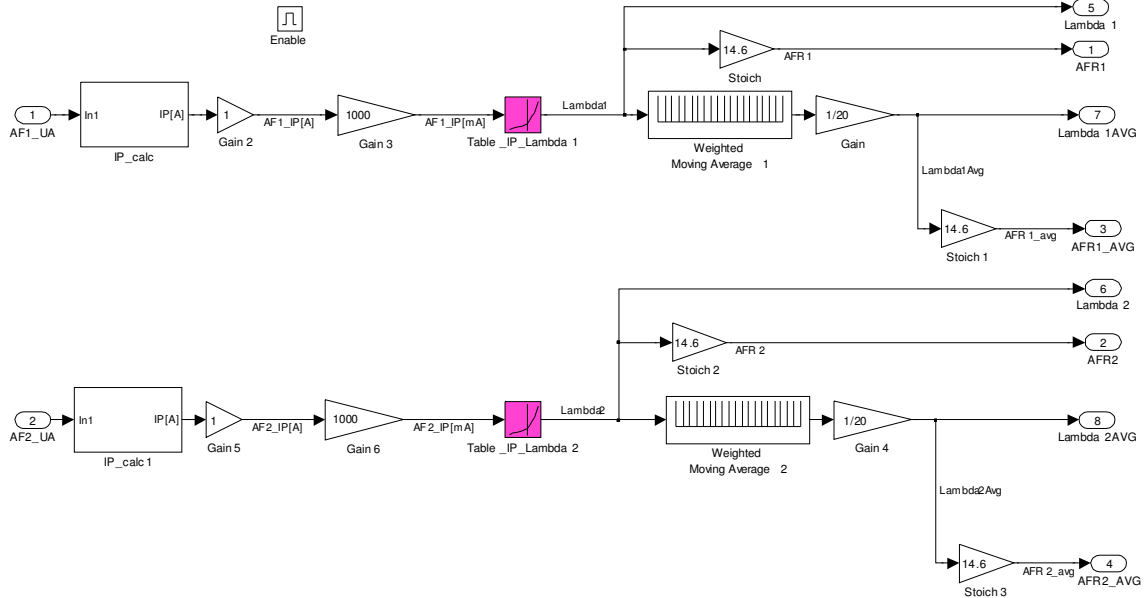


Figure A-XII-7: Sample_Hold_UA, adapted from [80]

Sample_Hold_UA is where the transfer function for the lambda sensor is implemented.

Table A-XII-7: SampleHold_UA Summary

| # | Block Name | Description |
|---|------------------------------|--|
| 1 | IP_calc & IP_calc1 | Converts the AFR voltage into a pumping current depending on the RPCU setup |
| 2 | Table_IP_Lambda1 & 2 | Transfer function to convert the pumping current from a mA value into a Lambda value |
| 3 | Weighted Moving Average1 & 2 | Applies a rectangular weighted moving average over the past 20 measurements to smooth out AFR measurements |
| 4 | Stoich, Stoich1, 2 & 3 | Converts from a Lambda value to an AFR value |

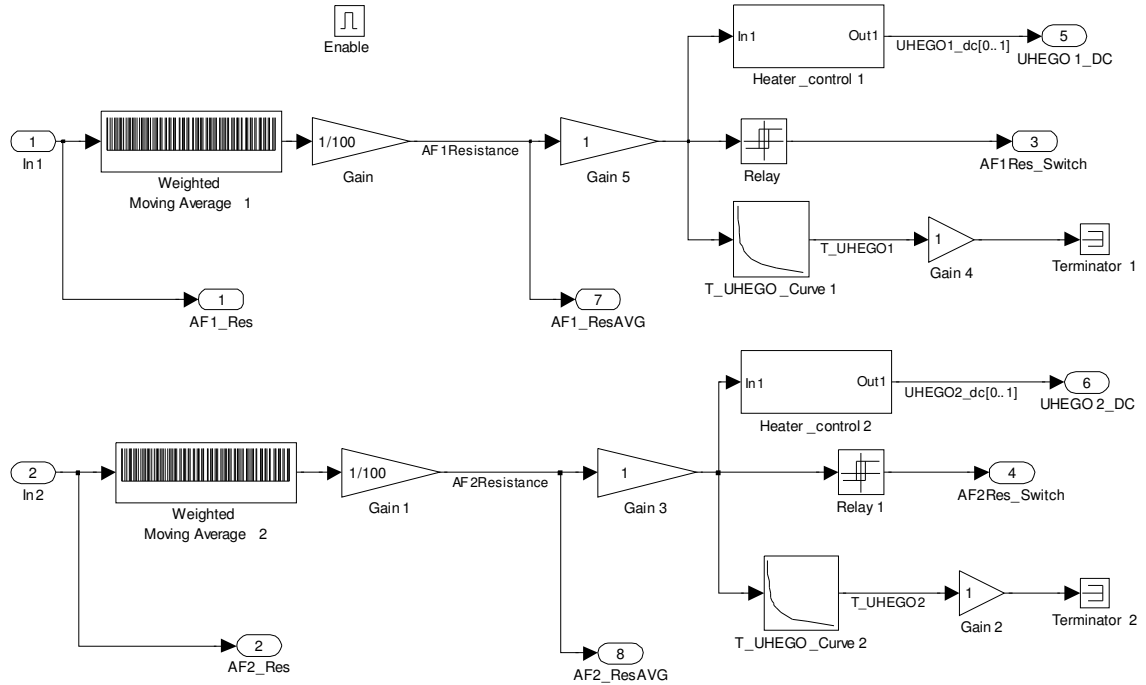


Figure A-XII-8: Sample_Hold_UR, adapted from [80]

Sample_Hold_UR is where the lambda sensor heater controller is implemented; also the resistance is converted into a temperature.

Table A-XII-8: SampleHold_UR Summary

| # | Block Name | Description |
|---|------------------------------|---|
| 1 | Weighted Moving Average1 & 2 | Averages the past 100 resistance measurements to smooth out and improve control of the resistance |
| 2 | Heater_controll1 & 2 | PID controller to maintain the AFR Sensor resistance at 300 Ω |
| 3 | Relay & Relay1 | Used to switch resistance measurement on and off depending on the resistance value. Switch on point 420 Ω, Switch off point 370 Ω. Output when on = 1 |
| 4 | T_UHEGO_Curve1 & 2 | Transfer function to convert the resistance measurement into a temperature value |

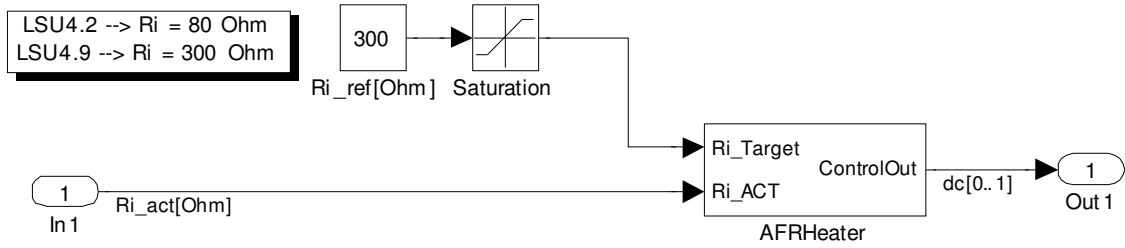


Figure A-XII-9: Heater_Control1, adapted from [80]

Heater_Control1 sets the required lambda sensor resistance for heater control.

Table A-XII-9: Heater_Control1 Summary

| # | Block Name | Description |
|---|-------------|--|
| 1 | Ri_ref[Ohm] | Desired UHEGO sensor resistance or operating setpoint |
| 2 | AFRHeater | AFR heater PID controller |
| 3 | Saturation | This saturation block was implemented to prevent the user from entering sensor resistances that are too small or too large. Limits are 70 and 500 Ω. |

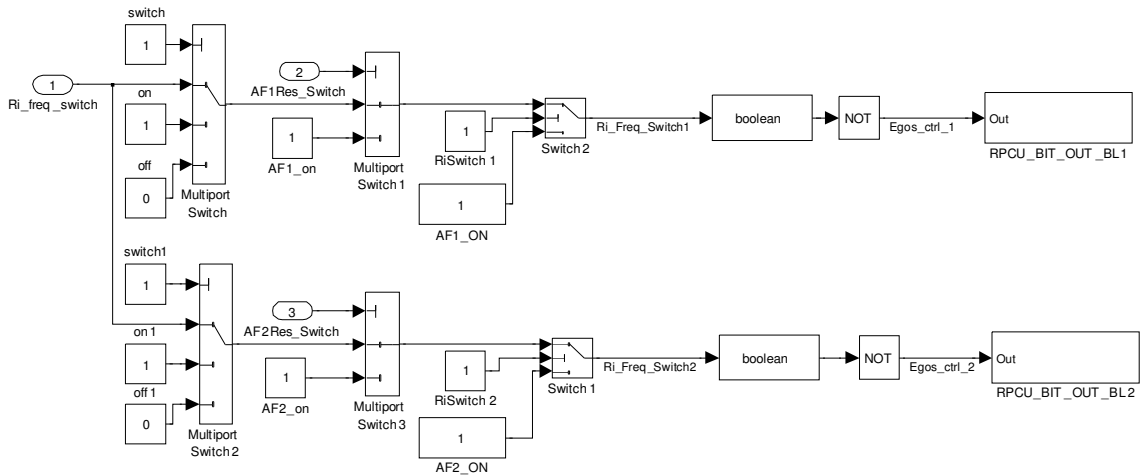


Figure A-XII-10: Resistance_Switch, adapted from [80]

Resistance_Switch is used to output the signal required to control resistance measurement of the lambda sensor for heater control.

Table A-XII-10: Resistance_Switch Summary

| # | Block Name | Description |
|---|-------------------|---|
| 1 | Ri_freq_switch | Output from stateflow chart Control_Ri_mes |
| 2 | switch | Used to control the source of Multiport Switch . |
| 3 | on | Can be used to force the output of Multiport Switch to 1 |
| 4 | off | Can be used to force the output of Multiport Switch to 0 |
| 5 | Multiport Switch | Selector for the state of Ri_freq_switch |
| 6 | AF1Res_Switch | This signal comes from the relay in Sample_Hold_UR and is used to lock the resistance measurement ON to prevent it from cycling if the sensor is detected as cold (high resistance). |
| 7 | AF1_on | This variable is used by Multiport Switch 1 to force resistance measurement on |
| 8 | Multiport Switch1 | This block allows for the relay feature to lock resistance measurement in the ON state |
| 9 | Switch2 | Used to bypass all the logic ahead of it |

| | | |
|----|------------------|---|
| 10 | AF1_ON | Used to bypass all the logic ahead of it |
| 11 | RiSwitch1 | Actuates Switch2 |
| 12 | boolean | Ensures the data type for the bit out is Boolean |
| 13 | NOT | Inverts the signal to match the hardware configuration |
| 14 | RPCU_BIT_OUT_BL1 | This bit out sends the signal to the hardware to measure the resistance |

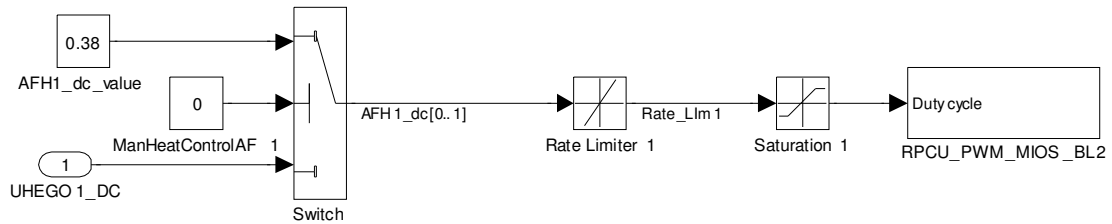


Figure A-XII-11: Heater_Switch, adapted from [80]

Heater_Switch allows for bypassing the lambda sensor heater controller and manually setting the controller to the desired duty cycle.

Table A-XII-11: Heater_Switch Summary

| # | Block Name | Description |
|---|-------------------|---|
| 1 | AFH1_dc_value | Used to manually bypass the AFR Heater Duty Cycle Controller. This is the setpoint variable |
| 2 | ManHeatControlAF1 | Controls Switch to bypass AFR Heater Control, 1 = OL, 0 = CL control |
| 3 | UHEGO1_DC | This is the duty cycle output by the PID controller (Heater_Control1) |
| 4 | Rate Limiter 1 | Used to limit the rate at which the heater duty cycle can change (slew rate = 1) |
| 5 | Saturation 1 | Limits the output to between 0 and 1 duty cycle |
| 6 | RPCU_PWM_MIOS_BL2 | Outputs the PWM signal to the UHEGO sensor to control the heater element |

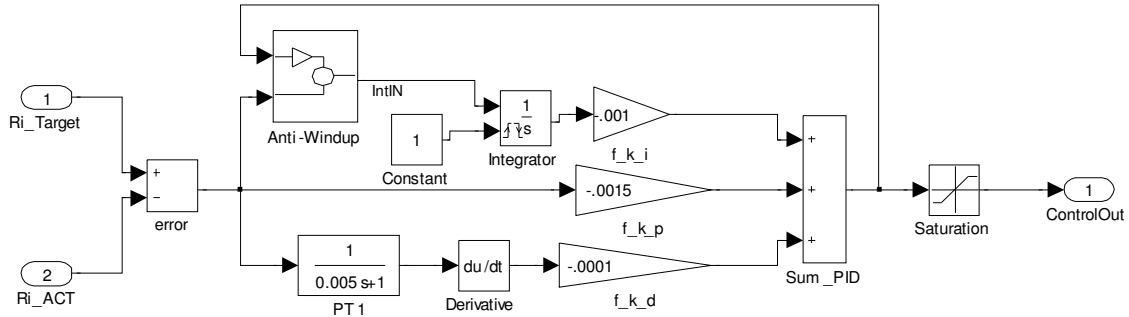


Figure A-XII-12: AFRHeater, adapted from [80]

AFRHeater is the PID controller that was implemented to control the heating of the lambda sensor.

Table A-XII-12: AFRHeater Summary

| # | Block Name | Description |
|----|-------------|--|
| 1 | Ri_Target | This is the target heater resistance setpoint value |
| 2 | Ri_ACT | This is the sensor feedback, measured resistance |
| 3 | Anti-Windup | Used to prevent the Integrator from winding up. Limits are 1 to -1 DC |
| 4 | Constant | This variable is used for resetting the Integrator |
| 5 | f_k_i | Integral gain value |
| 6 | f_k_d | Derivative gain value |
| 7 | error | The difference between the setpoint and the actual sensor feedback (setpoint – feedback) |
| 8 | PT1 | Filter applied in order to allow the derivative controller to act on a clean signal |
| 9 | Derivative | This block calculates the derivative for the PID controller |
| 10 | Integrator | This block calculates the integral fro the PID controller |
| 11 | f_k_p | Proportional gain value |
| 12 | Saturation | Limits between 0 and 1 |

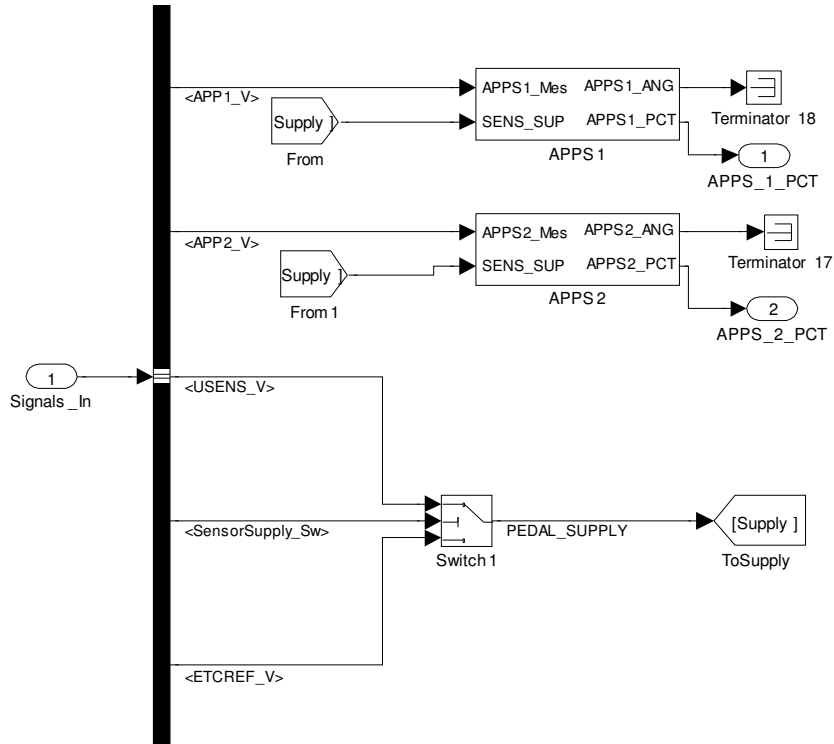


Figure A-XII-13: Pedal Subsystem

The **Pedal** subsystem contains the required transfer functions to convert the pedal output signals into pedal position/angle.

Table A-XII-13: Pedal Summary

| # | Block Name | Description |
|---|------------|--|
| 1 | Switch1 | Used to choose what the sensor voltage supply source is used. |
| 2 | APPS1 & 2 | Normalizes the voltage supply and generates an angle 0 to 15.5 and percent value between 0 & 1 |

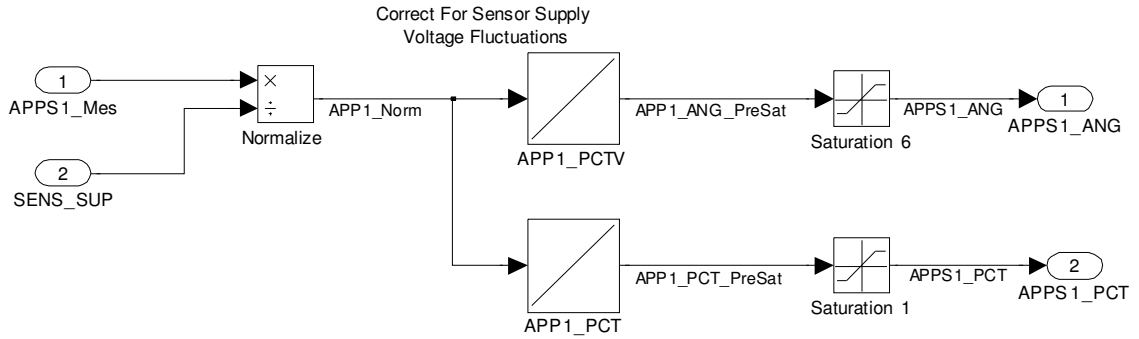


Figure A-XII-14: APPS1 Subsystem

APPS1 is shown above but **APPS2** is similar to **APPS1**. This is the way the transfer functions were implemented for converting the voltages to pedal positions.

Table A-XII-14: APPS1 & APPS2 Summary

| # | Block Name | Descriptions |
|---|-------------|---|
| 1 | Normalize | Divides the measured voltage by the supplied sensor voltage to account for sensor supply voltage fluctuations |
| 2 | APPS1_PCTV | Converts the normalized voltage from 0-1 to an angle between 0 to 15.5 |
| 3 | APPS1_PCT | Converts the normalized voltage from 0-1 to a percent value where 1 = 100% or an angle of 15.5 |
| 4 | Saturation6 | Upper Limit = 15.5, Lower Limit = 0 |
| 5 | Saturation1 | Upper Limit = 1, Lower Limit = 0 |

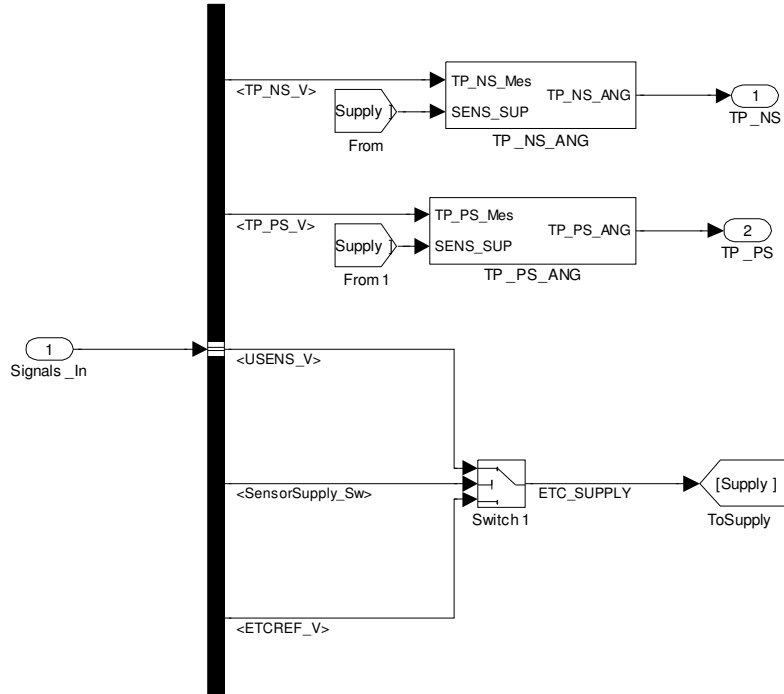


Figure A-XII-15: Throttle Subsystem

The **Throttle** subsystem contains subsystems to define the sensor transfer functions for throttle position/angle.

Table A-XII-15: Throttle Summary

| # | Block Name | Description |
|---|------------|---|
| 1 | Switch1 | Used to choose what the sensor voltage supply source is |
| 2 | TP_NS_ANG | Transfer function to output the negative slope of the throttle position |
| 3 | TP_PS_ANG | Transfer function to output the negative slope of the throttle position |

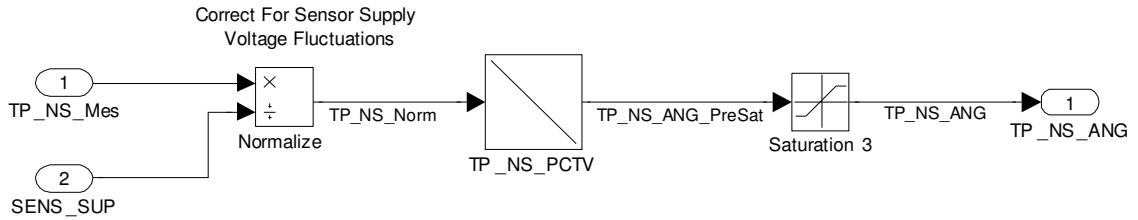


Figure A-XII-16: TP_NS_ANG Subsystem

TP_NS_ANG defines the throttle position negative slope angle transfer function.

Table A-XII-16: TP_NS_ANG Summary

| # | Block Name | Description |
|---|-------------|---|
| 1 | Normalize | Divides the measured voltage by the supplied sensor voltage to account for sensor supply voltage fluctuations |
| 2 | TP_NS_PCTV | Converts the normalized voltage from 0-1 to an angle between -6.4 to 103.7 |
| 3 | Saturation3 | Upper Limit = 103.7, Lower Limit = -6.4 |

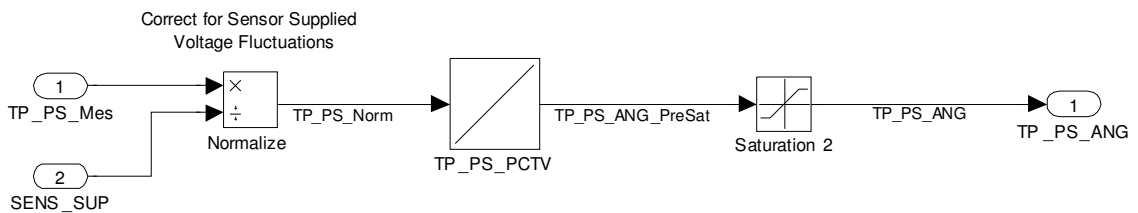


Figure A-XII-17: TP_PS_ANG Subsystem

TP_PS_ANG defines the throttle position positive slope angle transfer function.

Table A-XII-17: TP_PS_ANG Summary

| # | Block Name | Description |
|---|-------------|---|
| 1 | Normalize | Divides the measured voltage by the supplied sensor voltage to account for sensor supply voltage fluctuations |
| 2 | TP_PS_PCTV | Converts the normalized voltage from 0-1 to an angle between -3.4 to 56 |
| 3 | Saturation2 | Upper Limit = 56, Lower Limit = -3.4 |

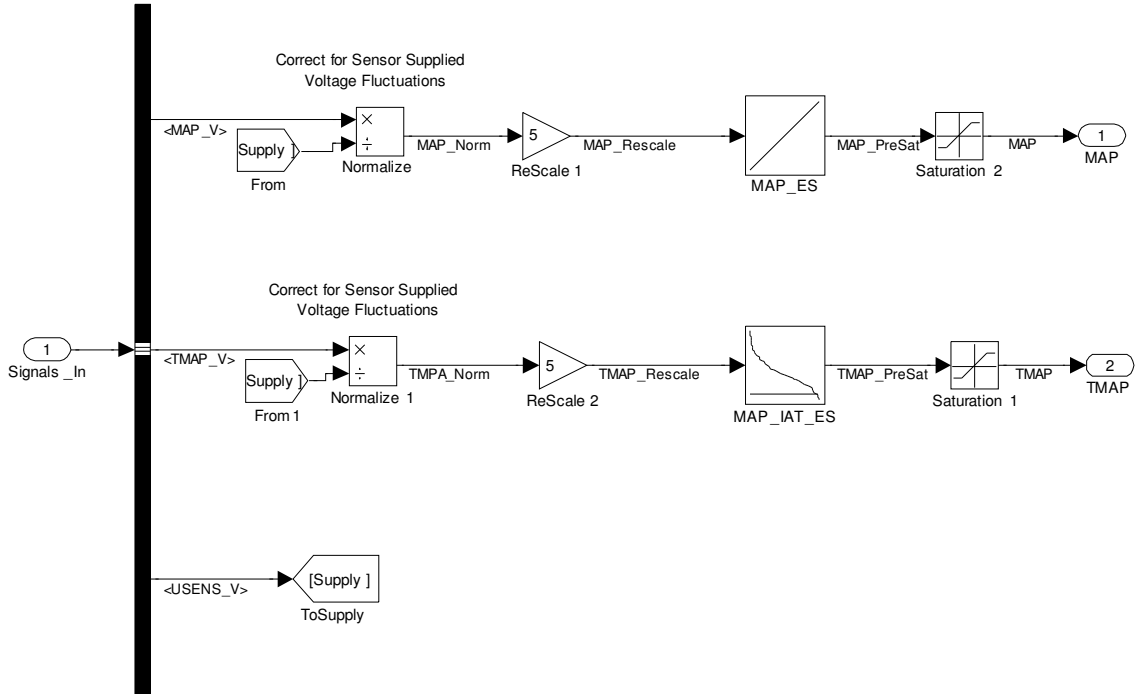


Figure A-XII-18: MAP Subsystem

Both **MAP** and **TIP** use the same model of sensor. The transfer functions would be identical with different names block names. Only the MAP subsystem was shown.

Table A-XII-18: MAP & TIP Summary

| # | Block Name | Description |
|---|-------------------------|---|
| 1 | Normalize & Normalize1 | Divides the measured voltage by the supplied sensor voltage to account for sensor supply voltage fluctuations |
| 2 | ReScale1 & 2 | Scale normalized voltage back to between 0 and 5V |
| 3 | MAP_ES / TIP_ES | Converts the voltage from 0-5 to a pressure between 10 and 200kpa |
| 4 | MAP_IAT_ES / TIP_IAT_ES | Converts the voltage from 0-5 to a temperature between -40 and 329F |
| 5 | Saturation1 | Upper Limit = 329, Lower Limit = -40 |
| 6 | Saturation2 | Upper Limit = 200, Lower Limit = 10 |

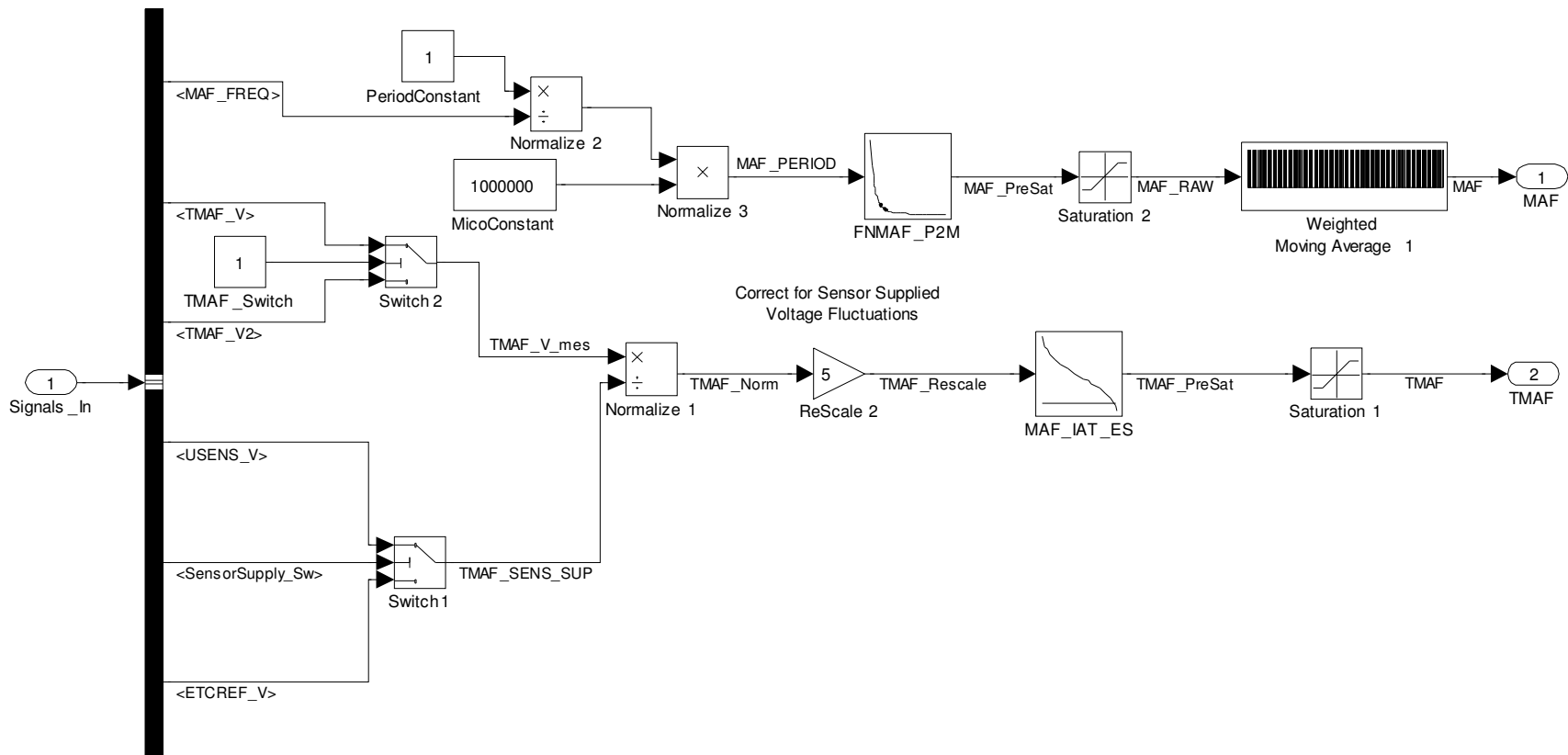


Figure A-XII-19: MAF Subsystem

The **MAF** subsystem contains the transfer functions for the MAF sensor temperature measurement and the MAF that are measured.

Table A-XII-19: MAF Summary

| # | Block Name | Description |
|----|--------------------------|---|
| 1 | Normalize2 & Normalize3 | Converts the measured MAF frequency to a period (microseconds) |
| 2 | FNMAF_P2M | Converts the period to a mass air flow between 0.3 and 65 lb/min |
| 3 | Switch1 | Chooses the sensor supply voltage source |
| 4 | Switch2 | Chooses the MAF sensor voltage temperature source |
| 5 | Saturation1 | Upper Limit = 248, Lower Limit = -40 |
| 6 | Saturation2 | Upper Limit = 65, Lower Limit = 0.3 |
| 7 | Normalize1 | Normalizes the measured MAF temperature sensor voltage for sensor supply voltage fluctuations |
| 8 | Rescale2 | Converts the normalized voltage back to a range between 0 and 5V |
| 9 | MAF_IAT_ES | Converts the MAF temperature sensor voltage into a temperature between -40 and 248F |
| | TMAF_Switch | Used to control Switch 2 voltage source |
| 10 | Weighted Moving Average1 | Applies an equally weighted rectangular moving average to the MAF signal over the past 1000 points (1 second of data) |

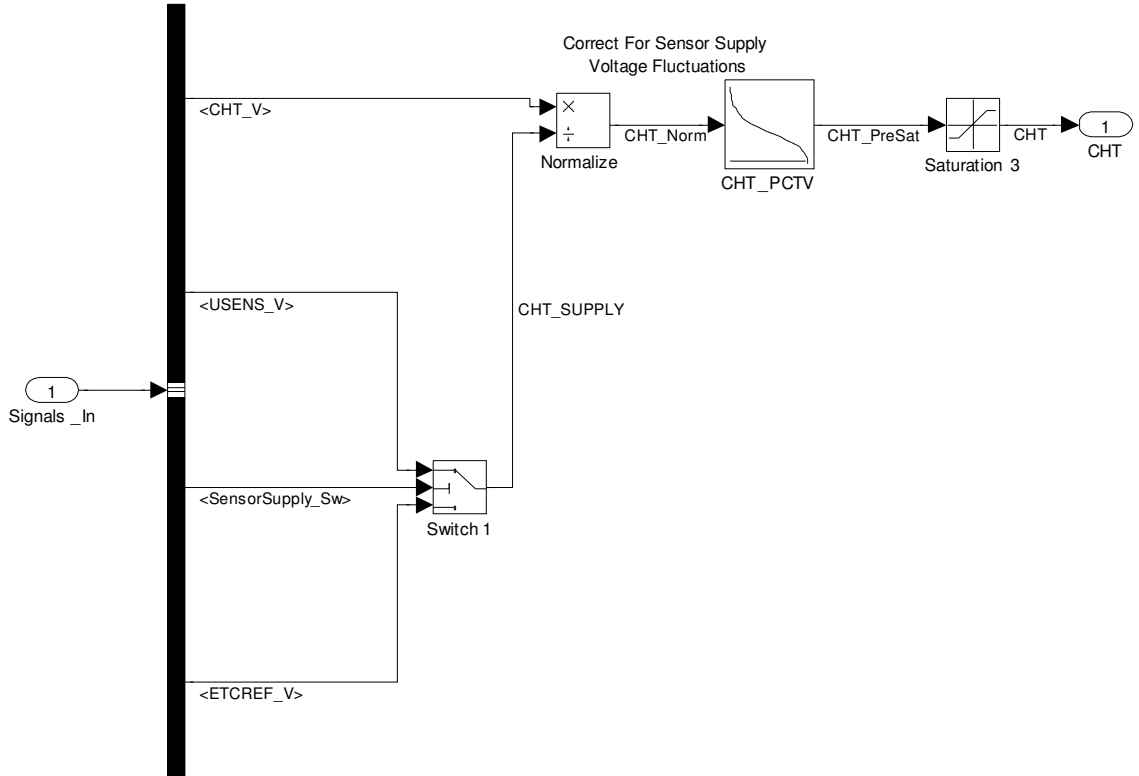


Figure A-XII-20: CHT Subsystem

The **CHT** subsystem contains the transfer function for the CHT sensor.

Table A-XII-20: CHT Summary

| # | Block Name | Description |
|---|-------------|---|
| 1 | Normalize | Divides the measured voltage by the supplied sensor voltage to account for sensor supply voltage fluctuations |
| 2 | CHT_PCTV | Converts the normalized voltage to a temperature in the range of -40 to 482F |
| 3 | Saturation3 | Upper Limit = 482, Lower Limit = -40 |
| 4 | Switch1 | Chooses the sensor supply voltage source for normalization |

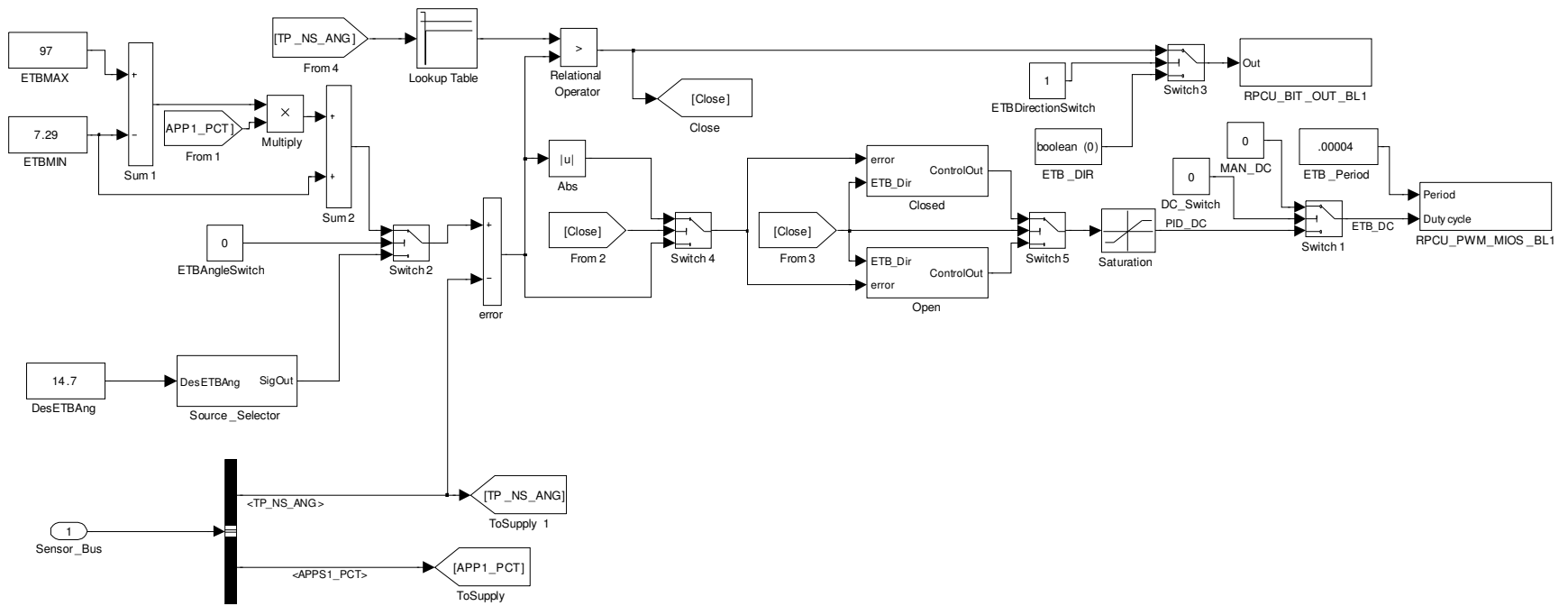


Figure A-XII-21: ETC Subsystem

ETC subsystem is the entire electronic throttle controller to control the position of the throttle plate.

Table A-XII-21: ETC Summary

| # | Block Name | Description |
|----|---------------------|---|
| 1 | ETBMAX | Maximum Angle the throttle body may go to |
| 2 | ETBMIN | Minimum angle the throttle body may go to |
| 3 | Sum1 | Calculation of the total travel possible by the throttle body |
| 4 | Multiply | Scales the pedal position into a commanded throttle body angle setpoint |
| 5 | Sum2 | Adds the scaled output from Multiply to create a final setpoint based on the pedal position |
| 6 | error | Calculates the error using the throttle body negative slope position |
| 7 | DesETBAng | This is the desired electronic throttle body angle for manual setpoint control |
| 8 | Subsystem | This system is used to select various signals to feed into the PID controller for manual setpoints |
| 9 | Switch2 | This switch allows the user to switch between pedal control and manual throttle body setpoint control |
| 10 | Abs | Takes the absolute value of the error for use in the PID controllers |
| 11 | Relational Operator | If the Lookup Table output is greater then the error switch the motor direction to open or close the throttle body |
| 12 | Switch4 & 5 | Used to switch between the open and close PID controllers |
| 13 | Closed | This is the PID controller used for closing the throttle body |
| 14 | Open | This is the PID controller used for opening the throttle body |
| 15 | Saturation | Duty Cycle Upper Limit = 1, Lower Limit = 0 |

| | | |
|----|--------------------|--|
| 16 | Switch1 | If DC_Switch >= 1 switch to open loop duty cycle control to control the throttle body using MAN_DC |
| 17 | Switch3 | If ETBDirectionSwitch >= 1 use the relation operator to choose the motor direction otherwise use ETB_DIR |
| 18 | ETBDirectionSwitch | Chooses between automatic motor direction reversal or manual |
| 19 | ETB_DIR | Used for manual motor direction reversal |
| 20 | DC_Switch | Chooses between open loop and closed loop ETB control |
| 21 | MAN_DC | Open loop throttle body duty cycle setpoint |
| 22 | ETB_Period | Period used for throttle body control |
| 23 | RPCU_BIT_OUT_BL1 | Provides write access to the digital output used to flip the H-bridge/motor direction |
| 24 | RPCU_PWM_MIOS_BL1 | Used to update the PWM duty cycle for the throttle body motor |
| 25 | Lookup Table | This table provides a variable error that is allowed before the motor direction is switched to open or close the throttle body |

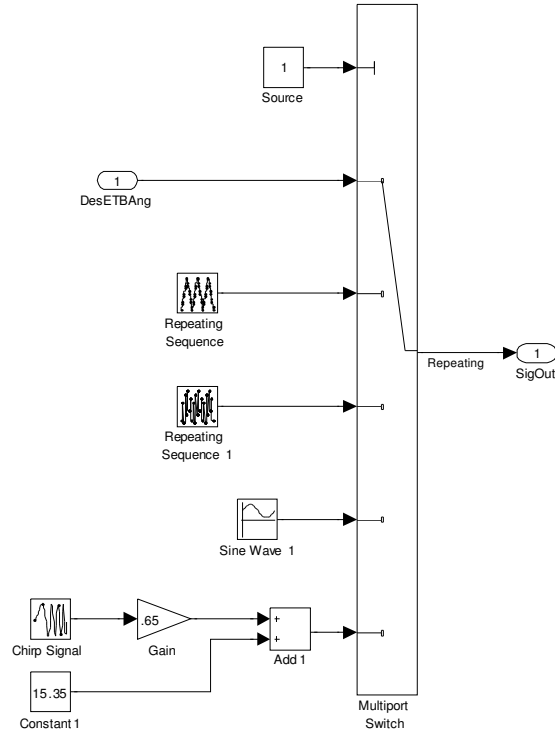


Figure A-XII-22: Source_Selector Subsystem

Source_Selector was used to supply various throttle position commanded signal patterns to the throttle position controller in order to monitor the response of the throttle controller.

Table A-XII-22: Source_Selector Summary

| # | Block Name | Description |
|---|------------------------------------|--|
| 1 | Source | Used to choose what the source/output of the Multiport switch will be |
| 2 | Repeating Sequence | This is the pyramid output signal used to test the throttle body |
| 3 | Repeating Sequence1 | This is the step response used to test the throttle body controller |
| 4 | Sine Wave1 | This is the sine wave that was used to test out the throttle body |
| 5 | Chirp Signal, Gain, Constant, Add1 | The chirp signal was not used but is another signal that may be used to test the throttle body |
| 6 | Multiport Switch | Uses the constant Source to choose what input is used for the subsystem output |

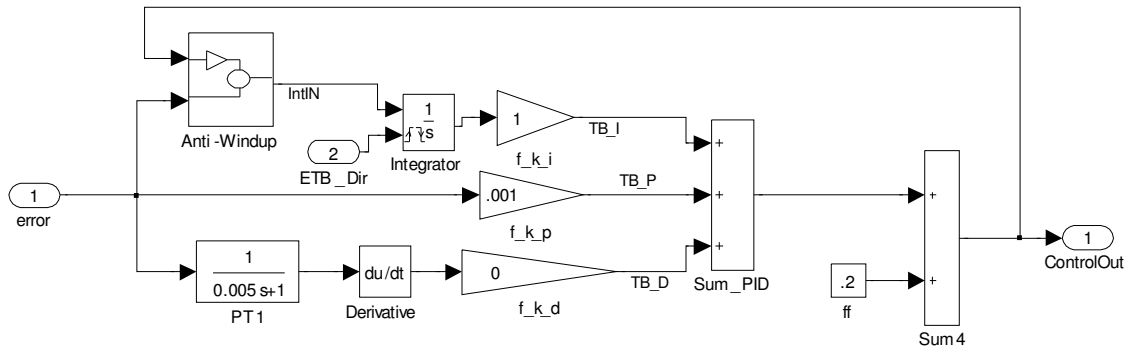


Figure A-XII-23: Closed Subsystem

The **Closed** subsystem was used to control the closing of the throttle plate.

Table A-XII-23: Closed Summary

| # | Block Name | Description |
|---|-------------|--|
| 1 | ff | Feedforward term was fixed at 0.2 since it was found that the throttle body duty cycle was always near 0.2 |
| 2 | PT1 | This is a filter to improve / remove the effect of noise on the derivative |
| 3 | Derivative | Numerical derivative, derivative action was removed from this PID controller |
| 4 | Integrator | Continuous Time Integration with reset switch, initial condition = 0, Every time the direction is swapped the integrator is reset |
| 5 | Anti-Windup | Allows the integral to integrate the error providing the feedback term absolute value does not exceed 1. Otherwise the integral receives a value of 0. |
| 6 | Sum_PID | Sums up the P, I and D parts of the controller |

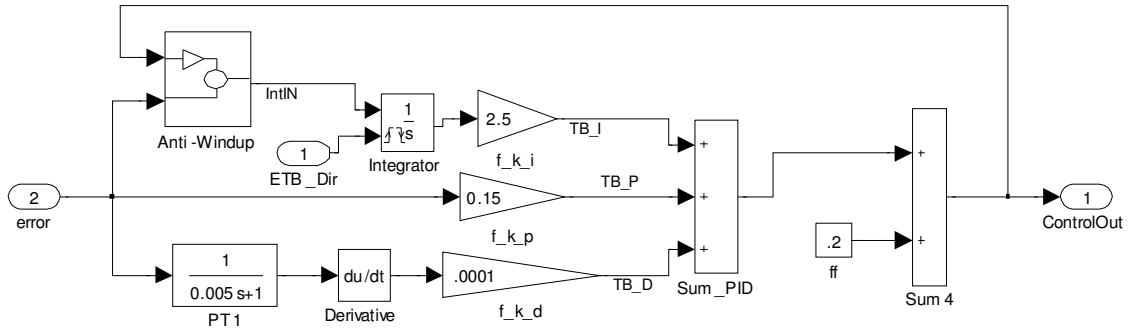


Figure A-XII-24: Open Subsystem

The **Open** subsystem was used to control the closing of the throttle plate.

Table A-XII-24: Open Summary

| # | Block Name | Description |
|---|-------------|--|
| 1 | ff | Feedforward term was fixed at 0.2 since it was found that the throttle body duty cycle was always near 0.2 |
| 2 | PT1 | This is a filter to improve / remove the effect of noise on the derivative |
| 3 | Derivative | Numerical derivative |
| 4 | Integrator | Continuous Time Integration with reset switch, initial condition = 0, Every time the direction is swapped the integrator is reset |
| 5 | Anti-Windup | Allows the integral to integrate the error providing the feedback term absolute value does not exceed 1. Otherwise the integral receives a value of 0. |
| 6 | Sum_PID | Sums up the P, I and D parts of the controller |

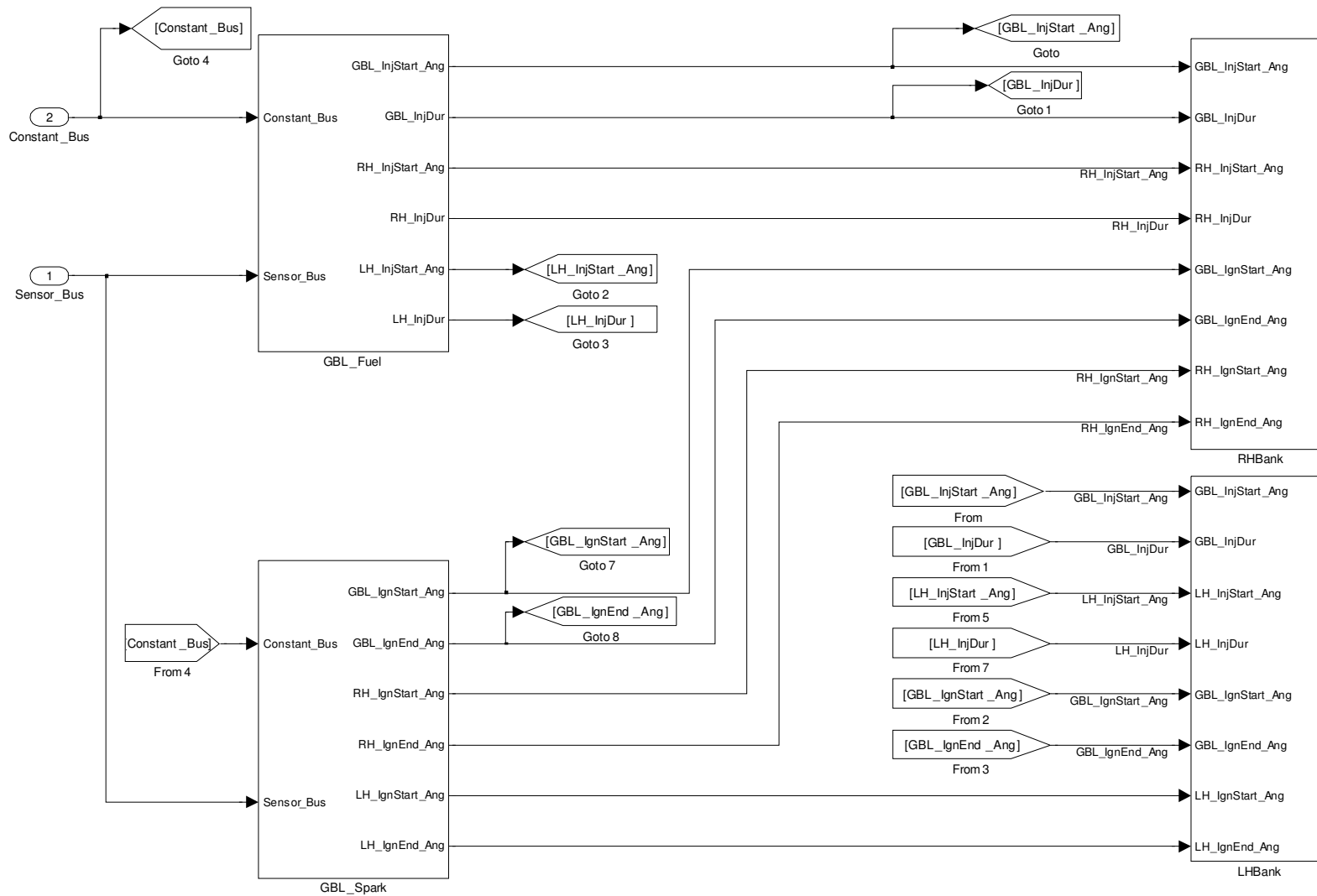


Figure A-XII-25: RPCU_Control_InjIgn Subsystem

RPCU_Control_InjIgn was used to control the injection events and the spark events that occur every combustion cycle.

Table A-XII-25: RPCU_Control_InjIgn Summary

| # | Block Name | Description |
|---|------------|--|
| 1 | GBL_Fuel | Includes subsystems to define bank specific fuelling, or global fuelling of the engine |
| 2 | GBL_Spark | Includes subsystems to define bank specific spark events, or global spark events of the engine |
| 3 | RH_Bank | Includes subsystems to schedule fuel and spark events for cylinder 1 to 4 |
| 4 | LH_Bank | Includes subsystems to schedule fuel and spark events for cylinder 5 to 8 |

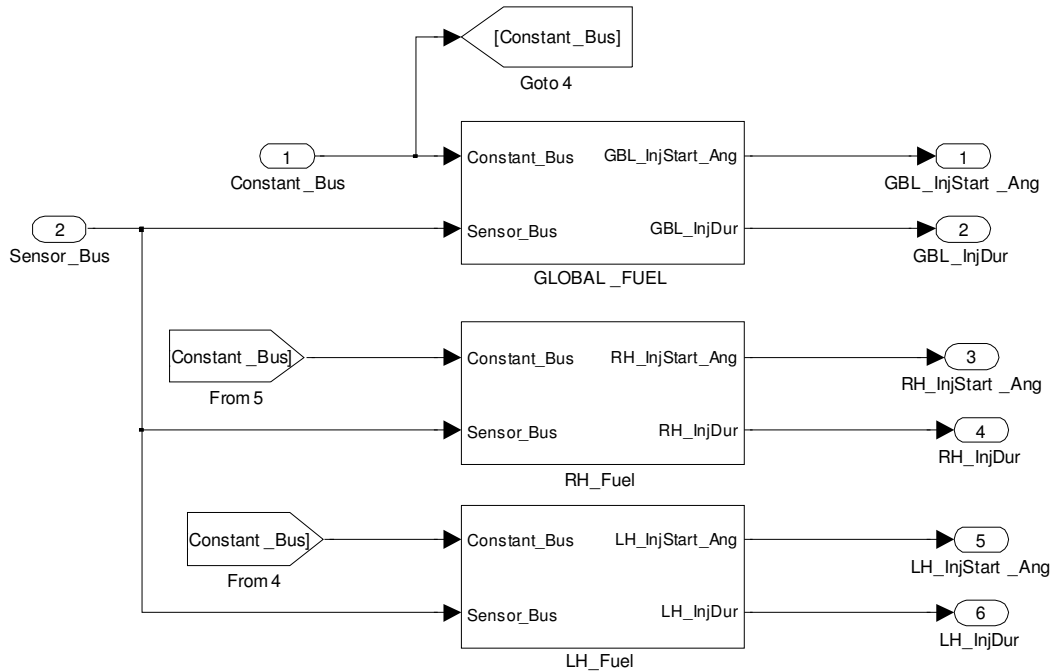


Figure A-XII-26: GBL_Fuel Subsystem

GBL_Fuel was implemented to allow various AFR control methods.

Table A-XII-26: GBL_Fuel Summary

| # | Block Name | Description |
|---|-------------|--|
| 1 | GLOBAL_FUEL | Includes subsystems for global scheduling of fuelling. One sensor may control both right and left bank AFR. |
| 2 | RH_FUEL | Includes subsystems for only right bank fuel scheduling. Right bank AFR sensor controls the right bank AFR sensor. |
| 3 | LH_FUEL | Includes subsystems for only left bank fuel scheduling. Left bank AFR sensor controls the left bank AFR sensor. |

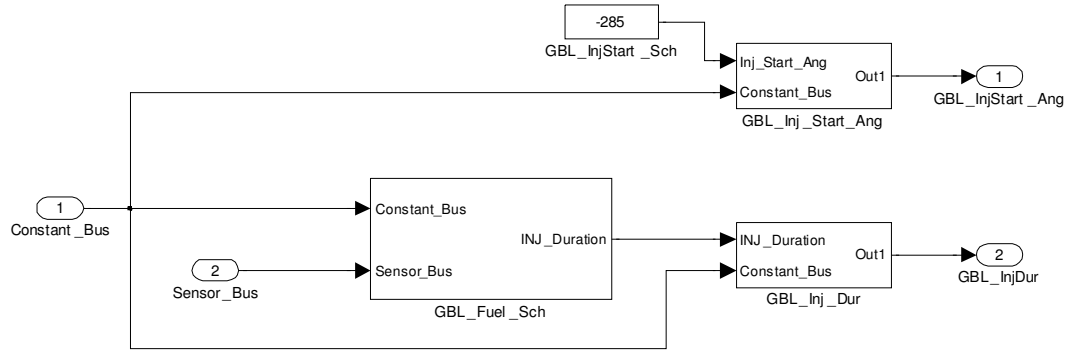


Figure A-XII-27:GLOBAL_FUEL Subsystem

GLOBAL_FUEL was implemented to allow one sensor the ability to control both right and left bank AFR/fuel injection duration.

Table A-XII-27: GLOBAL_FUEL Summary

| # | Block Name | Description |
|---|-------------------|---|
| 1 | GBL_Fuel_Sch | Contains subsystems for calculation of the required fuel to obtain the desired AFR setpoints in open and closed loop controller |
| 2 | GBL_Inj_Dur | Up to 15 injection events can be scheduled per combustion cycle, this subsystem is used to define the individual injection event durations |
| 3 | GBL_Inj_Start_Ang | Up to 15 injection events can be scheduled per combustion cycle, this subsystem is used to define the individual injection event start angles |
| 4 | GBL_InjStart_Sch | Default global injection start angle |

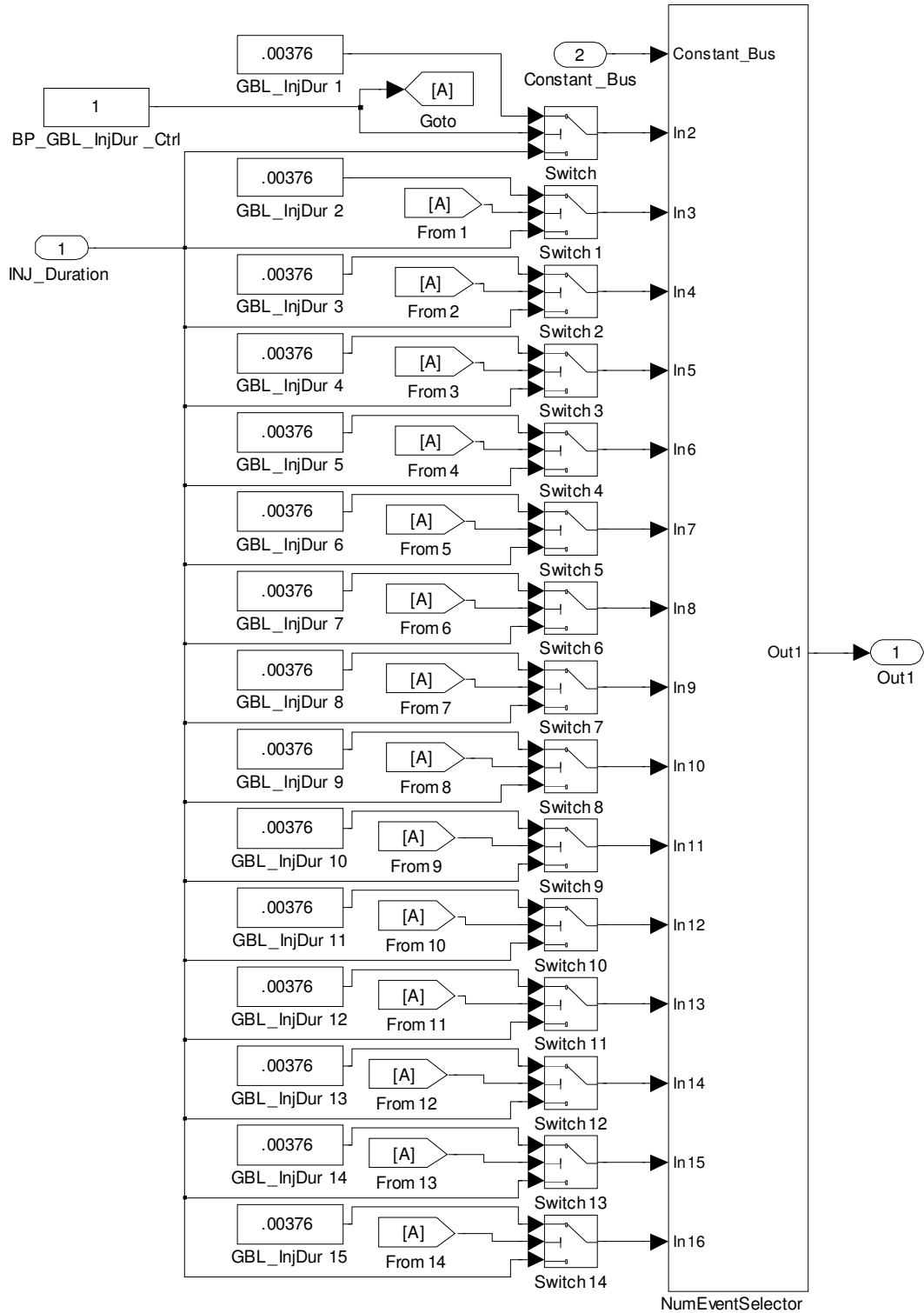


Figure A-XII-28: GBL_Inj_Dur Subsystem

GBL_Inj_Dur allows setting up to 15 injection duration events.

Table A-XII-28: GBL_Inj_Dur Summary

| # | Block Name | Description |
|---|--------------------|--|
| 1 | BP_GBL_InjDur_Ctrl | This constant is used to bypass the global injection duration control and manually command the 15 durations |
| 2 | Switch to Switch14 | If BP_GBL_InjDur_Ctrl \geq 1 use manual setpoints for all 15 injection events |
| 3 | GBL_Inj_Dur1 to 15 | Manual injection duration for the 15 injection events |
| 4 | NumEventSelector | 15 events are always programmed and this block is used to populate the extra events to be the same as the last commanded event of the 15 commanded events. If only one event is commanded then all 15 events will use the one setpoint |

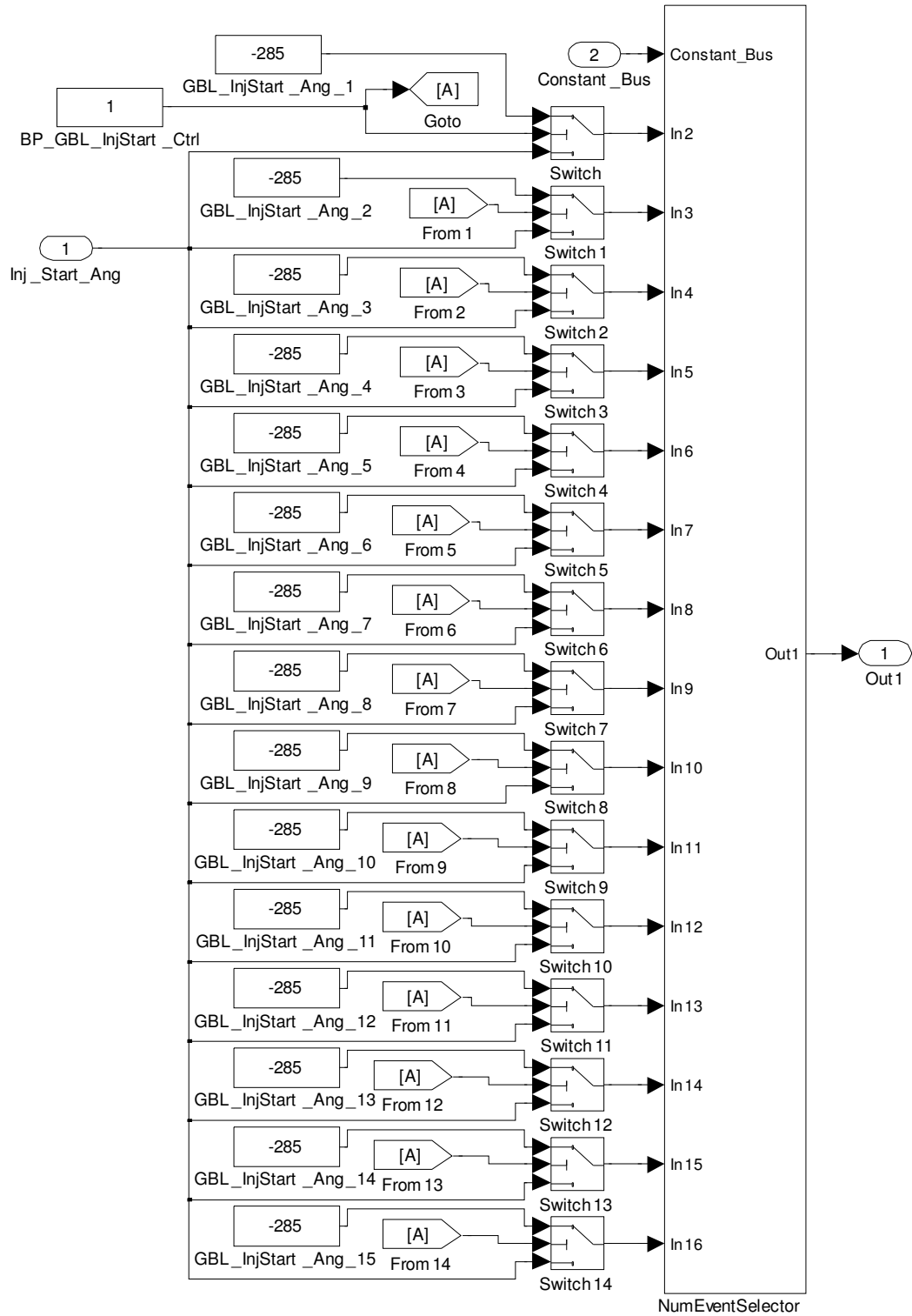


Figure A-XII-29: GBL_Inj_Start_Ang Subsystem

GBL_Inj_Start_Ang allows setting up to 15 injection start angles. Overlapping injection events are merged together. It is important to note how the dSPACE hardware/software is expecting its crank angles for injection and spark to be commanded. dSPACE assigns TDC compression as zero in the CAD for injection and spark (see Figure A-XII-30). In order to inject fuel at 645°CA, the dSPACE software requires a commanded input of -285°BTDC (see Figure A-XII-27 and Figure A-XII-30). Similarly in order to inject fuel at 260°CA, 100°BTDC would be commanded instead. The dSPACE software expects values between -360 and 360°CA. Presently no safety has been put in the model to prevent the user from commanding values outside of these bounds.

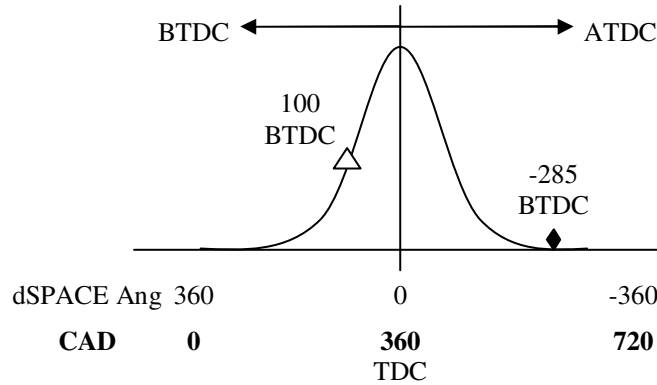


Figure A-XII-30: dSPACE Crank Angle Commands vs Actual Crank Angle Domain

Table A-XII-29: GBL_Inj_Start_Ang Summary

| # | Block Name | Description |
|---|--------------------------|---|
| 1 | Inj_Start_Ang | Globally available Injection Start Angle |
| 2 | BP_GBL_InjStart_Ctrl | Used to control the switches to choose between Inj_Start_Ang and GBL_InjStart_Ang values. |
| 3 | GBL_InjStart_Ang_1 to 15 | Includes subsystems for only left bank spark events |
| 4 | Switch to Switch 14 | Switches to choose between one single injection start angle or individual start angles for multiple pulses. |
| 5 | ConstantBus | Supplies the number of injection events to schedule |
| 6 | NumEventSelector | Creates the vector of injection events |

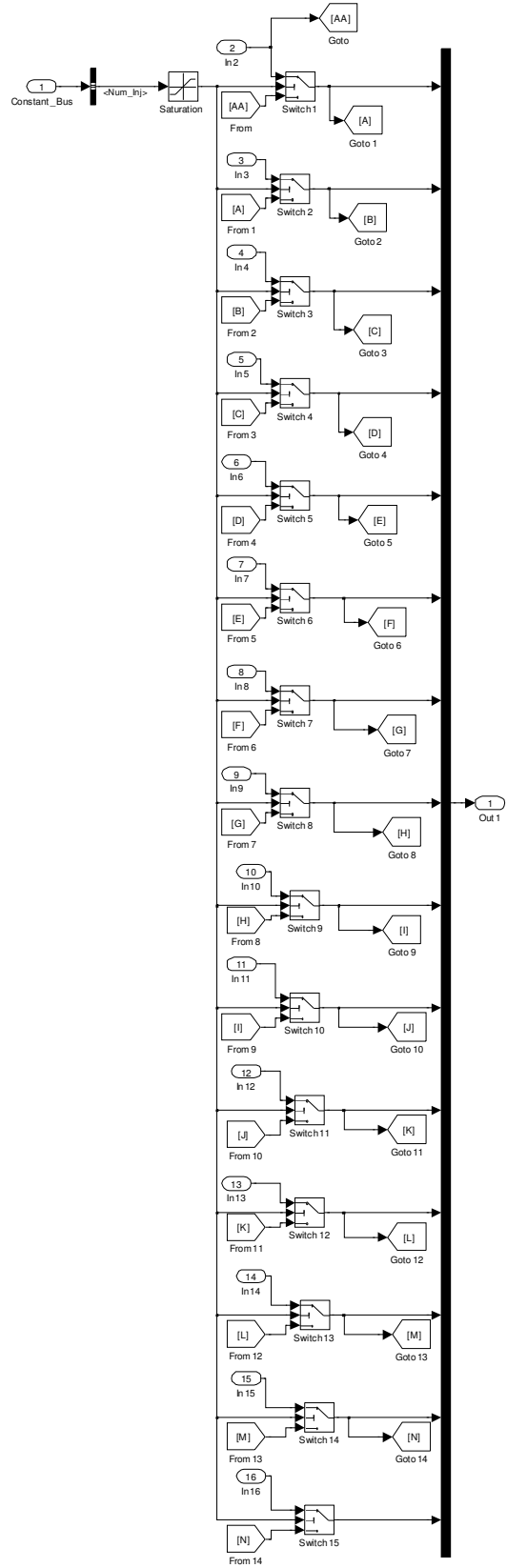


Figure A-XII-31: NumEventSelector Subsystem

Table A-XII-30: NumEventSelector Summary

| # | Block Name | Description |
|----------|-------------------|--|
| 1 | ConstantBus | Supplies the number of injection events |
| 2 | Saturation | Includes subsystems for only right bank spark events |
| 3 | Switch 1 to 15 | Includes subsystems for only left bank spark events |
| 4 | From, Goto | The From and Goto blocks were used to cascade down the last unique injection event and fill the remaining events until all 15 events are filled. |

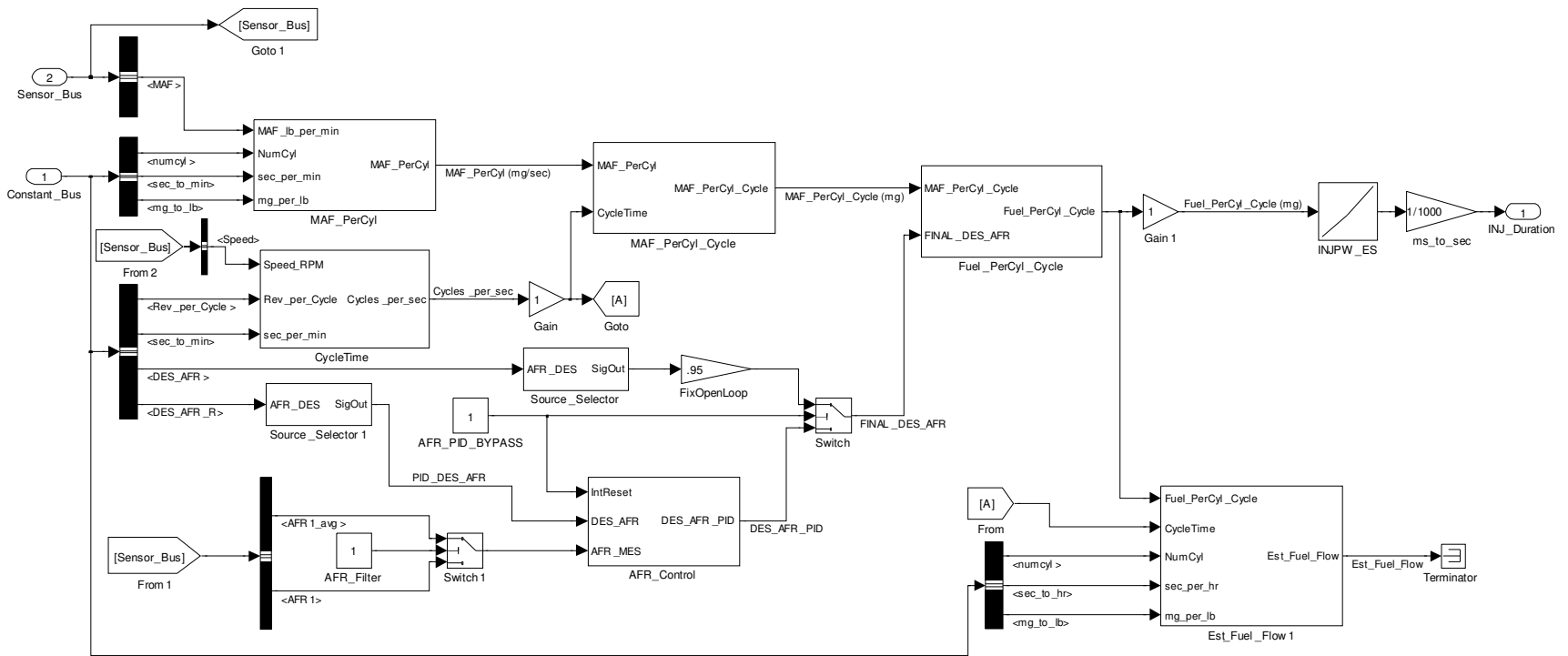


Figure A-XII-32: GBL_Fuel_Sch, Global Fuel Pulse Width Control

GBL_Fuel_Sch receives the sensor feedback (**AFR1_avg**, **MAF**, **Speed**, see Figure A-XII-32) and is used to determine the required fuel PW based on the open loop or closed loop commanded AFR setpoint.

Table A-XII-31: GBL_Fuel_Sch Summary

| # | Block Name | Description |
|----|------------------------------------|--|
| 1 | Sensor_Bus | Supplies AFR1_avg , MAF , Speed |
| | Constant_Bus | Supplies required constants for calculations |
| 2 | MAF_PerCyl | Calculates the air flow rate consumed by each cylinder in mg/sec using Eq. 2-3. |
| 3 | CycleTime | Calculates how many combustion cycles occur every second (Speed /(2*60)). |
| 4 | MAF_PerCyl_Cycle | Calculates how many mg of air are consumed by each cylinder (MAF_PerCyl/CycleTime). |
| 5 | Fuel_PerCyl_Cycle | Calculates how many mg of fuel is required based on the desired AFR (FINAL_DES_AFR) that is commanded (MAF_PerCyl_Cycle/FINAL_DES_AFR). |
| 6 | INJPW_ES | Determines the required PW to inject the required amount of fuel. |
| 7 | Source_Selector & Source_Selector1 | Allow the user the ability to supply various changing command setpoints such as; a step function, sine wave or other user defined repeating signals, if the basic manual setpoint was not desired. |
| 8 | AFR_PID_BYPASS | Used to switch between open loop (OL) and closed loop (CL) control (1 = OL, 0 = CL), it was also used to reset the integrator initial condition to the desired AFR (IntReset). |
| 9 | AFR_Filter | Allowed the user to choose between a filtered and unfiltered AFR sensor feedback signal (1 = Average, 0 = Raw). |
| | Switch | Used to choose between open and closed loop control of the Final AFR used to calculate fuel pulse width |
| | FixOpenLoop | Used to compensate for steady state offset that was observed in AFR |
| 10 | Est_Fuel_Flow1 | Estimates the fuel flow rate (lb/hr) to compare with the test cell flow rate, but has no purpose in the fuel PW controller. |

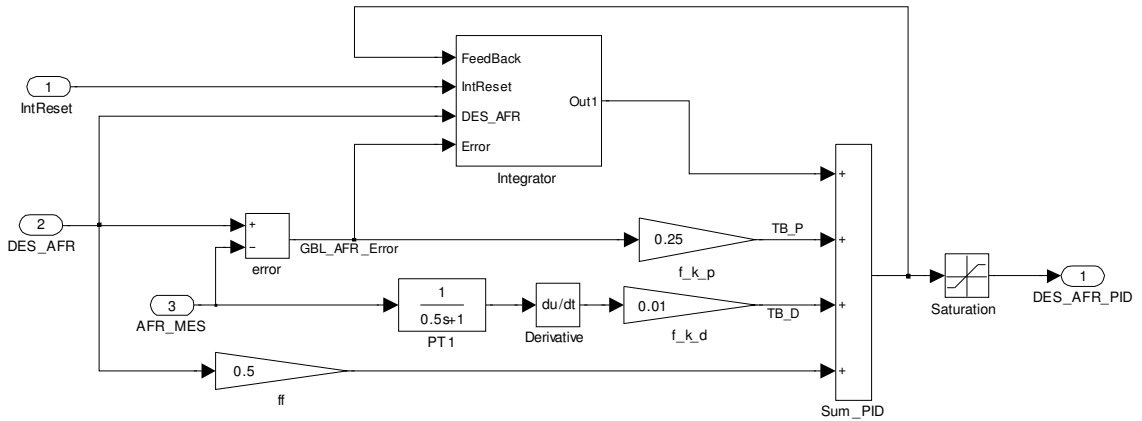


Figure A-XII-33: AFR_Control Subsystem

AFR_Control includes the PID controller that was implemented in order to control the update value of **Final_DES_AFR**. The derivative was relocated to use the sensor feedback signal as opposed to the error signal to reduce the derivative kick (see Figure A-XII-33) as discussed in chapter 2.3.4. The **Anti-Windup** block was reworked to allow different low and high saturation limits (see Figure A-XII-3). The gains were all manually tuned until the system performance was reasonable. The final gain values used can be found in Table 3.6.

Table A-XII-1: AFR_Control Summary

| # | Block Name | Description |
|----|-------------|--|
| 1 | IntReset | This signal is used to reset the integrator to allow for bumpless transfer into PID control from open loop control |
| 2 | DES_AFR | This is the desired AFR value |
| 3 | AFR_MES | This is the measured AFR signal |
| 4 | error | Calculates the difference between the setpoint and the feedback measurement |
| 5 | PT1 | This is a filter applied on the sensor feedback signal before the derivative is calculated. |
| 6 | Derivative | Calculates the derivative of the measured AFR signal |
| 7 | Integrator | Calculates the integral of the error signal |
| 8 | f_k_p | This is the proportional gain |
| 9 | f_k_d | This is the derivative gain |
| 10 | ff | This is the feedforward gain |
| 11 | Sum_PID | Used to sum up the P, I and D components |
| 12 | Saturation | Upper Limit = 50 Lower Limit = 10 |
| 13 | DES_AFR_PID | Desired AFR setpoint |

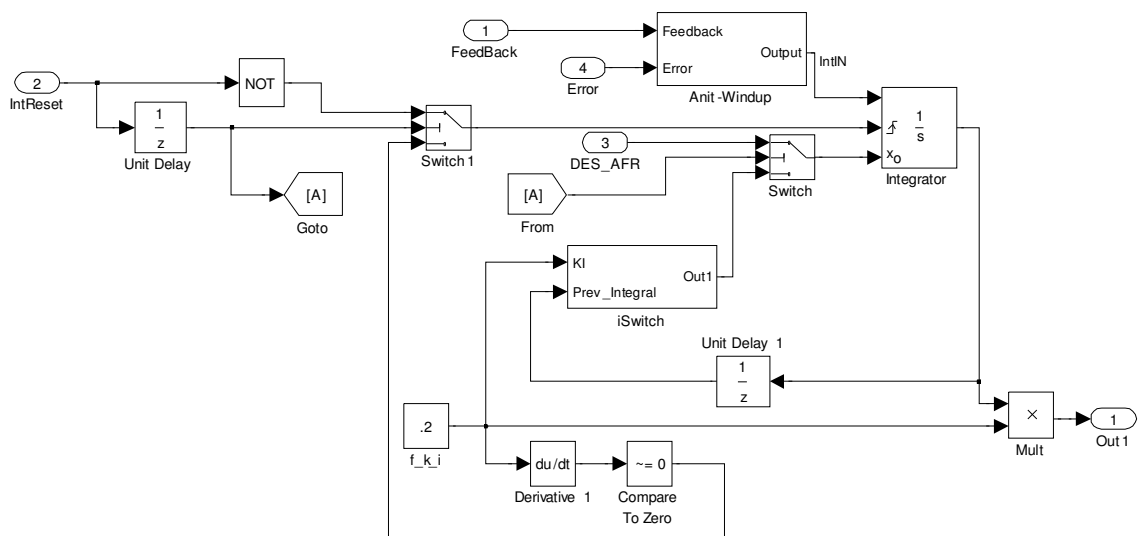


Figure A-XII-1: Integrator Subsystem w/Bumpless Transfer

The **Integrator** subsystem was reworked to include bumpless transfer. This allows a smoother transition from OL to CL control by supplying **AFR_PID_BYPASS** to **IntReset** (see Figure A-XII-1). Taking the derivative of **f_k_i** (the integral gain), allows the detection of when the gain has been modified, as the derivative will always be zero unless it was modified. Once **Derivative1** triggers the **Compare to Zero** block, the **Integrator** is reset to the initial condition, output by **iSwitch** (see Figure A-XII-2).

Table A-XII-2: Integrator Summary

| # | Block Name | Description |
|----|-----------------|--|
| 1 | IntReset | Receives input from AFR_PID_BYPASS |
| 2 | Unit Delay | Delays the output of IntReset |
| 3 | NOT | Used to invert IntReset and create a rising edge signal to reset the integrator initial condition to DES_AFR |
| 4 | Switch, Switch1 | Used to switch after the first cycle of running the PID controller to detect when the integral gain is modified. |
| 5 | Anti-Windup | Used to cut off the integrator when the output is out of range |
| 6 | Integrator | Integrates the error signal |
| 7 | Mult | Multiplies the integrator output by the integrator gain |
| 8 | Unit Delay1 | Used to store the last known value of the integrator |
| 9 | Compare To Zero | Triggered by Derivative 1 when the integral gain is modified |
| 10 | Derivative 1 | Used to detect when the integral gain f_k_i is modified |
| 11 | Feedback | Output from Sum_PID |
| 12 | error | Calculated error signal (AFR setpoint - measured AFR) |
| 13 | f_k_i | Integrator gain |
| 14 | iSwitch | Used to calculate the new integrator initial condition based on the changed integrator gain |
| 15 | DES_AFR | This is the desired AFR |

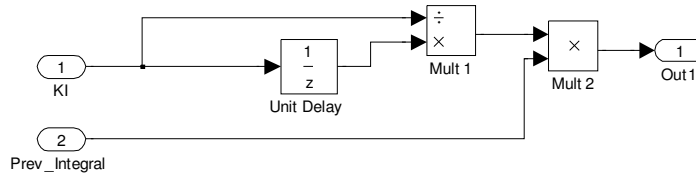


Figure A-XII-2: iSwitch Subsystem

iSwitch was used to allow for parameter changes to the **KI** gain. It was implemented to prevent the Integrator from becoming stuck.

Table A-XII-3: iSwitch Summary

| # | Block Name | Description |
|---|---------------|---|
| 1 | KI | This is the integral gain value |
| 2 | Prev_Integral | This is the last known value output by the integral |
| 3 | Unit Delay | This is used to store the last known value of KI |
| 4 | Mult1 | Calculates KI_{new}/KI_{old} |
| 5 | Mult2 | Calculates $Prev_Integral * KI_{new}/KI_{old}$ |
| 6 | Out1 | This is the new integral initial condition |

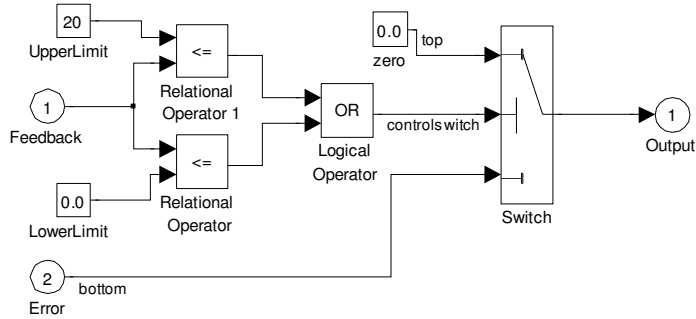


Figure A-XII-3: Anti-Windup Subsystem

This **Anti-Windup** subsystem was designed to allow different upper and lower limit values to cut off the integration.

Table A-XII-4: Anti-Windup Summary

| # | Block Name | Description |
|---|-----------------------|--|
| 1 | Feedback | This is the output from Sum_PID |
| 2 | error | Difference between the desired AFR and the measured AFR |
| 3 | UpperLimit | When the AFR exceeds this UpperLimit then integration is cut off |
| 4 | LowerLimit | When the AFR is below the LowerLimit the integration is cut off |
| 5 | Relational Operator | If Feedback \leq LowerLimit the output is 1 |
| 6 | Relational Operator 1 | If Feedback \geq UpperLimit the output is 1 |
| 7 | Logical Operator | If one of the Relational Operators is = 1 then the integrator uses the value of zero for integration |
| 8 | zero | zero is integrated when the relational operators output 1 since the controller is said to be winding up |
| 9 | Switch | Used to choose the source signal for integration |

APPENDIX XIII : MOTORING RESULTS

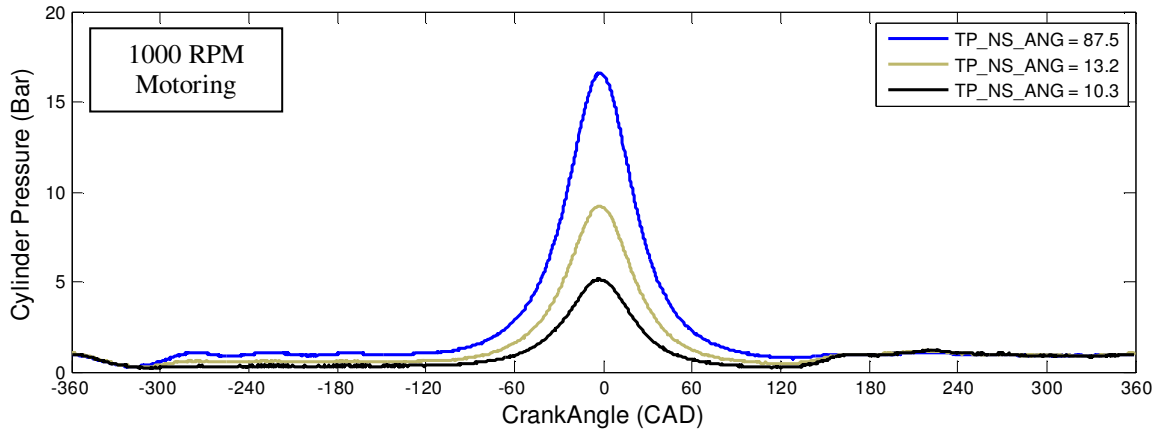


Figure A-XIII-1: 1000 RPM Motoring Curves

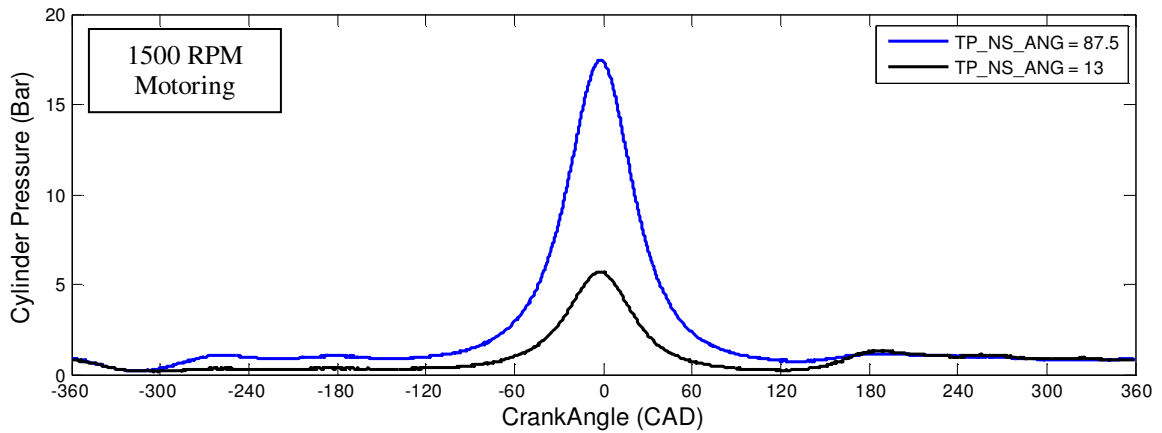


Figure A-XIII-2: 1500 RPM Motoring Curves

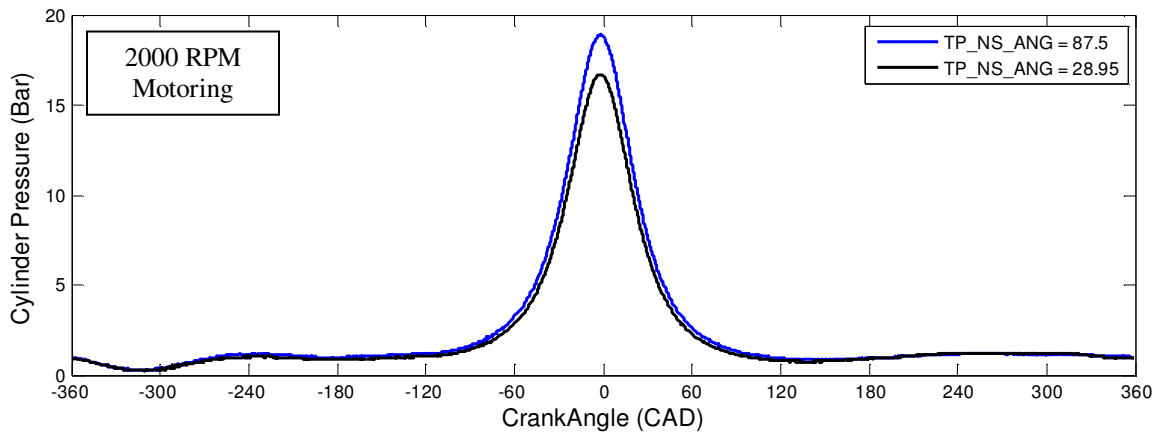


Figure A-XIII-3: 2000 RPM Motoring Curves

APPENDIX XIV : ADDITIONAL ENGINE OPERATION RESULTS

This following section includes the results from the additional load points that were tested. Data from 1000 RPM -17.7 inHg and 2000 RPM WOT for both production PCM operation and OL dSPACE operation are not included in this appendix, since they are presented in section 4.5 of the thesis main body. The CL results were nearly identical to the OL results, therefore only the results for 1000 RPM -17.7 inHg and 2000 RPM WOT are included at the end of this appendix as they were omitted from the main thesis body. All remaining load points for CL have been omitted as they were redundant. Each of the load points listed in Table 3.3, were successfully operated and controlled.

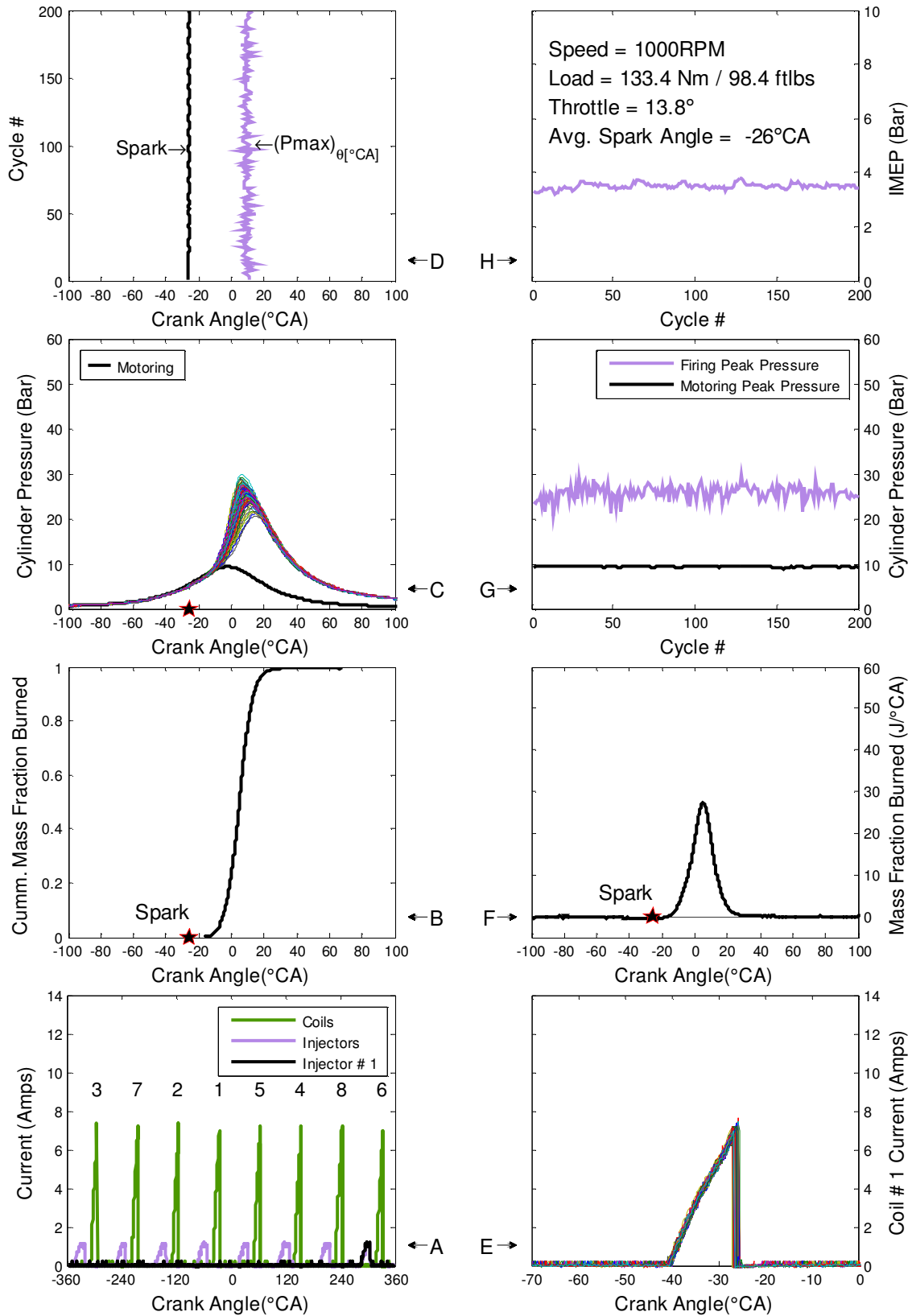


Figure A-XIV-1: Production 1000 RPM 100 ft-lb Combustion Data

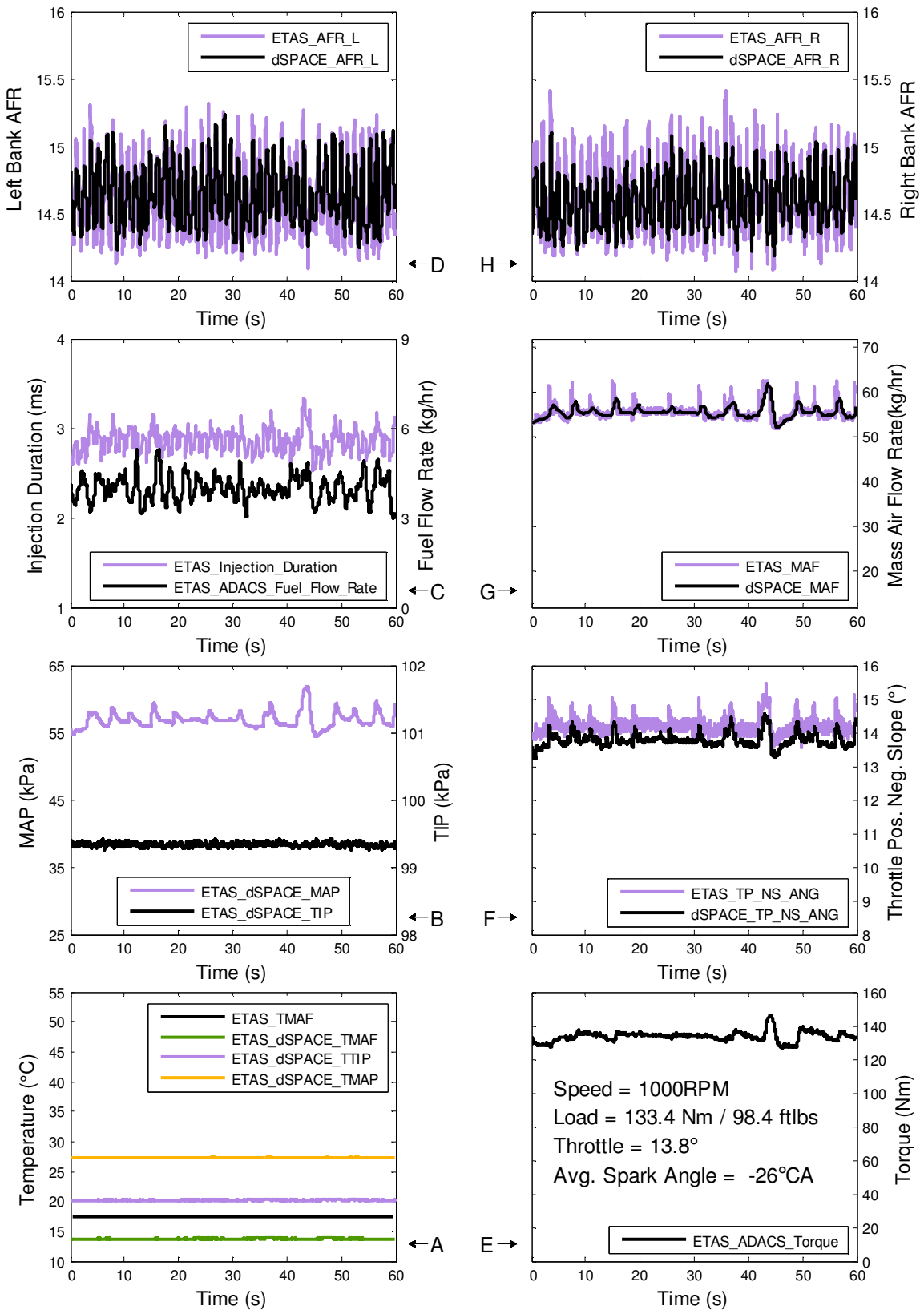


Figure A-XIV-2: Production 1000 RPM 100 ft-lb PCM Measurements

Table A-XIV-1: 1000 RPM 100 ft-lb Production Controller Data Summary

| | Left Bank AFR | | | Right Bank AFR | | |
|-----------------|---------------|------|--------|----------------|------|--------|
| | ETAS | LA4 | dSPACE | ETAS | LA4 | dSPACE |
| Mean | 14.59 | 8.02 | 14.64 | 14.59 | 8.02 | 14.60 |
| Std. | 0.28 | 0.00 | 0.22 | 0.26 | 0.00 | 0.20 |
| Coeff. Var. (%) | 1.90 | 0.01 | 1.50 | 1.78 | 0.00 | 1.37 |

| | Inj. Dur. (ms) | | Fuel Flow (kg/hr) | | MAF (kg/hr) | |
|-----------------|----------------|--------|-------------------|--------|-------------|--------|
| | ETAS | dSPACE | ETAS | dSPACE | ETAS | dSPACE |
| Mean | 2.86 | 0.00 | 3.99 | 3.99 | 55.72 | 55.48 |
| Std. | 0.12 | 0.00 | 0.42 | 0.42 | 1.84 | 1.38 |
| Coeff. Var. (%) | 4.33 | 0.00 | 10.42 | 10.42 | 3.30 | 2.49 |

| | MAP (kPa) | | TIP (kPa) | | TP_NS (°) | |
|-----------------|-----------|--------|-----------|--------|-----------|--------|
| | ETAS | dSPACE | ETAS | dSPACE | ETAS | dSPACE |
| Mean | 56.87 | 56.87 | 99.33 | 99.33 | 14.22 | 13.78 |
| Std. | 1.19 | 1.19 | 0.02 | 0.02 | 0.23 | 0.21 |
| Coeff. Var. (%) | 2.09 | 2.09 | 0.02 | 0.02 | 1.64 | 1.50 |

| | TMAP (°C) | | TTIP (°C) | | TMAF (°C) | |
|-----------------|-----------|--------|-----------|--------|-----------|--------|
| | ETAS | dSPACE | ETAS | dSPACE | ETAS | dSPACE |
| Mean | 27.34 | 27.34 | 20.17 | 20.17 | 17.45 | 13.72 |
| Std. | 0.03 | 0.03 | 0.02 | 0.02 | 0.02 | 0.04 |
| Coeff. Var. (%) | 0.10 | 0.10 | 0.12 | 0.12 | 0.11 | 0.30 |

| | Torque (Nm) | | CA50 (°CA) | | Spark (°CA) | |
|-----------------|-------------|--------|------------|--------|-------------|--------|
| | ETAS | dSPACE | ETAS | dSPACE | ETAS | dSPACE |
| Mean | 133.45 | 133.45 | 4.67 | 4.67 | -26.04 | -26.04 |
| Std. | 2.96 | 2.96 | 1.80 | 1.80 | 0.37 | 0.37 |
| Coeff. Var. (%) | 0.00 | 2.22 | 38.56 | 38.56 | 1.43 | 1.43 |

| | Pmax (bar) | | CA Pmax (°CA) | | IMEP (bar) | |
|-----------------|------------|--------|---------------|--------|------------|--------|
| | ETAS | dSPACE | ETAS | dSPACE | ETAS | dSPACE |
| Mean | 25.78 | 25.78 | 9.33 | 9.33 | 3.50 | 3.50 |
| Std. | 1.52 | 1.52 | 1.74 | 1.74 | 0.10 | 0.10 |
| Coeff. Var. (%) | 5.88 | 5.88 | 18.62 | 18.62 | 2.92 | 2.92 |

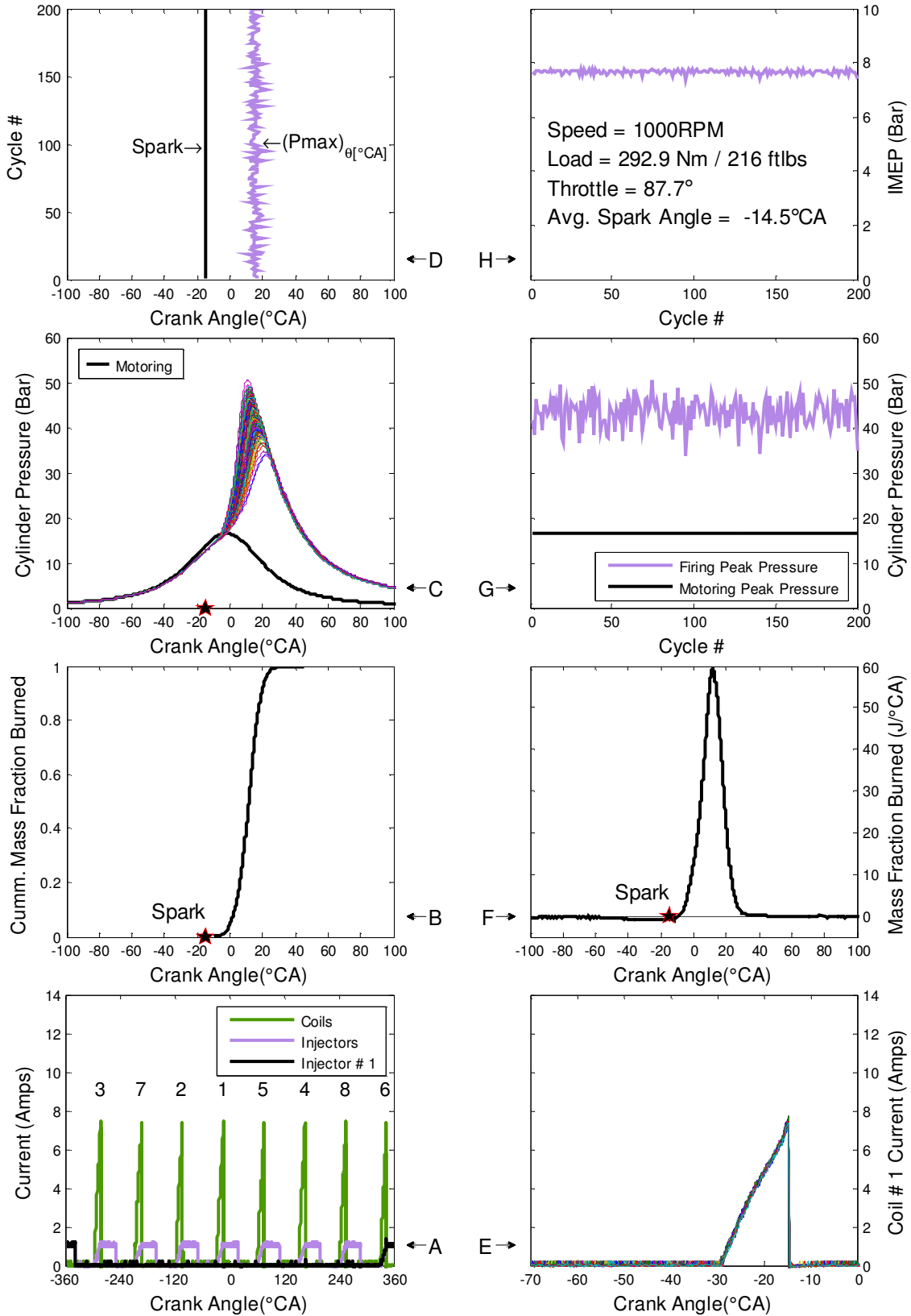


Figure A-XIV-3: Production 1000 RPM WOT Combustion Data

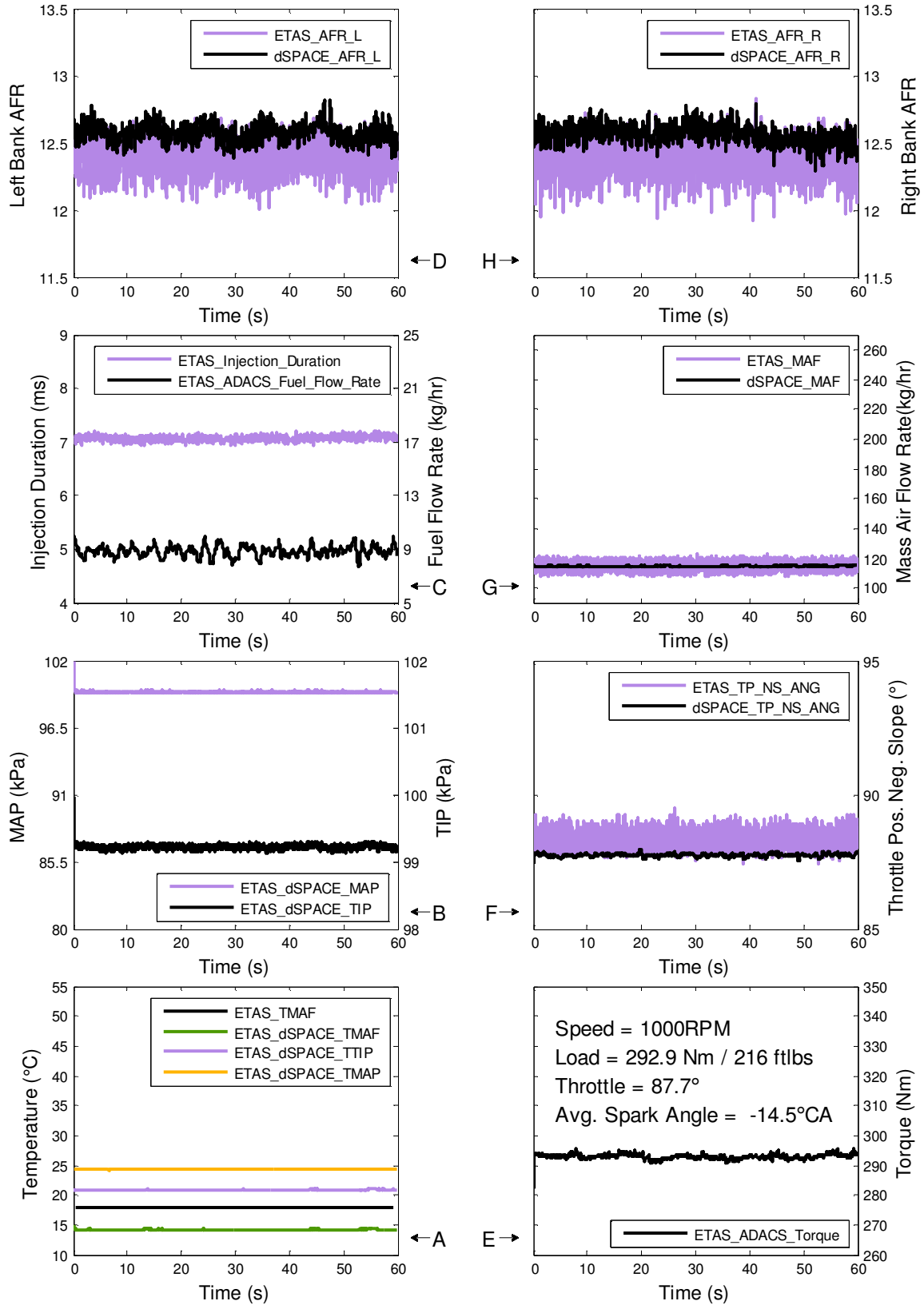


Figure A-XIV-4: Production 1000 RPM WOT PCM Measurements

Table A-XIV-2: 1000 RPM WOT Production Controller Data Summary

| | Left Bank AFR | | | Right Bank AFR | | |
|-----------------|---------------|-----|--------|----------------|-----|--------|
| | ETAS | LA4 | dSPACE | ETAS | LA4 | dSPACE |
| Mean | 12.40 | NA | 12.57 | 12.39 | NA | 12.56 |
| Std. | 0.11 | NA | 0.06 | 0.12 | NA | 0.07 |
| Coeff. Var. (%) | 0.86 | NA | 0.51 | 0.99 | NA | 0.54 |

| | Inj. Dur. (ms) | | Fuel Flow (kg/hr) | | MAF (kg/hr) | |
|-----------------|----------------|--------|-------------------|--------|-------------|--------|
| | ETAS | dSPACE | ETAS | dSPACE | ETAS | dSPACE |
| Mean | 7.07 | NA | 8.84 | NA | 115.14 | 114.44 |
| Std. | 0.05 | NA | 0.41 | NA | 2.69 | 0.27 |
| Coeff. Var. (%) | 0.66 | NA | 4.64 | NA | 2.34 | 0.24 |

| | MAP (kPa) | | TIP (kPa) | | TP_NS (°) | |
|-----------------|-----------|--------|-----------|--------|-----------|--------|
| | ETAS | dSPACE | ETAS | dSPACE | ETAS | dSPACE |
| Mean | 99.43 | NA | 99.22 | NA | 88.22 | 87.75 |
| Std. | 0.08 | NA | 0.03 | NA | 0.30 | 0.05 |
| Coeff. Var. (%) | 0.08 | NA | 0.03 | NA | 0.34 | 0.06 |

| | TMAP (°C) | | TTIP (°C) | | TMAF (°C) | |
|-----------------|-----------|--------|-----------|--------|-----------|--------|
| | ETAS | dSPACE | ETAS | dSPACE | ETAS | dSPACE |
| Mean | 24.27 | NA | 20.93 | NA | 17.89 | 14.23 |
| Std. | 0.02 | NA | 0.03 | NA | 0.02 | 0.05 |
| Coeff. Var. (%) | 0.10 | NA | 0.13 | NA | 0.10 | 0.33 |

| | Torque (Nm) | | CA50 (°CA) | | Spark (°CA) | |
|-----------------|-------------|--------|------------|--------|-------------|--------|
| | ETAS | dSPACE | ETAS | dSPACE | ETAS | dSPACE |
| Mean | 292.86 | NA | 11.24 | NA | -14.52 | NA |
| Std. | 0.80 | NA | 2.13 | NA | 0.10 | NA |
| Coeff. Var. (%) | 0.00 | NA | 18.95 | NA | 0.67 | NA |

| | Pmax (bar) | | CA Pmax (°CA) | | IMEP (bar) | |
|-----------------|------------|--------|---------------|--------|------------|--------|
| | ETAS | dSPACE | ETAS | dSPACE | ETAS | dSPACE |
| Mean | 43.25 | NA | 15.31 | NA | 7.66 | NA |
| Std. | 3.17 | NA | 2.23 | NA | 0.08 | NA |
| Coeff. Var. (%) | 7.33 | NA | 14.56 | NA | 0.98 | NA |

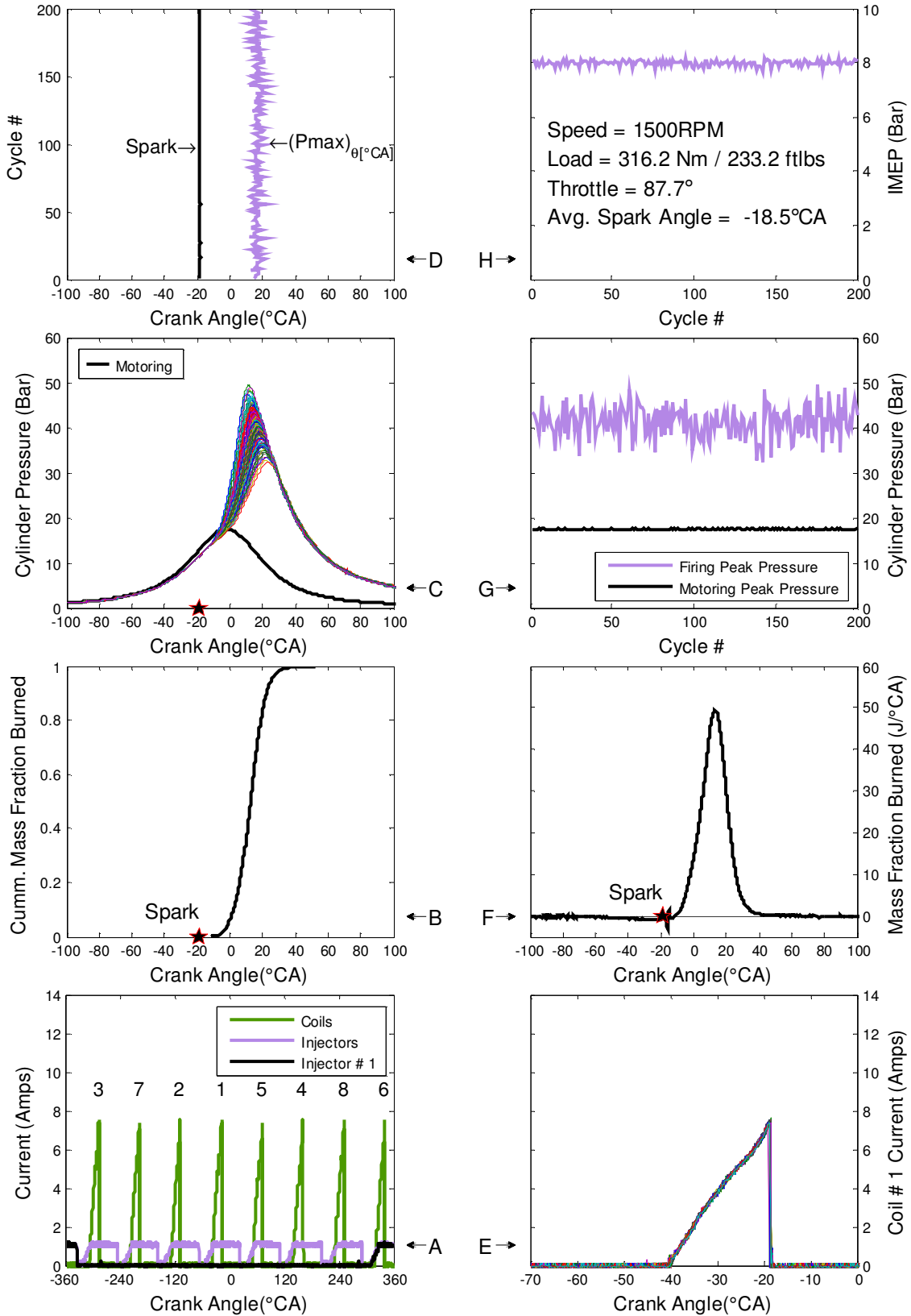


Figure A-XIV-5: Production 1500 RPM WOT Combustion Data

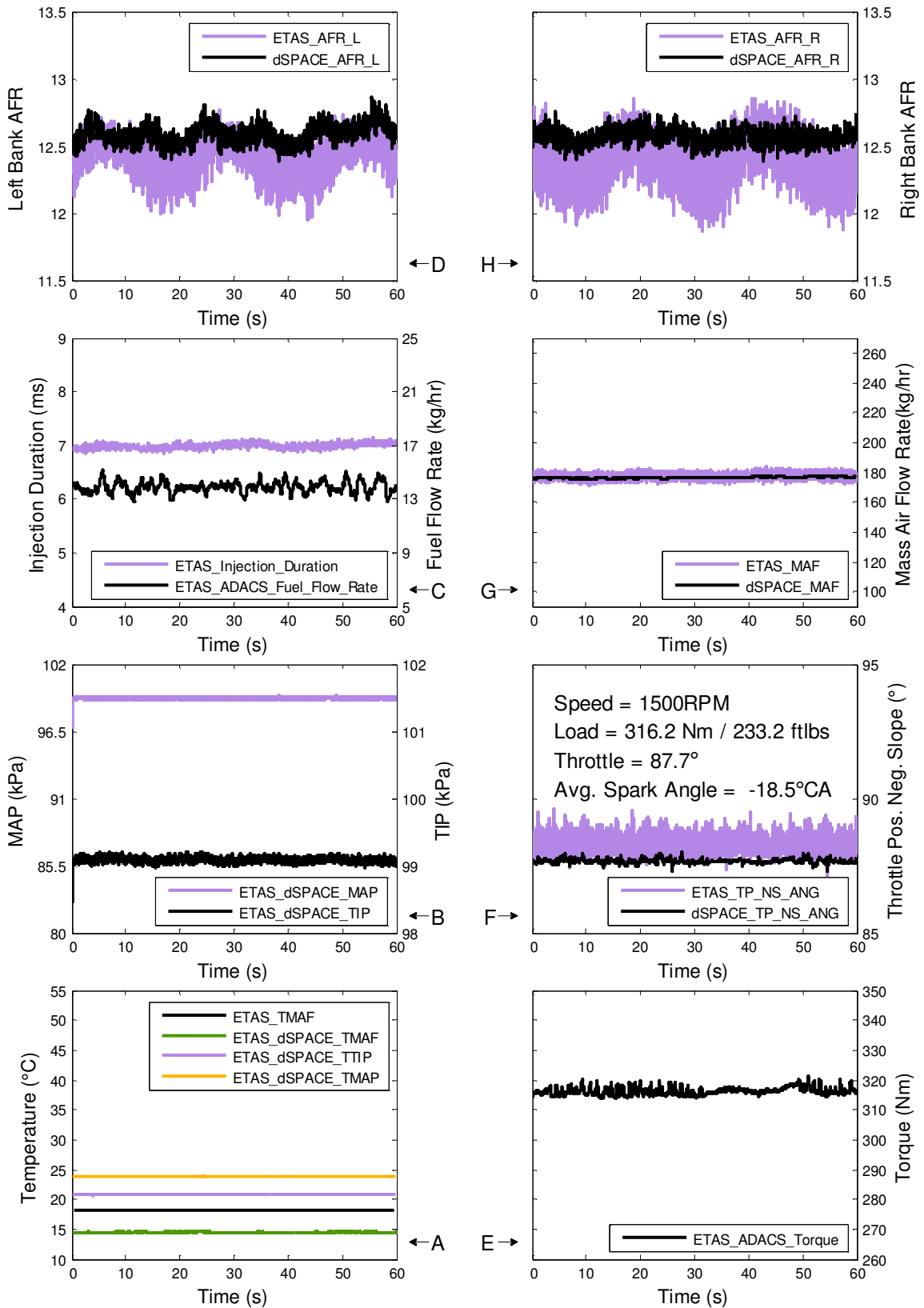


Figure A-XIV-6: Production 1500 RPM WOT PCM Measurements

Table A-XIV-3: 1500 RPM WOT Production Controller Data Summary

| | Left Bank AFR | | | Right Bank AFR | | |
|-----------------|---------------|-----|--------|----------------|-----|--------|
| | ETAS | LA4 | dSPACE | ETAS | LA4 | dSPACE |
| Mean | 12.41 | NA | 12.59 | 12.38 | NA | 12.57 |
| Std. | 0.13 | NA | 0.07 | 0.16 | NA | 0.06 |
| Coeff. Var. (%) | 1.05 | NA | 0.59 | 1.33 | NA | 0.45 |

| | Inj. Dur. (ms) | | Fuel Flow (kg/hr) | | MAF (kg/hr) | |
|-----------------|----------------|--------|-------------------|--------|-------------|--------|
| | ETAS | dSPACE | ETAS | dSPACE | ETAS | dSPACE |
| Mean | 6.99 | NA | 13.88 | NA | 177.17 | 176.26 |
| Std. | 0.05 | NA | 0.43 | NA | 2.12 | 0.46 |
| Coeff. Var. (%) | 0.68 | NA | 3.11 | NA | 1.20 | 0.26 |

| | MAP (kPa) | | TIP (kPa) | | TP_NS (°) | |
|-----------------|-----------|--------|-----------|--------|-----------|--------|
| | ETAS | dSPACE | ETAS | dSPACE | ETAS | dSPACE |
| Mean | 99.24 | NA | 99.08 | NA | 88.23 | 87.67 |
| Std. | 0.09 | NA | 0.04 | NA | 0.33 | 0.08 |
| Coeff. Var. (%) | 0.09 | NA | 0.04 | NA | 0.37 | 0.10 |

| | TMAP (°C) | | TTIP (°C) | | TMAF (°C) | |
|-----------------|-----------|--------|-----------|--------|-----------|--------|
| | ETAS | dSPACE | ETAS | dSPACE | ETAS | dSPACE |
| Mean | 23.82 | NA | 20.83 | NA | 18.19 | 14.51 |
| Std. | 0.03 | NA | 0.03 | NA | 0.04 | 0.05 |
| Coeff. Var. (%) | 0.14 | NA | 0.16 | NA | 0.21 | 0.36 |

| | Torque (Nm) | | CA50 (°CA) | | Spark (°CA) | |
|-----------------|-------------|--------|------------|--------|-------------|--------|
| | ETAS | dSPACE | ETAS | dSPACE | ETAS | dSPACE |
| Mean | 316.24 | NA | 12.45 | NA | -18.52 | NA |
| Std. | 1.22 | NA | 2.37 | NA | 0.11 | NA |
| Coeff. Var. (%) | 0.00 | NA | 19.07 | NA | 0.57 | NA |

| | Pmax (bar) | | CA Pmax (°CA) | | IMEP (bar) | |
|-----------------|------------|--------|---------------|--------|------------|--------|
| | ETAS | dSPACE | ETAS | dSPACE | ETAS | dSPACE |
| Mean | 41.18 | NA | 16.75 | NA | 7.98 | NA |
| Std. | 3.44 | NA | 2.42 | NA | 0.10 | NA |
| Coeff. Var. (%) | 8.36 | NA | 14.46 | NA | 1.25 | NA |

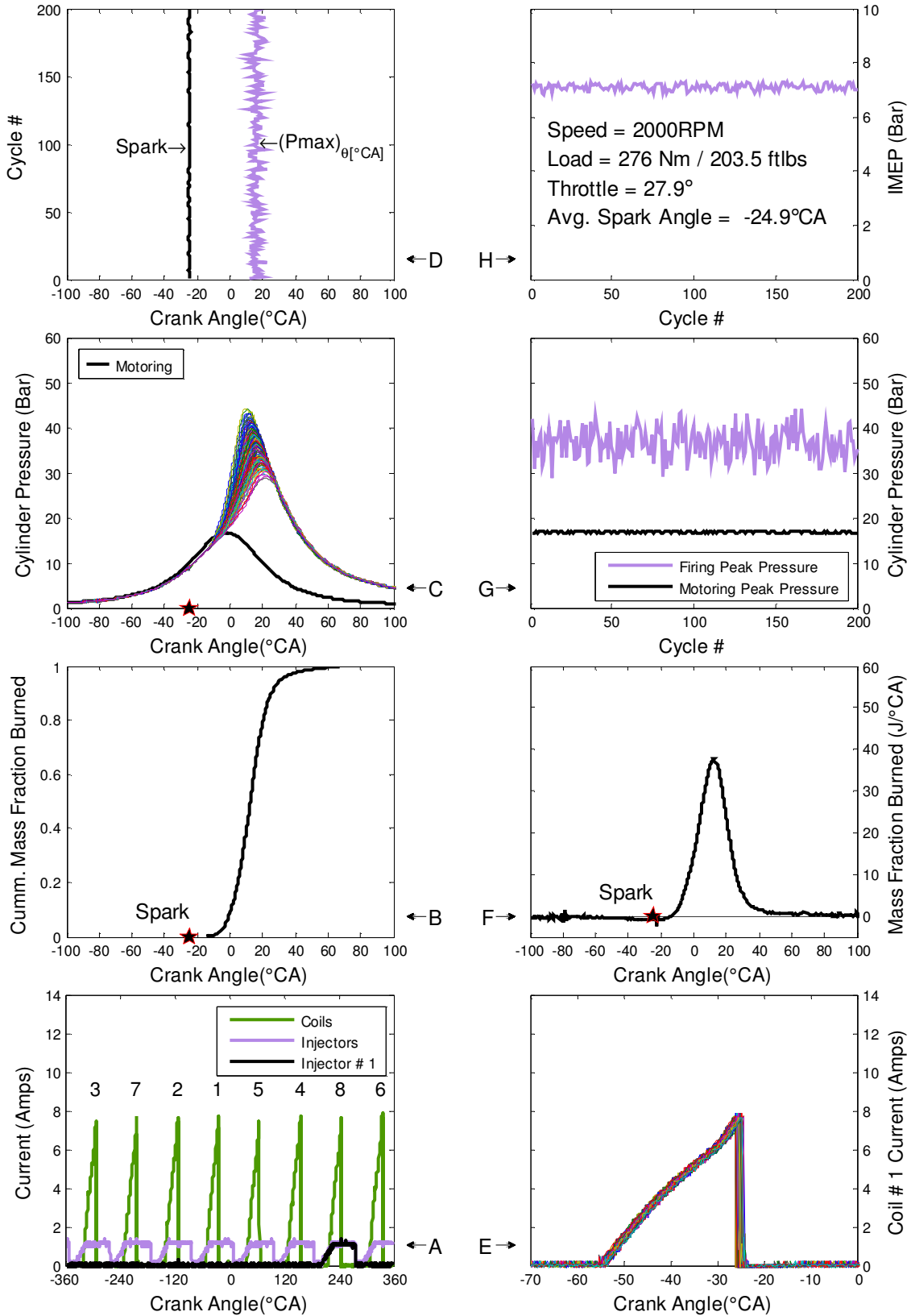


Figure A-XIV-7: Production 2000 RPM 35% Pedal Combustion Data

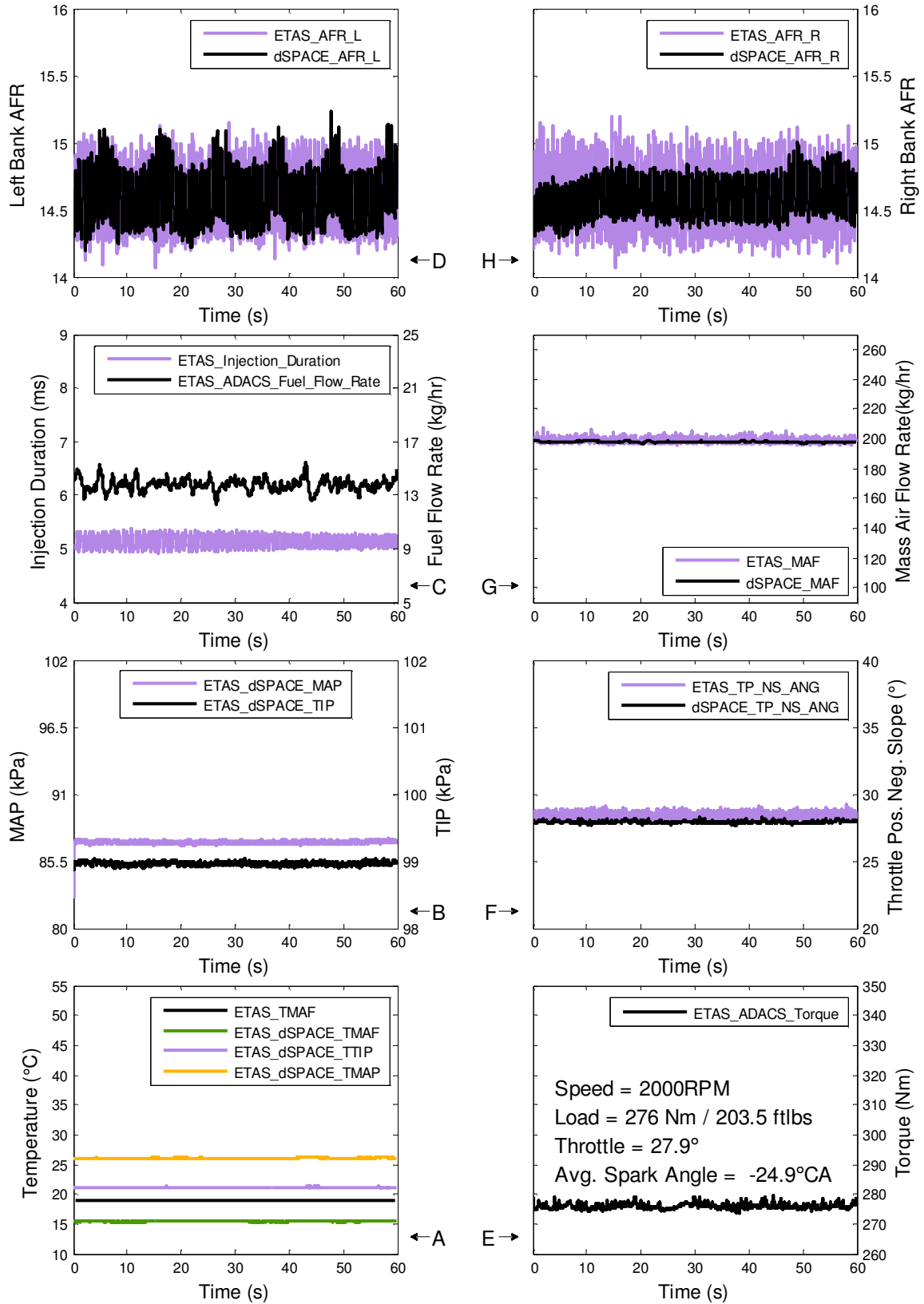


Figure A-XIV-8: Production 2000 RPM 35% Pedal PCM Measurements

Table A-XIV-4: 2000 RPM WOT Production Controller Data Summary

| | Left Bank AFR | | | Right Bank AFR | | |
|-----------------|---------------|-----|--------|----------------|-----|--------|
| | ETAS | LA4 | dSPACE | ETAS | LA4 | dSPACE |
| Mean | 14.58 | NA | 14.60 | 14.57 | NA | 14.59 |
| Std. | 0.24 | NA | 0.21 | 0.23 | NA | 0.15 |
| Coeff. Var. (%) | 1.61 | NA | 1.45 | 1.57 | NA | 1.02 |

| | Inj. Dur. (ms) | | Fuel Flow (kg/hr) | | MAF (kg/hr) | |
|-----------------|----------------|--------|-------------------|--------|-------------|--------|
| | ETAS | dSPACE | ETAS | dSPACE | ETAS | dSPACE |
| Mean | 5.15 | NA | 13.78 | NA | 199.00 | 197.80 |
| Std. | 0.11 | NA | 0.47 | NA | 1.33 | 0.38 |
| Coeff. Var. (%) | 2.23 | NA | 3.40 | NA | 0.67 | 0.19 |

| | MAP (kPa) | | TIP (kPa) | | TP_NS (°) | |
|-----------------|-----------|--------|-----------|--------|-----------|--------|
| | ETAS | dSPACE | ETAS | dSPACE | ETAS | dSPACE |
| Mean | 87.06 | NA | 98.96 | NA | 28.40 | 27.90 |
| Std. | 0.15 | NA | 0.02 | NA | 0.20 | 0.08 |
| Coeff. Var. (%) | 0.17 | NA | 0.02 | NA | 0.69 | 0.28 |

| | TMAP (°C) | | TTIP (°C) | | TMAF (°C) | |
|-----------------|-----------|--------|-----------|--------|-----------|--------|
| | ETAS | dSPACE | ETAS | dSPACE | ETAS | dSPACE |
| Mean | 26.04 | NA | 21.18 | NA | 18.94 | 15.41 |
| Std. | 0.03 | NA | 0.03 | NA | 0.02 | 0.05 |
| Coeff. Var. (%) | 0.10 | NA | 0.14 | NA | 0.13 | 0.31 |

| | Torque (Nm) | | CA50 (°CA) | | Spark (°CA) | |
|-----------------|-------------|--------|------------|--------|-------------|--------|
| | ETAS | dSPACE | ETAS | dSPACE | ETAS | dSPACE |
| Mean | 275.96 | NA | 12.28 | NA | -24.95 | NA |
| Std. | 0.84 | NA | 2.64 | NA | 0.40 | NA |
| Coeff. Var. (%) | 0.00 | NA | 21.54 | NA | 1.62 | NA |

| | Pmax (bar) | | CA Pmax (°CA) | | IMEP (bar) | |
|-----------------|------------|--------|---------------|--------|------------|--------|
| | ETAS | dSPACE | ETAS | dSPACE | ETAS | dSPACE |
| Mean | 36.62 | NA | 16.09 | NA | 7.10 | NA |
| Std. | 3.34 | NA | 2.43 | NA | 0.12 | NA |
| Coeff. Var. (%) | 9.13 | NA | 15.08 | NA | 1.63 | NA |

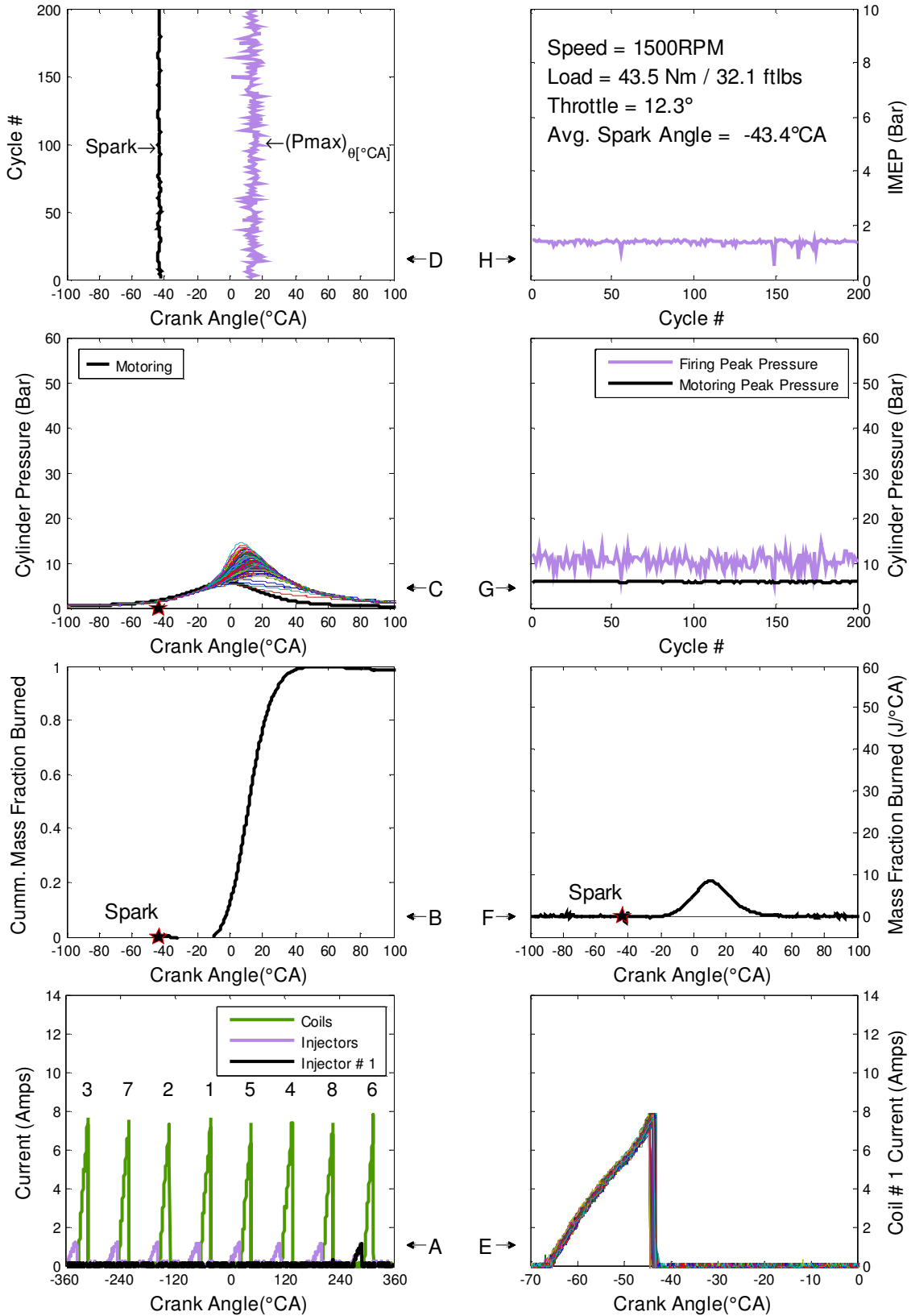


Figure A-XIV-9: Production 1500 RPM -17.7 inHg Combustion Data

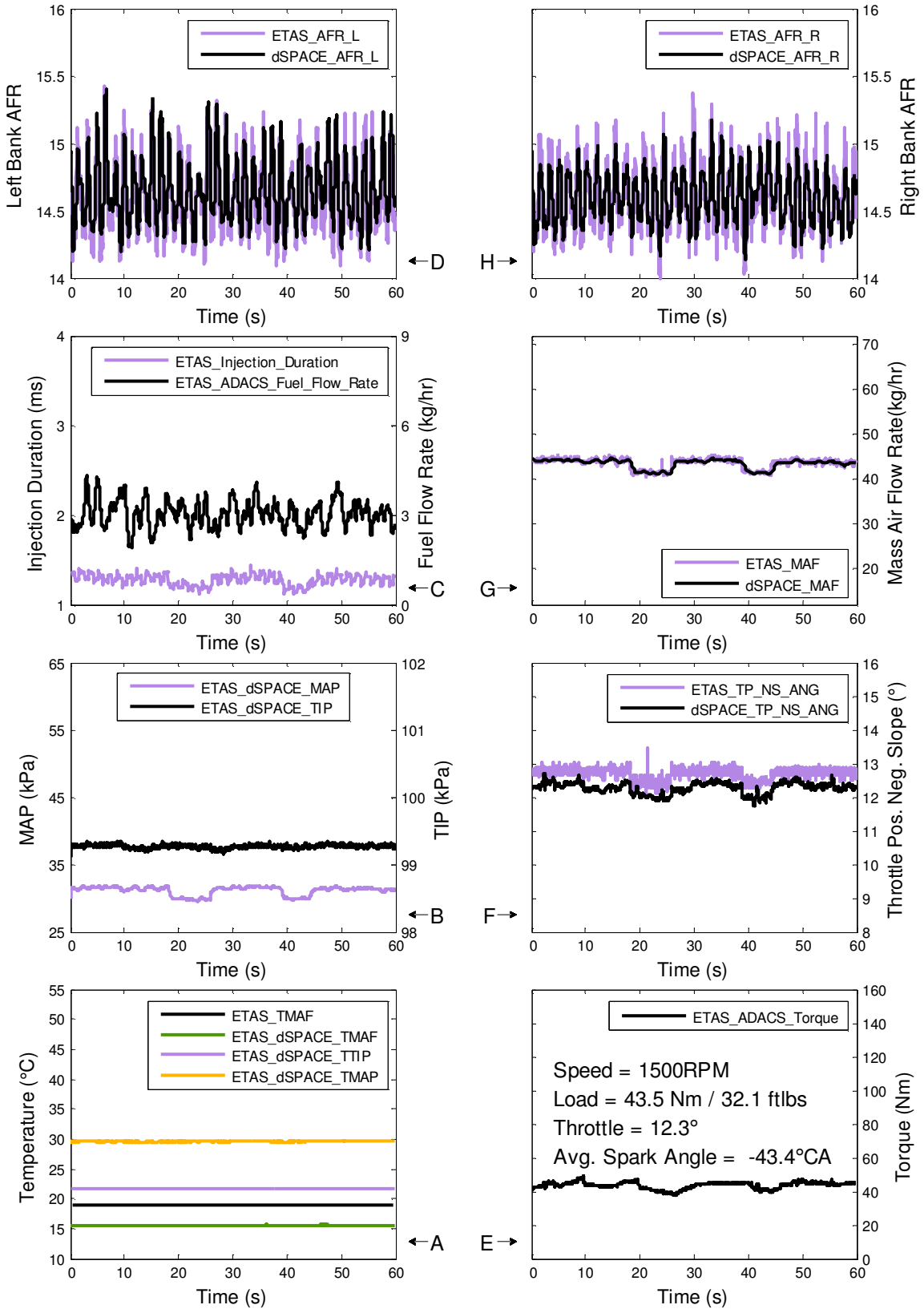


Figure A-XIV-10: Production 1500 RPM -17.7 inHg PCM Measurements

Table A-XIV-5: 1500 RPM –17.7 inHg Production Controller Data Summary

| | Left Bank AFR | | | Right Bank AFR | | |
|-----------------|---------------|-----|--------|----------------|-----|--------|
| | ETAS | LA4 | dSPACE | ETAS | LA4 | dSPACE |
| Mean | 14.58 | NA | 14.65 | 14.58 | NA | 14.60 |
| Std. | 0.28 | NA | 0.25 | 0.24 | NA | 0.19 |
| Coeff. Var. (%) | 1.93 | NA | 1.70 | 1.67 | NA | 1.31 |

| | Inj. Dur. (ms) | | Fuel Flow (kg/hr) | | MAF (kg/hr) | |
|-----------------|----------------|--------|-------------------|--------|-------------|--------|
| | ETAS | dSPACE | ETAS | dSPACE | ETAS | dSPACE |
| Mean | 1.28 | NA | 3.04 | NA | 43.54 | 43.40 |
| Std. | 0.06 | NA | 0.45 | NA | 1.13 | 1.05 |
| Coeff. Var. (%) | 4.74 | NA | 14.85 | NA | 2.59 | 2.42 |

| | MAP (kPa) | | TIP (kPa) | | TP_NS (°) | |
|-----------------|-----------|--------|-----------|--------|-----------|--------|
| | ETAS | dSPACE | ETAS | dSPACE | ETAS | dSPACE |
| Mean | 31.10 | NA | 99.27 | NA | 12.70 | 12.27 |
| Std. | 0.66 | NA | 0.03 | NA | 0.16 | 0.17 |
| Coeff. Var. (%) | 2.12 | NA | 0.03 | NA | 1.25 | 1.35 |

| | TMAP (°C) | | TTIP (°C) | | TMAF (°C) | |
|-----------------|-----------|--------|-----------|--------|-----------|--------|
| | ETAS | dSPACE | ETAS | dSPACE | ETAS | dSPACE |
| Mean | 29.58 | NA | 21.69 | NA | 18.92 | 15.52 |
| Std. | 0.03 | NA | 0.02 | NA | 0.03 | 0.04 |
| Coeff. Var. (%) | 0.11 | NA | 0.11 | NA | 0.15 | 0.29 |

| | Torque (Nm) | | CA50 (°CA) | | Spark (°CA) | |
|-----------------|-------------|--------|------------|--------|-------------|--------|
| | ETAS | dSPACE | ETAS | dSPACE | ETAS | dSPACE |
| Mean | 43.53 | NA | 12.30 | NA | -43.40 | NA |
| Std. | 2.05 | NA | 5.87 | NA | 0.42 | NA |
| Coeff. Var. (%) | 0.00 | NA | 47.69 | NA | 0.98 | NA |

| | Pmax (bar) | | CA Pmax (°CA) | | IMEP (bar) | |
|-----------------|------------|--------|---------------|--------|------------|--------|
| | ETAS | dSPACE | ETAS | dSPACE | ETAS | dSPACE |
| Mean | 10.43 | NA | 13.94 | NA | 1.36 | NA |
| Std. | 1.58 | NA | 2.86 | NA | 0.10 | NA |
| Coeff. Var. (%) | 15.12 | NA | 20.54 | NA | 7.32 | NA |

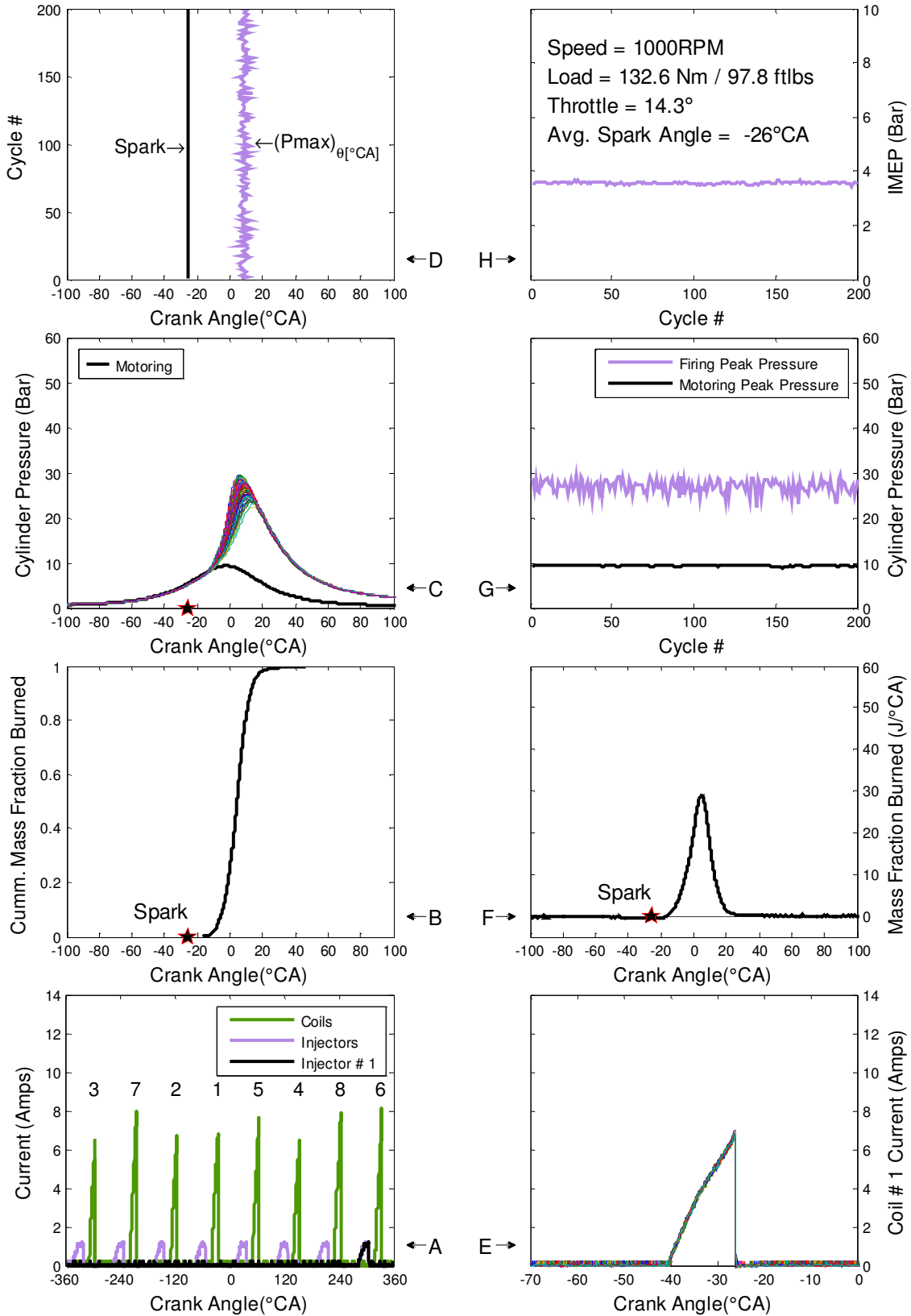


Figure A-XIV-11: dSPACE OL 1000 RPM 100 ft-lb Combustion Data

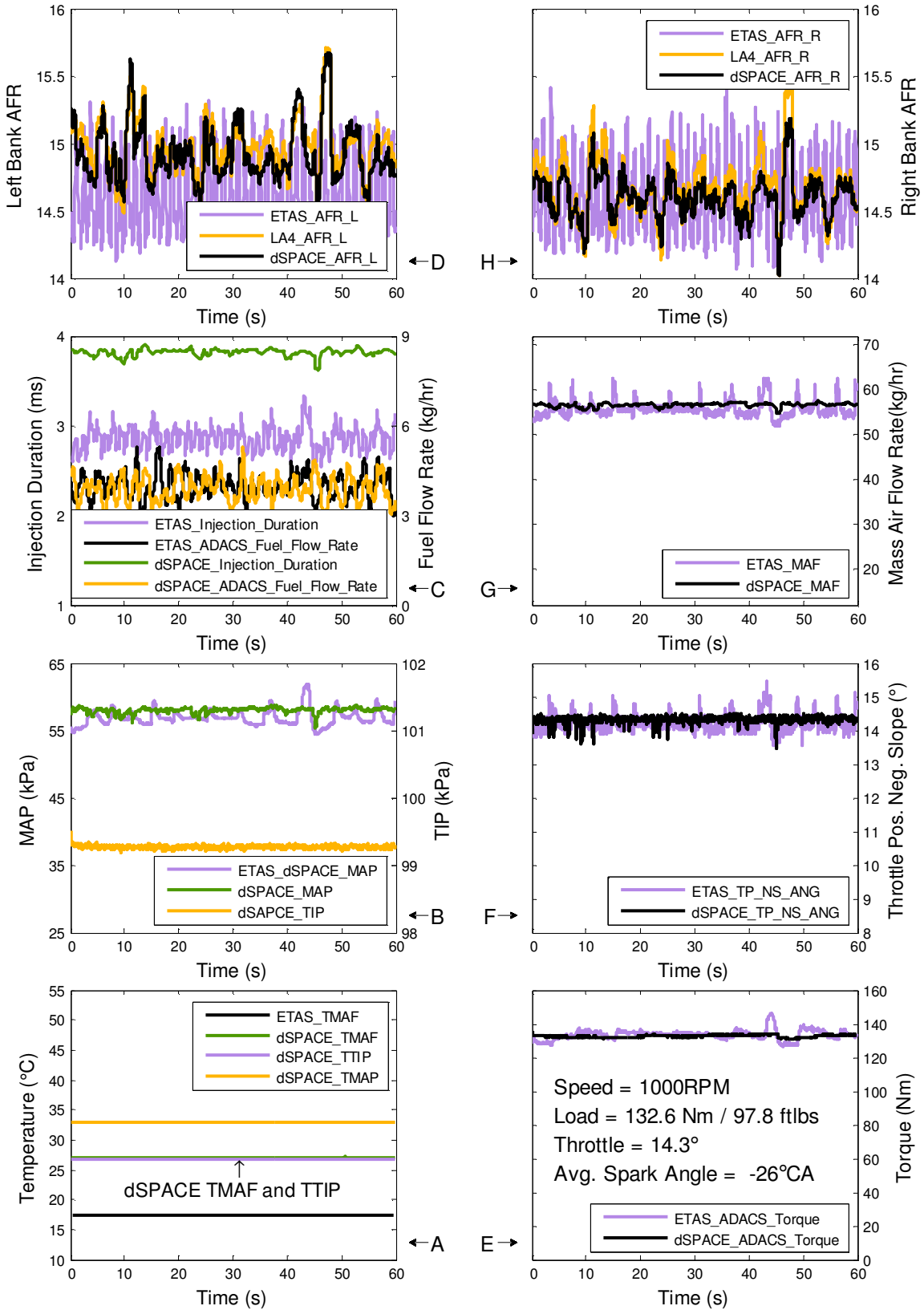


Figure A-XIV-12: dSPACE OL 1000 RPM 100 ft-lb PCM Measurements

Table A-XIV-6: 1000 RPM 100 ft-lb dSPACE Controller Data Summary

| | Left Bank AFR | | | Right Bank AFR | | |
|-----------------|---------------|-------|--------|----------------|-------|--------|
| | ETAS | LA4 | dSPACE | ETAS | LA4 | dSPACE |
| Mean | 14.59 | 14.98 | 14.92 | 14.59 | 14.67 | 14.60 |
| Std. | 0.28 | 0.20 | 0.22 | 0.26 | 0.22 | 0.16 |
| Coeff. Var. (%) | 1.90 | 1.33 | 1.45 | 1.78 | 1.53 | 1.11 |

| | Inj. Dur. (ms) | | Fuel Flow (kg/hr) | | MAF (kg/hr) | |
|-----------------|----------------|--------|-------------------|--------|-------------|--------|
| | ETAS | dSPACE | ETAS | dSPACE | ETAS | dSPACE |
| Mean | 2.86 | 3.82 | 3.99 | 3.88 | 55.72 | 56.60 |
| Std. | 0.12 | 0.04 | 0.42 | 0.43 | 1.84 | 0.44 |
| Coeff. Var. (%) | 4.33 | 1.08 | 10.42 | 11.08 | 3.30 | 0.78 |

| | MAP (kPa) | | TIP (kPa) | | TP_NS (°) | |
|-----------------|-----------|--------|-----------|--------|-----------|--------|
| | ETAS | dSPACE | ETAS | dSPACE | ETAS | dSPACE |
| Mean | 56.87 | 57.96 | 99.33 | 99.27 | 14.22 | 14.30 |
| Std. | 1.19 | 0.40 | 0.02 | 0.02 | 0.23 | 0.11 |
| Coeff. Var. (%) | 2.09 | 0.70 | 0.02 | 0.02 | 1.64 | 0.78 |

| | TMAP (°C) | | TTIP (°C) | | TMAF (°C) | |
|-----------------|-----------|--------|-----------|--------|-----------|--------|
| | ETAS | dSPACE | ETAS | dSPACE | ETAS | dSPACE |
| Mean | 27.34 | 32.91 | 20.17 | 26.78 | 17.45 | 27.05 |
| Std. | 0.03 | 0.03 | 0.02 | 0.02 | 0.02 | 0.03 |
| Coeff. Var. (%) | 0.10 | 0.08 | 0.12 | 0.08 | 0.11 | 0.11 |

| | Torque (Nm) | | CA50 (°CA) | | Spark (°CA) | |
|-----------------|-------------|--------|------------|--------|-------------|--------|
| | ETAS | dSPACE | ETAS | dSPACE | ETAS | dSPACE |
| Mean | 133.45 | 132.59 | 4.67 | 4.08 | -26.04 | -26.00 |
| Std. | 2.96 | 0.64 | 1.80 | 1.77 | 0.37 | 0.00 |
| Coeff. Var. (%) | 0.00 | 0.48 | 38.56 | 43.33 | 1.43 | 0.00 |

| | Pmax (bar) | | CA Pmax (°CA) | | IMEP (bar) | |
|-----------------|------------|--------|---------------|--------|------------|--------|
| | ETAS | dSPACE | ETAS | dSPACE | ETAS | dSPACE |
| Mean | 25.78 | 26.91 | 9.33 | 8.80 | 3.50 | 3.57 |
| Std. | 1.52 | 1.44 | 1.74 | 1.77 | 0.10 | 0.04 |
| Coeff. Var. (%) | 5.88 | 5.33 | 18.62 | 20.10 | 2.92 | 1.05 |

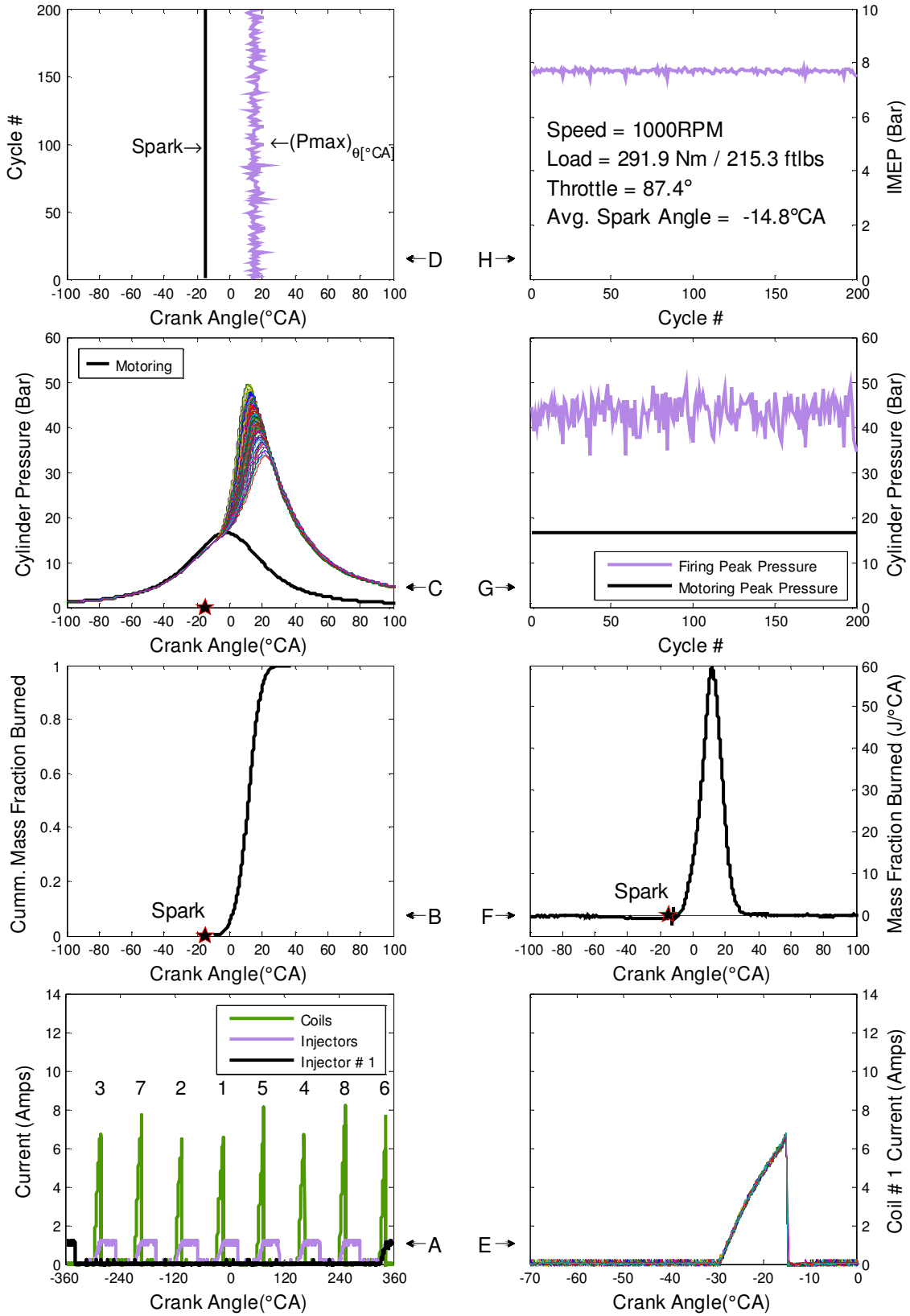


Figure A-XIV-13: dSPACE OL 1000 RPM WOT Combustion Data

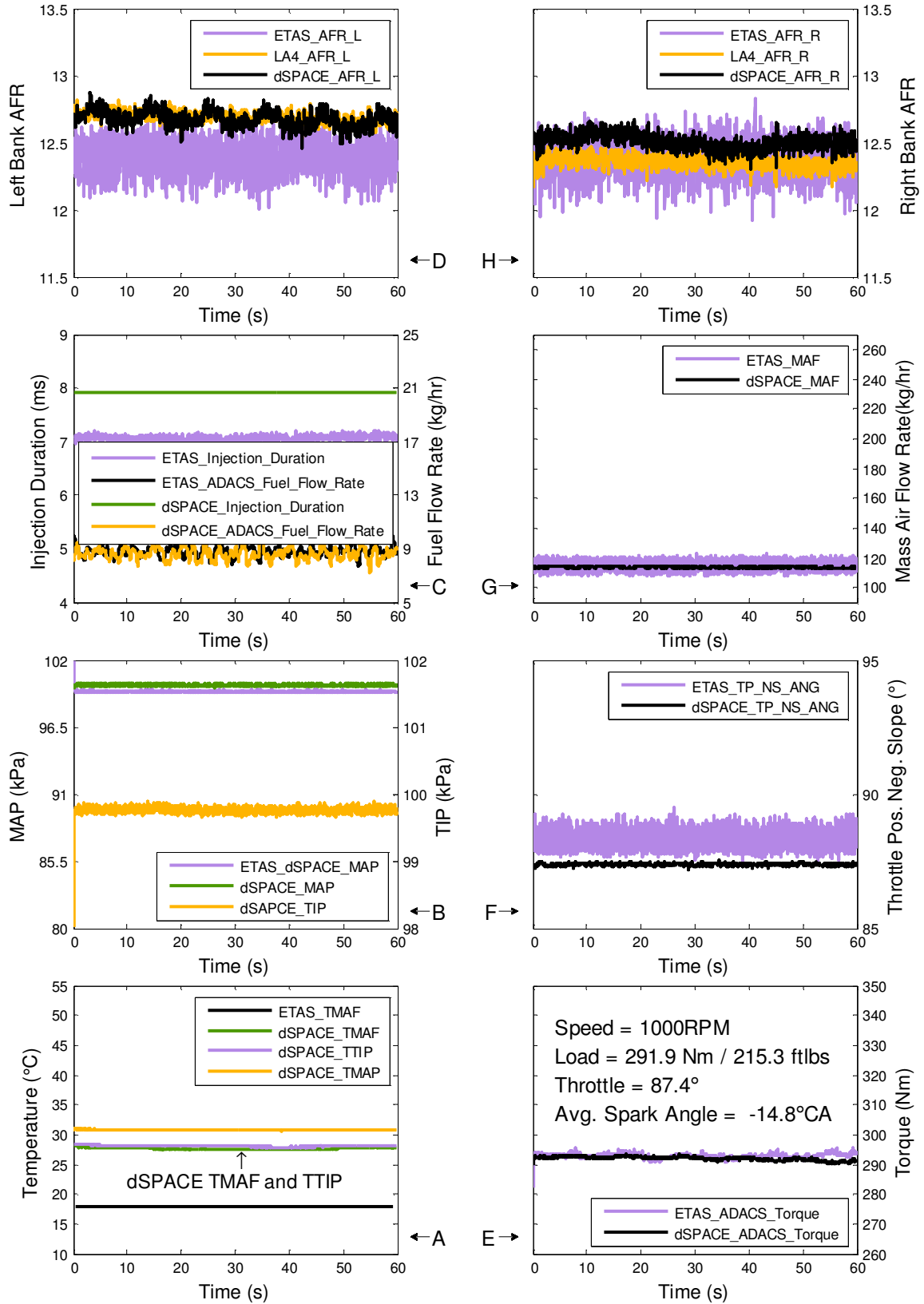


Figure A-XIV-14: dSPACE OL 1000 RPM WOT PCM Measurements

Table A-XIV-7: 1000 RPM WOT dSPACE Controller Data Summary

| | Left Bank AFR | | | Right Bank AFR | | |
|-----------------|---------------|-------|--------|----------------|-------|--------|
| | ETAS | LA4 | dSPACE | ETAS | LA4 | dSPACE |
| Mean | 12.40 | 12.69 | 12.68 | 12.39 | 12.36 | 12.51 |
| Std. | 0.11 | 0.04 | 0.06 | 0.12 | 0.04 | 0.05 |
| Coeff. Var. (%) | 0.86 | 0.31 | 0.47 | 0.99 | 0.36 | 0.44 |

| | Inj. Dur. (ms) | | Fuel Flow (kg/hr) | | MAF (kg/hr) | |
|-----------------|----------------|--------|-------------------|--------|-------------|--------|
| | ETAS | dSPACE | ETAS | dSPACE | ETAS | dSPACE |
| Mean | 7.07 | 7.90 | 8.84 | 8.62 | 115.14 | 113.60 |
| Std. | 0.05 | 0.00 | 0.41 | 0.47 | 2.69 | 0.23 |
| Coeff. Var. (%) | 0.66 | 0.00 | 4.64 | 5.40 | 2.34 | 0.20 |

| | MAP (kPa) | | TIP (kPa) | | TP_NS (°) | |
|-----------------|-----------|--------|-----------|--------|-----------|--------|
| | ETAS | dSPACE | ETAS | dSPACE | ETAS | dSPACE |
| Mean | 99.43 | 99.96 | 99.22 | 99.76 | 88.22 | 87.37 |
| Std. | 0.08 | 0.05 | 0.03 | 0.06 | 0.30 | 0.04 |
| Coeff. Var. (%) | 0.08 | 0.05 | 0.03 | 0.06 | 0.34 | 0.04 |

| | TMAP (°C) | | TTIP (°C) | | TMAF (°C) | |
|-----------------|-----------|--------|-----------|--------|-----------|--------|
| | ETAS | dSPACE | ETAS | dSPACE | ETAS | dSPACE |
| Mean | 24.27 | 30.75 | 20.93 | 28.05 | 17.89 | 27.70 |
| Std. | 0.02 | 0.06 | 0.03 | 0.10 | 0.02 | 0.13 |
| Coeff. Var. (%) | 0.10 | 0.20 | 0.13 | 0.35 | 0.10 | 0.48 |

| | Torque (Nm) | | CA50 (°CA) | | Spark (°CA) | |
|-----------------|-------------|--------|------------|--------|-------------|--------|
| | ETAS | dSPACE | ETAS | dSPACE | ETAS | dSPACE |
| Mean | 292.86 | 291.94 | 11.24 | 11.28 | -14.52 | -14.80 |
| Std. | 0.80 | 0.58 | 2.13 | 2.12 | 0.10 | 0.00 |
| Coeff. Var. (%) | 0.00 | 0.20 | 18.95 | 18.79 | 0.67 | 0.00 |

| | Pmax (bar) | | CA Pmax (°CA) | | IMEP (bar) | |
|-----------------|------------|--------|---------------|--------|------------|--------|
| | ETAS | dSPACE | ETAS | dSPACE | ETAS | dSPACE |
| Mean | 43.25 | 43.29 | 15.31 | 15.43 | 7.66 | 7.69 |
| Std. | 3.17 | 3.25 | 2.23 | 2.23 | 0.08 | 0.07 |
| Coeff. Var. (%) | 7.33 | 7.50 | 14.56 | 14.47 | 0.98 | 0.95 |

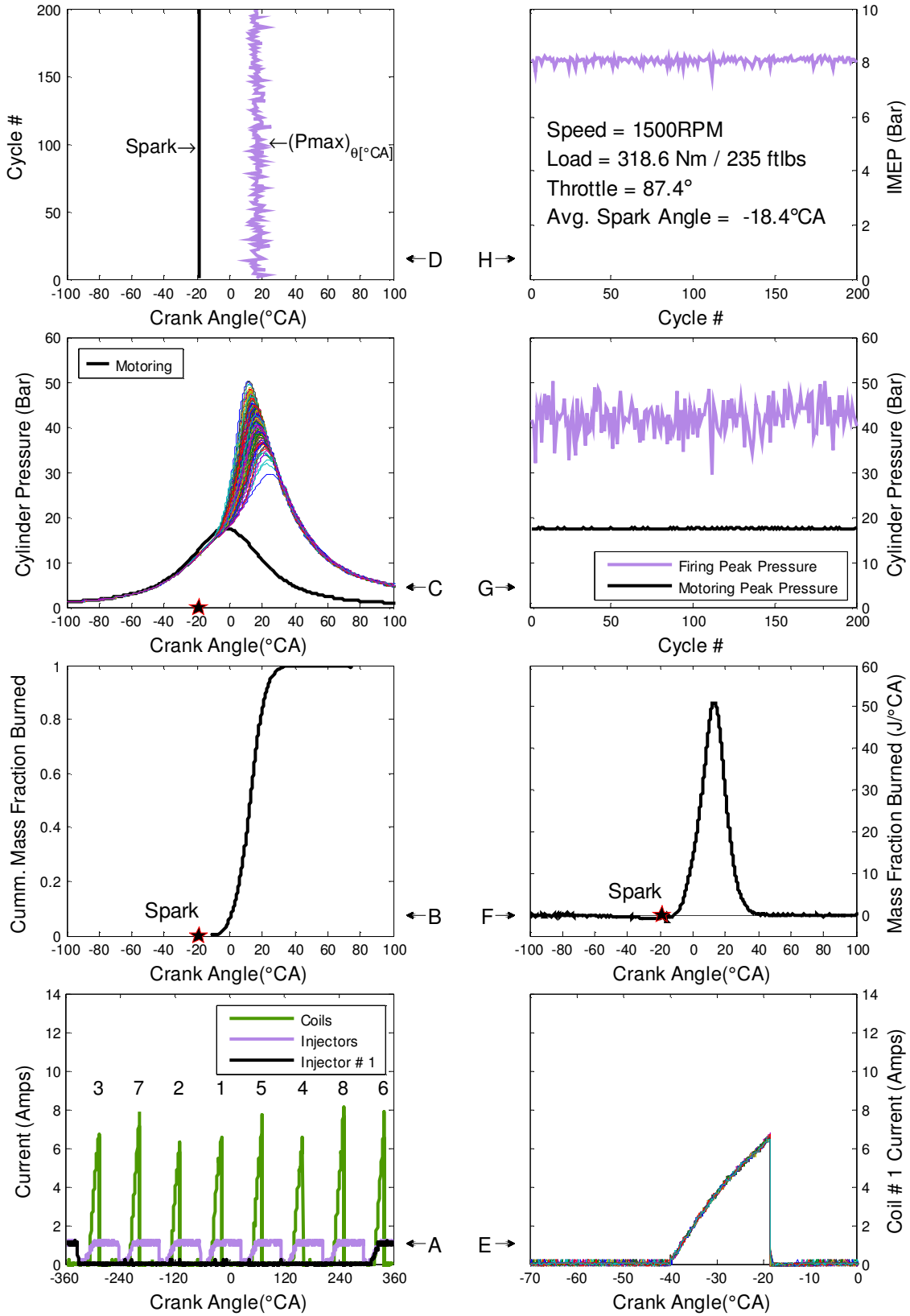


Figure A-XIV-15: dSPACE OL 1500 RPM WOT Combustion Data

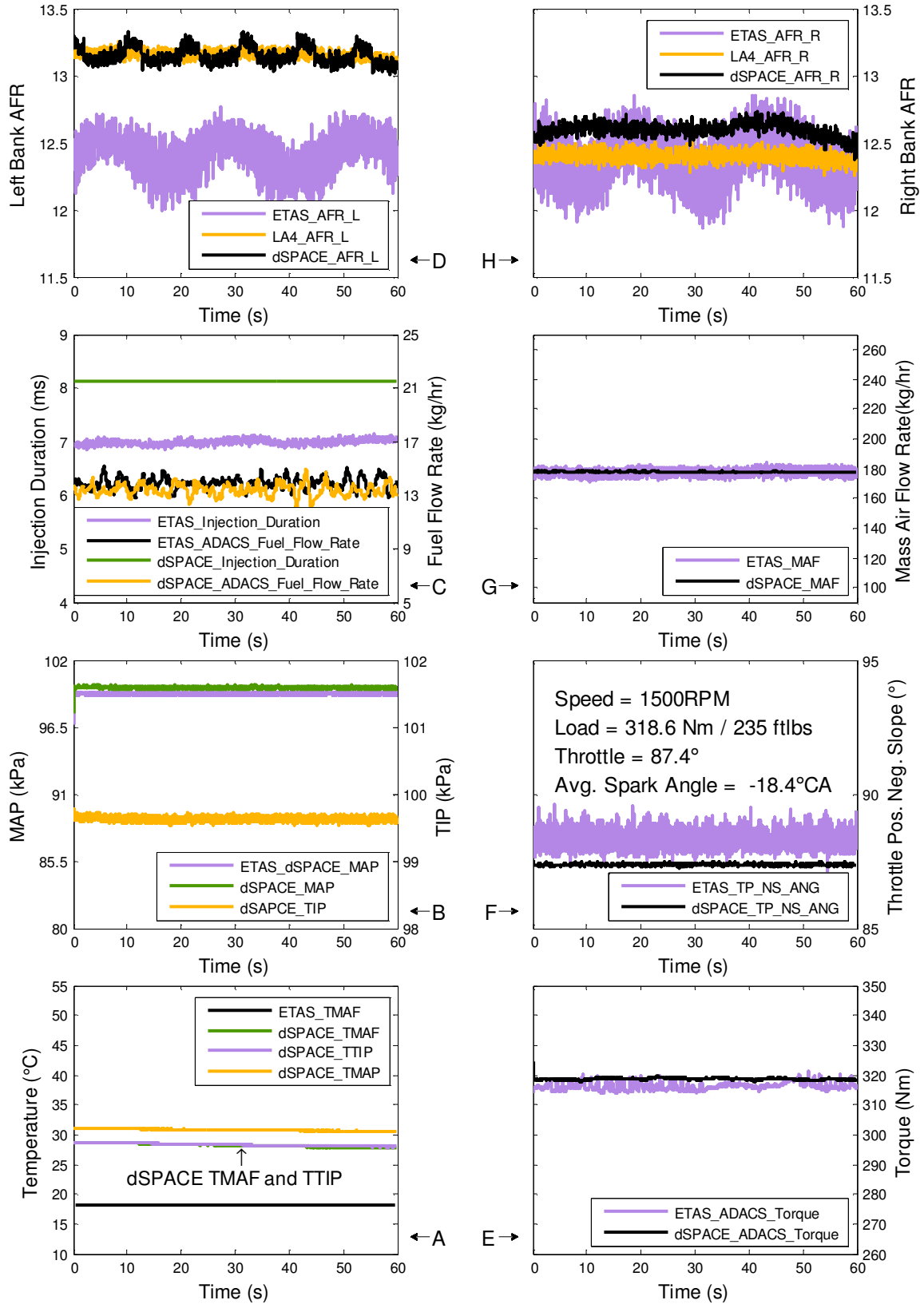


Figure A-XIV-16: dSPACE OL 1500 RPM WOT PCM Measurements

Table A-XIV-8: 1500 RPM WOT dSPACE Controller Data Summary

| | Left Bank AFR | | | Right Bank AFR | | |
|-----------------|---------------|-------|--------|----------------|-------|--------|
| | ETAS | LA4 | dSPACE | ETAS | LA4 | dSPACE |
| Mean | 12.41 | 13.16 | 13.15 | 12.38 | 12.40 | 12.60 |
| Std. | 0.13 | 0.03 | 0.06 | 0.16 | 0.04 | 0.05 |
| Coeff. Var. (%) | 1.05 | 0.22 | 0.47 | 1.33 | 0.30 | 0.38 |

| | Inj. Dur. (ms) | | Fuel Flow (kg/hr) | | MAF (kg/hr) | |
|-----------------|----------------|--------|-------------------|--------|-------------|--------|
| | ETAS | dSPACE | ETAS | dSPACE | ETAS | dSPACE |
| Mean | 6.99 | 8.13 | 13.88 | 13.38 | 177.17 | 177.62 |
| Std. | 0.05 | 0.00 | 0.43 | 0.45 | 2.12 | 0.23 |
| Coeff. Var. (%) | 0.68 | 0.00 | 3.11 | 3.35 | 1.20 | 0.13 |

| | MAP (kPa) | | TIP (kPa) | | TP_NS (°) | |
|-----------------|-----------|--------|-----------|--------|-----------|--------|
| | ETAS | dSPACE | ETAS | dSPACE | ETAS | dSPACE |
| Mean | 99.24 | 99.79 | 99.08 | 99.63 | 88.23 | 87.37 |
| Std. | 0.09 | 0.08 | 0.04 | 0.03 | 0.33 | 0.03 |
| Coeff. Var. (%) | 0.09 | 0.08 | 0.04 | 0.03 | 0.37 | 0.03 |

| | TMAP (°C) | | TTIP (°C) | | TMAF (°C) | |
|-----------------|-----------|--------|-----------|--------|-----------|--------|
| | ETAS | dSPACE | ETAS | dSPACE | ETAS | dSPACE |
| Mean | 23.82 | 30.76 | 20.83 | 28.29 | 18.19 | 28.20 |
| Std. | 0.03 | 0.15 | 0.03 | 0.23 | 0.04 | 0.28 |
| Coeff. Var. (%) | 0.14 | 0.49 | 0.16 | 0.81 | 0.21 | 1.00 |

| | Torque (Nm) | | CA50 (°CA) | | Spark (°CA) | |
|-----------------|-------------|--------|------------|--------|-------------|--------|
| | ETAS | dSPACE | ETAS | dSPACE | ETAS | dSPACE |
| Mean | 316.24 | 318.63 | 12.45 | 12.44 | -18.52 | -18.40 |
| Std. | 1.22 | 0.34 | 2.37 | 2.39 | 0.11 | 0.00 |
| Coeff. Var. (%) | 0.00 | 0.11 | 19.07 | 19.19 | 0.57 | 0.00 |

| | Pmax (bar) | | CA Pmax (°CA) | | IMEP (bar) | |
|-----------------|------------|--------|---------------|--------|------------|--------|
| | ETAS | dSPACE | ETAS | dSPACE | ETAS | dSPACE |
| Mean | 41.18 | 42.01 | 16.75 | 16.69 | 7.98 | 8.08 |
| Std. | 3.44 | 3.66 | 2.42 | 2.49 | 0.10 | 0.12 |
| Coeff. Var. (%) | 8.36 | 8.71 | 14.46 | 14.94 | 1.25 | 1.50 |

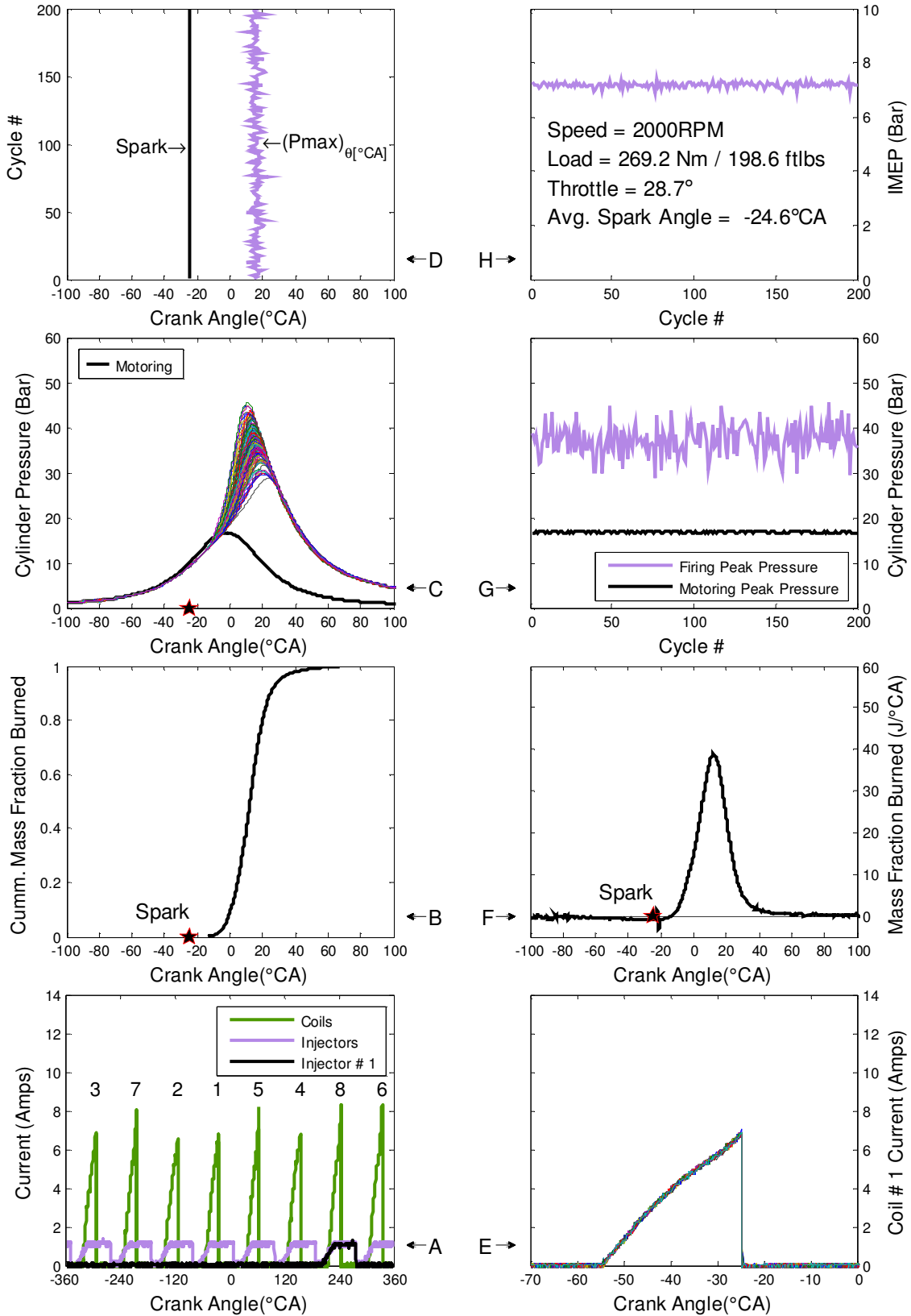


Figure A-XIV-17: dSPACE OL 2000 RPM 35% Pedal Combustion Data

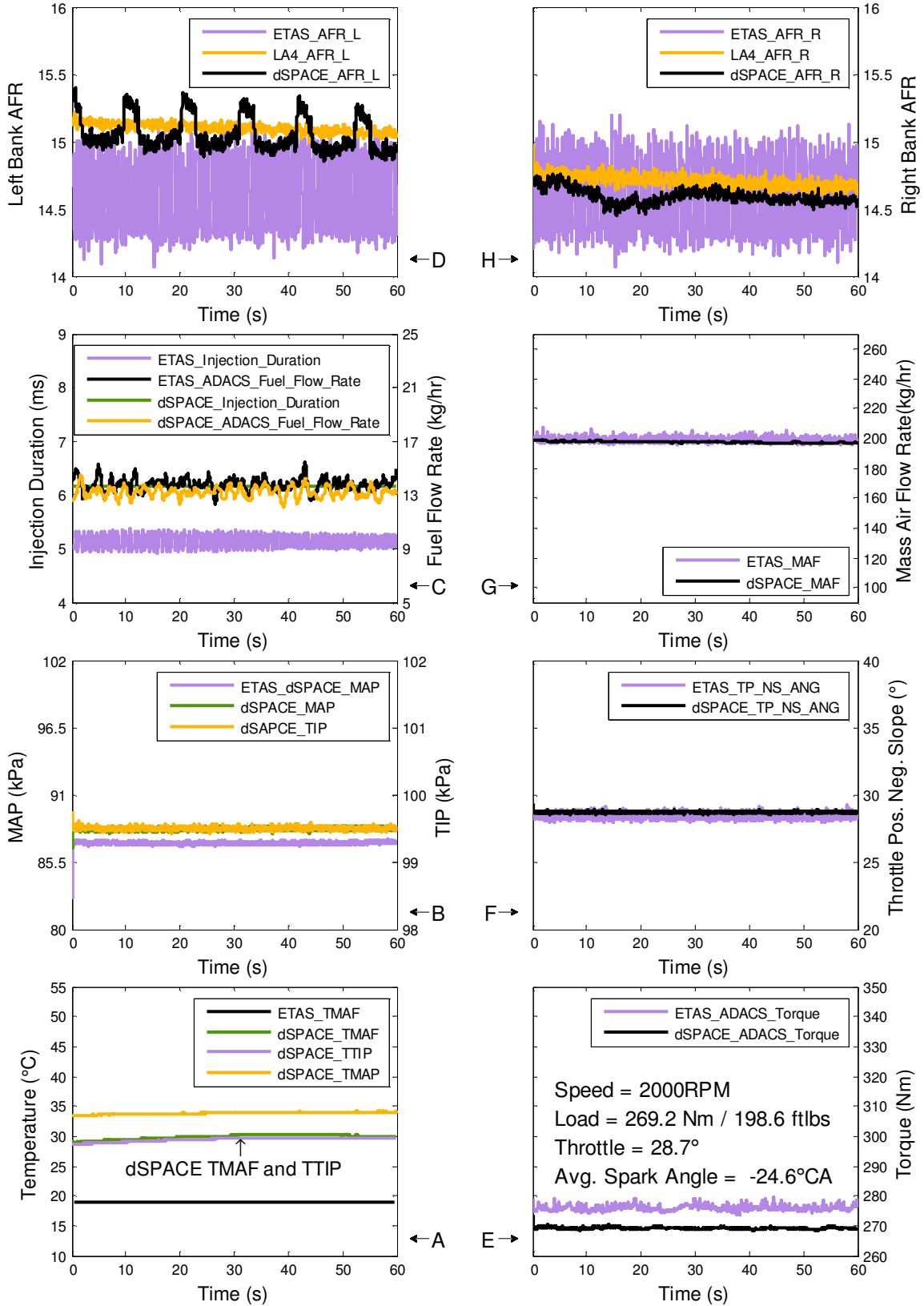


Figure A-XIV-18: dSPACE OL 2000 RPM 35% Pedal PCM Measurements

Table A-XIV-9: 2000 RPM WOT dSPACE OL Controller Data Summary

| | Left Bank AFR | | | Right Bank AFR | | |
|-----------------|---------------|-------|--------|----------------|-------|--------|
| | ETAS | LA4 | dSPACE | ETAS | LA4 | dSPACE |
| Mean | 14.58 | 15.10 | 15.05 | 14.57 | 14.70 | 14.59 |
| Std. | 0.24 | 0.03 | 0.12 | 0.23 | 0.04 | 0.05 |
| Coeff. Var. (%) | 1.61 | 0.21 | 0.82 | 1.57 | 0.29 | 0.36 |

| | Inj. Dur. (ms) | | Fuel Flow (kg/hr) | | MAF (kg/hr) | |
|-----------------|----------------|--------|-------------------|--------|-------------|--------|
| | ETAS | dSPACE | ETAS | dSPACE | ETAS | dSPACE |
| Mean | 5.15 | 6.15 | 13.78 | 13.20 | 199.00 | 197.45 |
| Std. | 0.11 | 0.00 | 0.47 | 0.39 | 1.33 | 0.53 |
| Coeff. Var. (%) | 2.23 | 0.00 | 3.40 | 2.95 | 0.67 | 0.27 |

| | MAP (kPa) | | TIP (kPa) | | TP_NS (°) | |
|-----------------|-----------|--------|-----------|--------|-----------|--------|
| | ETAS | dSPACE | ETAS | dSPACE | ETAS | dSPACE |
| Mean | 87.06 | 88.22 | 98.96 | 99.50 | 28.40 | 28.70 |
| Std. | 0.15 | 0.10 | 0.02 | 0.02 | 0.20 | 0.05 |
| Coeff. Var. (%) | 0.17 | 0.11 | 0.02 | 0.02 | 0.69 | 0.16 |

| | TMAP (°C) | | TTIP (°C) | | TMAF (°C) | |
|-----------------|-----------|--------|-----------|--------|-----------|--------|
| | ETAS | dSPACE | ETAS | dSPACE | ETAS | dSPACE |
| Mean | 26.04 | 33.87 | 21.18 | 29.45 | 18.94 | 29.86 |
| Std. | 0.03 | 0.20 | 0.03 | 0.33 | 0.02 | 0.36 |
| Coeff. Var. (%) | 0.10 | 0.58 | 0.14 | 1.13 | 0.13 | 1.20 |

| | Torque (Nm) | | CA50 (°CA) | | Spark (°CA) | |
|-----------------|-------------|--------|------------|--------|-------------|--------|
| | ETAS | dSPACE | ETAS | dSPACE | ETAS | dSPACE |
| Mean | 275.96 | 269.22 | 12.28 | 12.18 | -24.95 | -24.60 |
| Std. | 0.84 | 0.30 | 2.64 | 2.51 | 0.40 | 0.00 |
| Coeff. Var. (%) | 0.00 | 0.11 | 21.54 | 20.63 | 1.62 | 0.00 |

| | Pmax (bar) | | CA Pmax (°CA) | | IMEP (bar) | |
|-----------------|------------|--------|---------------|--------|------------|--------|
| | ETAS | dSPACE | ETAS | dSPACE | ETAS | dSPACE |
| Mean | 36.62 | 37.23 | 16.09 | 15.92 | 7.10 | 7.18 |
| Std. | 3.34 | 3.33 | 2.43 | 2.32 | 0.12 | 0.10 |
| Coeff. Var. (%) | 9.13 | 8.95 | 15.08 | 14.58 | 1.63 | 1.36 |

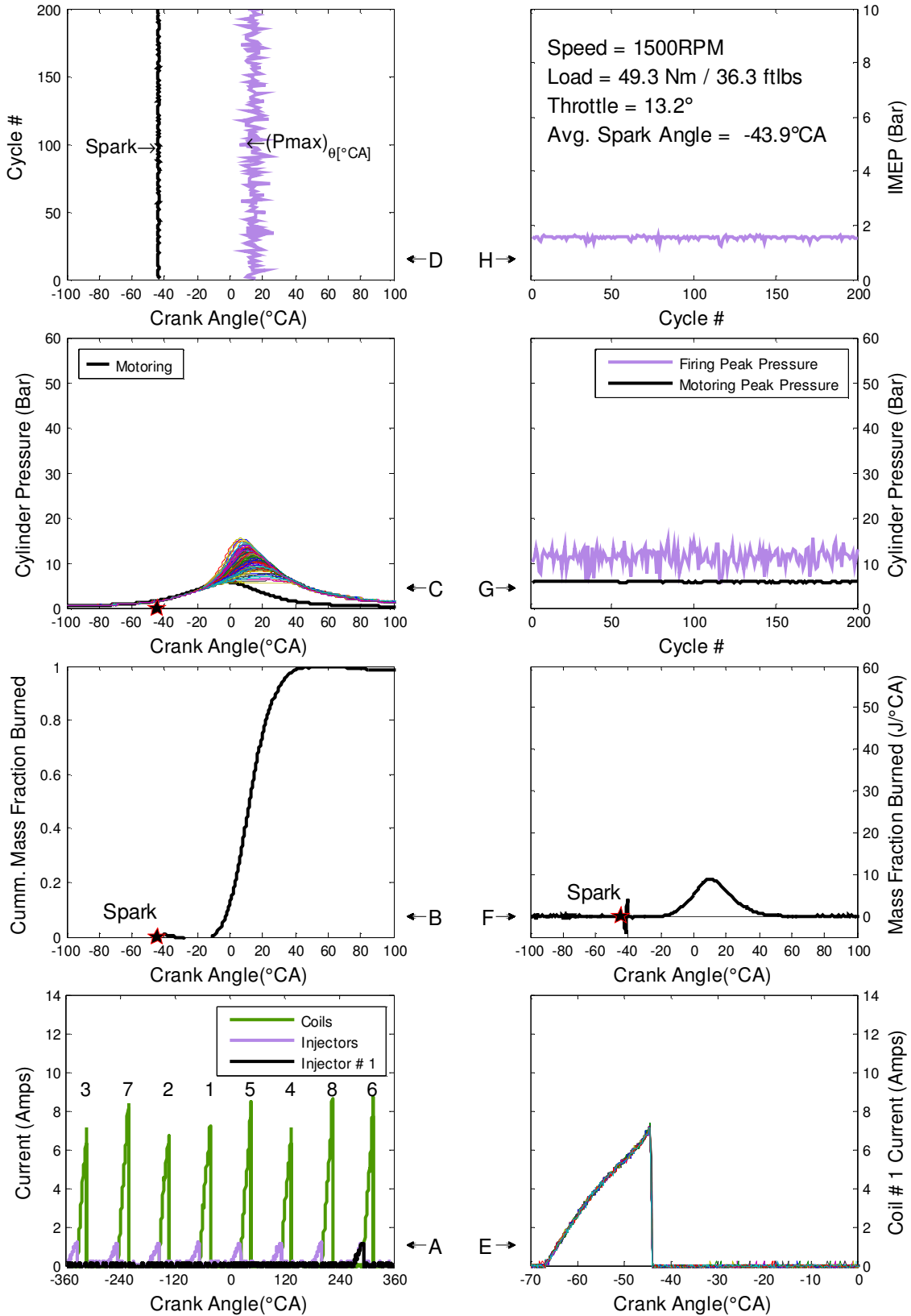


Figure A-XIV-19: dSPACE OL 1500 RPM -17.7 inHg Combustion Data

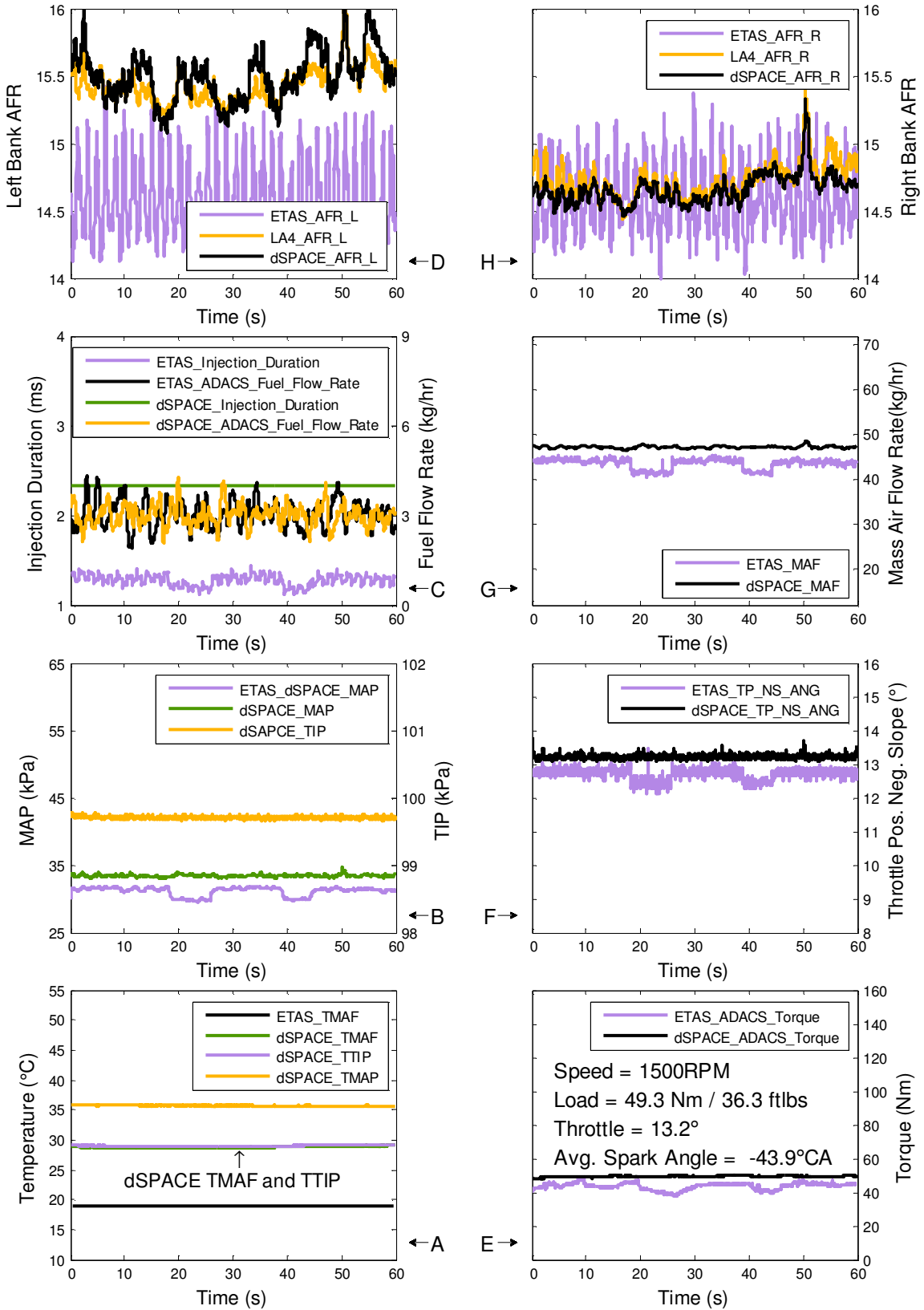


Figure A-XIV-20: dSPACE OL 1500 RPM -17.7inHg PCM Measurements

Table A-XIV-10: 1500 RPM –17.7 inHg dSPACE OL Controller Data Summary

| | Left Bank AFR | | | Right Bank AFR | | |
|-----------------|---------------|-------|--------|----------------|-------|--------|
| | ETAS | LA4 | dSPACE | ETAS | LA4 | dSPACE |
| Mean | 14.58 | 15.43 | 15.50 | 14.58 | 14.73 | 14.66 |
| Std. | 0.28 | 0.13 | 0.19 | 0.24 | 0.13 | 0.11 |
| Coeff. Var. (%) | 1.93 | 0.83 | 1.20 | 1.67 | 0.91 | 0.74 |

| | Inj. Dur. (ms) | | Fuel Flow (kg/hr) | | MAF (kg/hr) | |
|-----------------|----------------|--------|-------------------|--------|-------------|--------|
| | ETAS | dSPACE | ETAS | dSPACE | ETAS | dSPACE |
| Mean | 1.28 | 2.33 | 3.04 | 3.00 | 43.54 | 47.19 |
| Std. | 0.06 | 0.00 | 0.45 | 0.36 | 1.13 | 0.28 |
| Coeff. Var. (%) | 4.74 | 0.00 | 14.85 | 12.08 | 2.59 | 0.59 |

| | MAP (kPa) | | TIP (kPa) | | TP_NS (°) | |
|-----------------|-----------|--------|-----------|--------|-----------|--------|
| | ETAS | dSPACE | ETAS | dSPACE | ETAS | dSPACE |
| Mean | 31.10 | 33.39 | 99.27 | 99.71 | 12.70 | 13.21 |
| Std. | 0.66 | 0.19 | 0.03 | 0.02 | 0.16 | 0.06 |
| Coeff. Var. (%) | 2.12 | 0.56 | 0.03 | 0.02 | 1.25 | 0.47 |

| | TMAP (°C) | | TTIP (°C) | | TMAF (°C) | |
|-----------------|-----------|--------|-----------|--------|-----------|--------|
| | ETAS | dSPACE | ETAS | dSPACE | ETAS | dSPACE |
| Mean | 29.58 | 35.71 | 21.69 | 29.01 | 18.92 | 28.77 |
| Std. | 0.03 | 0.03 | 0.02 | 0.07 | 0.03 | 0.12 |
| Coeff. Var. (%) | 0.11 | 0.08 | 0.11 | 0.26 | 0.15 | 0.42 |

| | Torque (Nm) | | CA50 (°CA) | | Spark (°CA) | |
|-----------------|-------------|--------|------------|--------|-------------|--------|
| | ETAS | dSPACE | ETAS | dSPACE | ETAS | dSPACE |
| Mean | 43.53 | 49.28 | 12.30 | 12.20 | -43.40 | -43.93 |
| Std. | 2.05 | 0.36 | 5.87 | 5.67 | 0.42 | 0.09 |
| Coeff. Var. (%) | 0.00 | 0.72 | 47.69 | 46.43 | 0.98 | 0.22 |

| | Pmax (bar) | | CA Pmax (°CA) | | IMEP (bar) | |
|-----------------|------------|--------|---------------|--------|------------|--------|
| | ETAS | dSPACE | ETAS | dSPACE | ETAS | dSPACE |
| Mean | 10.43 | 11.19 | 13.94 | 14.46 | 1.36 | 1.54 |
| Std. | 1.58 | 1.91 | 2.86 | 3.50 | 0.10 | 0.06 |
| Coeff. Var. (%) | 15.12 | 17.07 | 20.54 | 24.24 | 7.32 | 4.18 |

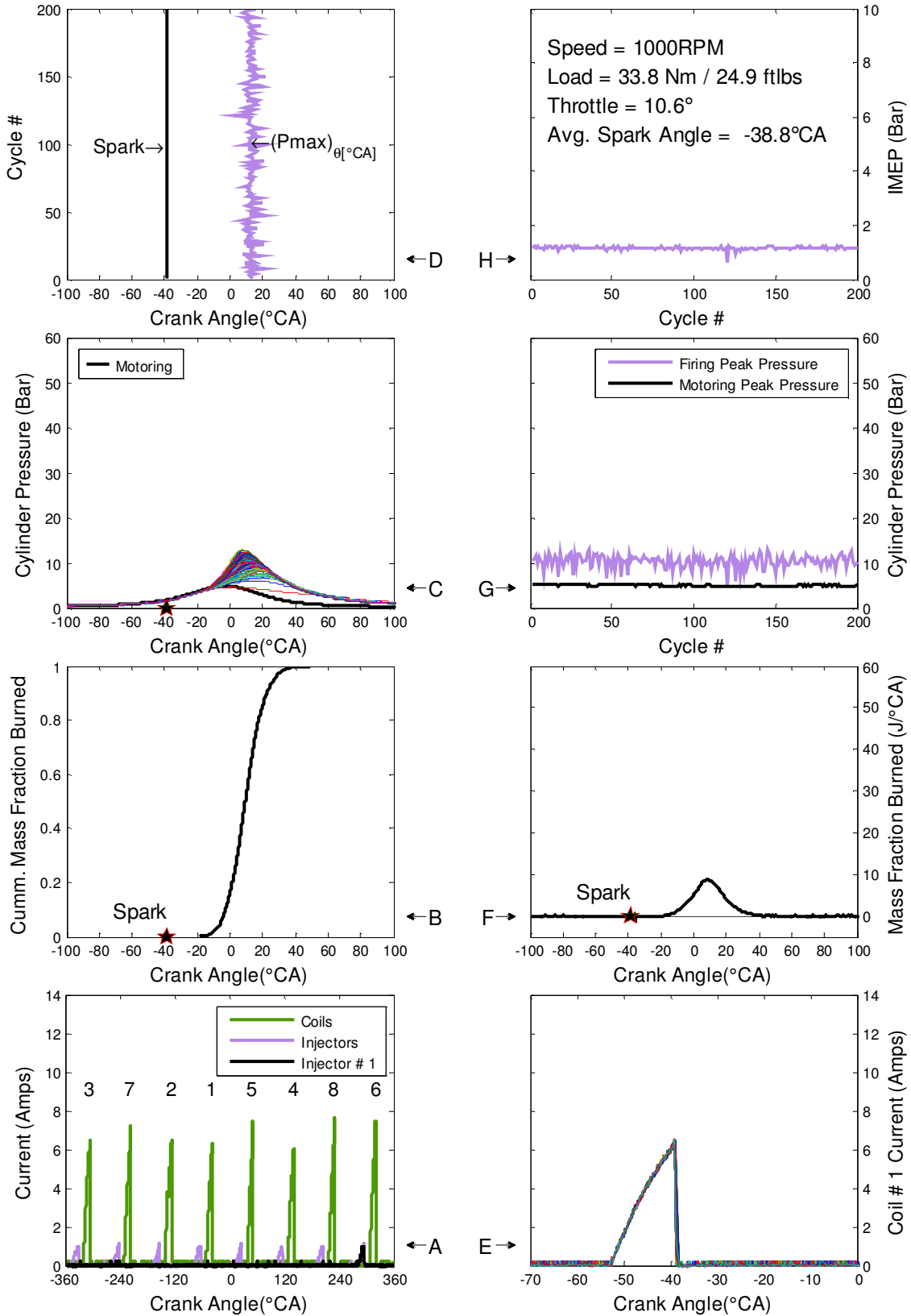


Figure A-XIV-21: dSPACE CL 1000 RPM -17.7 inHg Combustion Data

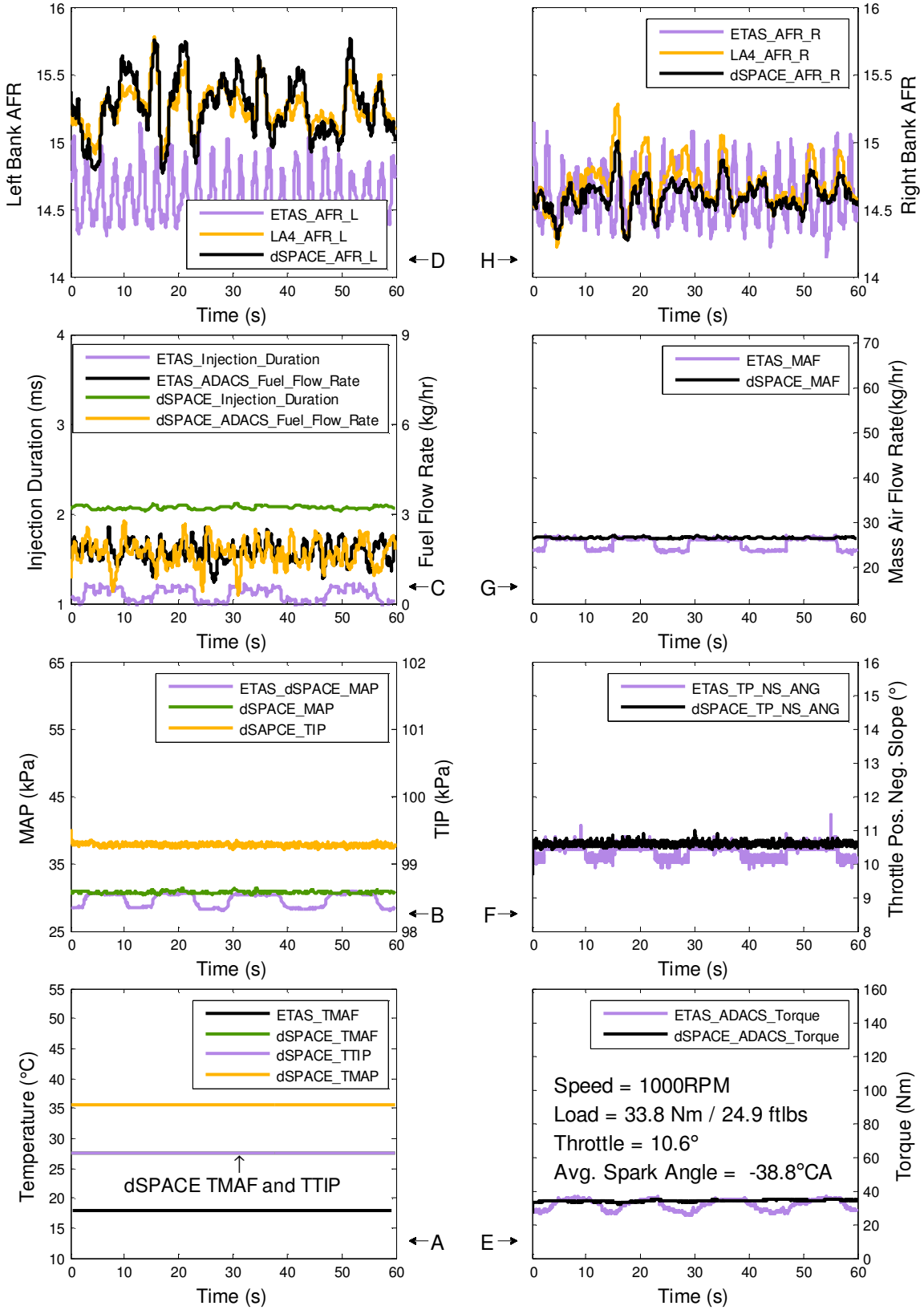


Figure A-XIV-22: dSPACE CL 1000 RPM -17.7 inHg PCM Measurements

Table A-XIV-11: 1000 RPM –17.7inHg dSPACE CL Controller Data Summary

| | Left Bank AFR | | | Right Bank AFR | | |
|-----------------|---------------|-------|--------|----------------|-------|--------|
| | ETAS | LA4 | dSPACE | ETAS | LA4 | dSPACE |
| Mean | 14.59 | 15.25 | 15.26 | 14.58 | 14.67 | 14.60 |
| Std. | 0.18 | 0.15 | 0.22 | 0.18 | 0.17 | 0.11 |
| Coeff. Var. (%) | 1.25 | 0.99 | 1.44 | 1.26 | 1.17 | 0.77 |

| | Inj. Dur. (ms) | | Fuel Flow (kg/hr) | | MAF (kg/hr) | |
|-----------------|----------------|--------|-------------------|--------|-------------|--------|
| | ETAS | dSPACE | ETAS | dSPACE | ETAS | dSPACE |
| Mean | 1.10 | 2.07 | 1.74 | 1.68 | 25.30 | 26.63 |
| Std. | 0.07 | 0.02 | 0.33 | 0.42 | 1.30 | 0.15 |
| Coeff. Var. (%) | 6.74 | 0.84 | 19.21 | 25.14 | 5.13 | 0.58 |

| | MAP (kPa) | | TIP (kPa) | | TP_NS (°) | |
|-----------------|-----------|--------|-----------|--------|-----------|--------|
| | ETAS | dSPACE | ETAS | dSPACE | ETAS | dSPACE |
| Mean | 29.58 | 30.71 | 99.36 | 99.27 | 10.35 | 10.58 |
| Std. | 1.01 | 0.14 | 0.02 | 0.02 | 0.21 | 0.06 |
| Coeff. Var. (%) | 3.40 | 0.44 | 0.02 | 0.02 | 1.99 | 0.59 |

| | TMAP (°C) | | TTIP (°C) | | TMAF (°C) | |
|-----------------|-----------|--------|-----------|--------|-----------|--------|
| | ETAS | dSPACE | ETAS | dSPACE | ETAS | dSPACE |
| Mean | 30.72 | 35.56 | 21.09 | 27.53 | 17.97 | 27.54 |
| Std. | 0.03 | 0.02 | 0.02 | 0.02 | 0.02 | 0.02 |
| Coeff. Var. (%) | 0.11 | 0.07 | 0.08 | 0.06 | 0.09 | 0.09 |

| | Torque (Nm) | | CA50 (°CA) | | Spark (°CA) | |
|-----------------|-------------|--------|------------|--------|-------------|--------|
| | ETAS | dSPACE | ETAS | dSPACE | ETAS | dSPACE |
| Mean | 31.57 | 33.81 | 12.25 | 10.22 | -38.42 | -38.76 |
| Std. | 3.08 | 0.56 | 3.90 | 4.71 | 0.93 | 0.08 |
| Coeff. Var. (%) | 0.00 | 1.65 | 31.83 | 46.04 | 2.42 | 0.20 |

| | Pmax (bar) | | CA Pmax (°CA) | | IMEP (bar) | |
|-----------------|------------|--------|---------------|--------|------------|--------|
| | ETAS | dSPACE | ETAS | dSPACE | ETAS | dSPACE |
| Mean | 9.22 | 10.31 | 14.28 | 13.07 | 1.09 | 1.17 |
| Std. | 1.30 | 1.38 | 2.34 | 2.97 | 0.10 | 0.05 |
| Coeff. Var. (%) | 14.15 | 13.40 | 16.38 | 22.70 | 8.92 | 4.40 |

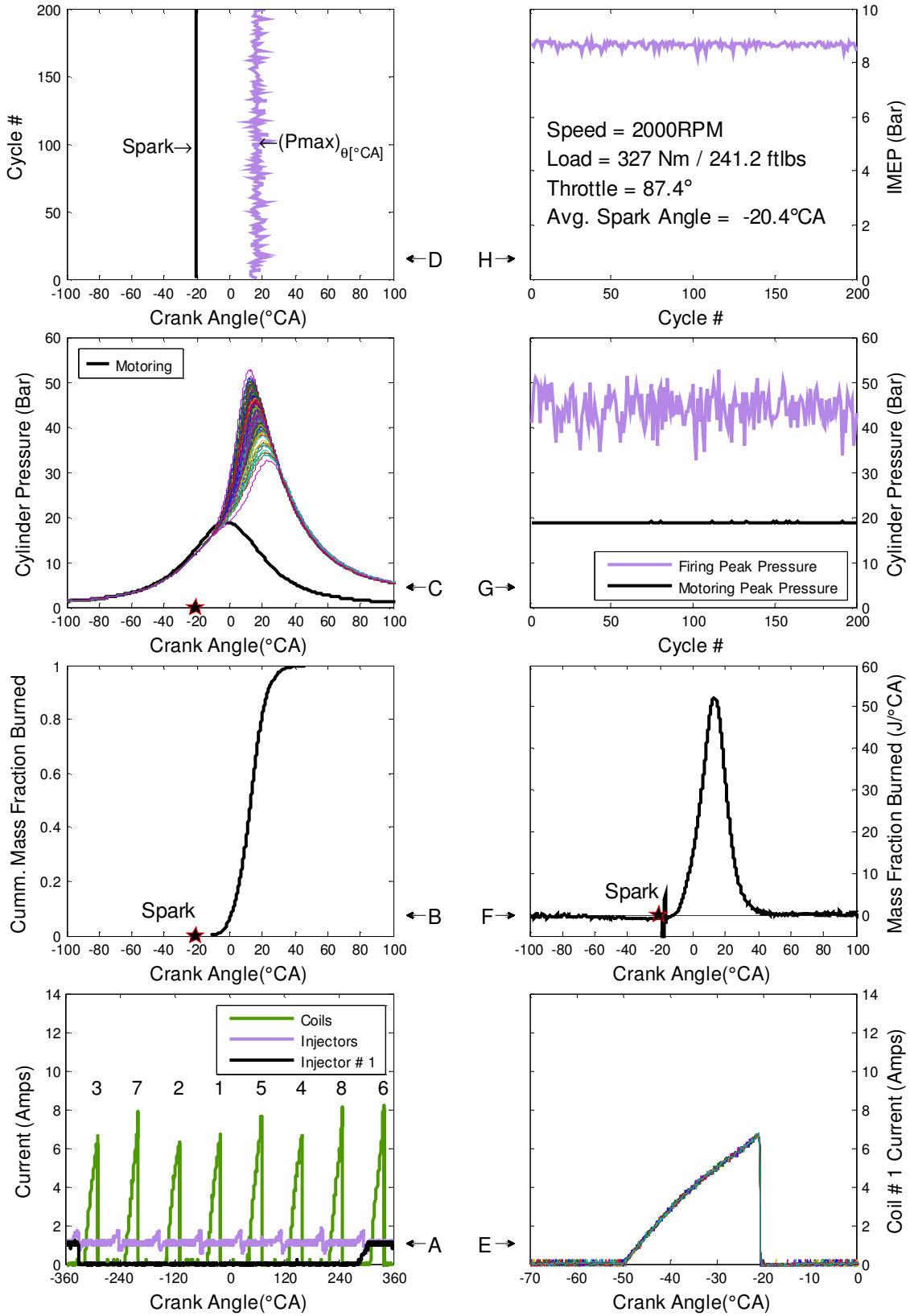


Figure A-XIV-23: dSPACE CL 2000 RPM WOT Combustion Data

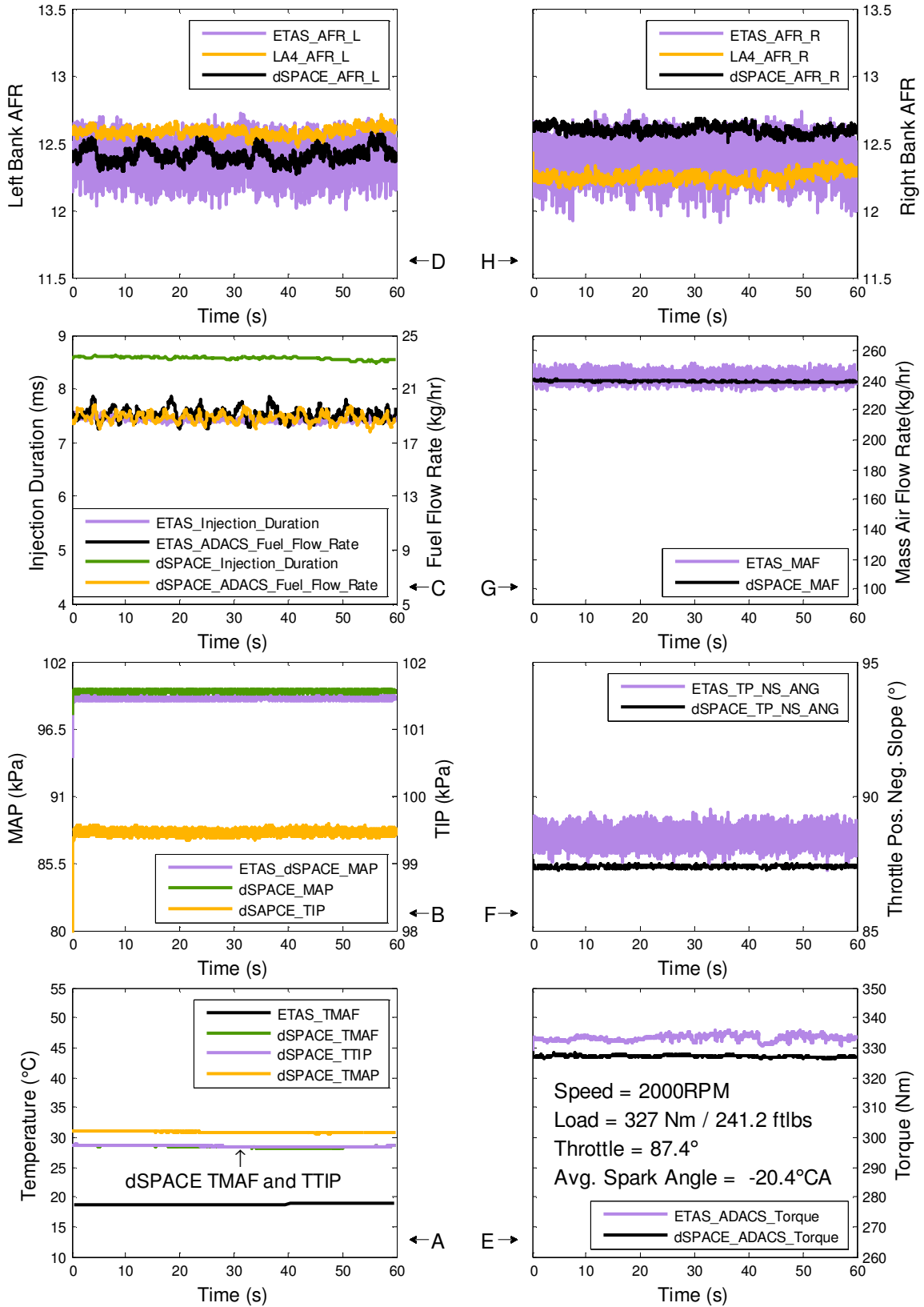


Figure A-XIV-24: dSPACE CL 2000 RPM WOT PCM Measurements

Table A-XIV-12: 2000 RPM WOT dSPACE CL Controller Data Summary

| | Left Bank AFR | | | Right Bank AFR | | |
|-----------------|---------------|-------|--------|----------------|-------|--------|
| | ETAS | LA4 | dSPACE | ETAS | LA4 | dSPACE |
| Mean | 12.40 | 12.58 | 12.42 | 12.40 | 12.25 | 12.60 |
| Std. | 0.13 | 0.03 | 0.06 | 0.14 | 0.04 | 0.03 |
| Coeff. Var. (%) | 1.04 | 0.24 | 0.44 | 1.16 | 0.29 | 0.24 |

| | Inj. Dur. (ms) | | Fuel Flow (kg/hr) | | MAF (kg/hr) | |
|-----------------|----------------|--------|-------------------|--------|-------------|--------|
| | ETAS | dSPACE | ETAS | dSPACE | ETAS | dSPACE |
| Mean | 7.43 | 8.57 | 19.12 | 18.82 | 240.84 | 238.96 |
| Std. | 0.04 | 0.03 | 0.43 | 0.37 | 3.28 | 0.47 |
| Coeff. Var. (%) | 0.49 | 0.31 | 2.23 | 1.95 | 1.36 | 0.20 |

| | MAP (kPa) | | TIP (kPa) | | TP_NS (°) | |
|-----------------|-----------|--------|-----------|--------|-----------|--------|
| | ETAS | dSPACE | ETAS | dSPACE | ETAS | dSPACE |
| Mean | 99.00 | 99.56 | 98.87 | 99.45 | 88.36 | 87.36 |
| Std. | 0.15 | 0.08 | 0.03 | 0.09 | 0.34 | 0.03 |
| Coeff. Var. (%) | 0.15 | 0.08 | 0.04 | 0.09 | 0.39 | 0.04 |

| | TMAP (°C) | | TTIP (°C) | | TMAF (°C) | |
|-----------------|-----------|--------|-----------|--------|-----------|--------|
| | ETAS | dSPACE | ETAS | dSPACE | ETAS | dSPACE |
| Mean | 23.80 | 30.82 | 21.34 | 28.48 | 18.85 | 28.36 |
| Std. | 0.04 | 0.12 | 0.06 | 0.15 | 0.06 | 0.16 |
| Coeff. Var. (%) | 0.18 | 0.39 | 0.29 | 0.51 | 0.34 | 0.56 |

| | Torque (Nm) | | CA50 (°CA) | | Spark (°CA) | |
|-----------------|-------------|--------|------------|--------|-------------|--------|
| | ETAS | dSPACE | ETAS | dSPACE | ETAS | dSPACE |
| Mean | 333.17 | 327.04 | 12.70 | 12.73 | -20.49 | -20.40 |
| Std. | 0.96 | 0.32 | 2.19 | 2.39 | 0.16 | 0.02 |
| Coeff. Var. (%) | 0.00 | 0.10 | 17.22 | 18.77 | 0.77 | 0.12 |

| | Pmax (bar) | | CA Pmax (°CA) | | IMEP (bar) | |
|-----------------|------------|--------|---------------|--------|------------|--------|
| | ETAS | dSPACE | ETAS | dSPACE | ETAS | dSPACE |
| Mean | 44.71 | 44.03 | 16.67 | 16.90 | 8.81 | 8.66 |
| Std. | 3.84 | 3.84 | 2.46 | 2.36 | 0.10 | 0.11 |
| Coeff. Var. (%) | 8.59 | 8.73 | 14.73 | 13.98 | 1.08 | 1.25 |

APPENDIX XV : ADDITIONAL THROTTLE BODY RESULTS

The throttle body was commanded to follow different patterns with the engine off and with the engine motoring at 1000, 1500 and 2000 RPM. First the error is plotted for the entire pyramid test and a zoomed region is also shown between 7 and 13 s (see Figure A-XV-1). The majority of the error is less than 1 degree there is slightly more error when the throttle body is controlled to the lower angles. The error plot is then shown for the pyramid test with the engine off and at the 2000 RPM conditions (see Figure A-XV-2). Since the results from the other motoring conditions provided similar results they were not included below. This figure shows that the controller performance did not drastically change; however, there was some slight improvement as the difference plot shows less drastic disturbances.

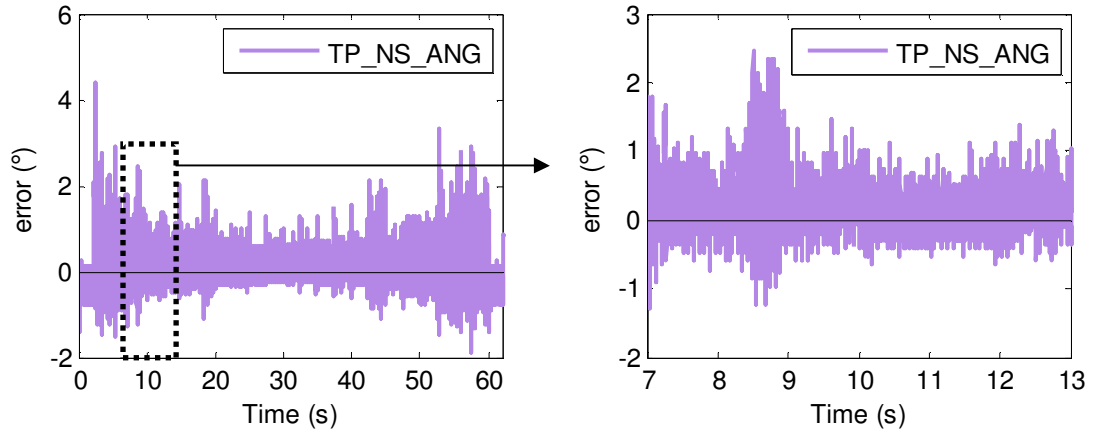


Figure A-XV-1: Pyramid Diff. Plots, Left – Engine Off, Right – Zoomed (7-13 s)

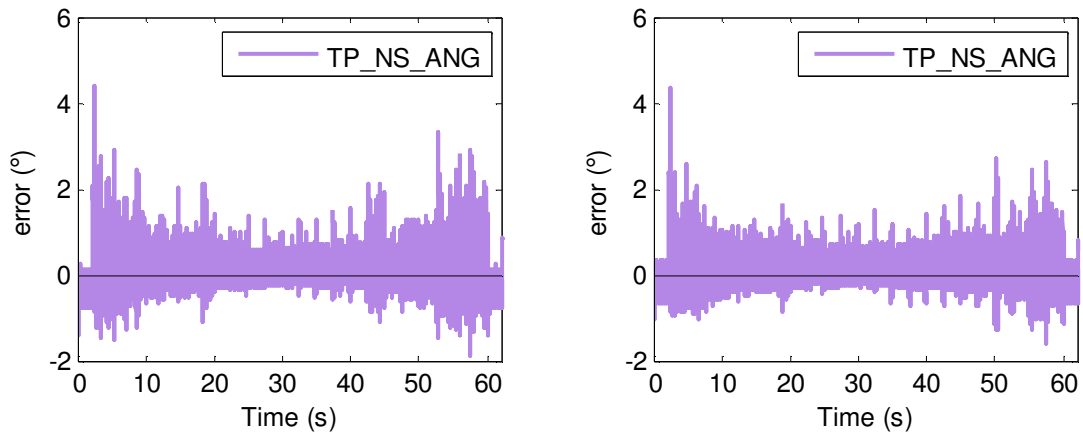


Figure A-XV-2: Pyramid Diff. Plots, Left – Engine Off, Right – Motoring 2000

The error is also plotted for the RSIT and the zoomed region shows an example of the region where the throttle body had overshoot and quickly stabilized (see Figure A-XV-3) The error was also compared for the 1500 RPM motoring conditions with the engine off conditions and the results looked similar (see Figure A-XV-4).

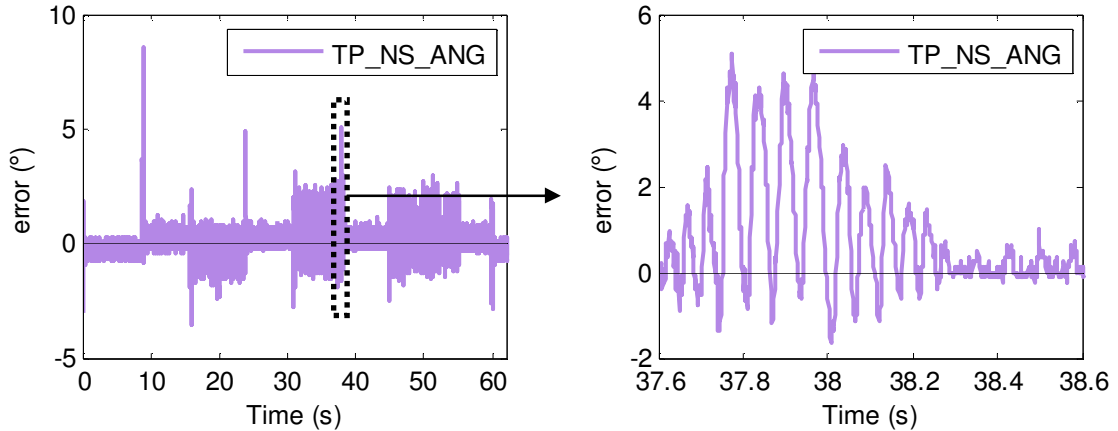


Figure A-XV-3: RSIT Diff. Plots, Left – Engine Off, Right – Zoomed (23-45 s)

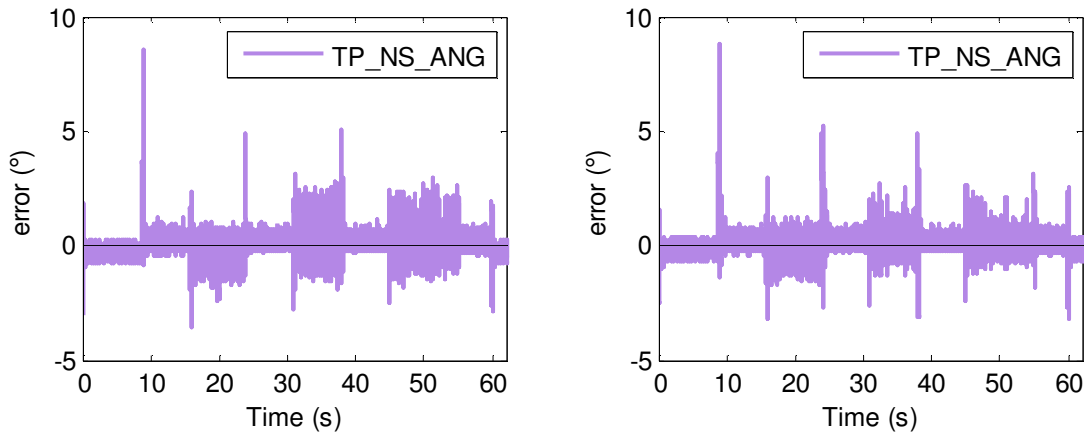


Figure A-XV-4: RSIT Diff. Plots, Left – Engine Off, Right – Motoring 1500 RPM

SWIT error plots were also created (see Figure A-XV-5), while Figure A-XV-6 again illustrates that the effect of motoring the engine at 2000RPM does not cause any additional disturbances on the ability of the throttle controller to hold a desired angle, but instead results in a very minimal improvement. Figure A-XV-7 shows a zoomed region of the throttle angle response which appears to be acceptable. Additional filtering on the measured angle could help improve the throttle control.

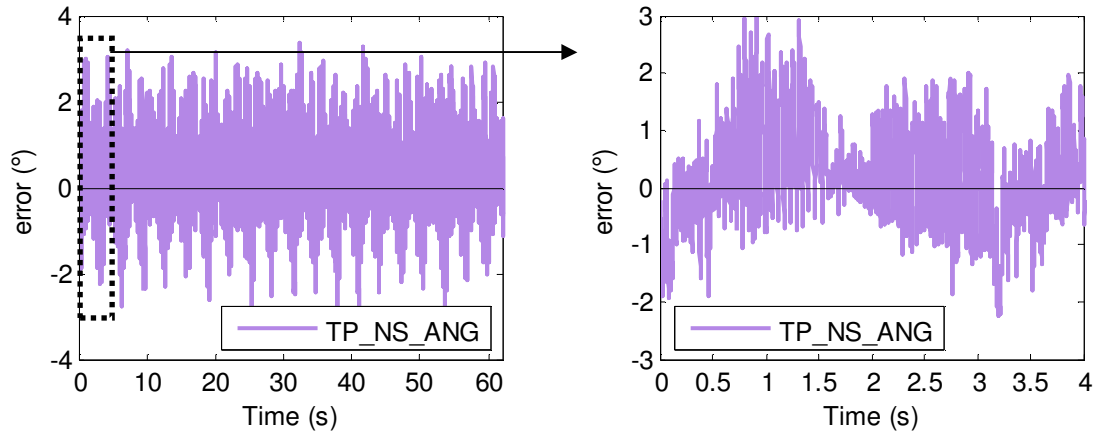


Figure A-XV-5: SWIT Diff. Plots, Left – Engine Off, Right – Zoomed (0-4 s)

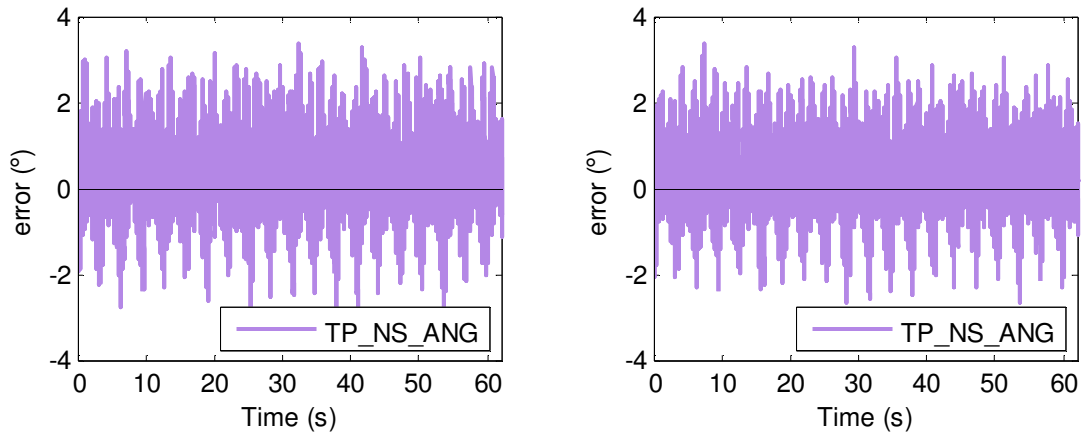


Figure A-XV-6: SWIT Diff. Plots, Left – Engine Off, Right – Motoring 2000 RPM

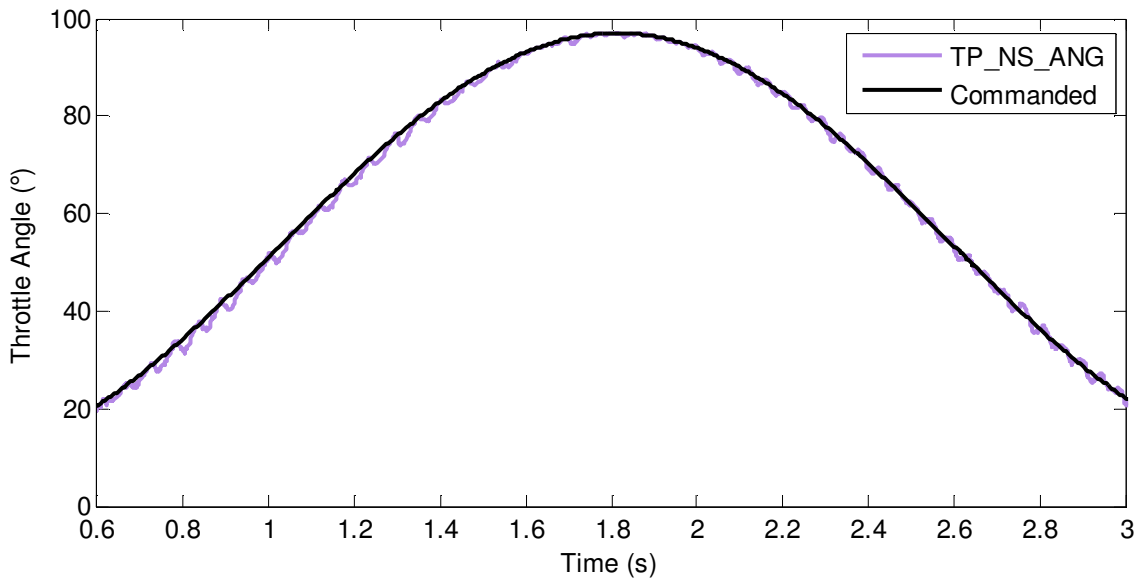


Figure A-XV-7: SWIT Engine Off, Zoomed (0.6-3 s)

APPENDIX XVI : COIL DRIVER CIRCUIT DESIGN

The following circuit/coil driver box was designed to allow easy operation of a two pin pencil on coil on spark plug by using a digital voltage supply which triggers a driver such as an IGBT. Figure A-XVI-1 is an image of the final assembled product that was used for engine testing.

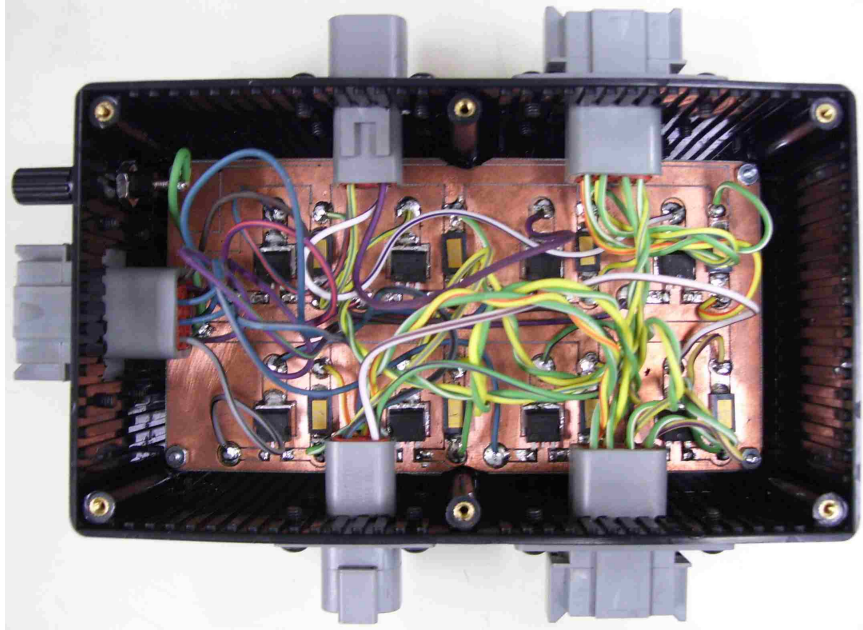


Figure A-XVI-1: Final Assembled Coil on Driver (Box Bottom View)

Figure A-XVI-2 describes the pads and their purpose for one set of the IGBT driver circuit, similarly the remaining pads serve the same purpose. This figure also shows where the IGBT and current resistor would be installed. Figure A-XVI-3 provides the pad numbers, which can be cross referenced to Table A-XVI-1 to identify, which connector the pad is wired to. Figure A-XVI-4 shows a top view of the box and the location for each of the connectors that are mounted on the side of the driver box. Figure A-XVI-5 shows how the driver box is expected to interface to the engine harness. It may be connected directly to the engine harness or a separate cable can be made to connect only to specific coils.

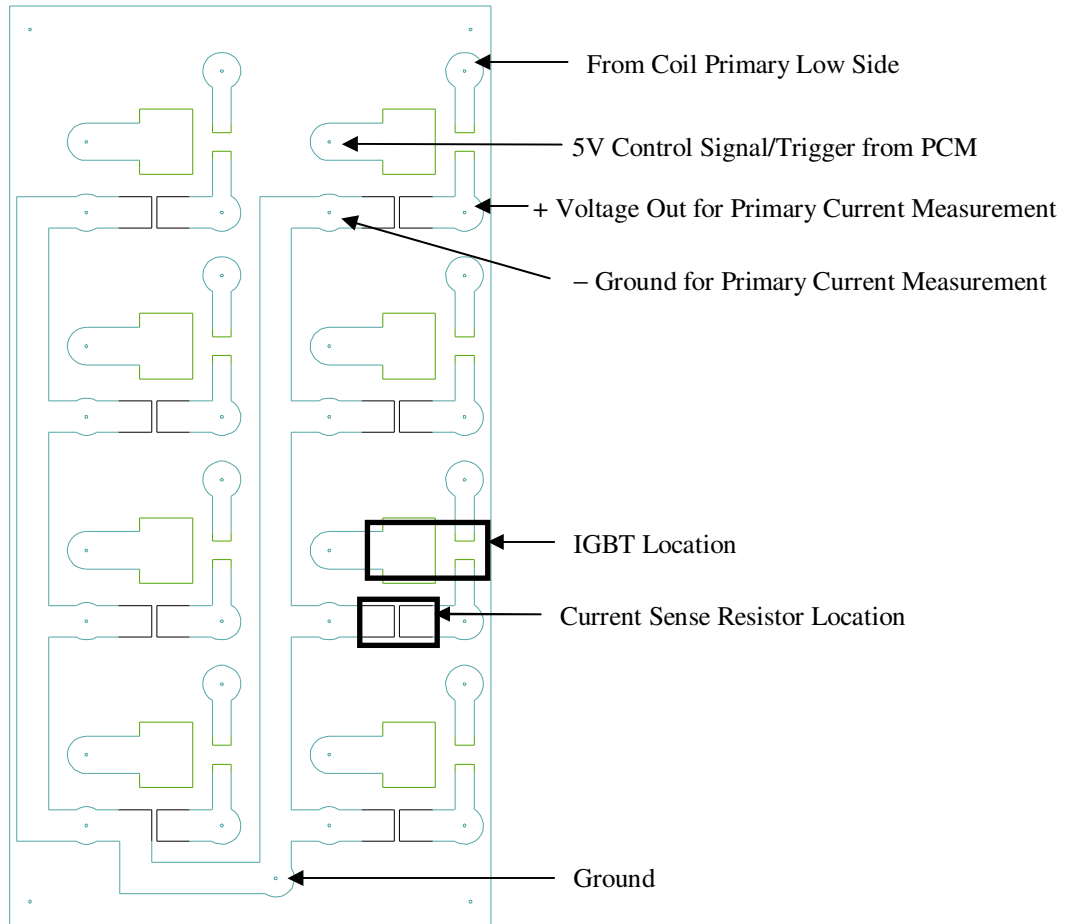


Figure A-XVI-2: Coil Driver Board Layout/Pad Descriptions

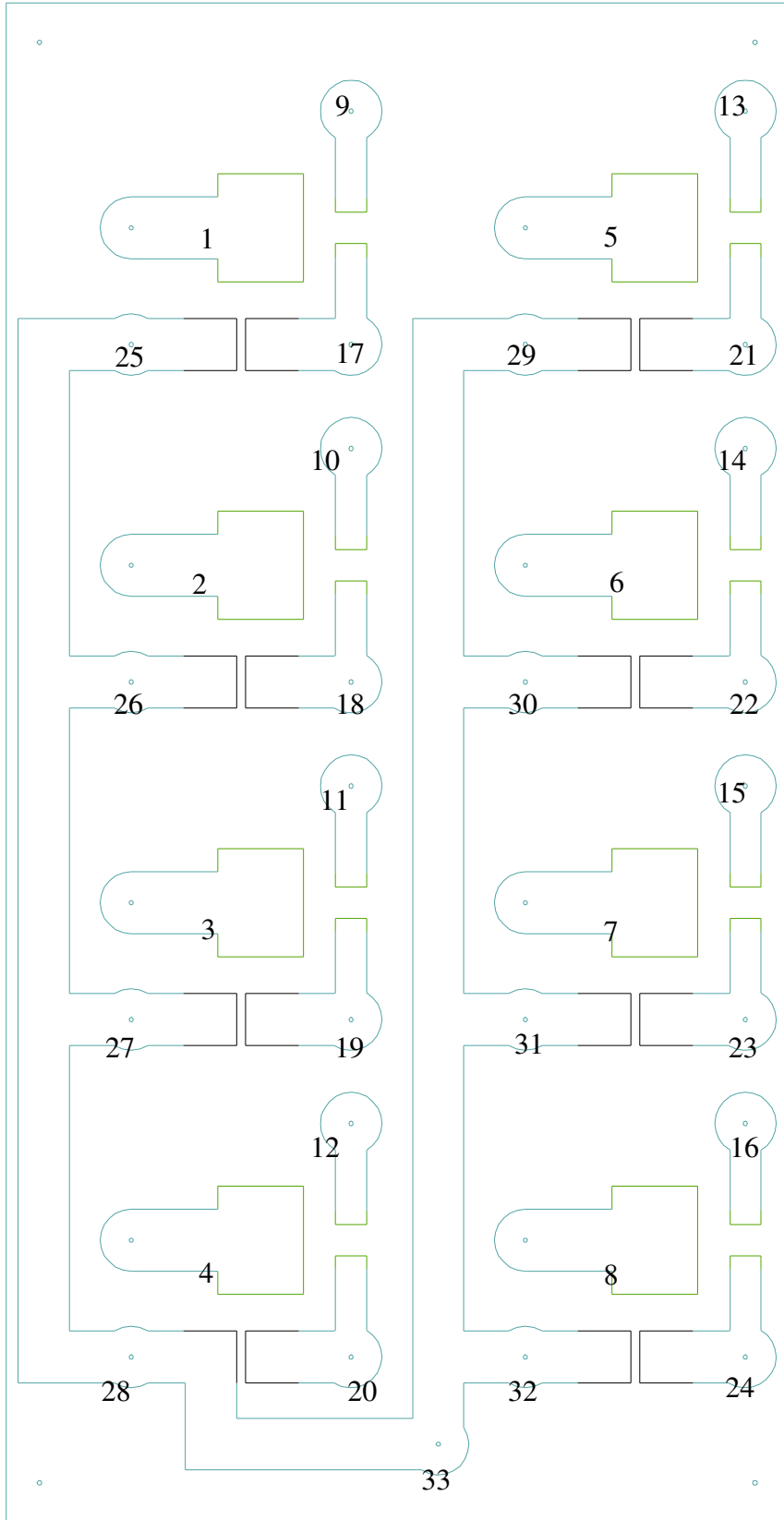


Figure A-XVI-3: PCB Circuit Board Pad Numbers

Table A-XVI-1: PCB Circuit Board Pad # to Connector Pin Numbers

| Circuit Pad # | Description | Connector # & Type on Box | Pin |
|---------------|------------------------------------|-------------------------------------|-----|
| 1 | 5V Trigger Coil 1 | Eight Pin Deutsch Connector 1 (DC1) | 1 |
| 2 | 5V Trigger Coil 2 | | 2 |
| 3 | 5V Trigger Coil 3 | | 3 |
| 4 | 5V Trigger Coil 4 | | 4 |
| 5 | 5V Trigger Coil 5 | | 5 |
| 6 | 5V Trigger Coil 6 | | 6 |
| 7 | 5V Trigger Coil 7 | | 7 |
| 8 | 5V Trigger Coil 8 | | 8 |
| 9 | Low Side Primary Coil 1 | Four Pin Deutsch Connector 2 (DC2) | 1 |
| 10 | Low Side Primary Coil 2 | | 2 |
| 11 | Low Side Primary Coil 3 | | 3 |
| 12 | Low Side Primary Coil 4 | | 4 |
| 13 | Low Side Primary Coil 5 | Four Pin Deutsch Connector 3 (DC3) | 1 |
| 14 | Low Side Primary Coil 6 | | 2 |
| 15 | Low Side Primary Coil 7 | | 3 |
| 16 | Low Side Primary Coil 8 | | 4 |
| 17 | + V _{currentsense} Coil 1 | Eight Pin Deutsch Connector 4 (DC4) | 1 |
| 18 | + V _{currentsense} Coil 2 | | 2 |
| 19 | + V _{currentsense} Coil 3 | | 3 |
| 20 | + V _{currentsense} Coil 4 | | 4 |
| 21 | + V _{currentsense} Coil 5 | Eight Pin Deutsch Connector 5 (DC5) | 1 |
| 22 | + V _{currentsense} Coil 6 | | 2 |
| 23 | + V _{currentsense} Coil 7 | | 3 |
| 24 | + V _{currentsense} Coil 8 | | 4 |
| 25 | - V _{currentsense} Coil 1 | Eight Pin Deutsch Connector 4 (DC4) | 8 |
| 26 | - V _{currentsense} Coil 2 | | 7 |
| 27 | - V _{currentsense} Coil 3 | | 6 |
| 28 | - V _{currentsense} Coil 4 | | 5 |
| 29 | - V _{currentsense} Coil 5 | Eight Pin Deutsch Connector 5 (DC5) | 8 |
| 30 | - V _{currentsense} Coil 6 | | 7 |
| 31 | - V _{currentsense} Coil 7 | | 6 |
| 32 | - V _{currentsense} Coil 8 | | 5 |
| 33 | Ground Connect to dSPACE Chassis | Banana Plug 1 | |

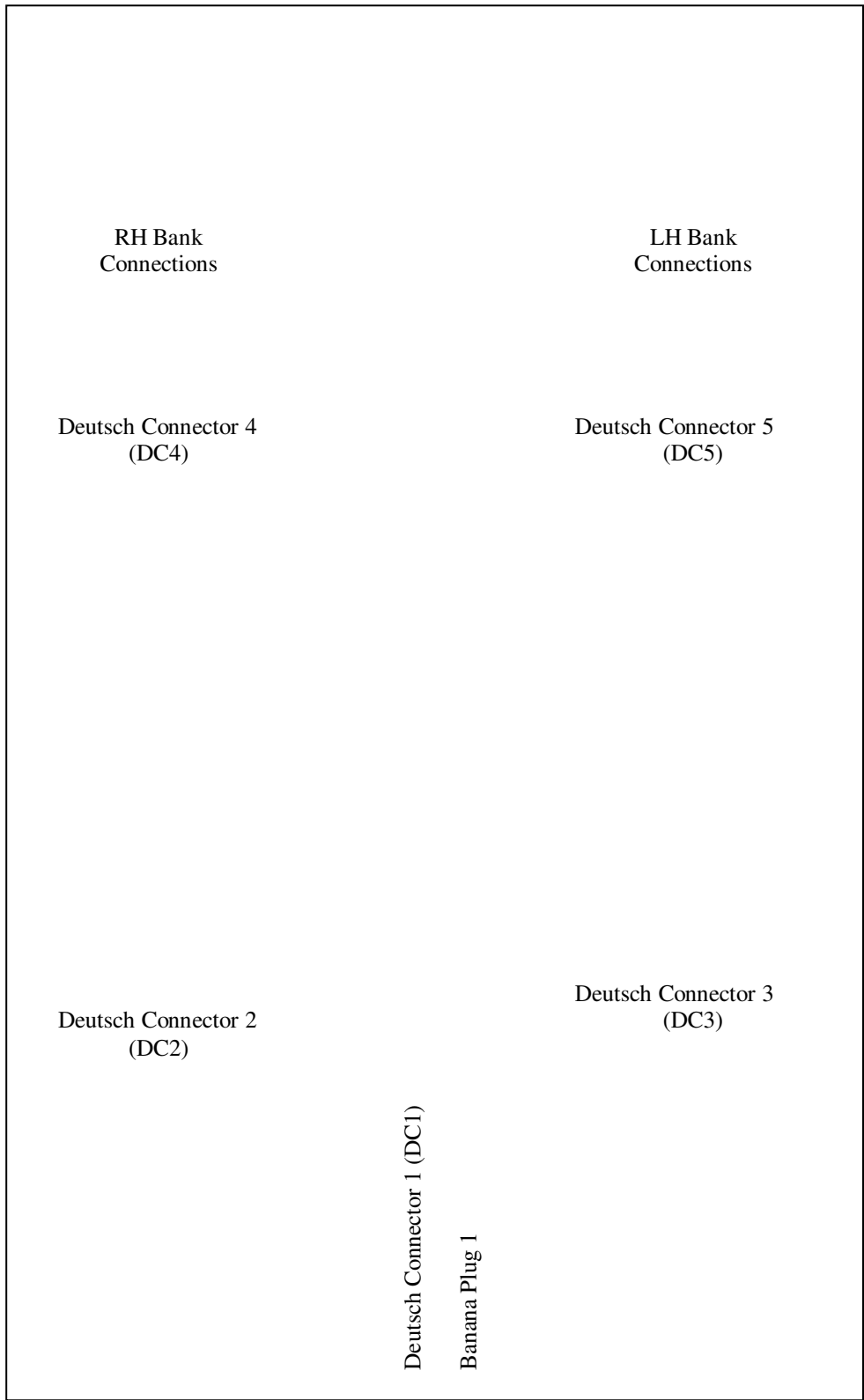


Figure A-XVI-4: Driver Box Top View - Connector Locations Names

The list below contains all the required parts that were used to construct the coil driver box including the mating connectors that were used. Two different IGBT chips are listed as both are feasible options that may be used. However, for the research conducted in this thesis the IGBT from STMicroelectronics was chosen due to its availability at the time of the project. Part numbers have been bolded.

- 1) IGBT Drivers (8 required) choose from one of the below parts
 - a. STMicroelectronics - **STGB18N40LZ** [46,47]
 - i. This is the part that was used in the research conducted
 - b. ON Semiconductor - **NGB8202N** [48,49]
 - i. This is an alternative driver that was sourced
- 2) 0.2 Ω Current Sense Resistor (8 required)
 - a. VISHAY - **WSR5R2000FEA** [45]
- 3) Driver Box (1 required)
 - a. HAMMOND MANUFACTURING - **1591EFLBK**
- 4) 8 Pin Connectors
 - a. 8 Pin Receptacle w/Flange - **DT04-08PA-L012** (3 required)
 - b. Male Pin, Size 16, 16-18AWG - **0460-202-16141** (24 required)
 - c. 8 Way Receptacle Wedgelock - **W8P** (3 required)

Optional Mating Connector Parts

 - d. **8DT06-08SA** (3 required)
 - e. Female Pin, Size 16, 16 to 18AWG - **0462-201-16141** (24 required)
 - f. 8 Way Plug Wedgelock - **W8S** (3 required)
- 5) 4 Pin Connectors
 - a. 4 Pin Receptacle w/ Flange - **DT04-4P-L012** (2 required)
 - b. Male Pin, Size 16, 16 to 18AWG - **0460-202-16141** (8 required)
 - c. 4 Way Receptacle Wedgelock - **W4P** (2 required)

Optional Mating Connector Parts

 - d. **DT06-4S** (2 required)
 - e. Female Pin, Size 16, 16-18AWG - **0462-201-16141** (8 required)
 - f. 4 Way Plug Wedgelock - **W4S** (2 required)
- 6) Banana (1 required)
 - a. Johnson/Emerson - Binding Post, Stud Black - **111-0103-001**

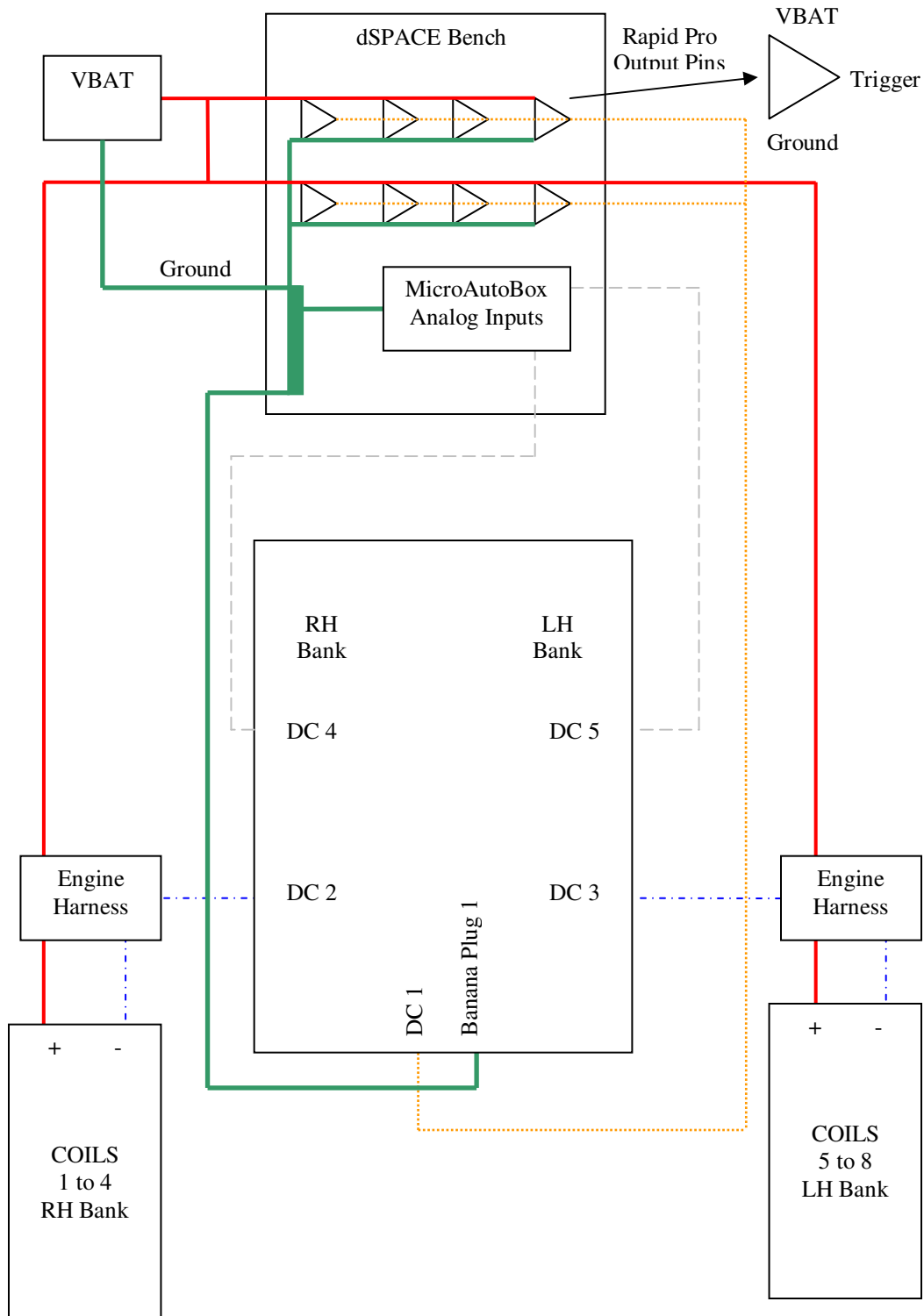


Figure A-XVI-5: Connection to dSPACE Bench & Components

APPENDIX XVII : OFFLINE ENGINE SIMULATOR

The first step was to simulate the engine rotation using a crank angle simulator through an electric motor. To do this, a CMC TORQUEMASTER 2130 servo motor [86, 87] was used together with a PS2X3W72 power supply [88] and 25A8K brush type PWM servo amplifier [89].



Figure A-XVII-1: Engine Speed/Crank Simulator Setup for Offline Testing

Using this hardware allowed a simple analog voltage input to control the motor speed as desired. The CKP VRS sensor signal was also used to generate a cam signal by detecting the negative slope zero crossings of the missing tooth. Using the CKP signal and the generated cam signal, synchronization was achieved. If synchronization was not achieved, it was not possible to use the dSPACE hardware to test injection/spark plug firing offline.

The offline test setup used a pump to supply pressurized water instead of gasoline, since injecting gasoline and operating a spark plug without a dividing barrier can be a dangerous thing to attempt (see Figure A-XVII-2). Ultimately, it would be beneficial to manufacture a test bench similar to that in Figure A-XVII-4. Digital inputs were verified using the UNOMAT Model MCX portable calibrator as a signal generator [90], while analog inputs were verified using the Agilent E3610A variable source power supply [91, 92]. Analog and digital outputs were verified using the Yokogawa DL850V ScopeCorder oscilloscope [93].

With all the hardware verified to operate properly, the second step was to have a production engine controller run an engine, while the sensor signals (engine speed, cam position, throttle position, mass air flow) could be teed off and sent to a parallel set of hardware (MicroAutoBox/RapidPro w/separate injectors, coils and spark plugs, see Figure A-XVII-2 and Figure A-XVII-3). This allowed for verification of the dyno wire harness that was built, while testing the MATLAB model under development. Injection and spark events were easily tested, while using Fluke 80i-110s current probes to monitor the current draw from both the coils and injectors, for both sets of hardware (production/development). The current probes output an analog voltage (proportional to the current draw), which was measured using the AVL IndiSmart 612 combustion system. The AVL combustion system allowed all the signals to be overlaid in the CAD (production/development). Individual cylinder coils on the development hardware were then tested and validated against the production hardware.

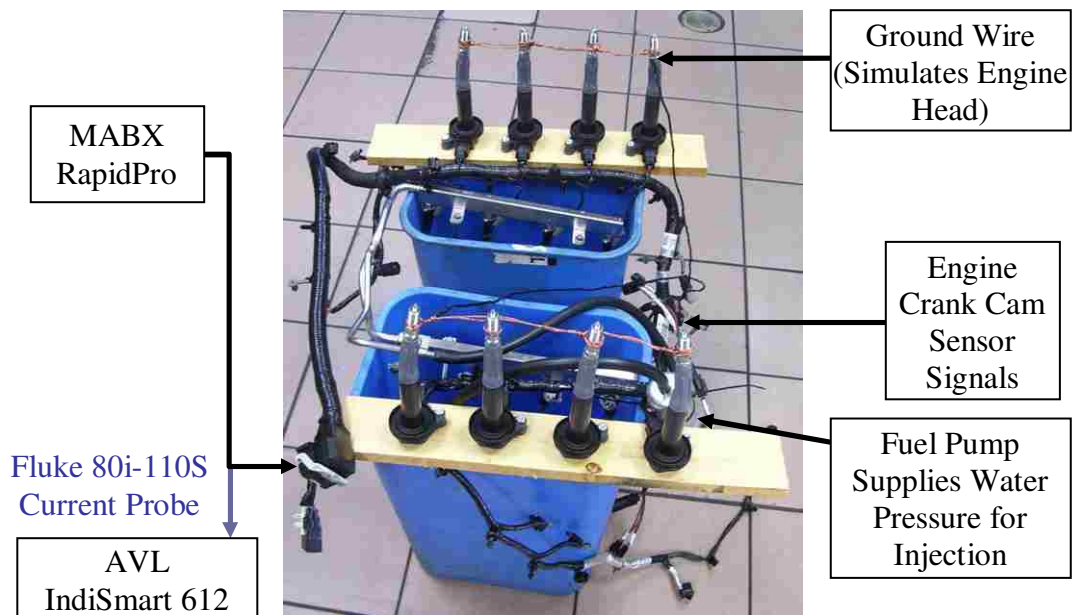


Figure A-XVII-2: Offline Injector and Spark Plug Test bench

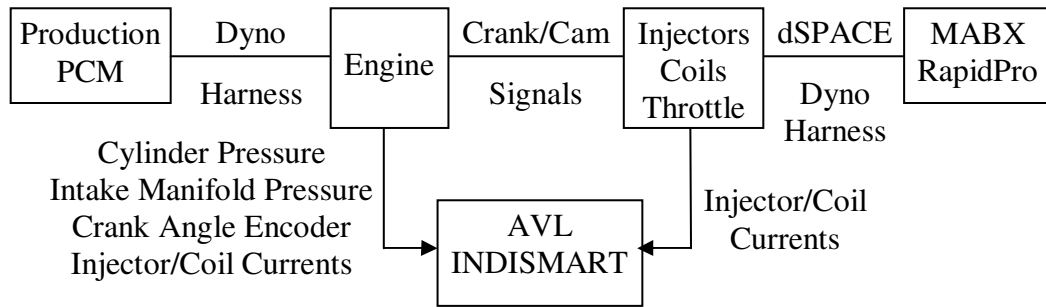


Figure A-XVII-3: Parallel Engine Hardware Testing

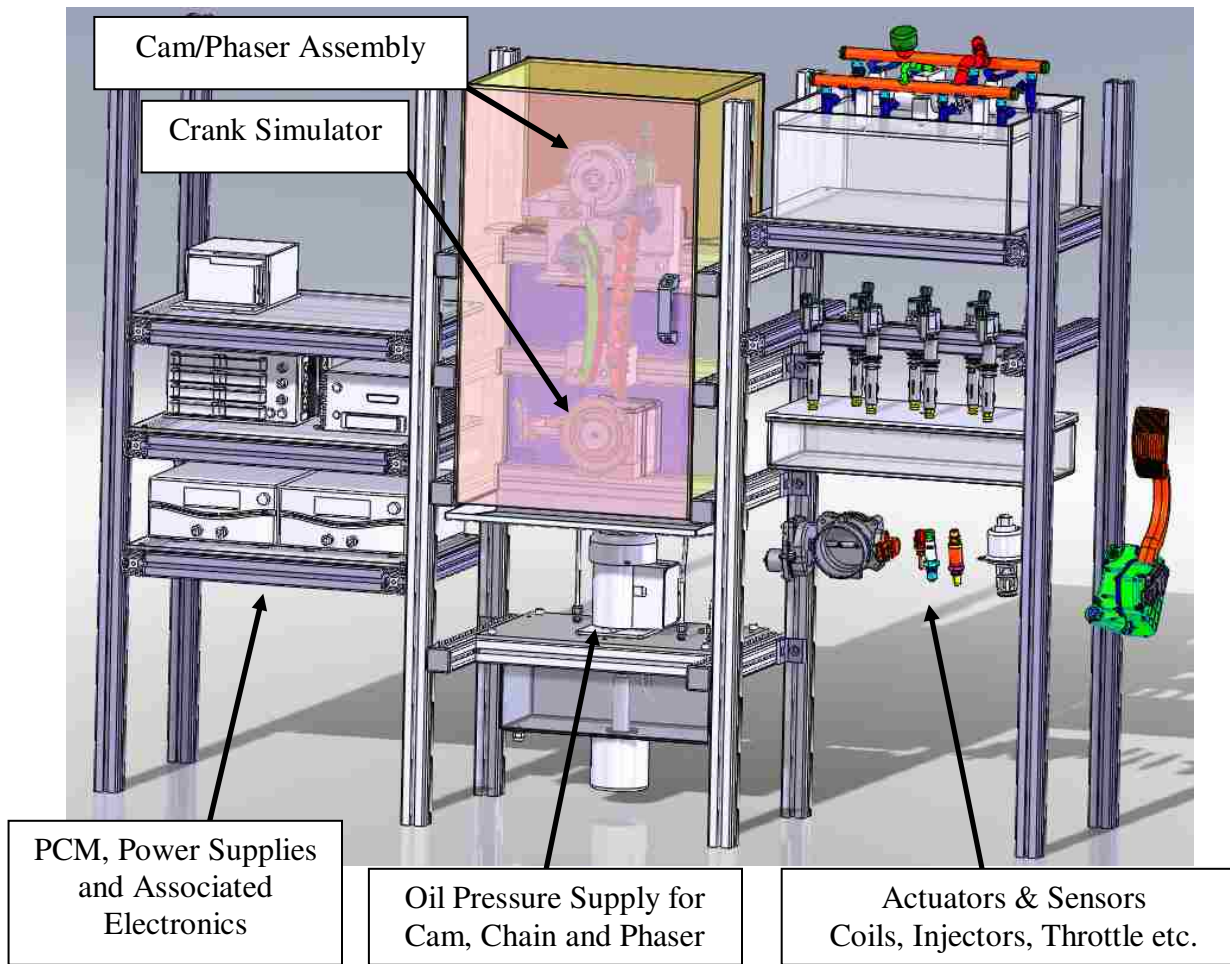


Figure A-XVII-4: Proposed Offline Engine Simulator

APPENDIX XVIII : MVEM MANIFOLD FILLING/EMPTYING

The MVEM is based on the conservation of mass which can be expressed for the engine as follows. For this thesis the Exhaust Gas Recirculation (EGR) mass flow rate (\dot{m}_{EGR}) was equivalent to zero since EGR is not setup for this engine. \dot{m}_{at} is the mass flow rate past the throttle body and \dot{m}_{ap} is the mass flow rate into the intake port. The conservation of mass for the intake manifold can be expressed using Eq. A-XVIII-1 [1].

$$\frac{dm_{at}}{dt} = \dot{m}_{at} - \dot{m}_{ap} + \dot{m}_{EGR} \quad \text{Eq. A-XVIII-1}$$

Throttle body mass flow rate can be calculated using Eq. A-XVIII-2 [1]

when $\rightarrow \left(\frac{P_m}{P_o}\right) > \left(\frac{2}{\gamma+1}\right)^{\gamma/\gamma-1}$

$$\dot{m}_{at} = \frac{C_d A_{th} P_o}{\sqrt{RT_o}} \left(\frac{P_m}{P_o}\right)^{1/\gamma} \sqrt{\left(\frac{2\gamma}{\gamma-1}\right) \left[1 - \left(\frac{P_m}{P_o}\right)^{\gamma+1/\gamma}\right]} \quad \text{Eq. A-XVIII-2}$$

or Eq. A-XVIII-3 [1] when $\rightarrow \left(\frac{P_m}{P_o}\right) \leq \left(\frac{2}{\gamma+1}\right)^{\gamma/\gamma-1}$

$$\dot{m}_{at} = \frac{C_d A_{th} P_o \sqrt{\gamma}}{\sqrt{RT_o}} \left[\frac{2}{\gamma+1}\right]^{(\gamma+1)/2(\gamma-1)} \quad \text{Eq. A-XVIII-3}$$

While A_{th} is the throttle area can be expressed by Eq. A-XVIII-4 [1]

$$A_{th} = \frac{\pi D^2}{4} \left(1 - \frac{\cos \alpha}{\cos \alpha_0}\right) + \frac{D^2}{2} [A - B - C + D] \quad \text{Eq. A-XVIII-4}$$

Where: $A = \frac{a}{\cos \alpha} \sqrt{\cos^2 \alpha - a^2 \cos^2 \alpha_0}$

$$B = \frac{\cos \alpha}{\cos \alpha_0} \sin^{-1} \left(\frac{a \cos \alpha_0}{\cos \alpha}\right)$$

$$C = a \sqrt{1 - a^2}$$

$$D = \sin^{-1} a$$

P_m is the intake manifold pressure, P_o is the ambient air pressure, $C_d = 0.5$ which is the coefficient of discharge [27], it will vary with throttle angle and must be found experimentally if it is not estimated [94-96], $R = 8.314$ J/K-mol which is the universal gas constant, $\gamma = 1.4$ which is the ratio of specific heats for air, d is the throttle shaft diameter, D is the throttle bore diameter and $a=d/D$. α_0 is the throttle angle when the throttle is closed. The throttle reaches its maximum value when $\alpha = \cos^{-1}(a \cos \alpha_0)$, which is $\cong \frac{\pi D}{4} - dD$ [1].

The port air mass flow rate can be found using the speed density equation (see Eq. A-XVIII-5) providing a Manifold Absolute Pressure (MAP) sensor is used or the intake manifold pressure is estimated.

$$\dot{m}_{ap} = \frac{\eta_{vol} N V_d P_m}{120 R T_m} \quad \text{Eq. A-XVIII-5}$$

Where, N is engine speed, V_d is the engine displacement T_m is the intake manifold air temperature. η_{vol} is the volumetric efficiency and can be expressed as a quadratic equation using both engine speed and intake manifold pressure. This equation is a curve fit to data collected by mapping the engine and c_1 to c_4 are the constants to fit the data (see Eq. A-XVIII-6).

$$\eta_{vol} = c_1 + c_2 N + c_3 N^2 + c_4 P_m \quad \text{Eq. A-XVIII-6}$$

A second method for obtaining volumetric efficiency would be to estimate it [94], or it can be expressed in a third form by fitting the following linear equation to experimental data (see Eq. A-XVIII-7 [98]) or through the use of a p-v diagram as explained in [98].

$$\eta_{vol} P_m = s_i P_m - y_i \quad \text{Eq. A-XVIII-7}$$

A volumetric efficiency model for variable valve timing is presented in [100] where the volumetric efficiency is first expressed as shown in Eq. A-XVIII-7 before developing their final equation which is not included here.

$$\eta_{vol} = \frac{m_{cyl} RT_m}{P_m V_d} \quad \text{Eq. A-XVIII-8}$$

The manifold state equation can be generated by assuming the intake manifold temperature is constant and the pressure is uniform, which allows the ideal gas law to be applied on Eq. A-XVIII-1.

$$\dot{P}_m = \frac{-\eta_{vol} N V_d P_m}{120 V_m} + \frac{RT_m}{V_m} \dot{m}_{at} \quad \text{Eq. A-XVIII-9}$$

When using a MAF sensor under steady state conditions, the mass of air entering the cylinder can be defined using Eq. A-XVIII-10 [101].

$$m_{cyl} = \frac{2 \dot{m}_{at}}{N n_{cyl}} \quad \text{Eq. A-XVIII-10}$$

From the ideal gas law the manifold pressure can be estimated using Eq. A-XVIII-11

$$P_m = \frac{m_{cyl} RT_m}{V_m} \quad \text{Eq. A-XVIII-11}$$

This estimated manifold pressure can then be applied in the speed density equations and the volumetric efficiency equations to find the port mass flow rate. Knowing the port mass flow allows for the calculation of the desired fuel flow rate (\dot{m}_{fdes}) providing that the desired air to fuel ratio (AFR_{des}) is given, see Eq. A-XVIII-12.

$$\dot{m}_{fdes} = \frac{\dot{m}_{ap}}{AFR_{des}} \quad \text{Eq. A-XVIII-12}$$

The mass of air entering the cylinder can be calculated using Eq. A-XVIII-13.

$$m_{cyl} = \frac{\eta_{vol} P_m V_d}{RT_m n_{cyl}} \quad \text{Eq. A-XVIII-13}$$

Knowing the mass of air that has entered the cylinder allows for the required mass of fuel to be calculated with Eq. A-XVIII-14

$$m_{fi} = \frac{m_{cyl}}{AFR_{des}} \quad \text{Eq. A-XVIII-14}$$

This desired fuel quantity can be used with a fuel injector characterization curve to then determine the required fuel injection pulse width. Knowing the desired fuel flow rate then allows for fuel film compensations calculations to take place and solve for the fuel mass flow rate injected (\dot{m}_{fi}). Since this thesis is dealing with steady state operation these equations are not required as the desired fuel flow rate into the cylinder will be equal to the flow rate of the injectors [26].

$$\dot{m}_{ff} = \left(\frac{1}{\hat{\tau}_f} \right) \left(-\dot{m}_{ff} + \hat{X} \left[\frac{1}{1 - \hat{X}} (\dot{m}_{fdes} - \dot{m}_{ff}) \right] \right) \quad \text{Eq. A-XVIII-15}$$

$$\dot{m}_{ff} = \left(\frac{1}{\hat{\tau}_f} \right) (-\dot{m}_{ff} + \hat{X} \dot{m}_{fi}) \quad \text{Eq. A-XVIII-16}$$

$$\dot{m}_{fi} = \left(\frac{1}{1 - \hat{X}} \right) (\dot{m}_{fdes} - \dot{m}_{ff}) \quad \text{Eq. A-XVIII-17}$$

Where $\hat{\tau}_f$ is an estimation of the fuel film evaporation time constant (0.1 seconds [26]), \hat{X} is the estimate of the fraction of the fuel that is deposited as fuel film (0.6 [26]), \dot{m}_{fdes} is the combustion chamber fuel mass flow rate, \dot{m}_{fi} is the injected fuel mass flow rate, \dot{m}_{ff} is the fuel film mass flow rate.

REFERENCES

1. Heywood, J.B., "Internal Combustion Engine Fundamentals" McGraw-Hill, New York, 1989
2. Stone, R., "Introduction to Internal Combustion Engines", 3rd edition, SAE Int., 1999
3. Robert BOSCH Gmbh, "Gasoline Engine Management", Wiley, 2006
4. Robert BOSCH Gmbh, "BOSCH Automotive Handbook", 6th edition, SAE Int., 2004
5. Ribbens, W. B., and Mansour, N.P., "Understanding Automotive Electronics", 6th edition, Elsevier, 2003
6. Bonnick, A., "Automotive Computer Controlled Systems", Butterworth-Heinemann, 2001
7. Kiencke, U., Nielsen, L., "Automotive Control Systems For Engine, Driveline, and Vehicle", 1st edition, SAE Int., 2000
8. Kiencke, U., Nielsen, L., "Automotive Control Systems For Engine, Driveline, and Vehicle", 2nd edition, Springer, 2005
9. Heisler, H. "Advanced Engine Technology", 2nd edition, SAE Int., 1995
10. Pickerrill, K. "Today's Technician Automotive Engine Performance: Classroom Manual", 5th edition, Delmar, 2010
11. Stone, R., Ball, J.K., "Automotive Engineering Fundamentals", SAE Int., 2004
12. Kang, J.M., "Advanced Control for Fuel Economy and Emissions Improvement in Spark Ignition Engines", PHD Thesis, The University of Michigan, 2000

13. Johansson, R., Rantzer, A., "Nonlinear and Hybrid Systems in Automotive Control", SAE In., 2003
14. Moskawa, J.J., "Automotive Engine Modeling For Real Time Control", PHD Thesis, M.I.T., 1988
15. Buckland, J.H., "Estimation Methods for Turbocharged Spark Ignition Engines", PHD Thesis, The University of Michigan, 2009
16. Andersson, P., "Air Charge Estimation in Turbocharged Spark Ignition Engines", PHD Thesis, Linköping University, 2005
17. Guerrier, M., Cawsey, P., "The Development of Model Based Methodologies for Gasoline IC Engine Calibration", SAE Int., 2004, 2004-01-1466
18. Caraceni, A., Cristofaro, F.D., Ferrara, F., Scala, S., "Benefits of Using a Real-Time Engine Model During Engine ECU Development", SAE Int., 2003, 2003-01-1049
19. Erkkinen, T., "Model Style Guidelines for Production Code Generation", SAE Int., 2005, 2005-01-1280
20. Dierker, L.T., "Automotive Systems Engineering, Modeling, and AutoCode Benefits or Burden", SAE Int., 2005, 2005-01-1287
21. Erkkinen, T., Breiner, S., "Automatic Code Generation - Technology Adoption Lessons Learned from Commercial Vehicle Studies", 2007, 2007-01-4249
22. Erkkinen, T., "Fixed-Point ECU Development with Model-Based Design", SAE Int., 2008, 2008-01-0744
23. Beine, M., Eisemann, U., Fleischer, D., Stamatov, S., "Key Factors for Successful Integration of Automatic Code Generation in Series Production Development", SAE Int., 2009, 2009-01-0154

24. Stürmer, I., Stamatov, S., Eisemann, U., “Automated Checking of MIRSA TargetLink and AUTOSAR Guidelines”, SAE Int., 2009, 2009-01-0267
25. Fleischer, D., Beine, M., Eisemann, U., “Applying Model-Based Design and Automatic Production Code Generation to Safety-Critical System Development”, SAE Int., 2009, 2009-01-0747
26. Guerquin, J., “The Development of An IC Engine Model-Based Fuel Injection Controller with Fuel Film Compensation”, Masters Thesis, University of Toronto, 2003
27. Mehrotra, R., “Air Fuel Ratio Control of Spark-Ignition Engines Using Sliding Modes”, Masters Thesis, The University of Calgary”, 1998
28. Honeywell Micro Switch Sensing and Control, “Hall Effect Sensing and Application”, http://sensing.honeywell.com/index.cfm/ci_id/154368/la_id/1/document/1/re_id/0, Accessed on May 1, 2011.
29. Borg, J.M., “Characterization and Measurement of Autoignition and Knock in a Spark Ignition Engine”, PHD Thesis, Oakland University, 2007
30. Gschweidl, K., Gotthard, E., Kampitsch, A., “Real Time Knock Analysis for Automatic Engine Mapping and Calibration”, SAE Int., 1994, 942399
31. Johansson, M. “Ion Current Interface”, Bachelor Thesis, Linköping Institute of Technology, Department of Electrical Engineering, Institutionen för systemteknik, 2005 <http://urn.kb.se/resolve?urn=urn:nbn:se:liu:diva-4000>, Accessed on May 1, 2011
32. Delphi Ionization Current Sensing Ignition Subsystem 2009, <http://delphi.com/manufacturers/auto/powertrain/gas/ignsys/ionized/>, Accessed on May 1, 2011

33. Eriksson, L., Nielsen, L., "Ionization Current Interpretation for Ignition Control in Internal Combustion Engines", Control Eng. Practice, Pergamon, Elsevier, 1997, Vol. 5, No. 8, pp.1107-1113
34. Calkins, F.T., Smith, R.C., and Flatau, A.B., "An Energy-Based Hysteresis Model for Magnetostrictive Transducers", IEEE Transactions on Magnetics, Vol. 36, No. 2, March 2000, pp.429-439 (DOI: 10.1109/20.825804)
35. Magnetostrictive Transducers, Actuators and Sensors @ ISU, <http://www.public.iastate.edu/~terfenol/homepage.html>, Accessed on May 1, 2011
36. BOSCH, "Product Information Oxygen Sensor", http://www.bosch.com.au/content/language1/downloads/Section_A.pdf, Accessed on Nov 27, 2011
37. BOSCH, "Lambda Sensor 4.9", <http://www.bosch-motorsport.com/pdf/sensors/lambda/LSU49.pdf>, Accessed on Nov 27, 2011
38. BOSCH, "Product Information LSU Planar Wide-Band Lambda Sensor", http://www.bosch-motorsport.com/pdf/sensors/lambda/LSU_En%20070905.pdf, Accessed on Nov 27, 2011
39. BOSCH, "Technical Product Information LSU4.9 Y 258 E00 015E", <http://www.breitband-lambda.de/media/Dateien%28Lambda%29/LSU49TechProductInfo.pdf>, Accessed on Nov 27, 2011
40. dSPACE, "RapidPro SC-EGOS 2/1 (DS1634) Application Notes", Version 1.0, Feb 3, 2006
41. Konzelmann, U., Hecht, H., Lembke, M., "Breakthrough in Reverse Flow Detection - A New Mass Air Flow Meter Using Micro Silicon Technology", SAE Int., 1995, 950433

42. Melexis, “MLX90316 Rotary Position Sensor IC”, <http://www.melexis.com/Hall-Effect-Sensor-ICs/Triaxis%C2%AE-Hall-ICs/MLX90316-566.aspx>, Accessed on Nov 27, 2011
43. Cassar, J., Saladano, D., “Rapid Pro Training Course”, 2009
44. Godfrey, T., “Ignition System Diagnostics Reading A Scope Pattern”, Manassas Campus Northern Virginia Community College, <http://www.nvcc.edu/home/tgodfrey/AUT%20242/8-7%20%20Chapter%20Ignition%20System%20Operation%20and%20Diagnosis.ppt> , Accessed on Dec 5, 2011
45. Vishay Dale., “WSR High Power Metal Strip Resistors”, <http://www.vishay.com/docs/31059/wsrhigh.pdf>, Accessed on May 1, 2011
46. STMicroelectronics, “STGB18N40LZ – STMicroelectronics”, <http://www.st.com/internet/analog/product/184846.jsp>, Accessed on Nov 27, 2011
47. STMicroelectronics, “STGB18N40LZ – Technical Data”, http://www.st.com/internet/com/TECHNICAL_RESOURCES/TECHNICAL_LITERATURE/DATASHEET/CD00182201.pdf, Accessed on Nov 27, 2011
48. ON Semiconductor, “NGB8202N: N-Channel Ignition IGBT 20 A, 400 V”, <http://www.onsemi.com/PowerSolutions/product.do?id=NGB8202N>, Accessed on Nov 27, 2011
49. ON Semiconductor, “NGB8202N, NGB8202AN Ignition IGBT Datasheet”, <http://www.onsemi.com/pub/Collateral/NGB8202N-D.PDF>
50. Estl, H., Preuschoff, C., Leteinturier, P., “Smart IGBT's for Advanced Distributed Ignition Systems”, SAE Int., 2004-01-0518
51. Palm III, W.J., “Modeling, Analysis and Control of Dynamic Systems”, 2nd edition, John Wiley & Sons, Inc, 2000

52. Åström, K.J., “Control System Design Lecture Notes for ME155A”, <http://www.cds.caltech.edu/~murray/courses/cds101/fa02/caltech/astrom.html>, Accessed on Nov 11, 2011.
53. Control Guru, <http://www.controlguru.com/>, Accessed on Nov 11, 2011.
54. Johnson, M.A., Moradi, M.H., “PID Control New Identification and Design Methods”, Springer, 2005
55. Ford, “Internal Documentation”
56. ETAS, “ES600 – Network Module”, http://www.etas.com/en/products/es600_network_module.php, Accessed on Nov 11, 2011
57. ETAS, “ES590/ES591 – Interface Module”, http://www.etas.com/en/products/es590_es591_interface_module.php, Accessed on Nov 11, 2011
58. ETAS, “ES650 – Thermo and A/D Module”, <http://www.etas.com/en/products/es650.php>, Accessed on Nov 11, 2011
59. dSPACE, “MicroAutoBox”, <http://www.dspace.com/en/inc/home/products/hw/micautob.cfm>, Accessed on Nov 27, 2011
60. dSPACE, “HelpDesk Documentation, dSPACE Software Release 7.0”, 2011
61. dSPACE, “RapidPro”, <http://www.dspace.com/en/inc/home/products/hw/rapidpro.cfm>, Accessed on Nov 27, 2011
62. AVL, “IndiCom Indicating Software”, <https://www.avl.com/indicom-indicating-software>, Accessed on Nov 14, 2011
63. AVL, “IndiSmart 612 Product Guide AT3042E”, 2009
64. AVL, “Angle Encoder 364CC/364XC AT1295E”, 2002

65. Kistler, “4005BA5F Piezoresistive Pressure Sensor”, http://www.kistler.com/US_en-us/13_Productfinder/App.4005BA5F/Piezoresistive-pressure-sensor-measuring-range-0-...-5-bar-fine-thread-M5x0-5-without-amplifier.html, Accessed on Nov 14, 2011
66. Kistler, “4005BA5F Piezoresistive Pressure Sensor Specification Sheet 4005B_000-594e-09.09”, http://www.kistler.com/mediaaccess/4005BA5F__000-594e-09.09.pdf, Accessed on Nov 14, 2011
67. Kistler, “4618A0 Piezoresistive Amplifier”, http://www.kistler.com/US_en-us/13_Productfinder/App.4618A0/Piezoresistive-amplifier-with-pressure-output-0-...-10-V-and-420-mA.html, Accessed on Nov 14, 2011
68. Kistler, “4618A0 Piezoresistive Amplifier Specification Sheet 4618A_000-293e-09.11”, http://www.kistler.com/mediaaccess/4618A0__000-293e-09.11.pdf, Accessed on Nov 14, 2011
69. AVL, “GU22CK Pressure Sensor Datasheet AT3391E”, https://www.avl.com/c/document_library/get_file?uuid=3135c203-3127-43e8-a619-f922d094c156&groupId=10138, Accessed on Nov 14, 2011
70. Fluke, “80i-110s AC/DC Current Probe Instruction Sheet”, http://assets.fluke.com/manuals/80i_110siseng0000.pdf, Accessed on Nov 14, 2011
71. Fluke, “80i-110s AC/DC Current Probe Technical Data”, <http://assets.fluke.com/datasheets/80i-110s-Spexs.pdf>, Accessed on Nov 14, 2011
72. NI, “PXI-1031”, <http://sine.ni.com/nips/cds/view/p/lang/en/nid/13906>, Accessed on Nov 14, 2011
73. NI, “PXI-1031/PXI-1031DC User Manual 371226G-01”, <http://www.ni.com/pdf/manuals/371226g.pdf>, Dec 2010, Accessed on Nov 14, 2011

74. NI, “BNC-2110”, <http://sine.ni.com/nips/cds/view/p/lang/en/nid/1865>, Accessed on Nov 14, 2011
75. NI, “BNC-2110 Installation Guide”, <http://www.ni.com/pdf/manuals/372121f.pdf>, Accessed on Nov 14, 2011
76. ETAS, “LA4 – Lambda Meter – Lambda Modules”, <http://www.etas.com/en/products/la4.php>, Accessed on Dec 5, 2011
77. ETAS, “Lambda Meter LA4 User’s Guide ”, 2011
78. dSPACE, “RapidPro Engine Controller Demo Model DemoRPCUEngineControl.mdl”, 2011
79. dSPACE, “MicroAutoBox 1401 Throttle Position Controller Demo Model demo1401_throttle_control.mdl”, 2011
80. dSPACE, “RapidPro BOSCH LSU 4.2 UHEGO Sensor Demo Model SC_EGOS_example.mdl”, 2011
81. dSPACE, “RapidPro SC-EGOS 2/1 (DS1634) Application Notes”, Version 1.0, 2006
82. Schmeißer, F., and Dietmayer, K., “Rotational Speed Sensors KMI15/16 AN98087”, Philips Semiconductors, http://www.nxp.com/documents/application_note/AN98087.pdf, Accessed on May 1, 2011
83. Philips Semiconductor “Magneto-resistive Sensors for Magnetic Field Measurement”, Sept 6, 2000, http://www.nxp.com/acrobat_download2/various/SC17_GENERAL_MAG_2.pdf, Accessed on May 1, 2011
84. Philips Semiconductor, “Rotational Speed Sensors”, <http://www.nxp.com/products/sensors/rotationalspeedsensors/index.html>, Accessed on May 1, 2011

85. Sugiura, M., Okazaki, I., Saikalis, G., "Hot Wire Mass Gas Flow Sensing Device", SAE Int., 1994, 940625
86. ITT, "DC Brush Servo Motor - Platform 2100", http://www.torquesystems.com/brush_servo_motor_platform2100.asp , Accessed on Nov 27, 2011
87. CMC, "TORQUEMASTER Brush Servo Motors 2100 Series", http://www.torquesystems.com/downloads/servo_motors/platform2100.pdf, Accessed on Nov 27, 2011
88. ADVANCED Motion Controls, "PS2X3 and PS4X3 SERIES", <http://www.a-m-c.com/download/datasheet/ps2x3w72.pdf> , Accessed on Nov 27, 2011
89. ADVANCED Motion Controls, "Analog Servo Driver 25A8", <http://www.a-m-c.com/download/datasheet/25a8.pdf>, Accessed on Nov 27, 2011
90. DRUCK, "MCX Portable Documenting Calibrator Specification Sheet", http://www.datacon.cz/pdf_druck/mcx.pdf, Accessed on Nov 14, 2011
91. Agilent Technologies, "E3610A 30W Power Supply, 8V, 3A or 15V, 2A", <http://www.home.agilent.com/agilent/product.jsp?pn=e3610a&cc=CA&lc=eng>, Accessed on Nov 14, 2011
92. Agilent Technologies, "E36XXA Series Non-Programmable DC Power Supplies Data Sheet", <http://cp.literature.agilent.com/litweb/pdf/5968-9727EN.pdf>, Accessed on Nov 14, 2011
93. Yokogawa, "Products - DL850/DL850V ScopeCorder", <http://tmi.yokogawa.com/products/oscilloscopes/scopeorders-oscillographic-recorders/dl850dl850v-scopeorder/>, Accessed on Nov 14, 2011
94. Turin, R., Dagci, O., Chang, M.F., "Low-Cost Air Estimation", SAE Int., 2009, 2009-01-0590

95. Butt., Q.R., Bhatti, A.I., Iqbal, M., M.A.Rizwi, Mufti, R., Kazmi, I.H., "Estimation of Automotive Engine Parameters: Part I: Discharge Coefficient of Throttle Body", IEEE Proceedings of International Bhurban Conference on Applied Sciences & Technology, 2009, pp. 275-280
96. Blair, G.P., Drouin, F.M.M., "Relationship Between Discharge Coefficients and Accuracy of Engine Simulation", SAE Int., 1996, 962527
97. Hendricks, E., Sorenson, S.C., "Mean Value Modeling of Spark Ignition Engines", SAE Int., 1990, 900616
98. Hendricks, E., Chevalier, A., Jensen, M., Sorenson, S.C., Trumpy, D., Asik, J., "Modeling of the Intake Manifold Filling Dynamics", SAE Int., 1996, 960037
99. Chevalier, A., Muller, M., Hendricks, E., "On the Validity of Mean Value Engine Models During Transient Operation", SAE Int., 2000, 2000-01-1261
100. Turnin, R.C., Zhang R., Chang, M.F., "Volumetric Efficiency Model for Variable Cam-Phasing and Variable Valve Lift Applications", SAE Int., 2008, 2008-01-0995
101. Kotwicki, A., Russell, J., Pursifull, R., Lewis, D., "An Air Meter Based Cylinder Air Charge Estimator", SAE Int., 1999, 1999-01-0856

VITA AUCTORIS

NAME: Christopher John Kelly

PLACE OF BIRTH: Windsor, Ontario

DATE OF BIRTH: June 24 1984

EDUCATION: Ontario Secondary School Diploma
Sandwich Secondary School
LaSalle, ON
1998-2003

Bachelor of Applied Science
Mechanical Engineering w/ Automotive Option
University of Windsor
Windsor, ON
2003-2007

Master of Applied Science
Mechanical Engineering
University of Windsor
Windsor, ON
2008 - 2011